THÈSE PRÉSENTÉE À

L'UNIVERSITÉ DU QUÉBEC À CHICOUTIMI

COMME EXIGENCE PARTIELLE

DU DOCTORAT EN SCIENCES DE LA TERRE ET DE L'ATMOSPHÈRE

PAR

CHARLEY J. DURAN

ORIGINE DES LENTILLES RICHES EN SULFURES DES GISEMENTS DE PALLADIUM DU LAC DES ILES, ONTARIO, CANADA

JANVIER 2015

RÉSUMÉ

Les gisements de Pd du Lac des Iles (Ouest de l'Ontario, Canada) sont connus pour être riches en Pd et pauvres en sulfures. Il y a un débat de longue date concernant l'origine de ces gisements, avec une école de pensée proposant qu'ils sont essentiellement d'origine magmatique, et une autre suggérant qu'ils sont hydrothermaux. En plus de la minéralisation pauvre en sulfures, des lentilles riches en sulfures sont présentes au travers de l'intrusion du Lac des Iles et celles-ci n'ont pas été étudiées précédemment. Le but de cette thèse de doctorat est d'aborder le problème de l'origine de ces lentilles riches en sulfures.

Les lentilles riches en sulfures (0,1 à 3 m de long) recoupent la stratigrphie et suivent des zones de cisaillement syn-magmatiques. La minéralogie des sulfures varie d'un assemblage composé de pyrrhotite (Po) pentlandite (Pn) ± pyrite (Py) ± chalcopyrite ± oxydes de Fe-Ti (magnétite and ilménite), à un assemblage dominé par la pyrite (Py). Les ratios Pd/Ir et Pd/Pt roche totale sont élevés et extrêmement variables (respectivement 5 à 258000 et 2 à 226), indépendamment de l'assemblage minéralogique. Les échantillons les plus riches en Py sont enrichis en As et Bi par rapport aux autres échantillons. Les analyses géochimiques roche totale montrent un découplage du Cu à partir du Ni. La plupart des échantillons ont des ratios S/Se d'approximativement 3000 et des valeurs $\delta^{34}S$ proches de celle du manteau. Les analyses LA-ICP-MS montrent que les compositions de Po, Pn et d'oxydes de Fe-Ti sont similaires à celles provenant de minéralisations magmatiques dérivées de magmas

évolués. Les Py sont riches en EGPI + Rh et montrent une zonation compositionnelle. Leur composition et leur distribution en éléments sont similaires à celles de Py trouvées dans des gisements de sulfures magmatiques.

Il est proposé que des liquides sulfurés magmatiques se soient accumulés au travers de l'intrusion en réponse à l'ouverture de zones de dilatation à un stade magmatique. Ces liquides sulfurés ont subit la cristallisation fractionnée et ont formé des cumulats de solution solide monosulfurée (MSS). Les liquides résiduels enrichis en Pd, Pt et Au complémentaires des cumulats de MSS ne sont plus associés avec les lentilles. La variation des ratios d'EGP est interprétée comme étant le résultat de différents degrés de fractionnement de liquides sulfurés évolués. Lors de la cristallisation de la MSS, l'oxigène a diffusé hors des liquides sulfurés et a réagit avec les magmas silicatés pour former les oxydes de Fe-Ti. Au cours du refroidissement, la MSS a exsolvé pour former Po et Pn. Lors de l'altération, le Fe ± Ni ont été redistribué depuis la MSS ou Po ± Pn vers les silicates intersticiels, entraînant le développement de Py. Il est suggéré que lorsque la Py s'est formée, elle a hérité des éléments trace de la MSS ou de la Po, mais en plus les éléments ont diffusés dans la Py à partir des sulfures alentours. Certains éléments mobiles (e.g., As et Bi) ont été introduits dans la Py par des fluides.

ABSTRACT

The Lac des Iles Pd-deposits (Western Ontario, Canada) are known to be Pd-rich and sulfide-poor. There is a long-standing debate as to the origin of these deposits, with one school of thought proposing that they are essentially of magmatic origin and one suggesting that they are hydrothermal. In addition to the sulfide-poor mineralization, sulfide-rich pods are present throughout the Lac des Iles intrusion and these have not previously been investigated. The purpose of this Ph.D. thesis is to address the origin of these sulfide-rich pods.

The sulfide-rich pods (0.1 to 3 m long) cross-cut the stratigraphy and follow syn-magmatic shear zones. The sulfide mineralogy varies from an assemblage that consists of pyrrhotite (Po) pentlandite (Pn) ± pyrite (Py) ± chalcopyrite ± Fe-Ti oxides (magnetite and ilmenite) to an assemblage dominated by pyrite. The whole-rock Pd/Ir and Pd/Pt ratios are high and extremely variable (5 to 258000 and 2 to 226, respectively), regardless of the mineralogical assemblages. The most Py-rich samples are enriched in As and Bi relative to the other samples. The whole-rock geochemical analyses show a decoupling of Cu from Ni. Most of the samples have S/Se ratios of approximately 3000 and $\delta^{34}S$ of near-mantle value. Laser ablation-ICP-MS analyses show that the compositions of Po, Pn and Fe-Ti oxides are similar to that from igneous mineralization derived from evolved magmas. The Py are rich

in IPGE + Rh and exhibit compositional zoning. Their composition and element distribution are similar to those of Py found in magmatic sulfide deposits.

It is proposed that magmatic sulfide liquids accumulated throughout the intrusion in response to the opening of dilation zones at magmatic stage. These sulfide liquids experienced crystal fractionation and formed cumulus monosulfide solid solution (MSS). The residual liquids enriched in Pd, Pt and Au and complimentary to the cumulus MSS are no longer associated with the pods. The variation in PGE ratios is interpreted as being the result of different degrees of fractionation of evolving sulfide liquids. During MSS crystallization, oxygen diffused out of the sulfide liquids and reacted with silicate magmas to form the Fe-Ti oxides. Upon cooling, MSS exsolved to form Po and Pn. During alteration, Fe ± Ni were redistributed from MSS or Po ± Pn to interstitial silicates, resulting in the development of Py. It is suggested that as the Py formed it inherited the trace elements from the MSS or Po, but in addition elements diffused from the surrounding sulfides into the Py. Some mobile elements (e.g., As and Bi) were introduced into the Py by fluids.

REMERCIEMENTS

Quelle aventure! Depuis mon arrivée au Québec en septembre 2010, en passant par Thunder Bay, la Chine et la Scandinavie, un long chemin a été parcouru pour aboutir à cette thèse de doctorat. Ainsi s'achèvent plus de 4 années de recherche, avec certes le sentiment d'avoir fait des découvertes, mais surtout avec la conviction de m'être découvert moi-même. Pour ne citer que Sir Edmund Hillary, premier homme à avoir atteint le sommet de l'Everest :

« It is not the mountain we conquer, but ourselves »

Il y a tant de personne qui m'ont aidé dans cette quête personnelle. Je tiens sincèrement à leur témoigner ma gratitude.

J'ai l'honneur de remercier ma directrice Sarah-Jane Barnes qui m'a donné cette opportunité exceptionnelle. Sa confiance et son soutien sans relâche m'ont poussé à donner le meilleur de moi-même, surtout dans les moments difficiles. Ce fut un véritable privilège d'avoir pu bénéficier de son mentorat, j'ai tant appris depuis que je l'ai rencontré. Merci Sarah!

J'ai le plaisir de remercier John Corkery, grâce à qui j'ai pu découvrir le monde de l'exploration minière. Son aide et sa disponibilité, que ce soit à Thunder Bay ou par courriel, ont été très importantes au cours de mon cheminement. Merci John!

J'ai également le plaisir de remercier mon ami Lionnel Djon qui à guider mes premiers pas à Thunder Bay et sur le terrain. Merci Lionnel!

Ce projet a été entièrement financé par une bourse de recherche de North American Palladium octroyée à la Chaire de Recherche du Canada en Métallogénie Magmatique. Je tiens donc à exprimer toute ma gratitude envers North American Palladium.

Au cours de ce projet j'ai pu bénéficier de l'assistance technique de nombreuses personnes. Je tiens à remercier tous les membres de l'équipe d'exploration de North American Palladium au cours des années pour leur aide avec la logistique, l'échantillonnage, la géolocalisation, et pour avoir partagé leur expérience avec moi. Plus particulièrement je

remercie Cameron McLean, Jim Finch, Arnaud Tchalikian, Skylar Schmidt, Bob Stewart, Gary De Schutter, Roland Landry, Dean Crick, Krista Nelson, Mike Grieve, Lesa Mihichuk, John Stoltz, Herin Hoxie, Devin Tait, Andrea Perrego, Timothy Lenane, Martin Tuffour, Jason Arnold, Suzanne Tatom, Jesse Koroscil, Tim Hannon, Ahmad Mumin, Matt Porter, Tyler Power, Matt Bodnar, David Benson et Dave Peck.

Je remercie également Dany Savard et Sadia Mehdi du LabMaTer, sans qui je n'aurais pu effectuer toutes les analyses géochimiques.

J'ai pu aussi profiter du support intellectuel et scientifique de Philippe Pagé, Sarah Dare et Ed Sawyer. Ils ont toujours été là pour m'éclairer dans les moments obscurs de ma recherche. Merci Philippe, Sarah et Ed.

Cette thèse a largement bénéficié des révisions des examinateurs. Je remercie sincèrement Sarah-Jane Barnes, Ed Sawyer, Jacob Hanley et Michael Higgins.

Ensuite je tiens à remercier l'ensemble du personnel de l'unité d'enseignement en Sciences de la Terre de l'UQAC et les étudiants du bac et du REDiST au cours des années. À leurs côtés, j'ai pu profiter d'un environnement de travail optimal.

Comment ne pourrais-je pas mentionner mes compagnons de galère (et occasionnellement de brosse!) qui sont devenus de véritables amis. Merci Cliff, Matthias, Lucas, Jérôme, Dominique, Sam, Edouard, Jean-Philippe, Bruna et Renato. Merci à vous pour ces moments partagés et les moments à venir!

Je remercie tout particulièrement ma famille et mes amis en France qui m'ont toujours soutenu et encouragé. Je dédie ce travail à mes parents, mon frère et mes grands-parents, qui, je le sais, sont fiers de moi, où qu'ils soient.

Enfin et surtout, je remercie ma compagne, Ariane, pour son soutien et sa compréhension. La fin du doctorat ne se serait pas aussi bien passée si tu n'avais pas été là.

TABLE DES MATIÈRES

LISTE DES FIGURES

CHAPITRE 1

CHAPITRE 2

CHAPITRE 3

LISTE DES TABLEAUX

CHAPITRE 3

CHAPITRE 4

LISTE DES ANNEXES

CHAPITRE 1

INTRODUCTION

1.1 INTRODUCTION

Ce chapitre présente le cadre d'étude de la thèse et s'organise en sept parties. La première partie place la thèse dans son contexte scientifique général. Suite à la mise en contexte, la deuxième partie présente la problématique spécifique de la thèse et les hypothèses relatives à la problématique. Cette partie présente également une vue d'ensemble des concepts fondamentaux nécessaires pour aborder la problématique ainsi que les objectifs et la méthodologie envisagés pour tester les hypothèses. La troisième partie décrit la zone d'étude afin d'établir les bases de l'étude. La quatrième partie décrit le format sous lequel la thèse est présentée. La cinquième partie est une déclaration de contribution originale. Enfin la dernière partie revendique les contributions de l'auteur et de ses collaborateurs.

1.2 CONTEXTE

La mine de palladium (Pd) du Lac des Iles (Fig. 1.1a), située dans l'ouest de l'Ontario, est le seul producteur primaire d'éléments du groupe du platine (EGP) au Canada. Même si le Lac des Iles est le cinquième plus important producteur de Pd au monde (Fig. 1.1b), il ne fournit que 2,6 % de la production mondiale (Johnson Matthey, Platinum 2013). La plupart de la production mondiale de Pd provient des minéralisations stratiformes de type *reef* présentes au sein de larges intrusions litées (e.g., le *Merensky Reef* et le *Platreef* du Complexe du Bushveld en Afrique du Sud; la *Main Sulfide Zone* du Great Dyke au Zimbabwe; le *J-M Reef* du Complexe du Stillwater aux États-Unis) et des gisements de

sulfures magmatiques associés aux coulées basaltiques de la région de Noril'sk en Russie (Naldrett, 2004 et références citées; Fig. 1.1b).

Les gisements de Pd du Lac des Iles (Roby, Offset, Twilight et High-grade zones) présentent des aspects bien différents de la plupart des autres gisements de Pd. Contrairement aux *reefs* des larges intrusions litées, les gisements du Lac des Iles sont contenus dans une intrusion ayant une faible superficie en surface (1,5 km x 3 km). Les zones minéralisées du Lac des Iles (~ 900 m x 700 m) sont présentes au sein de l'intrusion et s'étendent en profondeur. En revanche, tous les *reefs* (sauf le *Platreef*) sont des zones stratiformes étroites (1 à 3 m d'épaisseur). Le Platreef est plus large, mais à l'inverse des gisements du Lac des Iles, il est localisé à la marge du Complexe du Bushveld. Les roches des zones minéralisées du Lac des Iles sont caractérisées par des textures ignées complexes (e.g., brèches magmatiques, pegmatites …), des degrés d'altération variables, et une faible proportion de sulfures (0,1 à 3 %) qui sont finement disséminés. La minéralisation, qui est constituée de sulfures de métaux de base (i.e., pyrrhotite, pentlandite et chalcopyrite) et de minéraux du groupe du platine (MGP), est caractérisée par un fractionnement du Pd par rapport aux EGP plus importants que dans les autres gisements (Barnes et Gomwe, 2011 et références citées) qui ont généralement des ratios similaires aux magmas dérivés du manteau.

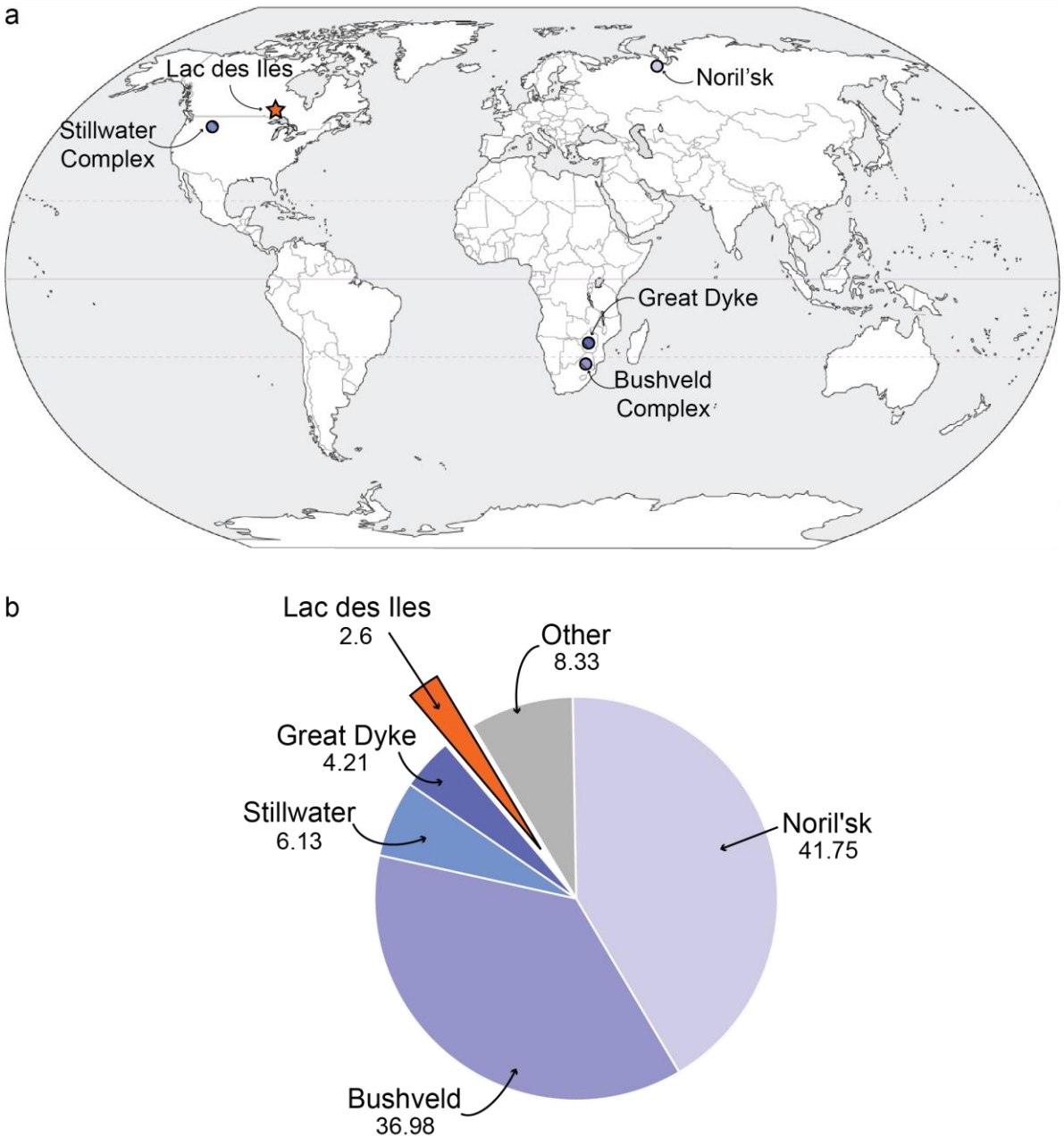

Figure 1.1 (a) Carte de localisation des principaux gisements producteurs de Pd à travers le monde; (b) Proportions (%) de la production mondiale de Pd en 2012 (Données issues de Johnson Matthey, Platinum 2013).

Depuis la découverte du Lac des Iles dans les années 1960 et la mise en opération de la mine en 1993, l'origine de la minéralisation en Pd a suscité une véritable controverse qui est encore d'actualité. Les caractéristiques inhabituelles mentionnées précédemment ont alimenté le débat et de nombreux auteurs ont suggéré que les fluides avaient contribué à la formation de la minéralisation. S'il est désormais admit que dans certaines zones minéralisées (High-grade Zone) les fluides ont contribué à un enrichissement subséquent de la minéralisation (Hinchey et Hattori, 2005; Gomwe, 2008; Barnes et Gomwe, 2011; Djon et Barnes, 2012), l'origine de la minéralisation dans les zones principales (Roby et Offset) est toujours controversée.

Des modèles hydrothermaux suggèrent que les métaux ont été enrichis par la séparation d'un fluide aqueux immiscible contenant du Pd. La présence de MGP contenant Te, As et Bi, spatialement associés avec des minéraux secondaires (e.g., chlorite, actinolite et pyrite) a été interprétée comme l'évidence d'un contrôle hydrothermal (Watkinson et Dunning, 1979; Talkington et Watkinson, 1984; Macdonald, 1988; Watkinson et al., 2002). Brügmann et al. (1989) ont proposé que la minéralisation ait été formée par *constitutional zone refining.* Cela implique la formation par cristallisation fractitonnée de magmas riches en volatiles qui par la suite ont provoqué la fusion partielle de cumulats précédemment formés, libérant ainsi les EGP des sulfures dans un magma leucocratique. Lavigne et Michaud (2001) ont proposé que la minéralisation ait été formée par l'intrusion de liquides sulfurés dans la chambre partiellement cristallisée, entraînant ainsi l'exsolution d'un fluide aqueux et la redistribution des métaux par ce dernier. Les travaux de Hanley et Gladney

(2011) basés sur l'étude d'inclusions fluides dans les pegmatites montrent que des fluides salins riches en CO_2 et pauvres en H_2O contiennent des métaux. Ces fluides magmatiques précoces ont pu collecter et transporter les métaux pour former la minéralisation. Les travaux de Boudreau et al. (2014) et Schisa et al. (2014) basés respectivement sur l'évaluation quantitative des réactions d'altération et sur la géochimie des halogènes contenus dans l'apatite, suggèrent que la minéralisation ait été formée par le dégasage de fluides magmatiques puis modifiée par des fluides au faciès schiste vert qui ont lessivé le S, Cu, Pt et Au.

En revanche, Hinchey et al. (2005) ont proposé que la minéralisation ait été formée par la ségrégation de sulfures à partir de magmas leucocratiques précoces et l'incorporation de ces sulfures par des magmas mélanocratiques tardifs. Barnes et Gomwe (2011) ont proposé que la minéralisation ait été formée suite à la ségrégation de sulfures dans une chambre magmatique en profondeur et à l'accumulation de ces sulfures dans un piège structural situé entre les deux chambres. Une nouvelle injection de magma sous-saturé en S aurait partiellement fusionné les sulfures, enrichissant ainsi le magma en S, Cu et Pd. Le magma enrichit en Pd aurait alors été injecté dans la chambre du Lac des Iles et ségrégué des sulfures en se mélangeant avec le magma partiellement consolidé déjà en place.

Un élément qui n'a pas été considéré précédemment est la présence de lentilles riches en sulfures. La découverte de ces lentilles ajoute une nouvelle dimension au débat en cours. Cette thèse de doctorat aborde la problématique de l'origine de ces lentilles de sulfures. Notre étude est basée sur un échantillonnage détaillé et une investigation rigoureuse des

lentilles riches en sulfures. Nous proposons un modèle pétrogénétique pour expliquer l'origine des lentilles de sulfures et nous considérons les processus qui ont influencé la minéralogie, la pétrographie et la géochimie.

1.3 PROBLÉMATIQUE

Historiquement, la minéralisation des gisements de Pd du Lac des Iles a été caractérisée comme pauvre en sulfures. De par leur importante concentration en sulfures, les lentilles ne correspondent pas à cette caractérisation et constituent un nouvel axe de recherche. L'origine de ces lentilles riches en sulfures et leur lien potentiel avec la minéralisation n'ont pas été considéré dans les études antérieures. Dans le cadre du débat concernant l'origine de la minéralisation à Lac des Iles, il est important de considérer les origines possibles des lentilles riches en sulfures. L'objet de ce travail de recherche est de s'interroger sur l'origine de ces lentilles de sulfures et d'étudier les processus qui les ont affectés afin de pouvoir retracer leur évolution. Il sera alors possible d'établir les éventuelles relations des lentilles riches en sulfures avec la minéralisation disséminée. Cela permettra d'améliorer nos connaissances sur les gisements du Lac des Iles.

1.3.1 HYPOTHÈSES

D’après les différents modèles proposés pour l’origine de la minéralisation à Lac des Iles, plusieurs hypothèses peuvent être envisagées pour expliquer l’origine des lentilles riches en sulfures. Les lentilles riches en sulfures pourraient être soit d’origine magmatique (cristallisées à partir de liquides sulfurés; Fig. 1.2a), soit d’origine hydrothermale (précipitées à partir de fluides; Fig. 1.2b).

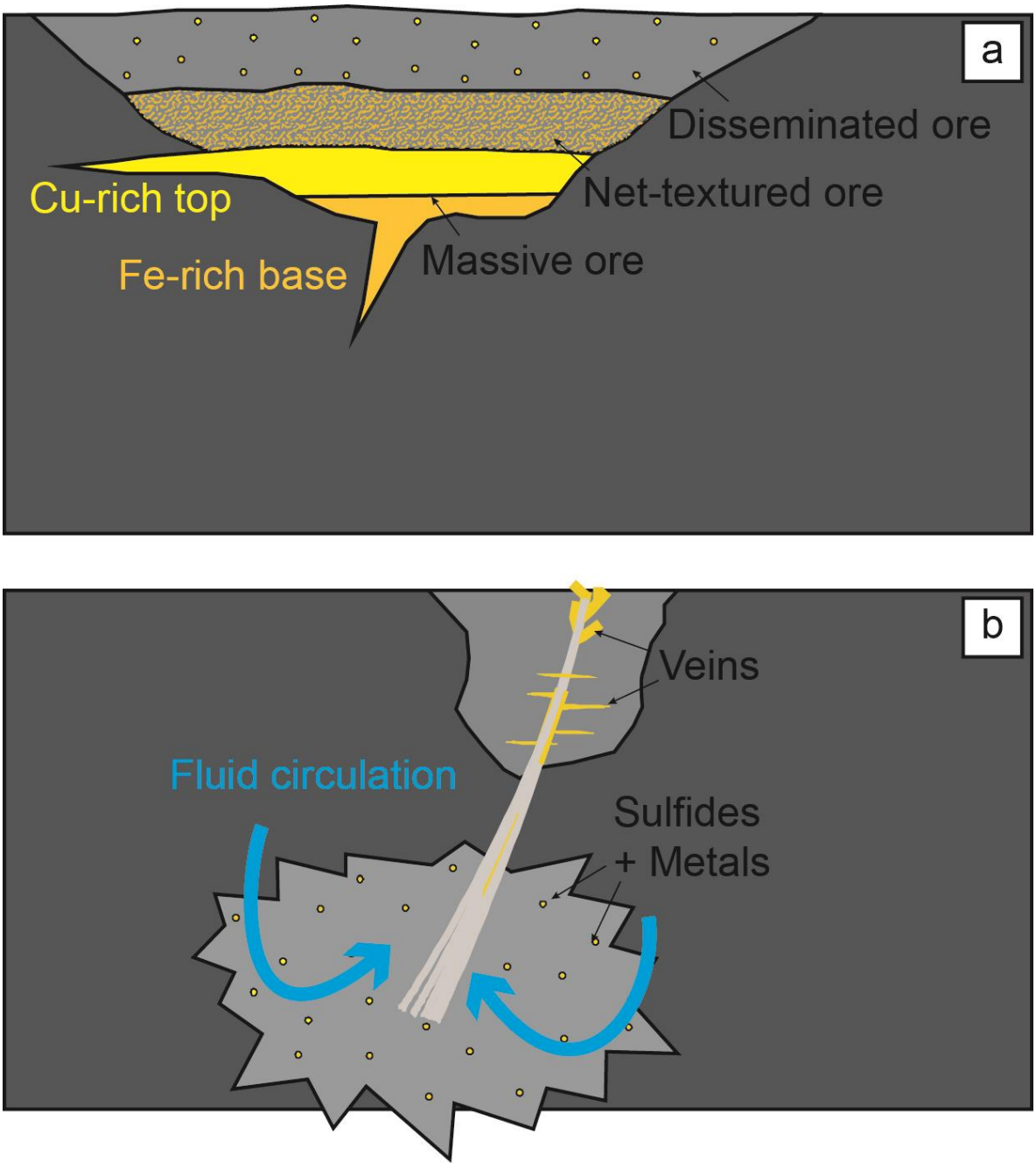

Figure 1.2 Représentation shcématique des possibles origines des lentilles de sulfures: (a) magmatique;(b) hydrothermale.

Des observations préliminaires ont montré que les lentilles de sulfures étaient réparties au travers de l'intrusion. Si l'intrusion a été déformée au cours de sa mise en place et de sa cristallisation, la position des lentilles au sein de l'intrusion pourrait être expliquée par la migration de liquides sulfurés dans des zones de dilatation. Si l'intrusion a été déformée après sa mise en place et sa cristallisation, la position des lentilles pourrait être expliquée soit par la tectonique (écoulement ductile et plasitque), le métamorphisme (anatexie des sulfures), ou l'hydrothermalisme (précipitations des sulfures), qui auraient permis la mise en place des sulfures le long de zones de cisaillement ou de failles. Par ailleurs, un grand nombre des échantillons collectés présente un contenu en pyrite significatif. La présence de pyrite pourrait alors indiquer que les sulfures ont été altérés s'ils sont d'origine magmatique, ou que les sulfures ont précipité à partir de fluides magmatiques/hydrothermaux.

Avant de présenter nos objectifs pour tester ces hypothèses, il est nécessaire de présenter aux lecteurs intéressés l'état des connaissances actuel relatif à la formation de gisements d'EGP associés à des sulfures. Les concepts fondamentaux en matière de géochimie du Pd, ségrégation de liquide sulfurés, dépôt des sulfures dans la croûte, processus d'enrichissement des liquides sulfurés, cristallisation fractionnée des liquides sulfurés, organisation des sulfures, solubilité et spéciation des EGP dans les fluides, et précipitation de sulfures à partir de fluides, sont définis afin que les lecteurs potentiels puissent être familiés avec le contenu de la thèse.

1.3.2 CONCEPTS FONDAMENTAUX

1.3.2.1 GÉOCHIMIE DU PALLADIUM

D'après Goldschmidt (1937), le Pd et autres EGP sont des éléments au comportement sidérophile dans les conditions du système solaire. Le Pd incorpore donc préférentiellement des alliages de Fe-Ni, entraînant alors son appauvrissement dans le manteau lors de la formation du noyau. Par conséquence, les EGP sont présents en faibles proportions dans le manteau (Lorand et Allard, 2001). Mitchell et Keays (1981) ont déterminé que dans le manteau, les EGP sont accommodés par des phases sulfurées et que la concentration moyenne en Pd y est d'environ 4 ppb.

Au cours de la fusion partielle du manteau, les phases sulfurées contenant les EGP se dissolvent dans le magma. Keays (1995) a calculé qu'approximativement 25% de fusion partielle été requit pour que le magma nouvellement formé puisse absorber tous les sulfures disponibles dans le manteau. Un taux élevé de fusion partielle est donc nécessaire pour dissoudre les sulfures dans le magma nouvellement formé et augmenter sa concentration en Pd (Barnes et Lightfood, 2005). Barnes et al. (1985) ont montré que le fractionnement des EGP au cours de la fusion partielle du manteau se faisait par ordre décroissant de point de fusion, témoignant de différence de solubilité entre les éléments. Ainsi il est possible de répartir les EGP en deux sous-groupes en fonction de leur comportement : les EGP du groupe de l'Ir (EGPI) qui sont compatibles, et les EGP du groupe du Pd (EGPP) qui sont

incompatibles. La différence de comportement entre les EGPI et les EGPP entraîne alors le fractionnement des EGP pendant la fusion partielle du manteau (Barnes et al., 1985 ; Bockrath et al., 2004). Borisov et al. (1994) ont démontré que la solubilité du Pd dans le magma silicaté était de l'ordre de la centaine de ppb.

Borisov et al. (1994) ont également démontré que dans les conditions de fugacité d'O et de température du manteau, la forme prédominante du Pd dans le magma était ionique et non pas métallique. Ringwood (1955) a mis en évidence le rôle de l'électronégativité des éléments lors de leur distribution durant la cristallisation magmatique. Il suggère qu'un cation de plus faible électronégativité se combinera préférentiellement à un anion. Ainsi dans des milieux riches en O tels que ceux du manteau et de la croûte, les cations faiblement électronégatifs se combinent en priorité à O^{2-}. Par conséquence, les éléments hautement électronégatifs tel que le Pd (2,2) possèdent une forte tendance à créer des liaisons covalentes avec le S, l'anion le plus disponible après l'O. Sous des conditions crustales, le Pd devient alors chalcophile et c'est la raison pour laquelle il se trouve dans les sulfures plutôt que dans les silicates ou les oxydes (Barnes et Maier, 1999). Cela se manifeste par le coefficient de partage élevé du Pd entre les sulfures et le magma silicaté (Barnes et Lightfood, 2005).

1.3.2.2 SATURATION EN SOUFRE DU MAGMA

Les sulfures magmatiques cristallisent à partir de liquide sulfurés qui se forment lorsqu'un magma silicaté issu de la fusion partielle du manteau devient sursaturé en soufre (S) (Haughton et al., 1974). Les magmas issus de la fusion partielle du manteau sont généralement sous-saturés en S (Mavrogenes et O'Neill, 1999 ; Keays, 1995). Par conséquence, le magma doit atteindre la saturation en S au cours de son évolution afin qu'un liquide sulfuré immiscible puisse se former. Pour se faire, soit le magma contient initialement du S et un changement de certains paramètres physiques peut entraîner la sursaturation, soit le magma doit subir un apport de S.

Dans le premier cas, les travaux expérimentaux de Wallace et Carmichael (1992) et Mavrogenes et O'Neill (1999) ont montré que la diminution de la température ainsi que de la fugacité du S, et l'augmentation de la pression ainsi que de la fugacité d'oxygène (O), abaissent la solubilité du S dans le magma et permettent sa sursaturation sans apport de S supplémentaire. Haughton et al. (1974) et Liu et al. (2007) suggèrent également que la variation de la composition initiale du magma peut influencer la solubilité du S, notamment l'influence du Fe sur les fugacités d'O et de S. Par exemple, la cristallisation fractionnée ou une modification du taux de fusion peuvent engendrer des variations de composition du magma.

Dans le second cas, du S peut être apporté au magma par la contamination de l'encaissant lors de l'intrusion. Généralement les encaissants sédimentaires sont susceptibles de fournir

le S nécessaire pour atteindre le point de saturation dans le magma (Ripley et Li, 2003). Du S peut également être apporté par le mélange de magmas survenu à la suite de pulses successifs. L'origine du S peut alors être mise en évidence par le $\delta^{34}S$ et le rapport S/Se (Lesher et Burnham, 2001).

Cependant, dans des conditions oxydantes le S est beaucoup plus soluble et les sulfures ne sont pas stables. En effet, les expériences de Jugo et al., (2005) ont montré qu'à plus basse fugacité d'O ce sont les sulfates qui sont stables. Comme les éléments chalcophiles tel que le Pd partitionne préférentiellement dans les phases sulfurées, des conditions suffisamment oxydantes dans lesquelles les sulfures ne sont pas stables, favoriserait l'incorporation de ces éléments dans le magma silicaté ainsi produit. De tels magmas pourraient alors dissoudre de grandes quantités de S et d'éléments chalcophiles qui par la suite seraient susceptibles d'incorporer des phases volatiles lors de leur exsolution du magma. Pokrovski et Dubrovinski (2011) ont montré que la forme chimique dominante du S dans des solutions aqueuses à plus de 250°C et 0,5 GPa était l'ion trisulfure (S^{3-}) qui est stable dans une large gamme de conditions géologiques.

1.3.2.3 DÉPÔT DES SULFURES DANS LA CROÛTE

Pour que les sulfures acquièrent un intérêt économique, il est indispensable qu'ils soient déposés à proximité de la surface afin d'être accessibles. Le magma étant moins dense que le liquide sulfuré, il est alors nécessaire que son transfert, du manteau vers la croûte, se

fasse au préalable de la saturation en S afin d'atténuer la perte des sulfures (Barnes et al., 1997). Le dépôt de sulfures dans la croûte dépend donc du *timing* de saturation en S du magma. Par conséquence, le transport vers la croûte doit se faire le plus rapidement possible (Maier, 2005), ce qui implique un flux dynamique. Les sutures crustales proéminentes jouent alors un rôle important en fournissant des zones de faiblesse par lesquelles l'ascension du magma s'effectue vers les roches supracrustales (Naldrett, 1999).

1.3.2.4 PROCESSUS D'ENRICHISSEMENT DES SULFURES EN MÉTAUX

Lors de l'ascention du magma dans la croûte et après sa saturation en S, les EGP sont collectés par les liquides sulfurés du fait de leurs coefficients de partage élevés. Cependant, le simple comportement chalcophile des EGP n'est pas suffisant pour que les sulfures soient enrichis de manière économique et un autre processus est requit. D'après Campbell et Naldrett (1979), pour que les EGP soient enrichis dans les sulfures, il est nécessaire qu'une faible quantité de liquide sulfuré interagisse avec de larges volumes de magma initialement pourvu de métaux. Cela implique alors un système extrêmement dynamique. Cette notion est illustrée par le R factor qui correspond au rapport entre le volume de magma silicaté et le volume de liquide sulfuré (Campbell et Naldrett, 1979).

Barnes et al. (1993) ont démontré que le rapport Cu/Pd changeait dans un magma au cours de la formation des sulfures du fait du coefficient de partage entre le magma et le liquide sulfuré plus élevé pour le Pd que pour le Cu. Ainsi un rapport Cu/Pd plus élevé que celui du

manteau primitif implique un retrait précoce des sulfures du magma, ou une rétention à la source avant que les sulfures n'aient pu collecter les EGP. À l'inverse un rapport plus faible indique une interaction plus longue entre le liquide sulfuré et le magma, susceptible de concentrer les EGP.

1.3.2.5 CRISTALLISATION FRACTIONNÉE DES LIQUIDES SULFURÉS

Les travaux expérimentaux de Kullerud et al. (1969), Cabri (1973), Kelly et Vaughan (1983), Fleet et al. (1993), et Li et al. (1996) ont permis de mettre en évidence plusieurs phases lors de la cristallisation des sulfures, et sont résumés dans Barnes et al. (2006).

A 1200°C, les éléments chalcophiles sont dissous dans les gouttelettes de liquide sulfuré qui ont ségrégué du magma silicaté à l'origine des roches mafiques et ultramafiques. Le liquide sulfuré peut également contenir en solution des quantités d'O significatives (Kress et al., 2008; Fonseca et al. 2008). Au cours du refroidissement, à environ 1190°C, Fe, Ni, Co et les EGPI se concentrent dans la première phase qui cristallise, correspondant à une solution solide monosulfurée appelée *monosulfide solid solution* (MSS). Le Pt, Pd, Au, et les semi-métaux se concentrent dans un liquide résiduel riche en Cu, formé après la cristallisation de la MSS. A 900°C ce liquide résiduel cristallise et forme une seconde phase intermédiaire appelée *intermediate solid solution* (ISS). Cependant Pt, Pd, et Au sont incompatibles dans l'ISS et partitionnent dans un liquide immiscible enrichit en semi-métaux (Peregoedova et al., 2004; Helmy et al., 2007). Au cours de ce processus, de la

magnétite peut cristalliser à partir de l'O dissout et peut enregistrer l'évolution de la cristallisation fractionnée des sulfures (Dare et al., 2012).

A plus basse température, à partir de 650 °C, la MSS recristallise respectivement en pentlandite et pyrrhotite (Kullerud et al., 1969; Kelly et Vaughan, 1983) et l'ISS en chalcopyrite avec une faible composante de cubanite (Cabri, 1973). La cristallisation du liquide résiduel riche en semi-métaux peut former des MGP aux bords des sulfures et des silicates alentours.

1.3.2.6 ORGANISATION DES SULFURES

L'organisation des sulfures au sein d'un système magmatique dépend en partie des processus de cristallisation du liquide sulfuré, qui évoluent en fonction de la température. L'organisation des sulfures varie selon les différents types de gisements. Cependant, des mécanismes généraux sont admis et sont synthétisés dans Barnes et Lightfood (2005).

Les gouttelettes de liquide sulfuré, qui sont plus denses que le magma silicaté dans lequel elles sont en suspension, migrent par gravité vers la base de l'intrusion. Ainsi, leur accumulation dans des zones où la convection magmatique est faible, notamment dans des dépressions physiques ou des creux topographiques de l'encaissant, se traduit par la formation de lentilles de sulfures massifs. Au cours du refroidissement du système magmatique, les gouttelettes de liquide sulfuré peuvent se retrouver piégées, lors de leur

migration vers la base de l'intrusion, dans les interstices de cumulats de silicates qui cristallisent, formant ainsi des sulfures disséminés. Cependant, les cumulats de silicates sédimentent également vers la base de l'intrusion. De ce fait, le liquide sulfuré qui a migré à la base peut alors percoler au sein des cumulats au cours de leur compaction sous l'effet de la pression (Godel et al., 2007), formant aussi des sulfures disséminés. Selon l'environnement, calme ou dynamique, ces sulfures disséminés peuvent être respectivement stratiformes ou discordants (Maier, 2005). Dans certains cas, les cumulats de silicates peuvent migrer jusque dans les lentilles piégées à la base, formant alors une zone de sulfures matriciels.

La présence de sulfures massifs à la base des intrusions constitue des zones plus compétentes qui peuvent accommoder la déformation et donc fluer plastiquement. Thériault et Barnes (1998) et Duuring et al. (2007) ont montré que les sulfures massifs pouvaient se mettre en place par une remobilisation physique lors d'évènements tectoniques. Ainsi il est possible de rencontrer des lentilles de sulfures massifs dans des zones de faiblesse de l'intrusion, et non pas à sa base.

En général, les sulfures massifs ont des teneurs en métaux moins importantes que les sulfures disséminés associés. Barnes et Lightfood (2005) suggèrent que les sulfures disséminés représentent des gouttelettes de liquide sulfuré qui n'ont pas été excluent du magma, permettant ainsi des interactions plus importantes avec le magma (R factor plus élevé). Les sulfures massifs se remarquent par leurs faibles ratios Pd/Ir, traduisant la cristallisation fractionnée d'une phase de MSS, enrichie en EGPI. Ce mécanisme se produit

aux alentours de 1190°C, entraînant alors la formation d'un liquide sulfuré résiduel enrichit en Cu-Pt-Pd. Cependant ce liquide n'est pas complètement solidifié au dessus de 900°C. Ainsi il peut être dissocié des cumulats de MSS et s'échapper du magma silicaté qui à cristalliser complètement à 950°C. Dans certains cas, le liquide résiduel peut être injecté sous forme de veine dans l'encaissant.

1.3.2.7 SOLUBILITÉ ET SPÉCIATION DU PD DANS LES FLUIDES

Les processus de formation de fluides aqueux (liquide + vapeur) ainsi que les processus de spéciation des métaux dans ces fluides sont résumés dans la revue de Pokrovski et al. (2013). La formation et l'évolution de fluides au cours des processus magmatiques est gouverné par les propriétés des systèmes eau-sel-gas qui permettent l'exsolution de fluides à partir de magmas silicatés. En général, ces fluides sont essentiellement aqueux mais ils peuvent contenir d'importantes quantités de volatiles tels que CO_2, CH_4, HCl, H_2S, et SO_2 et des quantités significatives de sels tels que NaCl. Les connaissances générales en matière de géochimie des EGP dans ces phases aqueuses sont présentées dans les revues de Wood (2002) et Hanley (2005) et références citées. Dans les fluides aqueux, les métaux peuvent former des complexes avec le Cl et S. En l'absence de sulfures, les coefficients de partages des métaux entre fluides et magmas sont en faveur des fluides, permettant ainsi l'extraction des métaux initiallement présent dans les magmas vers les phases issues de l'exsolution des fluides (Pokrovski et al. 2013).

Dans les fluides magmatiques/hydrothermaux de haute température, des volatiles magmatiques riches en Cl peuvent être responsable de la concentration et de la redistribution des EGP (Boudreau, 2009; Hanley, 2005). Des travaux expérimentaux (Hanley et al., 2005) ont démontré la solubilité des EGP dans ces fluides, et la présence d'EGP dans des fluides naturels ont été observés (Hanley et al., 2008 ; Hanley et Gladney, 2011).

En revanche dans les fluides de plus basse température, la mobilisation du Pd sous forme de complexe avec le Cl est limitée et n'est significative que dans un contexte oxydant dépourvu de sulfures (Bazarnika et al., 2014). Dans la plupart des fluides hydrothermaux de basse à moyenne température, la concentration de complexes Pd-Cl est trop faible pour expliquer un enrichissement en Pd et la complexation avec l'ion bisulfure (Hanley, 2005) ou avec S^{3-} (Bazarnika et al., 2014) sont envisageables pour expliquer un quelconque enrichissement hydrothermal.

1.3.2.8 PRÉCIPITATION DE SULFURES À PARTIR DE FLUIDES

Les sulfures peuvent précipiter à partir de solutions hydrothermales lorsque les métaux et les sulfures sont plus stables sous forme solide plutôt qu'en solution dans les fluides. Les processus de précipitation de sulfures à partir de fluides hydrothermaux ont été investigués par Reed et Palandri (2006). Deux processus majeurs ont été identifiés. Le premier processus consiste à la precipitation de sulfures où le S et les métaux dissous dans un même

fluide se combinent dû à un changement des conditions physico-chimiques. Par exemple, lors du refroidissement, les complexes métalliques peuvent être déstabilisés et les métaux deviennent disponibles pour se combiner avec le S. Si le refroidissement est suffisamment important, les sulfures peuvent précipiter dû à leur meilleure stabilité à plus basse température. L'augmentation du pH peut également entraîner la précipitation de sulfures en libérant le S de H_2S ou HS^-. Alternativement, la réduction de sulfate dissous dans les fluides peut entraîner la précipitation de sulfures. Le second processus consiste à la précipitation de sulfures où les métaux dissous dans un fluide sont combiné au S provenant d'une source différente.

1.3.3 OBJECTIFS

Cette étude se concentre sur les lentilles riches en sulfures du Lac des Iles. Les principaux objectifs sont:

- Identifier et caractériser les lentilles riches en sulfures.
- Déterminer le processus de mise en place des lentilles
- Proposer un modèle génétique
- Déterminer la distribution des éléments chalcophiles et des EGP entre les différents minéraux
- Évaluer l'influence de certains paramètres sur les signatures géochimiques tel que:
    - Magma parent

- Processus de formation des minéraux
- Deformation et altération

- Comparer les signatures géochimiques avec celles de sulfures provenant d'autres gisements de Ni-Cu-EGP.
- Proposer des recommandations susceptibles d'être utile en exploration.

1.3.4 MÉTHODOLOGIE

Le détail des procédures analytiques est fourni dans les sections décrivant la méthodologie dans chaque article. La partie qui suit met en évidence les relations entre les méthodes d'analyses et les différents objectifs spécifiques.

1.3.4.1 TRAVAIL DE TERRAIN

Le travail de terrain a permis de collecter des échantillons représentatifs des lentilles riches en sulfures nécessaires aux analyses. La majorité du travail de terrain a été effectuée durant l'été 2011. Des informations complémentaires ont été recueillies au cours d'emplois saisonniers durant l'été 2012 et l'automne 2013. La plupart des échantillons a été collectée dans la carrothèque de la mine et certains ont été échantillonnés dans la fosse à ciel ouvert et sur des affleurements. De plus les échantillons ont pu être géolocalisés et étudiés en contexte. Ces données permettent de déterminer le processus de mise en place des lentilles.

1.3.4.2 ANALYSE PETROGRAPHIQUE

L'analyse pétrographique a permis d'identifier les assemblages minéralogiques et d'estimer les proportions de chaque espèce minérale. Ces données permettent de déterminer les relations texturales des roches en cherchant, par exemple, les évidences d'exsolution, de déformation, de recristallisation et d'altération. Ces informations sont nécessaires pour interpréter la nature des lentilles riches en sulfures.

1.3.4.3 GÉOCHIMIE

Les compositions en éléments majeurs et traces en roche totale et *in situ* ont permis de caractériser la signature géochimique des lentilles de sulfures et de chaque espèce minérale. De plus, un calcul de bilan de masse ainsi que des cartographies élémentaires de certains minéraux ont été réalisés pour mettre en évidence la distribution des éléments. L'ensemble de ces données est indispensable pour retracer l'évolution des lentilles riches en sulfures.

1.3.4.4 ISOTOPES DU SOUFRE

Déterminer les ratios d'isotopes du soufre ($\delta^{34}S$) sur des échantillons de roche totale permet d'estimer si du S a été ajouté ou remobilisé des sulfures. Ces analyses permettent d'étudier la nature des sulfures et l'impact de l'altération.

1.4 ZONE D'ÉTUDE

Les détails relatifs à la géologie de la zone d'étude sont fournis dans chaque article, ce qui implique qu'une description du contexte géologique sera répétée dans les différents chapitres. Néanmoins, chacun mettra l'emphase sur les particularités propres à leur problématique spécifique. Cette section décrit seulement les caractéristiques majeures de la zone d'étude.

1.4.1 CONTEXTE GÉOLOGIQUE RÉGIONAL

Le complexe intrusif du Lac des Iles se situe environ à 80 km au nord de la ville de Thunder Bay (Ontario, Canada) et fait partie de la province archéenne du Supérieur (Fig. 1.3). La province du Supérieur est interprétée comme l'association de fragments continentaux, océaniques et d'arcs, méso à néo-archéen (Card, 1990). La détermination des âges isotopiques (Brügmann et al., 1997 ; Stone et al., 2003 ; Tomlison et al., 2004) montre

que les roches plutoniques et volcaniques de la province du Supérieur se sont formées entre 3,1 Ga et 2,6 Ga. Au cours de cette période, les épisodes magmatiques tholéiitiques, calco-alcalins, komatiitiques, et alcalins sont courants et associés à la mise en place de sédiments chimiques et à clastes volcanogèniques. Les épisodes magmatiques précoces ont été accompagnés et succédés par de la déformation régionale et des évènements métamorphiques, liés à plusieurs orogènes successifs. Cependant, les effets de ces épisodes précoces ont largement été atténués par la déformation polyphasée, le métamorphisme régional et le plutonisme répandu, associés à l'orogène Kenoran (Card, 1990).

Plus précisément, le complexe intrusif du Lac des Iles est localisé dans la sous-province de Wabigoon. La sous-province de Wabigoon est essentiellement constituée de granitoïdes et de ceintures de roches vertes (Pye, 1968 ; Sutcliffe, 1989). Les roches de la sous-province de Wabigoon se sont formées lors de plusieurs épisodes magmatiques (Sutcliffe, 1989 ; Brügmann et al., 1997 ; Tomlinson et al., 2004). La zone du Lac des Iles se trouve à proximité de la limite avec la sous-province de Quetico, le long de laquelle les intrusions mafiques et ultramafiques sont communes. La sous-province de Quetico, essentiellement composée de séries métavolcaniques et métasédimentaires, est interprétée comme une partie d'un prisme d'accrétion formé lors de la subduction de lithosphère océanique sous la sous-province de Wabigoon (Percival et Williams, 1989).

Le complexe intrusif du Lac des Iles, s'est mis en place dans les gneiss tonalitiques foliés (Brügmannn et al., 1997) à 2689 ± 1 Ma (Stone et al., 2003). Il constitue la suite la plus large d'une série mafique/ultramafique, également composée des intrusions Legris Lake,

Demars-Wakinoo Lake, Buck Lake et Tib Lake, définissant une structure circulaire d'environ 30 km de diamètre.

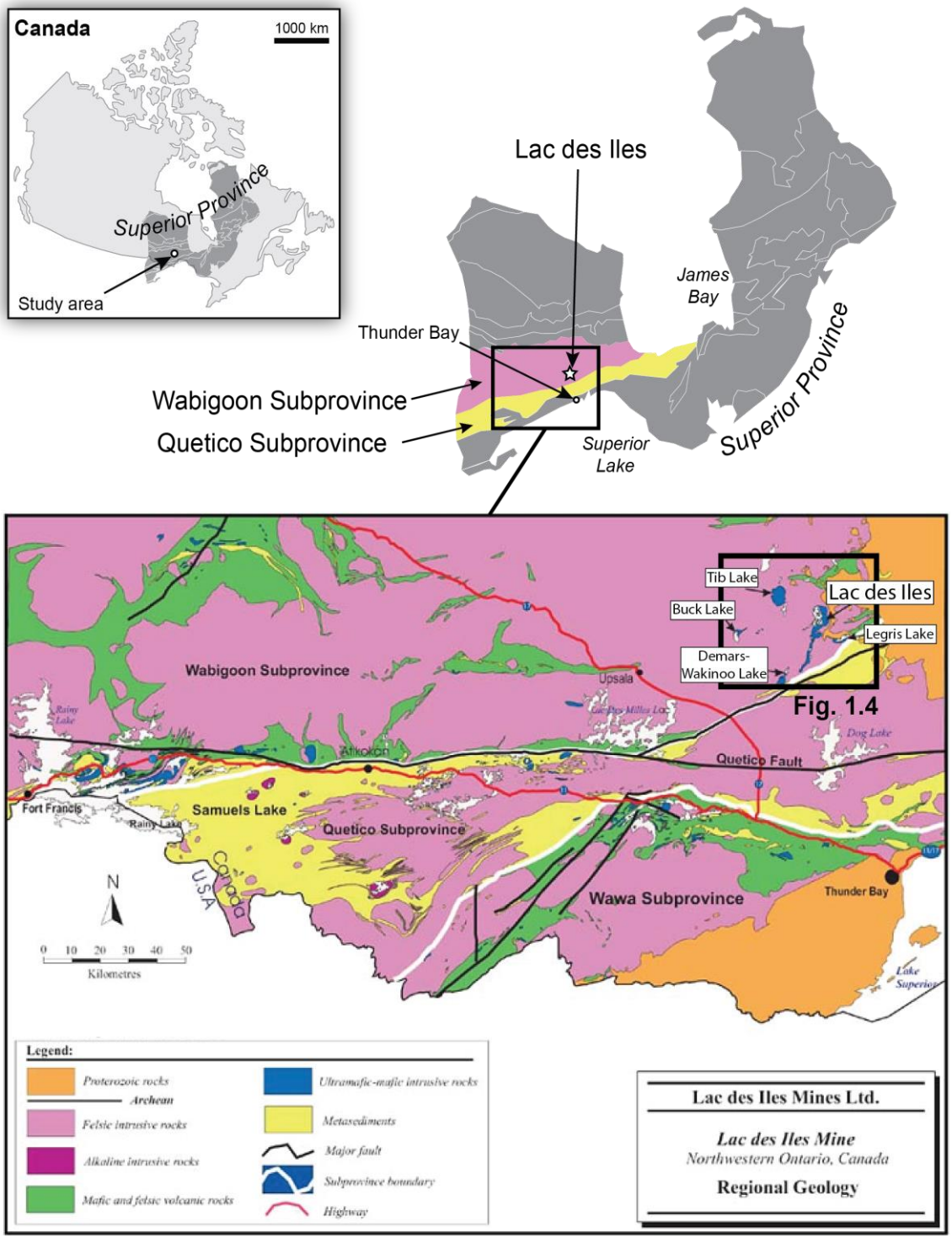

Figure 1.3 Carte géologique régionale (Modifié d'après Lavigne et al,. 2002)

1.4.2 CONTEXTE GÉOLOGIQUE LOCAL

Le complexe intrusif du Lac des Iles est composé de 3 intrusions (Fig. 1.4): la *North Lac-des-Iles Intrusion*, la *Mine Block Intrusion*, et la *Camp Lake Intrusion* (Lavigne et Michaud, 2001), qui sont séparées par leur encaissant tonalitique. La *North Lac-des-Iles Intrusion*, située au Nord du complexe, forme une intrusion litée composée de clinopyroxènites, webstérites et gabbronorites. La *Camp Lake Intrusion*, située au Sud, présente une composition plus homogène constituée de gabbros à hornblende. La *Mine Block Intrusion* constitue l'intrusion centrale du complexe. C'est dans cette intrusion que se trouvent les zones minéralisées (Roby, Offset, Twilight et High-grade). La *Mine Block Intrusion* est composée d'une gamme de roche allant des anorthosites jusqu'aux mélanonorites. Cependant la plupart des roches sont des métanorites/métagabbronorites. Ces roches présentent des textures extrêmenent variables (textures variées, pegmatites, brêches magmatiques) et les différentes unités lithologiques forment une stratigraphie concentrique.

Brügmann et al. (1997) ont noté que le contexte géologique du Lac des Iles, mis en place dans les granitoides situés juste au nord du prisme d'accrétion de Quetico, suggère la base d'un arc continental comme contexte tectonique. Les estimations du liquide initial de la *Mine Block Intrusion* établit par Barnes et Gomwe (2010) supportent cette interpétation et montrent que le magma parent du Lac des Iles est similaire aux andésites modernes. En revanche Hinchey et al. (2005) ont suggéré que le magma parent du Lac des Iles était de type E-MORB, ce qui requiert un contexte océanique d'île en arc.

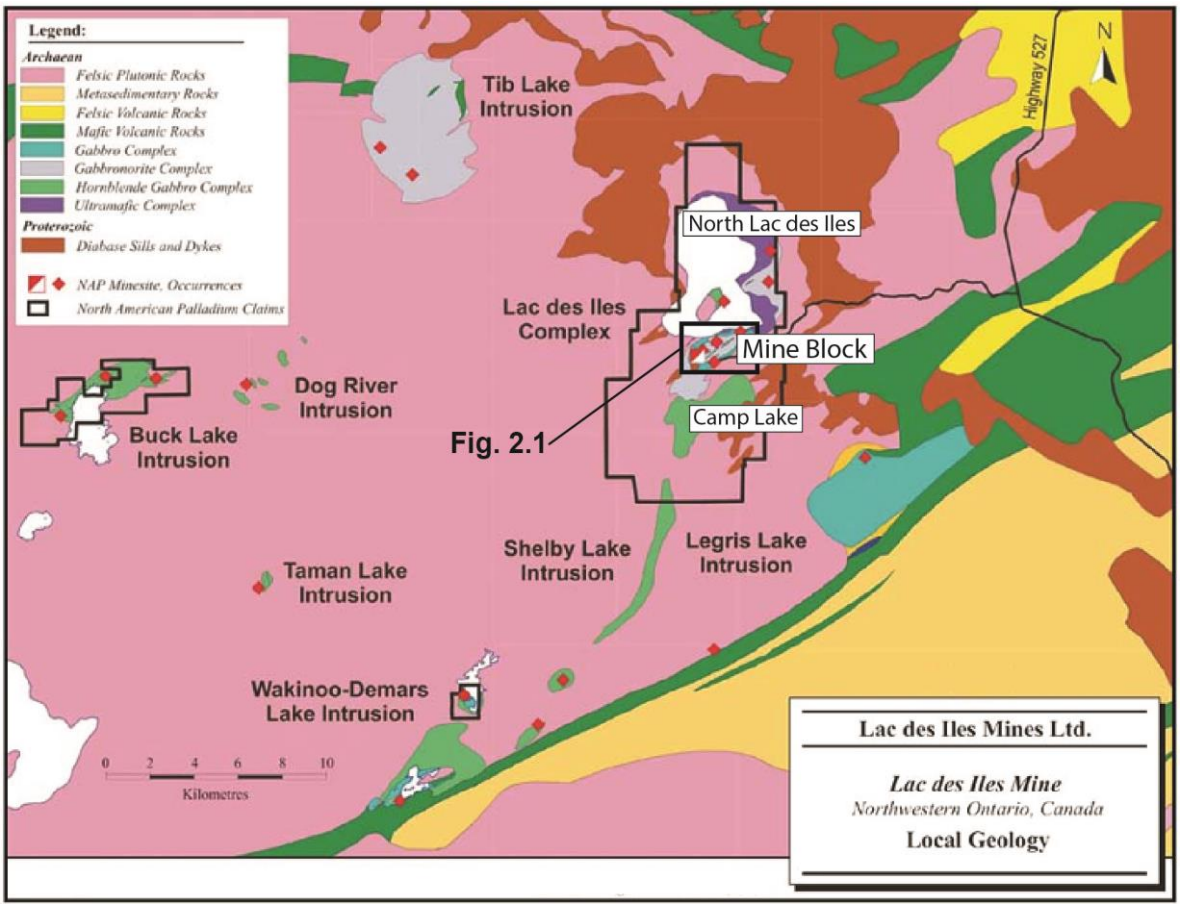

Figure 1.4 Carte géologique locale (D'après Lavigne et Michaud, 2001)

1.5 FORMAT DE LA THÈSE

Cette thèse de doctorat en Sciences de la Terre et de l'Atmosphère est présentée sous la forme d'un recueil de publications scientifiques et s'organise en cinq chapitres. Le premier chapitre (ci-présent) est une introduction qui place cette étude dans un contexte scientifique général. Les trois chapitres suivants correspondent à des manuscrits soumis dans des journaux spécialisés. Pour cette raison, ces chapitres ont été rédigés en anglais. Le premier manuscrit, intitulé *Geology, petrography and geochemistry of sulfide-rich pods from the Lac des Iles Pd deposits (Western Ontario, Canada) and a model for their genesis,* a été soumit à la revue *Mineralium Deposita*. Le deuxième manuscrit, intitulé *Chalcophile and platinum-group element distribution among primary sulfides and Fe-Ti oxides of the sulfide-rich pods from the Lac des Iles Pd deposits (Western Ontario, Canada): Constraints on processes controlling the composition of the ore,* a été soumit à la revue *Mineralogical Magazine*. Le troisième manuscrit, intitulé *Chalcophile and platinum-group element distribution in pyrites of the sulfide-rich pods from the Lac des Iles Pd deposits (Western Ontario, Canada): Implications for post-cumulus re-equilibration and the use of pyrite compositions for exploration,* a été soumit à la revue *Journal of Geochimical Exploration*. Enfin le dernier chapitre est une conclusion générale qui présente une synthèse de cette étude, ainsi que les retombées académiques et économiques. Chaque manuscrit a été soumit accompagné de matériel électronique supplémentaire. Ces données sont présentées dans les annexes ainsi que les résumés des affiches et présentations orales de conférences internationales.

1.6 DÉCLARATION DE CONTRIBUTION ORIGINALE

Cette thèse de doctorat est la première étude des lentilles de sulfures du Lac des Iles à ce jour. Les données présentées dans les trois manuscrits ont été collectées sur le terrain et en laboratoire dans le cadre de cette étude. Chaque manuscrit a été soumit aux revues spécialisées pour publication originale. Le format de recueil de manuscrits présente des redondances inévitables, notamment concernant le contexte géologique et la méthodologie. Au meilleur de notre connaissance, aucune autre étude n'a investigué les lentilles de sulfures du Lac des Iles.

1.7 CONTRIBUTION DES COLLABORATEURS

L'auteur de cette thèse est l'auteur principal des trois manuscrits soumis. Le premier auteur a échantillonné les roches sur le terrain, préparé les échantillons et effectué les analyses en laboratoire. Pour chaque manuscrit, l'auteur principal est responsable de la collecte et de l'interprétation des données, de la production des figures et de la rédaction de l'article. La deuxième auteure, Sarah-Jane Barnes, est responsable de la planification et de la supervision de l'étude dans son ensemble, ainsi que de la révision et de l'amélioration du manuscrit avant soumission. Le troisième auteur, John Corkery, a permis l'accès aux

échantillons et leur géolocalisation, et a contribué à la révision et à l'amélioration du manuscrit avant soumission.

1.8 RÉFÉRENCES

Barnes, S-J., Naldrett, A.J., Gorton, M.P., (1985) The origin of fractionation of platinum-group elements in terrestrial magmas. Chemical Geology, 53, 303-323.

Barnes, S-J., Zientek, M.L., Severson, M.J., (1997) Ni, Cu, Au, and platinum-group element contents of sulphides associated with intraplate magmatism: a synthesis. Canadian Journal of Earth Sciences, 34, 337-351.

Barnes, S-J., Maier, W.D., (1999) The fractionation of Ni, Cu and the noble metals in silicate and sulfide liquids. In Dynamic Processes in Magmatic Ore Deposits and their application in mineral exploration. Edited by Keays, R.R., Lesher, C.M., Lightfoot, P.C., Farrow, C.E.G. Geological Association of Canada, Short Course, 13, 69-106.

Barnes, S-J., Lightfoot, P.C., (2005) Formation of magmatic nickel-sulfide ore deposits and processes affecting their copper and Platinum-Group Element contents. Economic Geology, 100th Anniversary Volume, 179-213.

Barnes, S-J., Cox, R.A., Zientek, M.L., (2006) Platinum-group element, gold, silver and base metal distribution in compositionally zoned sulfide droplets from the Medvezky Creek Mine, Noril'sk, Russia. Contributions to Mineralogy and Petrology, 152, 187-200.

Barnes, S-J., Gomwe, T.S., (2010) Composition of the Lac des Iles magma and implications for the origin of the ore. In: 11th international platinum symposium, program abstracts, Ontario Geological Survey, miscellaneous release-data 269 (abstract).

Barnes, S-J., Gomwe, T.S., (2011) The Pd Deposits of the Lac des Iles Complex, Northwestern Ontario. Reviews in Economic Geology, 17, 351-370.

Bazarkina, E.F., Pokrovski, G.S., Hazemann, J-L., (2014) Structure, stability and geochemical role of palladium chloride complexes in hydrothermal fluids. Geochimica et Cosmochimica Acta, 146, 107-131.

Bockrath, C., Ballhaus, C., Holzheid, A., (2004) Fractionation of the platinum-group elements during mantle melting. Science, 305, 1951-1953.

Borisov, A., Palme, H., Spettel, B., (1994) Solubility of palladium in silicate melts: Implications for core formation in the Earth. Geochimica et Cosmochimica Acta, 58, 705-716.

Boudreau, A.E., (2009) Transport of the platinum-group elements by igneous fluids in layered intrusions. In: New Developments in Magmatic Ni–Cu and PGE Deposits (eds. C. Li and E.M. Ripley). Geological Publishing House, Beijing, pp. 229-249.

Boudreau, A., Djon, L., Tchalikian, A., Corkery, J., (2014) The Lac des Iles palladium deposit, Ontario, Canada. Part I. The effect of variable alteration on the Offset Zone. Mineralium Deposita, 49, 625-654.

Brügmann, G.E., Naldrett, A.J., Macdonald, A.J., (1989) Magma mixing and constitutional zone-refining in the Lac-des-Iles complex, Ontario - Genesis of Platinum-Group Element mineralization. Economic Geology, 84, 1557-1573.

Brügmann, G.E., Reischrnann, T., Naldrett, A.J., Sutcliffe, R.H., (1997) Roots of an Archean volcanic arc complex; the Lac des Iles area in Ontario, Canada. Precambrian Research, 81, 223-239.

Cabri, L., (1973) New data on phase relations in Cu–Fe–S system. Economic Geology, 68, 443-454.

Campbell, I.H., Naldrett, A.J., (1979) The influence of silicate: sulfide ratios on the geochemistry of magmatic sulfides. Economic Geology, 74, 1530-1505.

Card, K.D., (1990) A review of the Superior Province of the Canadian Shield, a product of Archean accretion. Precambrian Research, 48, 99-156.

Dare, S.A.S., Barnes, S-J., Beaudoin, G., (2012) Variation in trace element content of magnetite crystallized from a fractionating sulfide liquid, Sudbury, Canada: Implications for provenance discrimination. Geochimica and Cosmochimica Acta, 88, 27-50.

Djon, M.L.N., Barnes, S-J., (2012) Changes in sulphides and platinum-group minerals with the degree of alteration in the Roby, Twilight, and High Grade Zones of the Lac des Iles Complex, Ontario, Canada. Mineralium Deposita, 47, 875-896.

Duuring, P., Bleeker, W., Beresford, S.W., (2007) Structural modification of the komatiite-associated Harmony nickel sulfide deposit, Leinster, Western Australia. Economic Geology, 102, 277-297.

Fleet, M.E., Chryssoulis, S.L., Stone, W.E., Weisener, C.G., (1993) Partitioning of platinum-group elements and Au in the Fe - Ni - Cu - S system: experiments on the fractional crystallization of sulfide melt. Contributions to Mineralogy and Petrology, 115, 36-44.

Fonseca, R.O.C., Campbell, A.H., O'Neill, H.S.C., Fitzgerald, J.D., (2008) Oxygen solubility and speciation in sulphide-rich mattes. Geochimica and Cosmochimica Acta, 72, 2619-2635.

Godel, B., Barnes, S-J., Maier, W.D., (2007) Platinum-group elements in sulphide minerals, platinum-group minerals, and whole-rocks of the Merensky Reef (Bushveld Complex, South Africa): Implications for the formation of the reef. Journal of Petrology, 48, 1569-1604.

Goldschmidt, V.M., (1937) The principles of distribution of chemical elements in minerals and rocks. Journal of Chemical Society, 655-673.

Gomwe, T.S., (2008) The formation of the palladium-rich Roby, Twilight and High-Grade zones of the Lac des Iles complex. PhD Thesis, Université du Québec à Chicoutimi, 296 pp.

Hanley, J.J., (2005) The aqueous geochemistry of the platinum-group elements (PGE) in surficial, low-T hydrothermal and high-T magmatic-hydrothermal environments. In: Exploration for Platinum-Group Element Deposits, vol. 35 (ed. J.E. Mungall), pp. 35-56. Short Course Series. Mineralogical Association of Canada, Ottawa.

Hanley, J.J., Pettke, T., Mungall, J.E., Spooner, E.T.C., (2005) The solubility of platinum and gold in NaCl brines at 1.5 kbar, 600 to 800ºC: A laser ablation ICP-MS pilot study of synthetic fluid inclusions. Geochimica et Cosmochimica Acta, 69, 2593-2611.

Hanley, J.J., Mungall, J.E., Pettke, T., Spooner, E.T.C., Bray, C.J., (2008) Fluid and halide melt inclusions of magmatic origin in the ultramafic and lower banded series, Stillwater Complex, Montana, USA. Journal of Petrology,49, 1133-1160.

Hanley, J.J., Gladney, E.R., (2011) The presence of carbonic-dominant volatiles during the crystallization of sulfide-bearing mafic pegmatites in the North Roby Zone, Lac des Iles Complex, Ontario. Economic Geology, 106, 33-54.

Haughton, D.R., Roeder, P.L., Skinner, B.J., (1974) Solubility of sulfur in mafic magmas. Economic Geology, 69, 451-467.

Helmy, H.M., Ballhaus, C., Berndt, J., Bockrath C., Wohlgemuth-Ueberwasser, C., (2007) Formation of Pt, Pd and Ni tellurides: Experiments in sulfide-telluride systems. Contributions to Mineralogy and Petrology, 153, 577-591.

Hinchey, J.G., Hattori, K.H., Lavigne, M.J., (2005) Geology, petrology, and controls on PGE mineralization of the southern Roby and Twilight zones, Lac des Iles mine, Canada. Economic Geology, 100, 43-61.

Jugo, P.J., Luth, R.W., Richards, J.P., (2005) An experimental study of the sulfur content in basaltic melts saturated with immiscible sulfide or sulfate liquids at 1300°C and 1.0 GPa. Journal of Petrology, 46, 783-798.

Keays, R.R., (1995) The role of komatiitic and picritic magmatism and S-saturation in the formation of the ore deposits. Lithos, 34, 1-18.

Kelly, D.P., Vaughan, D.J., (1983) Pyrrhotine-pentlandite ore textures: a mechanistic approach. Mineralogical Magazine, 47, 453-463.

Kress, V., Greene, L.E., Ortiz, M.D., Mioduszewski, L., (2008) Thermochemistry of sulfide liquids IV: density measurements and the thermodynamics of O-S-Fe-Ni-Cu liquids a low to moderate pressures. Contribution to Mineralogy and Petrology, 156, 785-797.

Kullerud, G., Yund, R.A., Moh, G.H., (1969) Phase relations in the Cu–Fe–S, Cu–Ni–S and Fe–Ni–S systems. Economic Geology, 4, 323-343.

Lavigne, M.J., Michaud, M.J., (2001) Geology of North American Palladium Ltd.'s Roby zone deposit, Lac des Iles. Exploration and Mining Geology, 10, 1-17.

Lesher, C.M., et Burnham, O.M., (2001) Multicomponent elemental and isotopic mixing in Ni-Cu-(PGE) ores at Kambalda, Western Australia. The Canadian Mineralogist, 39, 421-446.

Li, C., Barnes, S-J., Makovicky, E., Rose-Hansen, J., Makovicky, M., (1996) Partitioning of Ni, Cu, Ir, Rh, Pt and Pd between monosulfide solid solution and sulfide liquid: effects of composition and temperature. Geochimica et Cosmochimica Acta, 60, 1231-1238.

Liu, Y., Samaha, N.T., Baker, D.R., (2007) Sulfur concentration at sulfide saturation (SCSS) in magmatic silicate melts. Geochimica et Cosmochimica Acta, 71, 1783-1799.

Lorand, J-P., Alard, O., (2001) Platinum-group element abundances in the upper mantle: New constraints from in situ and whole-rock analyses of Massif Central xenoliths (France). Geochimica et Cosmochimica Acta, 65, 2789-2806.

Macdonald, A.J., (1988) Platinum-group element mineralisation and the relative importance of magmatic and deuteric processes: field evidence from the Lac des Iles deposit, Ontario, Canada. In Geo-Platinum ’87. Edited by Prichard, H.M., Potts, P.J., Bowles, J.F.W., Cribb, S.J. Elsevier, London, 215-236.

Maier, W.D., (2005) Platinum-group element (PGE) deposits and occurrences: Mineralization styles, genetic concepts, and exploration criteria. Journal of African Earth Sciences, 41, 165-191.

Makovicky, M., Makovicky, E., Rose-Hansen, J., (1986) Experimental studies on the solubility and distribution of platinum group elements in base-metal sulphides in platinum deposits. In Metallogeny of basic and ultrabasic rocks. Edited by Gallagher, M., Ixer, R., Neary, C., Prichard, H. London, Inst. Mining Metallurgy, 415-425.

Mavrogenes, J.A., O'Neill, H.S.C., (1999) The relative effects of pressure, temperature and oxygen fugacity on the solubility of sulfide in mafic magmas. Geochimica et Cosmochimica Acta, 63, 1173-1180.

Mitchell, R.H., Keays, R.R., (1981) Abundance and distribution of gold, palladium and iridium in some spinel and garnet lherzolites: implications for the nature and origin of preciousmetal-rich intergranular components in the upper mantle. Geochimica et Cosmochimica Acta, 45, 2425-2442.

Naldrett, A.J., (1999) World-class Ni-Cu-PGE deposits: key factors in their genesis. Mineralium Deposita, 34, 227-240.

Naldrett, A.J., (2004) Magmatic sulfide deposits: geology, geochemistry and exploration. Springer, Berlin, 727 pp.

Peach, C.L., Mathez, E.A., Keays, R.R., (1990) Sulfide melt – silicate melt distribution coefficients for noble metals and other chalcophile elements as deduced from MORB: Implications for partial melting. Geochimica et Cosmochimica Acta, 54, 3379-3389.

Peregoedova, A., Barnes, S-J., Baker, D.R., (2004) The formation of Pt-Ir alloys and Cu-Pd-rich sulfide melts by partial desulfurization of Fe-Ni-Cu sulfides; results of experiments and implications for natural systems. Chemical Geology, 208, 247-264.

Percival, J.A., Williams, H.R., (1989) Late archean Quetico accretionary complex, Superior province, Canada. Geology, 17, 23-25.

Pokrovski, G.S., Dubrovinsky, L.S., (2011) The S^{3-} ion is stable in geological fluids at elevated temperatures and pressures. Science, 331, 1052-1054.

Pokrovski, G.S., Borisova, A.Y., Bychkov, A.Y., (2013) Speciation and transport of metals and metalloids in geological vapors. Reviews in Mineralogy and Geochemistry, 76, 165-218.

Pye, E.G., (1968) Geology of the Lac des Iles area, district of Thunder-Bay. Ontario. Department of Mines Geology Report, 64-47.

Reed, M.H., Palandri J., (2006) Sulfide mineral precipitation from hydrothermal fluids. Reviews in Mineralogy and Geochemistry, 61, 609-631.

Ringwood, A.E., (1955) The principles governing trace element distribution during magmatic crystallization; part I, The influence of electronegativity. Geochimica et Cosmochimica Acta, 7, 189-202.

Ripley, E.M., Li, C., (2003) Sulfur isotope exchange and metal enrichment in the formation of magmatic Cu-Ni-(PGE) deposits. Economic Geology, 98, 635-641.

Schisa, P., Boudreau, A., Djon, L., Tchalikian, A., Corkery, J., (2014) The Lac des Iles palladium deposit, Ontario, Canada. Part II. Halogen variations in apatite. Mineralium Deposita, doi10.1007/s00126-014-0541-4

Stone, D., Lavigne, M.J., Schnieders, B., Scott, J., Wagner, D., (2003) Regional geology of the Lac des Iles area. Summary of field work and other activities open file report 6120, Ontario Geological Survey.

Sutcliffe, R.H., (1989) Magma mixing in late Archean tonalitic and mafic rocks of the Lac des Iles area, Western Superior Province. Precambrian Research, 44, 81-101.

Talkington, R.W., Watkinson, D.H., (1984) Trends in the distribution of the precious metals in the Lac des Iles complex, Northwestern Ontario. The Canadian Mineralogist, 22, 125-136.

Thériault, R.D., et Barnes, S-J., (1998) Compositional variations in Cu-Ni-EGP sulfides of the Dunka Road deposit, Duluth complex, Minnesota: The importance of combined assimilation and magmatic processes. The Canadian Mineralogist, 36, 869-886.

Tomlinson, K.Y., Scott, G.M., Percival, J.A., Stone, D., (2004) Basement terrane correlations and crustal recycling in the western Superior Province: Nd isotopic character of granitoid and felsic volcanic rocks in the Wabigoon subprovince, N. Ontario, Canada. Precambrian Research, 132, 245-274.

Wallace, P., Carmichael, I.S.E., (1992) Sulfur in basaltic magmas. Geochimica et Cosmochimica Acta, 56, 1683-1874.

Watkinson, D.H., Dunning, G.R., (1979) Geology and platinum-group mineralization, Lac des Iles complex, Northwestern Ontario. The Canadian Mineralogist, 17, 453-462.

Watkinson, D.H., Lavigne, M.J., Fox, P.E., (2002) Magmatic-hydrothermal Cu and Pd-rich deposits in gabbroic rocks from North America. In: Cabri L.J. (ed) The geology,

geochemistry, mineralogy and mineral beneficiation of platinum-group elements. Canadian Institute of Mining and Metallurgy 54, 299–320.

Wood, S.A., (2002) The aqueous geochemistry of the platinum-group elements with applications to ore deposits. In: The Geology, Geochemistry, Mineralogy and Mineral Beneficiation of Platinum-Group Elements (ed. L.J. Cabri). Montréal, pp. 211-249, Special Volume 54.

CHAPITRE 2

GEOLOGY, PETROGRAPHY, AND GEOCHEMISTRY OF SULFIDE-RICH PODS FROM THE LAC DES ILES PALLADIUM DEPOSITS (WESTERN ONTARIO, CANADA) AND A MODEL FOR THEIR GENESIS

CHARLEY J. DURAN[1], SARAH-JANE BARNES[1], JOHN T. CORKERY[2]

[1] UNIVERSITÉ DU QUÉBEC À CHICOUTIMI

[2] NORTH AMERICAN PALLADIUM

MINERALIUM DEPOSITA, SUBMITTED NOVEMBER 6, 2014

2.1 RÉSUMÉ

La mine et les gisements de Pd du Lac des Iles sont connus pour leur minéralisation riche en Pd et pauvre en sulfures. Cependant, des lentilles riches en sulfures non documentées sont présentes au travers de la mine et des gisements. Nous montrons que l'origine de ces lentilles riches en sulfures est le résultat d'accumulation de solution solide monosulfurée (MSS) dans des zones de dilatation. Les lentilles riches en sulfures recoupent la stratigraphie et sont présentent le long de structures majeures. Elles vont de sulfures matriciels à massifs. L'assemblage de sulfures est constitué de pyrrhotite–pentlandite–pyrite ± chalcopyrite. La pyrrhotite et la pentlandite présentent des textures ignées d'exsolution typiques. Deux tendances ont été identifiées à partir de cet assemblage de pyrrhotite–pentlandite. La première tendance est une zonation vers un assemblage dominé par la chalcopyrite, ayant lieu vers la bordure de certaines lentilles. Les analyses géochimiques montrent que le Cu est découplé du Ni. La deuxième tendance est une transition vers un assemblage dominé par la pyrite, ayant lieu d'une lentille à l'autre. Les proportions molaires de métaux de bases et de S montrent une tendance de développement de pyrite au détriment d'une composition magmatique typique. Il est proposé que la pyrite ait remplacé la MSS/pyrrhotite au cours de processus d'altération subséquents. L'abondance de pyrite n'apparait pas influencer les ratios d'EGP. Les EGP montrent de fortes corrélations entre Os, Ir, Ru et Rh. Cependant, il y a de faibles corrélations entre Pd–Pt et le Cu. Ces données reflètent l'accumulation de MSS. La variabilité en compositions d'EGP est interprétée comme le résultat de différents degrés de fractionnement. Cela

suggèrerait que le Pd n'a pas été remobilisé. L'ensemble de ces résultats est consistent avec les liquides sulfurés ayant été concentrés dans des zones de dilatiton avant de cristalliser des cumulats de MSS. Les liquides résiduels enrichis en Pd et Pt ont pu migrer à l'écart des lentilles riches en sulfures, fournissant ainsi une excellente cible pour l'exploration.

2.2 ABSTRACT

The Lac des Iles Pd mine and deposits are known for their Pd-rich/sulfide-poor mineralization. However, undocumented sulfide-rich pods are present throughout Lac des Iles Pd mine and deposits. We show that the origin of these sulfide-rich pods is the result of MSS (monosulfide solid solution) accumulation into structural dilation zones. The sulfide-rich pods crosscut stratigraphy and occur along major structures. They range from net-textured to massive sulfides. The sulfide assemblage consists of pyrrhotite–pentlandite–pyrite ± chalcopyrite. Pyrrhotite and pentlandite display typical igneous exsolution textures. Two trends were identified from this pyrrhotite–pentlandite assemblage. The first trend is a zonation toward a chalcopyrite-dominated assemblage, occurring along the edge of some pods. Geochemical analyses show a decoupling of Cu from Ni. The second trend is a transition toward a pyrite-dominated assemblage, occurring from one pod to another. Molar proportions of base metals and S show a trend of pyrite development at the expense of a typical primary magmatic composition. It is proposed that pyrite replaced MSS/pyrrhotite during subsequent alteration processes. The pyrite abundance does not appear to influence

the PGE ratios. The PGE show strong correlations between Os, Ir, Ru and Rh. However, there are poor correlations between Pd–Pt and Cu. These data reflects the accumulation of MSS. The variability in PGE compositions is interpreted as the result of different degrees of fractionation. This would suggest that Pd has not been remobilized. These overall results are consistent with sulfide liquids having been concentrated into dilation zones prior to crystallization of cumulus MSS. The residual fractionated liquid, enriched in Pt and Pd, may have migrated away from the sulfide-rich pods, providing an excellent exploration target.

2.3 INTRODUCTION

The Lac des Iles (LDI) Complex, Western Ontario, Canada, (Fig. 2.1) is the world's fifth largest producer of Pd, providing 164 000 oz Pd for the year 2012, i.e., 2.6% of the world's mining supply (Platinum 2013 Johnson Matthey annual report). The LDI Pd mine and deposits are hosted by the Mine Block Intrusion of the LDI Complex. This intrusion does not resemble other intrusions containing Pd deposits. Further, the deposits (Roby, High-grade, Offset and Twilight zones; Fig. 2.1) do not resemble other PGE (platinum-group elements) deposits in terms of size, textures and composition (Brügmann et al. 1989; Lavigne and Michaud 2001; Hinchey et al. 2005; Barnes and Gomwe 2011). Indeed, most of the world's PGE come from thin, PGE-rich, stratiform layers (known as reefs) within large layered intrusions (Naldrett 2004 and references therein). In contrast, the Mine Block

Intrusion is small (3 km long by 1.5 km wide), concentrically zoned (Fig. 2.1) and its deposits occur within the intrusion as fairly wide zones (50-400 m) of disseminated sulfides in rocks with extremely varied textures.

Although Talkington and Watkinson (1984) mention the presence of a few pyrite-rich occurrences in their study, previous studies of the LDI deposits have not fully described the presence of occasional sulfide-rich pods. The sulfide-rich pods are unusual in that they are not found at the base or the margins of the intrusion. Furthermore, many of the sulfide-rich pods contain too much pyrite to represent the crystallization product of magmatic sulfide liquids. There has been a long-standing controversy about the role played by fluids in the ore-forming processes at LDI (Talkington and Watkinson 1984; Brügmann et al. 1989; Lavigne and Michaud 2001; Hinchey and Hattori 2005; Barnes and Gomwe 2011; Hanley and Gladney 2011; Djon and Barnes 2012; Boudreau et al. 2014; Schisa et al. 2014). The presence of these unusual sulfide-rich pods adds another dimension to the ongoing debate.

The purpose of this study is to describe the sulfide-rich pods of the Mine Block Intrusion and investigate how they could have formed. Two possible origins may be considered: (1) the pods could represent the sulfides crystallized from magmatic sulfide liquids in which case some have undergone subsequent alteration to produce the pyrite-rich pods; or (2) the pods could represent sulfides precipitated from magmatic-hydrothermal fluids. To assess whether the pods are of magmatic or hydrothermal origin, we investigated their geological setting, petrography, whole-rock geochemistry, and S isotopic compositions.

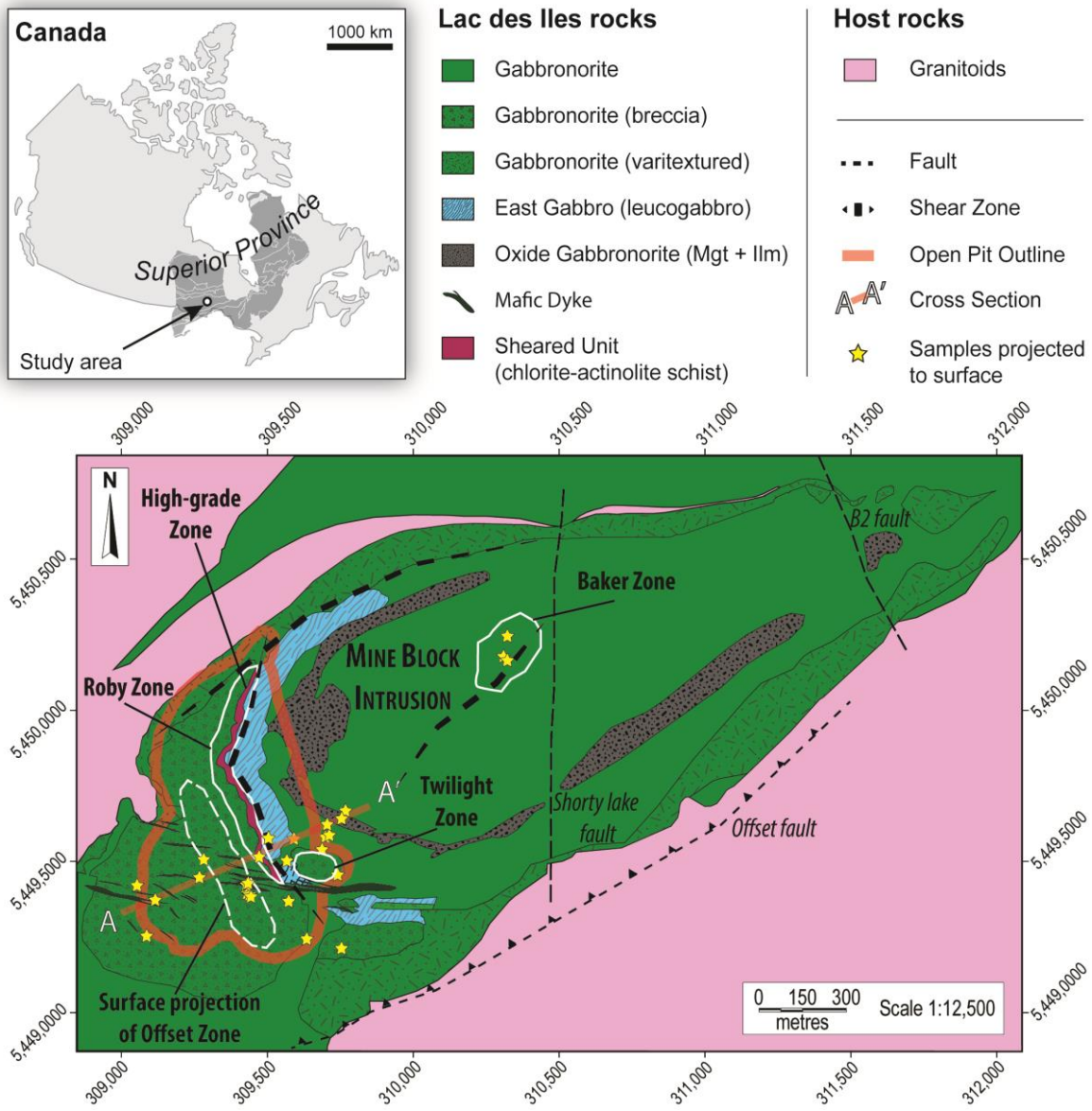

Figure 2.1 Simplified geological map of the Mine Block Intrusion of the Lac des Iles Complex (Modified from North American Palladium). Sulfide-rich samples are projected to surface and form a SW-NE trend.

2.4 GEOLOGICAL BACKGROUND

2.4.1 REGIONAL SETTING

The LDI Complex is part of a suite of mafic to ultramafic intrusions located approximately 80 km north of the city of Thunder Bay, Western Ontario, Canada (Fig. 2.1). This suite of plutons occurs within the Superior province, in the vicinity of the contact between the Wabigoon subprovince and the northwestern margin of the Quetico subprovince. The LDI Complex (2689 ± 1 Ma; Stone et al. 2003) intruded into foliated tonalitic gneisses (2775 to 2772 Ma; Stone et al. 2003). Furthermore, the mafic and ultramafic rocks of the Complex were in turn intruded by various granitoids, ranging from tonalitic gneisses to granodiorites, indicating the coexistence of mafic and felsic magmatism (Macdonald et al. 1988; Sutcliffe 1989). The Complex is usually subdivided, from north to south, into three main intrusions based on field relations (Lavigne and Michaud 2001): (a) the North Lac des Iles Intrusion that consists of a sequence of layered ultramafic cumulates and minor gabbronoritic cumulates; (b) the Mine Block Intrusion that consists mainly of gabbronorites hosting the ore zones; and (c) the Camp Lake Intrusion that consists of a homogeneous hornblende gabbro.

The Quetico metasedimentary rocks adjacent to the LDI Complex are interpreted to have formed during the subduction of oceanic lithosphere beneath the Wabigoon subprovince (Percival and Williams 1989). Brügmann et al. (1997) noted that the geological context of the LDI Complex suggests the root of a continental arc as the tectonic setting and Barnes

and Gomwe (2010) showed that LDI parental magmas most resemble andesites based on the estimate of the liquid composition. Hanley and Gladney (2011) suggested a maximum depth of emplacement of 10–12 km for the Mine Block Intrusion based on a thermobarometric study.

2.4.2 GEOLOGY AND PETROGRAPHY OF THE MINE BLOCK INTRUSION

The geology and petrology of the Mine Block Intrusion have been documented in numerous studies (Brügmann et al. 1989; Sutcliffe 1989; Brügmann et al. 1997; Lavigne and Michaud 2001). The Mine Block Intrusion (Fig. 2.1) has been mainly described as a gabbroic to gabbronoritic intrusion with extremely variable lithologies, comprising anorthosite, leuco- to melano-gabbro, chlorite-actinolite schist, oxide-rich gabbronorite and including numerous mafic and ultramafic dykes and sills. Based on whole-rock geochemistry Barnes and Gomwe (2011) most recently showed that the intrusion is rather of noritic to gabbronoritic composition and that most of the rocks are plagioclase-orthopyroxene adcumulates. The various lithologies also display a wide range of textures, from equigranular to varitextured (fine- to coarse-grained) and pegmatitc rocks. However, regardless of their textures the rocks have similar incompatible element ratios indicating that they all are co-magmatic (Barnes and Gomwe 2011). Pegmatitic and varitextured rocks in the Mine Block Intrusion have been interpreted to have formed when the magma became saturated in fluids which in turn caused recrystallization (Barnes and Gomwe 2011). The

presence of magmatic breccias and the scarcity of layers have been interpreted as the result of a dynamic intrusive system with disruptive pulses of magma (Lavigne and Michaud 2001).

2.4.3 DEFORMATION

Although intense deformation has been reported in the Mine Block Intrusion, only recently have studies focused on the role of deformation. Regional structural measurements record large-scale recumbent folds with S–N axes and later large-scale recumbent folds with SW–NE axes (Rankin 2013), following major regional faults (Gupta and Sutcliffe 1990). These indicate crustal shortening in the E–W direction followed by crustal shortening in the SE–NW direction. These crustal shortenings may have opened dilation zones in the SW–NE direction and the intrusion could have been emplaced along one of these.

The Mine Block Intrusion has two large-scale S–N dilation zones: (1) the Roby and Offset zones, and (2) the Shorty Lake Fault, which also carries PGE mineralization (Baker Zone) (Fig. 2.1). Interestingly, large shear zones and mylonites occur within the Mine Block Intrusion following the S–N and SW–NE structural trends, and post-intrusion major brittle faults (Offset, Shorty Lake, and B2) also follow these trends (Fig. 2.1). The presence of the chlorite-actinolite schist in the ore zones combined with the presence of shear zones, mylonites and brittle faults indicates a continuous deformation history, suggesting that the Mine Block Intrusion was being deformed during emplacement.

2.4.4 SHAPE AND STRATIGRAPHY

The surface and subsurface expressions of the Mine Block Intrusion give the appearance of an oval, funnel-shaped, and to some extent concentrically zoned body (Figs. 2.1, 2.2). However, the Mine Block Intrusion is cut off by the Offset Fault that separates the upper block (Roby Block) to the north from the lower block (Offset Block) to the south. The Offset Fault is a reverse fault thrusting the Roby Block over the Offset Block, which indicates a more complicated history at depth than the simple surface appearance.

The stratigraphy observed at surface may be summarized as follows. The marginal part of the intrusion consists of a varitextured gabbronoritic to gabbroic rim, where magmatic breccias are common and occur as pipes, pods and large blocks of varying composition (Lavigne and Michaud 2001). However, breccias have not been identified at depth. On the western side of the intrusion the varitextured unit and the breccias are in contact with a massive, foliated, steeply dipping leucogabbronorite known as the East Gabbro. The contact between the varitextured/breccia rocks and the East Gabbro consists of a shear zone mainly composed of chlorite-actinolite schist. The central part of the intrusion consists mainly of fairly homogeneous gabbronorites. Within the gabbronorites there is a weakly concentric zone with significant amounts of Fe-Ti oxides (i.e., magnetite and ilmenite) and there are also zones of variable textures and breccias (Baker Zone).

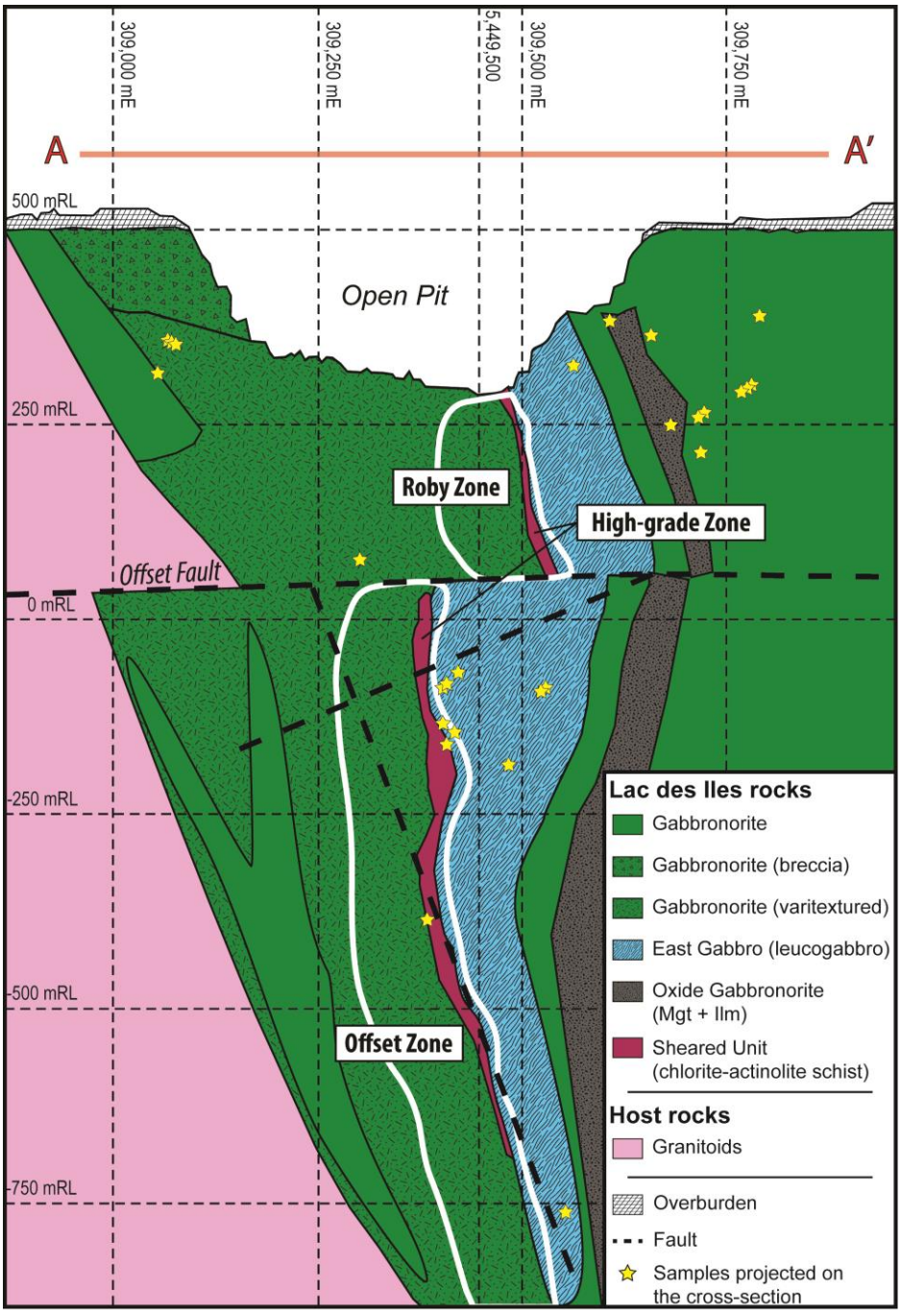

Figure 2.2 Idealized cross-section of the Mine Block Intrusion of the Lac des Iles Complex (Modified from North American Palladium) with projected locations of sulfide-rich samples from drill cores. Note that sulfides-rich pods sampled from the open pit and from Baker zone are not plotted on the cross-section.

2.4.5 ALTERATION

Although fresh rocks have been identified in the Mine Block Intrusion, most of the rocks are altered to greenschist and lower amphibolite facies (Boudreau et al. 2014). Based on the degree of alteration Barnes and Gomwe (2011) divided the rocks of the ore zones into three main lithologies: (a) gabbronorites; (b) metagabbronorites; and (c) chlorite-actinolite schist. In the gabbronorites, small amounts of biotite and hornblende (<1%) are present and the pyroxene is orthopyroxene. Gabbronorites are scarce in the Roby Zone and tend to be more common in the Offset Zone where they have been interpreted to represent the fresh protolith (Boudreau et al. 2014). In the metagabbronorites, the pyroxene is replaced by actinolite + chlorite ± talc. To a lesser extent plagioclase is altered to sericite + chlorite + epidote ± quartz ± carbonates. According to Boudreau et al. (2014) the difference in degree of alteration arises because pyroxene is altered at about twice the rate of plagioclase. In the chlorite-actinolite schist the alteration is complete and the igneous textures have been destroyed.

The alteration is in part thought to be due to late-magmatic rather than metamorphic fluids because minor amounts of primary hornblende and biotite are present, implying the presence of H_2O in the magmas (Watkinson et al. 2002). Further, the whole-rock geochemistry of fresh and altered rocks are similar (Barnes and Gomwe 2011). However, given the predominance of greenschist facies rocks, metamorphic fluids may have contributed to the alteration of the Mine Block Intrusion.

Based on halogen geochemistry of apatite and on previous work by Somarin et al. (2009) and Hanley and Gladney (2011), Schisa et al. (2014) identified three stages of fluid activity: (1) early degassing of Cl-rich CO_2-H_2O vapor from residual silicate liquid at high temperature; (2) late degassing of Cl-poor CO_2-H_2O vapor from residual silicate liquid at lower temperature, becoming enriched in CO_2 after dehydration during amphibole stabilization; and (3) mixing of country rock fluids of meteoric composition with late vapor under greenschist conditions.

2.4.6 MINERALIZATION

Several zones in the Mine Block Intrusion contain mineralization of economic interest, either currently exploited or being explored. Mining operations started with an open pit on three main zones defined at surface: the Roby, Twilight, and High-grade zones. These three zones have been the focus of most previous investigations (Lavigne and Michaud 2001; Hinchey et al. 2005; Barnes and Gomwe 2011; Djon and Barnes 2012). The Roby and Twilight Zones consist of varitextured gabbronorites and magmatic breccias with various degrees of alteration. The High-grade Zone consists of sheared chlorite-actinolite schist. Mining operations were extended underground by excavating the Roby and High-grade zones against the East Gabbro hanging wall. Underground drilling led to the discovery of the Offset Zone, which is an extension at depth of the Roby Zone, displaced approximately 250 m to the west by the Offset Fault. Further, two mineralized trends (i.e., Cowboy and

Outlaw zones) have been identified 40 m and 85 m west of the Offset Zone. Several new mineralized zones are the focus of intensive drilling from the surface: the Sheriff and South Norite zones to the south of the open pit; the North VT Rim and the Creek Zone in the north of the Mine Block Intrusion; and the Baker Zone in the center of the intrusion.

In the rocks of the Mine Block Intrusion, Pd is hosted by pentlandite and platinum-group minerals (PGM) closely associated with base metal sulfides (BMS) (Watkinson and Dunning 1979; Talkington and Watkinson 1984; Sutcliffe et al. 1989; Djon and Barnes 2012). The BMS content of the rocks is highly variable, ranging from <0.1 to 5%, but most of the rocks have less than 3% sulfides. Several assemblages have been observed in different studies, ranging from magmatic assemblage pyrrhotite–pentlandite–chalcopyrite to altered assemblages with the presence of pyrite, millerite, violarite, siegenite, sphalerite and magnetite (Talkington and Watkinson 1984; Hinchey and Hattori 2005; Djon and Barnes 2012). Djon and Barnes (2012) identified three main BMS assemblages according to host lithology. An assemblage consisting of pyrrhotite–pentlandite–chalcopyrite ± pyrite in the fresh gabbronorite was interpreted to represent a high temperature assemblage, crystallized upon cooling from magmatic sulfide liquids. A second assemblage consisting of chalcopyrite–pyrite–pentlandite and a third consisting of pyrite–chalcopyrite–millerite were both found in the metagabbronorite and in the chlorite-actinolite schist. Both of these assemblages were interpreted to result from re-equilibration of sulfides and silicates during moderate- to low-temperature alteration.

The strong correlation between S and PGE in the Roby and Twilight zones is consistent with the mineralization having been formed by sulfide liquids. However, the lack of correlation between S and PGE, and the higher Pd/Ir and Pd/Pt ratios observed in the High-grade Zone rocks, indicate that S has been lost and Pd has been upgraded in this zone (Hinchey and Hattori 2005; Djon and Barnes 2012; Barnes and Gomwe 2011). Given these considerations, Barnes and Gomwe (2011) suggested that Pd was scavenged from magmatic sulfides at depth by late-magmatic fluids, which were in turn concentrated in the shear zone as the rocks were converted to schist and sulfides were modified.

2.5 SAMPLING AND ANALYTICAL METHODS

The database from the extensive drilling program of North American Palladium was interrogated for sulfide-rich samples using Ni + Cu > 5 wt. % as a filter. Approximately one hundred borehole intersections were reported and in 34 cases sufficient drill core was available for sampling. Additionally, four massive pods were sampled in the Roby Zone open pit and five were sampled from the Baker Zone outcrop. The location of the samples within the intrusion was plotted using the three-dimensional geographic information system commercial software package Encom Discover 3D (Tetrad Computer Applications Inc., Vancouver) for MapInfo Professional (Pitney Bowes).

Samples were cut with a diamond saw and a representative hand specimen was retained for macroscopic characterization. The remaining material was cleaned by cutting off weathered

surfaces, and a representative piece of each sample was selected for polished thin sectioning. At least 500 g of each sample was crushed to <1 cm using a mild steel jaw crusher, and 250 g of this was pulverized to less than 200 mesh in an alumina ceramic mill.

Petrographic examinations of polished thin sections and polished blocks were completed using an OLYMPUS DP71 optical microscope coupled with a digital camera at Université du Québec à Chicoutimi (UQAC). Sulfide, oxide and silicate minerals were identified and described. Some PGM were observed in polished sections and were more closely investigated using a scanning electron microscope JEOL-840A at Laval University, Québec City.

Most of the whole-rock geochemical analyses were performed at LabMaTer (UQAC). Sulfur was determined by a HORIBA EMIA-220V infrared sulfur and carbon analyzer, using the method described by Bédard et al. (2008). Nickel and Cu were determined by aqua regia digestion coupled with atomic absorption spectrophotometry. The PGE (Os, Ir, Ru, Rh, Pd and Pt) and Au were determined by Ni sulfide fire assay followed by Te co-precipitation and ICP-MS (inductively coupled plasma–mass spectrometry) solution analysis using the method described by Savard et al. (2010). Aluminum, Ca, Cr, Fe, Na, Mg, Mn, Sc, Se, Ti, V, and Zn were determined by instrumental neutron activation analysis (INAA) after irradiation at the Slowpoke laboratory, Ecole Polytechnique, Montréal, and data reduction at UQAC, using the method described by Bédard et al. (2000). Data from Gomwe (2008) was used to constrain the composition of the disseminated sulfides, however Gomwe (2008) did not determine Se, therefore we analyzed 18 of her whole-rock

samples for Se using Thiol Cotton Fiber and INAA as described by Savard et al. (2006). In-house reference materials WMS-1a (Canada Certified Reference Material Projects, CCRMP) and KPT-1 (UQAC), respectively a massive and a disseminated sulfide, were analyzed with the samples to monitor data quality. In-house reference material MRG-1 (CCRMP), which is a gabbro, was analyzed with the samples from Gomwe (2008) to monitor Se data quality. The analyses of the in-house reference materials are consistent with the working values (see electronic supplementary materials).

Additionally Ag, As, Ba, Bi, Cd, Cs, Hg, Li, Mo, Pb, Rb, Sb, Sn, Te, and Tl were determined by aqua regia digestion coupled with ICP-MS at Geoscience Laboratories, Ontario Geological Survey, Sudbury. In-house reference material KPT-1, was submitted as unknown sample to monitor data quality. The analyses of the in-house reference materials are consistent with the working values (see electronic supplementary materials).

Sulfur isotope analyses were performed on an IsoChrom Continuous Flow Stable Isotope Ratio Mass Spectrometer coupled to a Carlo Erba Elemental Analyzer at the Environmental Isotope Laboratory of Waterloo University. All sulfur isotope compositions were determined in delta notation relative to the international standard Vienna Cañon Diablo Troilite (VCDT) with an analytical precision of ± 0.05‰ and a reproducibility of ± 0.2‰.

2.6 RESULTS AND INTERPRETATION

2.6.1 GEOLOGY OF SULFIDE-RICH PODS

Sulfide-rich pods (Fig. 2.3) occur in all rock types of the Mine Block Intrusion of the LDI Complex, cross-cutting the stratigraphy (Fig. 2.2). Further, the pods occur along a SW–NE trend (Fig. 2.1) approximately parallel to several SW–NE trending major ductile shear zones observed in the field and interpreted to have co-magmatic activity.

The amount of sulfides in the sulfide-rich pods vary from approximately 8 to 98 modal percent. The texture and basic mineralogy of the sulfides range from massive with a few oxide grains present (> 60% sulfides; Fig. 2.3b), net-textured sulfides with silicate and oxide inclusions (between 30 and 60% sulfides; Fig. 2.3d), to patches of interconnected sulfides within a sample that consists predominately of silicate minerals (< 30% sulfides; Fig. 2.3e). The pods consisting of massive and net-textured sulfides have thicknesses ranging from 10 to 162 cm, whereas the pods with patches of interconnected sulfides are up to 3 m thick. The geometry of the pods is unknown as most of the samples are from drill cores. A mineralogical transition can be readily observed on hand specimen, ranging from pyrrhotite-dominated rocks to pyrite-dominated rocks (Figs. 2.3f–h). Some massive pods are zoned, with pyrrhotite-dominated rock in the center and chalcopyrite-dominated rock along the edges (Fig. 2.3i).

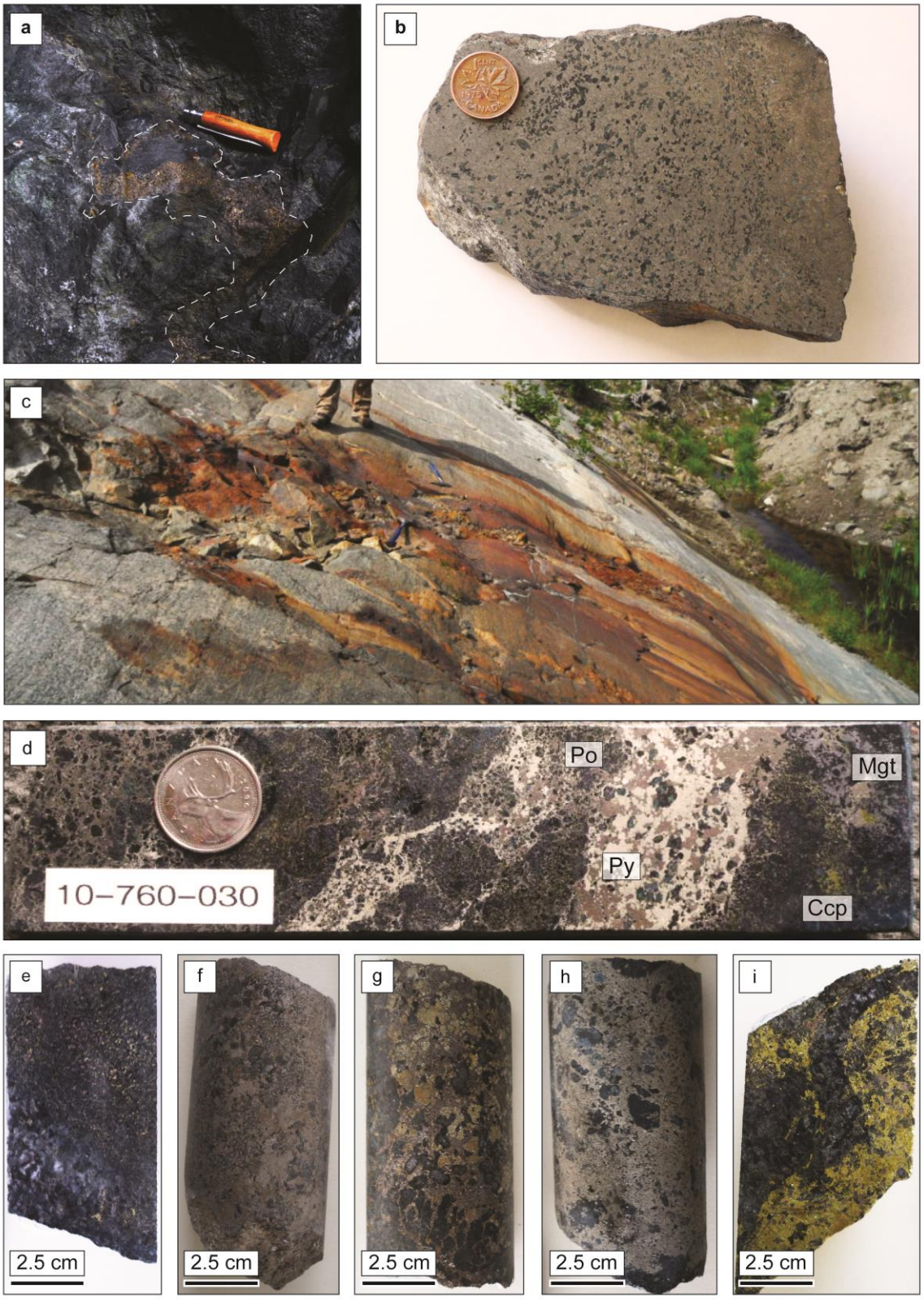
a
b
c
d
Po
Mgt
Py
Ccp
10–760–030
e
f
g
h
i
2.5 cm
2.5 cm
2.5 cm
2.5 cm
2.5 cm

Figure 2.3 Hand specimens, core samples, and outcrop expression of sulfide-rich pods. (a) Roby Zone outcrop in the open pit. (b) Massive sulfide from Roby Zone open pit. (c) Baker Zone outcrop. (d) Net-textured sulfides from drill core. (e) Patch of interconnected sulfides. (f) Massive pyrrhotite. (g) Net-textured pyrrhotite + pyrite. (h) Massive pyrite. (i) Net-textured chalcopyrite.

These overall observations are interpreted to suggest that sulfide-rich pods did not simply form by settling of a magmatic sulfide liquid out of a silicate liquid. On this basis we suggest three possible origins of the sulfide-rich pods. First, the sulfide-rich pods may represent crystallization products of magmatic sulfide liquids that collected in low pressure zones of the cumulus magma pile while it was not completely consolidated. Secondly, sulfide liquids may have crystallized at the base of the intrusion and were subsequently mobilized along shear zones. Finally, the sulfides may have been deposited along shear zones from hydrothermal fluids.

Based on field evidence we consider the first origin as most probable. The sulfide patches may be considered as examples of disseminated sulfide liquids that have partly migrated from high-pressure areas and the massive sulfides as sites where the sulfide liquids have collected. The second origin seems unlikely because mobilization of sulfides in a solid state requires that sulfides are massive. However, many of the pods consist of net-textured and patches of interconnected sulfides. Moreover, as presented in section 2.6.2, the observed sulfides lack features of ductile deformation at the grain scale, which could support this possibility. The third origin also lacks support from field evidence. If the sulfides were deposited from a hydrothermal fluid, then we should expect an increase of alteration in the silicate minerals present around the sulfides. However, we did not observed such relationship.

2.6.2 PETROLOGY AND MINERALOGY

2.6.2.1 SULFIDE ASSEMBLAGES AND TEXTURES

The ore-mineral assemblage is mainly composed of pyrrhotite (Po), pentlandite (Pn), pyrite (Py), chalcopyrite (Ccp) and magnetite (Mgt) with minor amounts of ilmenite (Ilm) and discrete PGM. The sulfide-rich pods may be divided into four main groups based on a combination of texture and mineral assemblage: (1) Po–Pn ± Py–Ccp–Mgt–Ilm; (2) Ccp ± Po–Pn–Py–Mgt–Ilm; (3) Py ± Pn–Ccp–Po–Mgt–Ilm; and (4) Mgt ± Ilm–Py–Pn–Po–Ccp. No evidence of ductile deformation or recrystallization such as twining, mineral banding, triple junctions, have been observed within the sample set.

The Po–Pn-rich assemblage exhibits igneous textures (Figs. 2.4a, b). Pyrrhotite forms large anhedral crystals (up to a few mm long) surrounded by irregular granular polycrystalline veinlets of fine to coarse Pn. Pentlandite also occurs as oriented exsolution flames within Po. Chalcopyrite is present as irregularly dispersed polycrystalline aggregates occurring along sulfide-sulfide grain boundaries, and as veinlets along actinolite cleavages. Pyrite occurs as disseminated, subhedral to anhedral grains and polycrystalline aggregates, associated with Po and Pn (Fig. 2.4b). In some cases Py forms an anhedral, spongy-textured mixture associated with silicates (Fig. 2.4c) and in rare cases Py occurs as small (up to 0.5 mm width) veins cross-cutting Po (Fig 2.4d). Magnetite is present as small rounded anhedral grains randomly dispersed in Po or in contact with silicates and is associated with Ilm (Fig. 2.4e). This assemblage and related textures are typical of magmatic Ni-Cu sulfide

deposits, although some samples contain more Py than would be expected in a magmatic assemblage.

The Ccp-rich assemblage occurs along the edges of some pods composed of Po–Pn-rich assemblage (Fig. 2.4f). The Ccp occurs as large anhedral polycrystalline aggregates (up to a few mm long) and as tiny grains (up to 100 microns) hosted in silicates. The small amount of Po and Pn present with Ccp exhibits igneous textures. Pyrite occurs as disseminated, subhedral to anhedral grains and polycrystalline aggregates, associated with Po and Pn. Magnetite and Ilm occur as small (up to hundreds of microns) anhedral grains hosted by Ccp or as large patches (up to a few mm long) at the Ccp–silicate grain boundary.

In the Py-rich assemblage (Figs. 2.4g, h) Py is the dominant Fe-sulfide and occurs as large (up to a few mm) anhedral individual grains and as polycrystalline aggregates. Pentlandite forms small anhedral polycrystalline aggregates. In the samples where Po is present it forms large anhedral grains associated with Pn, but it does not contain Pn flames. Chalcopyrite occurs as irregularly dispersed anhedral grains. Magnetite and Ilm occur as small (up to hundreds of microns) anhedral grains among the sulfide minerals.

In the Mgt-rich assemblage (Fig. 2.4i) the sulfide minerals have a similar relationship to the Py-rich assemblage, but Mgt is much more common and occurs as centimetric amorphous patches. Additionally, Py may occur as small (up to 0.5 mm width) veins cross-cutting Mgt.

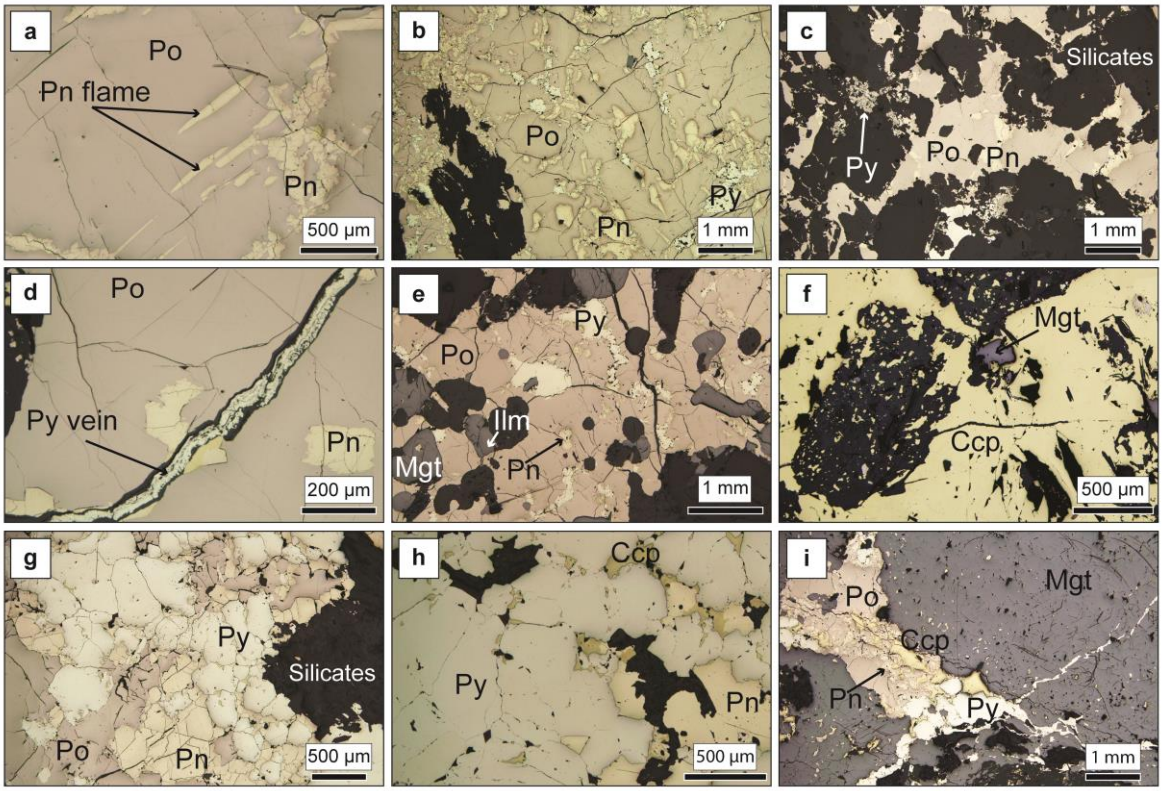

Figure 2.4 Photomicrographs in reflected light of the different assemblages and textures observed in the sulfide-rich pods. (a) Pyrrhotite–pentlandite-rich assemblage with oriented pentlandite exsolution flames. (b) Pyrrhotite–pentlandite-rich assemblage with minor pyrite. Pentlandite forms chain-like veinlets. (c) Pyrrhotite–pentlandite-rich assemblage with minor spongy-textured Py. (d) Pyrrhotite–pentlandite-rich assemblage with pyrite-vein. (e) Pyrrhotite–pentlandite-rich assemblage with minor pyrite, magnetite and ilmenite. (f) Chalcopyrite-rich assemblage. (g) Pyrite-rich assemblage with minor pyrrhotite and pentlandite. Pentlandite does not occur as exsolution flames. (h) Pyrite-rich assemblage with minor pentlandite and chalcopyrite but no pyrrhotite. (i) Magnetite-rich assemblage with minor pyrrhotite, pyrite, pentlandite and chalcopyrite.

2.6.2.2 PLATINUM-GROUP MINERALS

The PGM we have observed occur as euhedral to anhedral single grains (Fig. 2.5) that range from approximately 1 to 100 microns. Most of these grains are included in sulfides and along sulfide-silicate and sulfide-sulfide grain boundaries. Less commonly, PGM were observed associated with silicate minerals (e.g., actinolite and chlorite). Some of the PGM in the sulfide minerals exhibit exsolution textures and are associated with Pn (Figs. 2.5a, b). Euhedral PGM are generally bigger and are mainly associated with sulfides (Figs. 2.5c, d). Anhedral PGM are generally smaller and are mainly associated with silicates (Figs. 2.5e, f).

The majority of PGM are Pd-tellurides as observed by previous workers (Watkinson and Dunning 1979; Talkington and Watkinson 1984; Sutcliffe et al. 1989; Djon and Barnes 2012). They consist, in decreasing order of abundance, of merenskyite ($PdTe_2$), kotulskite (PdTe), and telluropalladinite (Pd_9Te_4). Some (Pd, Pt)-bismuthotellurides and (Pd, Pt)-sulfides have also been found in the sulfide-rich pods.

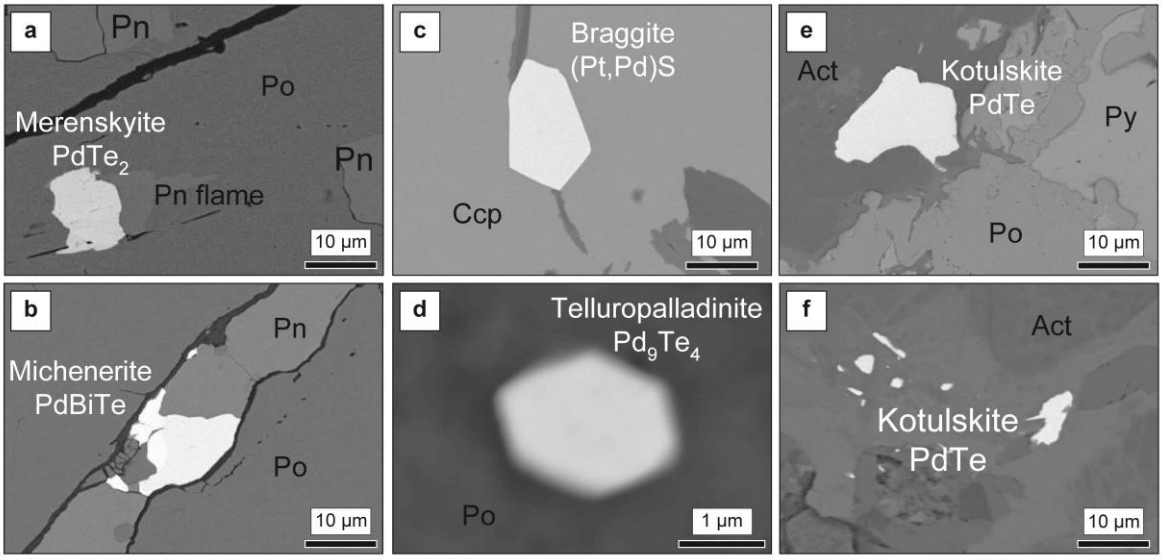

Fig. 5 Back-scattered electron photomicrographs of platinum-group minerals found within sulfide-rich pods. (a) Anhedral merenskyite associated with pentlandite exsolution flame hosted in pyrrhotite. (b) Anhedral michenirite hosted in fine grained pentlandite veinlet. (c) Euhedral braggite hosted in chalcopyrite. (d) Euhedral telluropalladinite hosted in pyrrhotite. (e) Anhedral kotulskite at silicate-sulfide grain boundary. (f) Anhedral kotulskite hosted in actinolite.

2.6.2.3 SILICATE MINERALS

The silicate minerals present in or around the sulfide-rich pods consist mainly of actinolite, chlorite, and plagioclase. Orthopyroxene (Opx) was completely altered and replaced by actinolite and chlorite, with partly altered Opx observed in only one sample. Minor hornblende, quartz, epidote and carbonates are also present.

All associated silicate minerals are anhedral. The plagioclase ranges from 1 to 6 mm. Most plagioclase contains spindle twins (Fig. 2.6a) and kink bands and has experienced moderate to strong sericitization. The actinolite ranges from 1 to 4 mm and commonly contains kink bands (Fig. 2.6b) and shows undulose extinctions. The quartz ranges from 0.5 to 6 mm and shows undulose extinctions (Fig. 2.6c) and subgrains (Fig. 2.6d). In some samples plagioclase and actinolite show preferential shape orientation in the vicinity of sulfide-rich pods (Fig. 2.6e). However, silicate minerals within sulfide-rich pods are randomly oriented and show different angle boundaries (Fig. 2.6f).

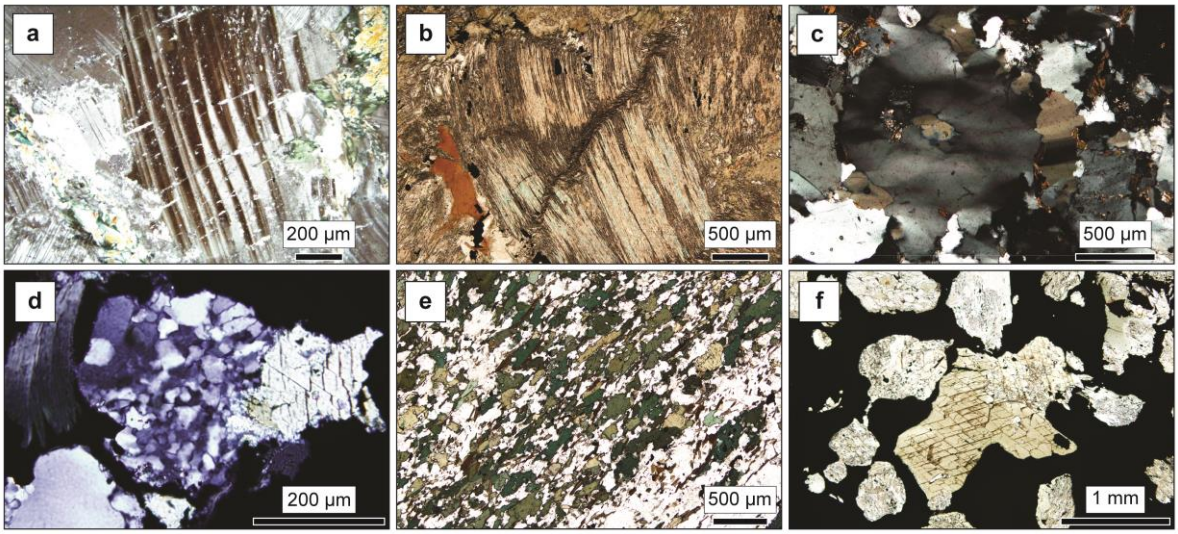

Figure 2.6 Photomicrographs in transmitted light of silicate-mineral assemblages in the vicinity of sulfide-rich pods showing evidence of deformation. (a) Spindle twins in plagioclase. (b) Kink-band in actinolite. (c) Undulose extinctions in quartz. (d) Subgrains in quartz. (e) Shape preferred orientation of plagioclase and actinolite. (f) Sulfides surrounding silicate minerals with random orientation and different angle boundaries.

2.6.2.4 INTERPRETATION OF THE PETROLOGY

Based on the exsolution textures and the lack of ductile deformation evidence in the Po–Pn-rich and Ccp-rich assemblages, these assemblages may represent the crystallization products of magmatic sulfide liquids. The relationship of sulfide minerals with silicate minerals showing evidence of high temperature deformation further supports the idea of sulfides being emplaced as a penetrating liquid while silicates were deformed.

The amount of Py present in some of the samples suggests that the Po–Pn-rich assemblage has undergone some modification, as discussed in detail in this section. The low modal proportion of Ccp in this assemblage suggests that it represents sulfide cumulate composition. When a sulfide liquid crystallizes the first phase to crystallize is monosulfide solid solution (MSS). As the temperature falls, Po and Pn exsolve from the MSS. Copper does not readily partition into the MSS and is concentrated in the fractionated liquids. Therefore, cumulus MSS generally consists predominantly of Po and Pn.

The Ccp-rich assemblage can be interpreted in a number of ways. It could be the product of crystallization from the fractionated sulfide liquid that becomes enriched in Cu as the MSS crystallizes. This liquid crystallizes into an intermediate solid solution (ISS) below 880°C (Dutrizac 1976). As the temperature falls, Ccp ± cubanite exsolves from ISS (Cabri 1973). Alternatively, the Ccp-rich assemblage could be remobilized material, formed either by subsolidus recrystallization or by precipitation from a hydrothermal fluid. As mentioned in sections 2.6.1 and 2.6.2, these two possibilities seem unlikely as no deformation features

have been observed in Ccp which absence is interpreted to suggest that Ccp was not emplaced by subsolidus recrystallization. Furthermore, the silicate assemblage surrounding the Ccp-rich assemblage is not more altered than the rest of the rocks. The association of the Ccp with massive pods that have igneous mineralogy and textures suggests to us that these samples crystallized from fractionated magmatic sulfide liquids.

The difference in PGM textures may result from various processes. The PGM with exsolution textures intimately associated with Pn might have exsolved from the Po–Pn-rich assemblage. The euhedral PGM associated with sulfides could be the products of crystallization from the residual liquid that becomes enriched in Pd, Pt, Au and semi-metals as ISS crystallizes. The anhedral PGM associated with silicates might have precipitated from late-magmatic fluids, or might have been previously associated with sulfides that have been dissolved by late-magmatic fluids.

The Py-rich assemblage cannot simply be the product of crystallization of magmatic sulfide liquids. Sulfides that crystallize from magmatic sulfide liquids contain approximately equal molar amounts of S and metals but Py contains twice as much S as metals. Furthermore, the Py-rich samples no longer exhibit igneous textures.

The Py could have formed by a number of reactions:

(a) by S addition from an external source (sulfidation)

$$FeS_{(1-x)} + 1/2\ S = FeS_2 \qquad \text{Eq. 1}$$

(b) by Fe redistribution from the sulfide assemblage to the silicates

$$FeS_{(1-x)} + H_2O + \text{pyroxene} = FeS_2 + \text{Fe-rich amphibole/chlorite} \qquad \text{Eq. 2}$$

(c) by oxidation of the sulfides to form Py+Mgt

$$6FeS_{(1-x)} + 2O_2 = 3FeS_2 + Fe_3O_4 \qquad \text{Eq. 3}$$

For the Py-rich samples, origins (a) or (b) are possible and will be more closely considered in section 4.3. Origin (c) requires that the modal proportion of Py to Mgt is approximately 62 to 38 modal percent. This might be a viable way of forming Py in the Mgt-rich assemblage, but requires too much Mgt for the Py-rich assemblage.

The Mgt in the Mgt-rich assemblage could also have formed in a number of ways. First, as outlined in Equation 3, it could have formed by oxidation of the igneous sulfide assemblage. Second, it could have crystallized from magmatic sulfide liquids that may contain some oxygen. Experimental work (Naldrett 1969; Kress et al. 2008) shows that up to 15% Mgt can crystallize from sulfide liquids. Third, it could have formed as oxygen diffused out of sulfide liquids and reacted with silicate liquids during early stages of crystallization of the sulfide liquids (Fonseca et al. 2008). Finally, it could have simply crystallized from the silicate liquids. The first three origins are possible and will be more closely considered in section 2.6.3. The last origin requires that the host rocks contain enough oxides to account for the amount observed in the ore-mineral assemblages. However, except for the oxide-rich gabbronorite, host rocks in the Mine Block Intrusion do

not contain enough oxides. Thus, oxides from the ore-mineral assemblage are unlikely to have crystallized from the silicate liquid.

2.6.3 WHOLE-ROCK GEOCHEMISTRY

Based on our interpretation of the petrographic observations in section 2.6.2.4, the influence of crystal fractionation of sulfide liquids must be considered. However, the effects of subsequent alteration on geochemistry must be assessed before present compositions can be related to igneous processes. The complete geochemical dataset is presented in the electronic supplementary materials.

2.6.3.1 MAJOR AND MINOR ELEMENTS

As outlined in section 2.6.2.4, the presence of Py in many of the sulfide-rich pods indicates that either S or Fe has been redistributed, or oxygen has been added. These possibilities may be considered on a Pearce plot for sulfides by plotting molar S versus molar Fe + Cu + Ni + Co (Fig. 2.7). An igneous sulfide assemblage would be expected to show a ratio of approximately one S to one Fe + Cu + Ni + Co. In figure 2.7, the disseminated sulfides (green circles) and some patches of interconnected sulfides fall slightly above the 1:1 line of an igneous assemblage due to the presence of silicate minerals containing Fe but no S.

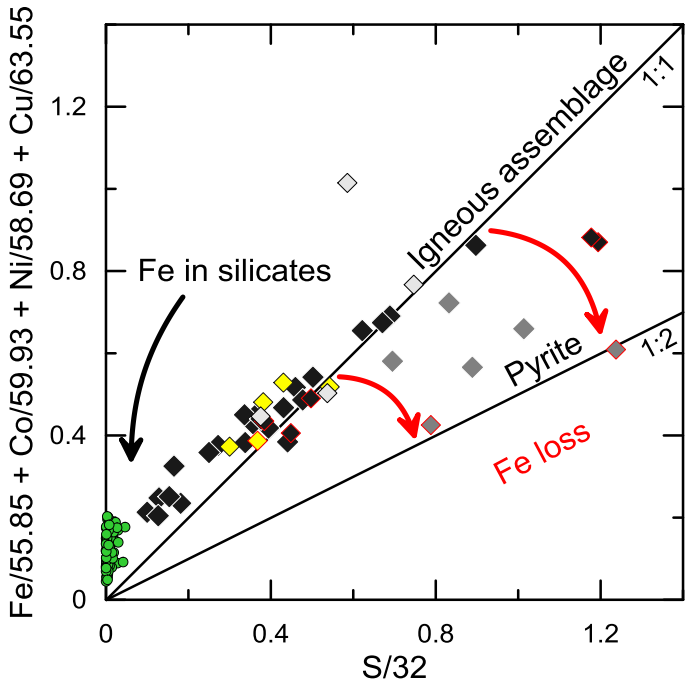

Figure 2.7 Pearce plot of molar proportions (S/32 vs Fe/55.84 + Co/59.93+Ni/58.6 + Cu/63.5). Green circles = disseminated sulfides; black diamonds = pyrrhotite–pentlandite-rich samples; yellow diamonds = chalcopyrite-rich samples; light grey diamonds = magnetite-rich samples; grey diamonds = pyrite-rich samples; red outline = samples from Baker Zone. Note that disseminated sulfides plot above the igneous line because of the Fe present in silicates. Most sulfide-rich pods plot on the igneous line indicating that neither Fe nor S has been mobile. One magnetite-rich sample plots above the igneous line indicating that either Fe has been added or S has been lost. Pyrite-rich samples from Baker Zone plot on the pyrite line indicating that either Fe has been lost or S added and the other Py-rich samples plot between both lines.

Most of the massive sulfide rocks plot close to the 1:1 line, indicating that neither S nor Fe has been gained or lost from the samples. The Py-rich samples from the Baker Zone (dark grey diamonds with red outline) and two of those from the Roby Zone are exceptions to this pattern: they plot below the igneous line, indicating either S gain or Fe loss. One Mgt-rich sample plots above the igneous line indicating either S loss or Fe gain.

To consider whether S gain or Fe loss has occurred, we plotted S versus S/Se (Fig. 2.8a). Generally, Se is considered less mobile than S (Auclair et al. 1987; Queffurus and Barnes 2014), so samples that have gained S will have higher S/Se ratios than igneous samples. On average, magmatic sulfides have S/Se ratios close to the mantle range of around 3000 (Eckstrand and Hulbert 1987). Most samples from the Mine Block Intrusion sulfide-rich pods have S/Se ratios between 2000 and 4000. In the Baker Zone Py-rich samples and one Ccp-rich sample have high S/Se ratios along with one sample from the Roby Zone. These high ratios indicate the samples have gained S (Fig. 2.8a). However, many of the disseminated sulfide samples have S/Se ratios less than 2000, which indicates a S loss. The possibility that some samples show modified S values is further supported by S isotopes.

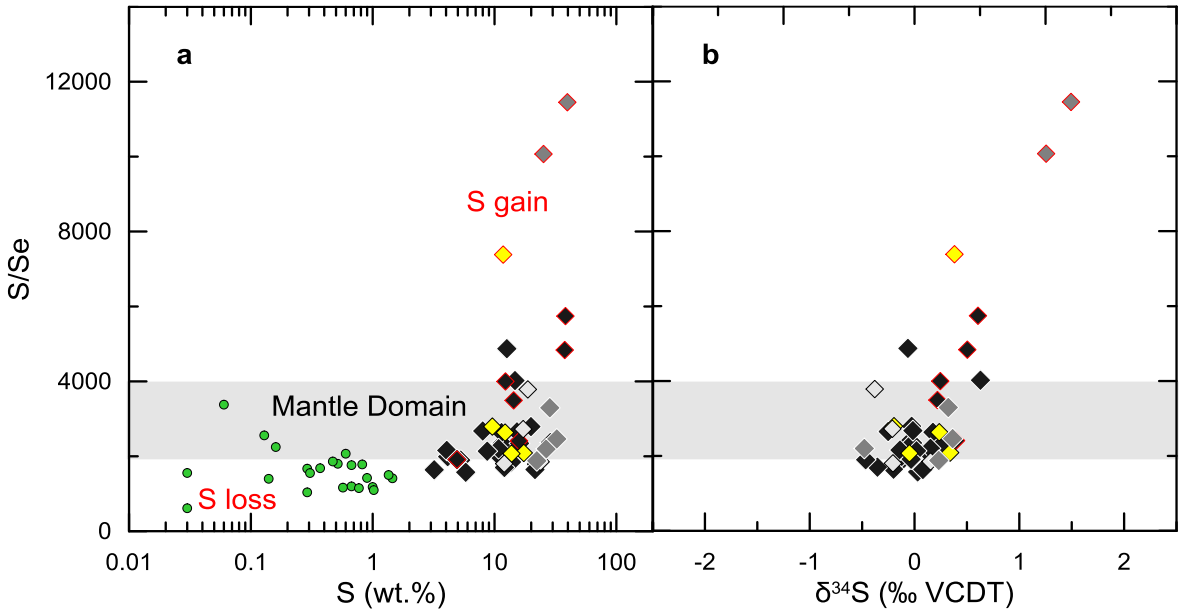

Figure 2.8 Binary diagram of S/Se ratio versus (a) S; and (b) δ34S. Note that pyrite-rich samples from Baker Zone have high S/Se ratios and δ34S values probably indicating S addition. In contrast disseminated sulfides have low S/Se ratios probably indicating S loss. Most sulfide-rich pods plot in the mantle domain indicating that S have neither been added nor lost. See Fig. 2.7 for legend.

Mantle values for $\delta^{34}S$ are around 0 (Ripley and Li, 2003). On a plot of $\delta^{34}S$ versus S/Se, most of the sulfide-rich pods have $\delta^{34}S$ values of -0.5 to 0.5. These data correspond with near-mantle values, suggesting these samples are unmodified and magmatic in origin. Conversely, the Py-rich samples from Baker Zone and one from Roby Zone have higher $\delta^{34}S$ values, in the 0.5 to 1.5 range (Fig. 2.8b).

The Py-rich samples from the Baker Zone may have formed by S addition. However, given the results shown in figures 2.7 and 2.8, other Py-rich samples may not have formed from the addition of S. Two explanations are proposed to account for the excess of Py in the remaining samples. First, the igneous assemblage was oxidized resulting in the formation of Py + Mgt. Secondly, Fe was lost from the igneous assemblage to surrounding silicates. The first explanation may account for the Mgt-rich assemblage. To investigate the origin of the Mgt from the sulfide-rich pods, the trace element contents of the Mgt were studied. Our results suggest that the Mgt is of igneous origin rather than an alteration product (Duran et al. in prep). Therefore, the oxidation model would not apply to the Py-rich assemblage. Consequently, we assume that in Py-rich samples where S has not been added some Fe has been lost from the sulfides to the surrounding silicates. This would explain why these Py-rich samples lie below the 1:1 line on the Pearce plot. In contrast, samples from the Po–Pn-rich and the Ccp-rich assemblages plot on the 1:1 line, which indicate that neither Fe nor S was mobile.

If the sulfides in these rocks represent the crystallization products of magmatic sulfide liquids, then the concentrations of the chalcophile elements should correlate with the S content of the rocks. Because S appears to have been mobile in some samples, Se is used as a proxy for S. For Ni and Co a positive correlation can be observed above 1 ppm Se (Fig. 2.9a, b). Below 1 ppm Se, the silicate minerals have an influence on the Ni and Co contents (up to 500 ppm Ni in silicates). For Cu there is a correlation with Se in the disseminated and patches of interconnected sulfides (between 1 and 10 ppm Se). However, the net-textured and massive sulfides are distributed on both sides of the trend, with Ccp-rich samples above and Po–Pn-rich, Py-rich and Mgt-rich samples below (Fig. 2.9c). The co-variance of Ni, Co and Cu in disseminated and patches of interconnected sulfides and the decoupling of Cu from Ni and Co in the net-textured and massive sulfides have been observed at other magmatic sulfide deposits, e.g., Duluth (Hauck et al. 1997). These correlations arise because the disseminated sulfides represent frozen sulfide liquids whereas the massive sulfides represent crystal fractionation products of sulfide liquids. Nickel and Co have partition coefficients into the first sulfide to crystallize (MSS) of close to 1. Therefore Ni and Co correlate with the Se content of the rocks and with each other (Fig. 2.9a, b). Copper does not partition into MSS and consequently early sulfide cumulates are Cu-poor whereas the later crystallization products are Cu-rich (Fig. 2.9c). Similarly, the later crystallization products are enriched in Ag, Cd and Zn, evidenced by the relatively high degree of correlation between these elements and Cu (Fig. 2.10).

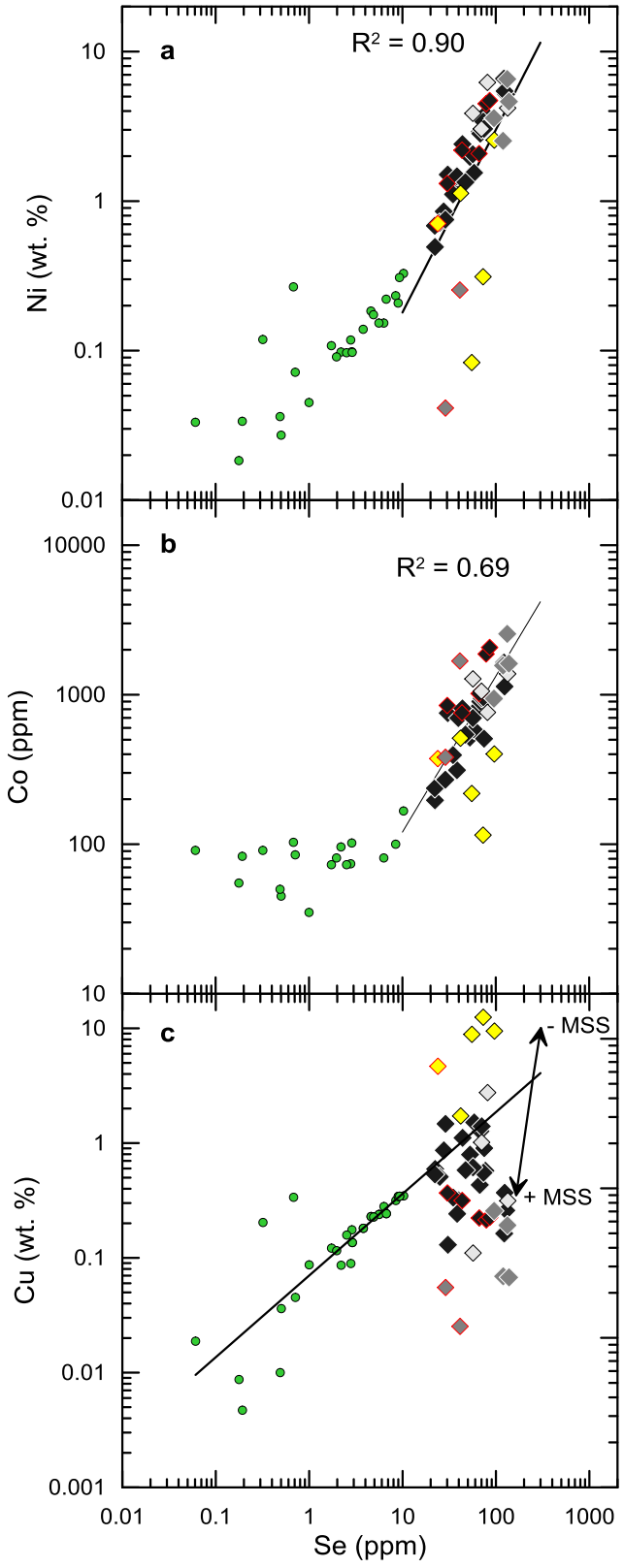
a
R² = 0.90
Ni (wt. %)
10
1
0.1
0.01
b
R² = 0.69
Co (ppm)
10000
1000
100
10
c
- MSS
+ MSS
Cu (wt. %)
10
1
0.1
0.01
0.001
0.01
0.1
1
10
100
1000
Se (ppm)

Figure 2.9 Binary diagrams of Se versus (a) Ni; (b) Co; and (c) Cu. Note the co-variance of Ni, Co and Cu with Se for disseminated sulfides. For sulfide-rich pods Ni and Co follow the trend of disseminated sulfides but there is a decoupling of Cu from Se due to MSS crystal fractionation as shown by the MSS vector. See Fig. 2.7 for legend.

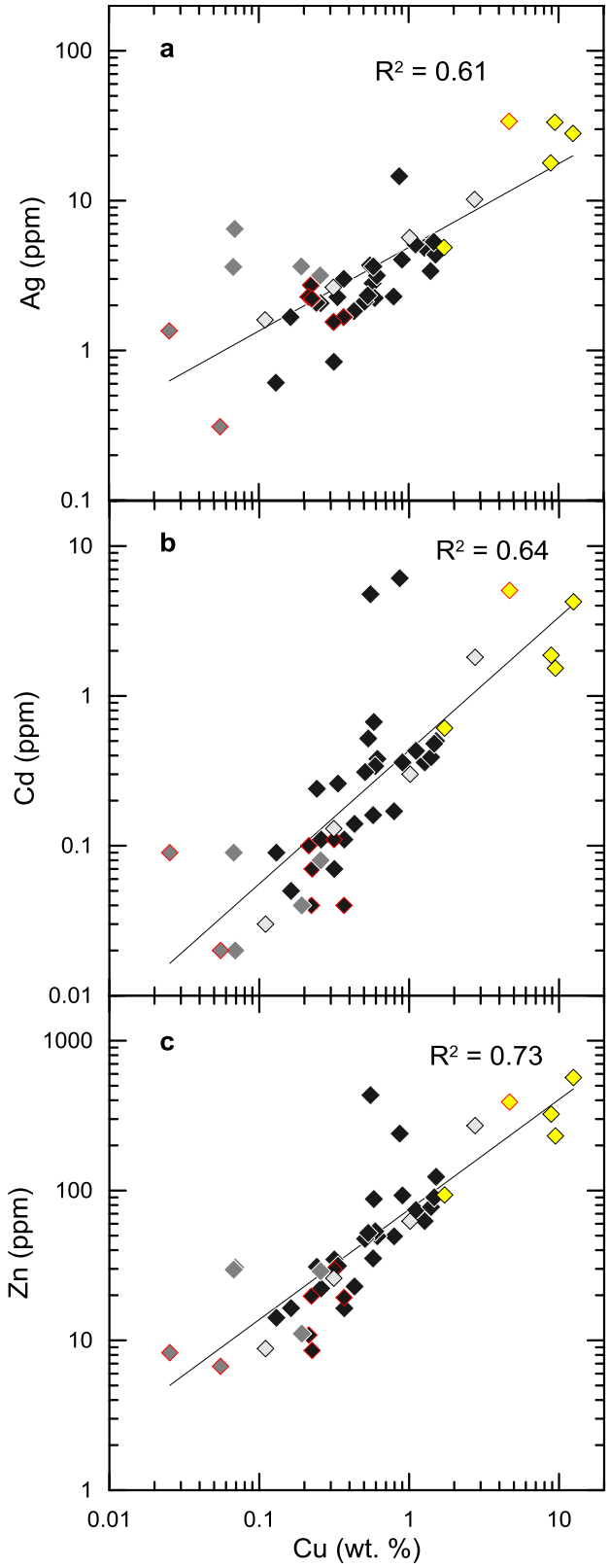
a
R² = 0.61
Ag (ppm)
100
10
1
0.1
b
R² = 0.64
Cd (ppm)
10
1
0.1
0.01
c
R² = 0.73
Zn (ppm)
1000
100
10
1
0.01
0.1
1
10
Cu (wt. %)

Figure 2.10 Binary diagrams of Cu versus (a) Ag; (b) Cd; and (c) Zn. Note the strong correlation between these elements. The Cu-rich samples are enriched in Ag, Cd and Zn as predicted by the MSS fractionation model. See Fig. 2.7 for legend.

Given these results, Ni, Co, Cu, Ag, Cd and Zn do not appear to have been mobile with the formation of Py. However, we could expect Py-rich samples to be enriched or depleted in some mobile elements usually incompatible into sulfide cumulates, i.e., semi-metals (Lui and Brenan 2012). The Py-rich samples are not measurably depleted in any elements relative to other samples. Elements such as Hg, Sb and Sn are below or close to detection limits. Therefore it is not possible to say whether or not they have been affected by alteration. In contrast Py-rich samples are slightly enriched in As, Bi and Mo, which is particularly apparent on a plot of As versus Bi (Fig. 2.11). This indicates that some elements have been introduced into Py during its formation, probably by fluids.

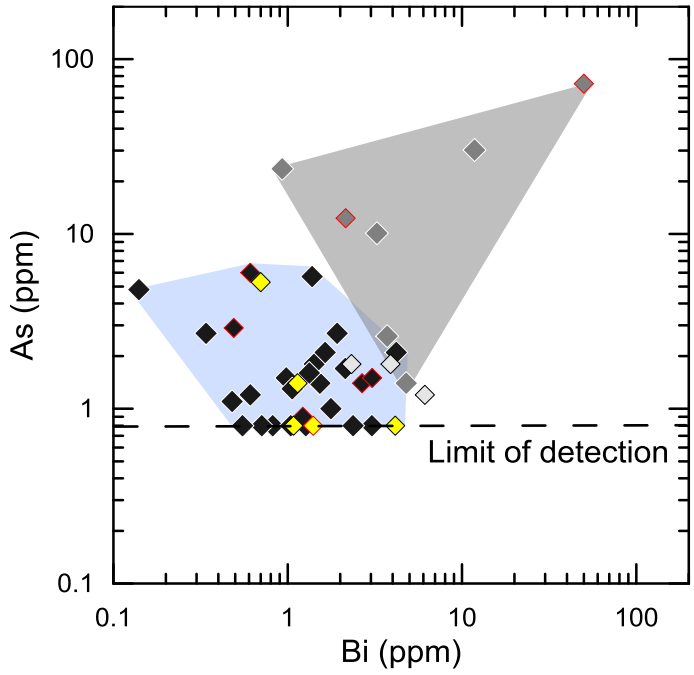

Figure 2.11 Binary diagram of As versus Bi. Although there is no correlation, note that pyrite-rich samples (grey field) are enriched in Bi and As relative to other samples (light blue field). See Fig. 2.7 for legend.

2.6.3.2 PLATINUM-GROUP ELEMENTS

Considering the Py-rich samples represent an altered igneous assemblage, it is necessary to assess whether PGE have been mobile with alteration prior to considering igneous processes. In general, IPGE + Rh are considered relatively immobile elements under hydrothermal conditions (Wood 2002) and partition sub-equally into MSS (Fleet et al. 1993; Li et al. 1996; Barnes et al. 1997b; Mungall et al. 2005, Lui and Brenan, 2012). Therefore, we may plot IPGE and Rh versus one another to illustrate the influence of crystal fractionation. All the sulfide-rich pods, regardless of their degree of alteration, exhibit strong correlations between IPGE and Rh. These correlations are particularly apparent between the pairs Os and Ru, and Ir and Rh (Fig. 2.12a, b). The strong correlations between IPGE and Rh arise because these elements have been concentrated into MSS during crystal fractionation of sulfide liquids.

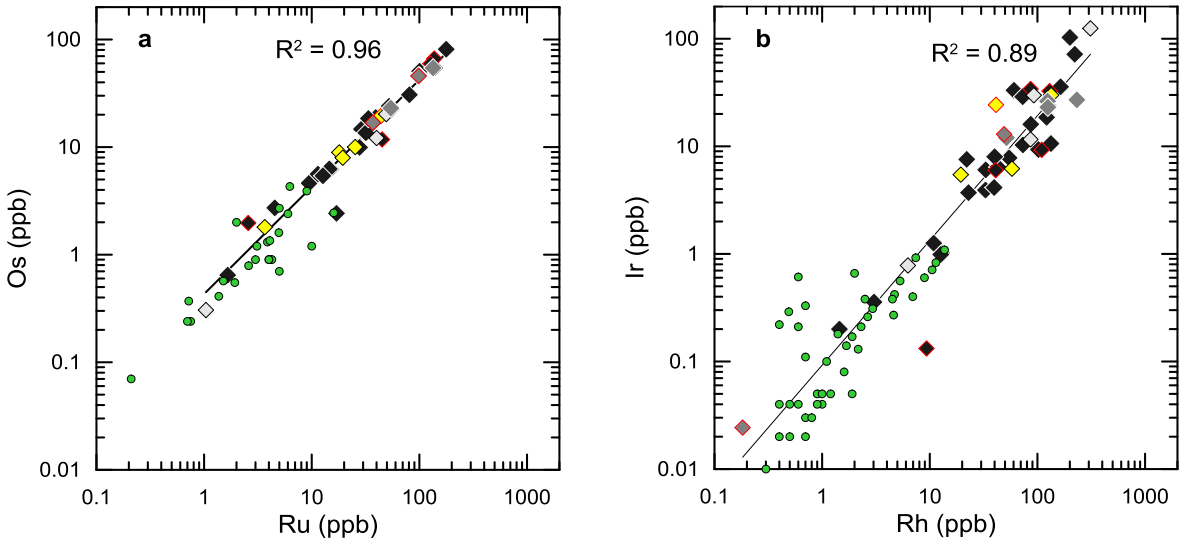

Figure 2.12 Binary diagrams of (a) Os versus Ir; and (b) Ir versus Rh. These diagrams show two processes. In the disseminated samples the correlation is because both in each diagram have been collected by a sulfide liquid. In the sulfide-rich samples there is the additional effect of the MSS accumulation. See Fig. 2.7 for legend.

Conversely, Pd and Pt do not correlate with IPGE and Rh. This feature may result either from incompatibility of Pd and Pt into MSS (Fleet et al. 1993; Li et al. 1996) or from preferential remobilization of Pd and Pt relative to IPGE and Rh under hydrothermal conditions (Wood 2002). In the case where Pd and Pt have been mobile with alteration, the most altered assemblage should be either enriched or depleted in these elements relative to igneous assemblage. However, we did not observe such relationships (Fig. 2.13). Furthermore, Pd is thought to be more mobile than Pt (Wood 2002; Barnes and Liu 2012). In the studied samples there is a reasonably strong degree of correlation between Pd and Pt in sulfide-rich pods. This should not be observed if one element had been preferentially mobilized over another (Fig. 2.13). These observation suggest that the distribution of Pd and Pt was controlled by the crystal fractionation of sulfide liquids.

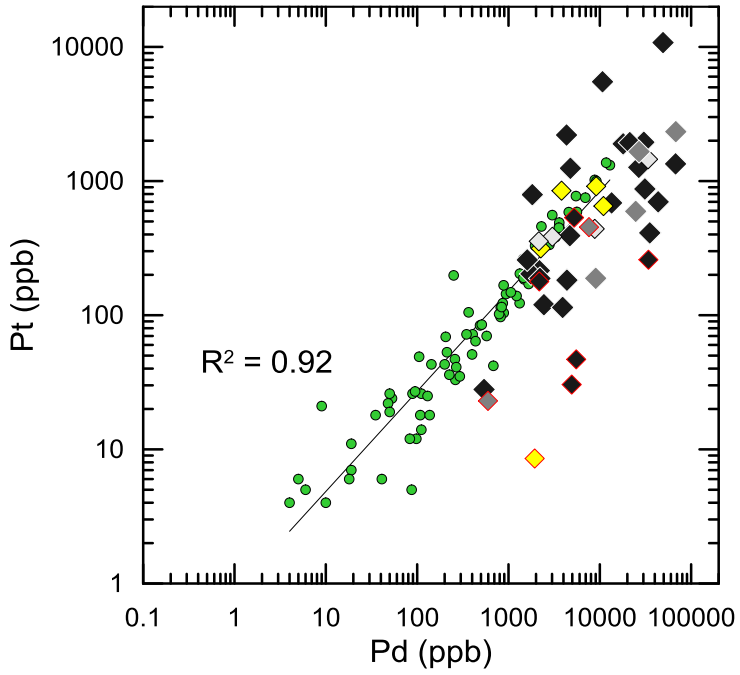

Figure 2.13 Binary diagrams of Pd versus Pt. Note the strong correlation between these elements, especially in disseminated sulfides, indicating that neither of these elements has been preferentially mobilized. Also note that there is no correlation between the Pt-Pd content and the sulfide mineralogy of the sulfide-rich pods. See Fig. 2.7 for legend.

Considering that the Ccp-rich assemblage represents the product of crystallization from fractionated sulfide liquids, it might be anticipated that Pd and Pt would be enriched in these samples. In many ore deposits e.g., Sudbury and Noril'sk (Li et al. 1992; Zientek et al. 1994) the Cu-rich ore is enriched in Pd, Pt and many semi-metals. However, in our samples plots of Pd and Pt versus Cu show that there is no correlation between these elements (Fig. 2.14). Further, the Ccp-rich samples are not enriched in Pd and Pt relative to the Po–Pn-rich, Py-rich and Mgt-rich assemblages. This suggests that the Ccp-rich assemblage may not represent the fractionated liquid. Alternatively, the Ccp-rich assemblage may represent cumulus ISS. It is believed that elements such as Ag, Cd and Zn partition into ISS whereas Pd, Pt and the semi-metals do not (Liu and Brenan 2012), and instead are thought to concentrate in the residual liquids (Barnes et al. 2006; Holwell and McDonald 2010). In Cu-rich ores possibly representing fractionated sulfide liquids, these elements are generally found in the form of accessory minerals among the Ccp grains (Dare et al. 2014). The similar amount of Pd and Pt in the Ccp-rich assemblage relative to Po–Pn-rich, Py-rich and Mgt-rich assemblages may be explained by the residual liquids having been squeezed out of the ISS.

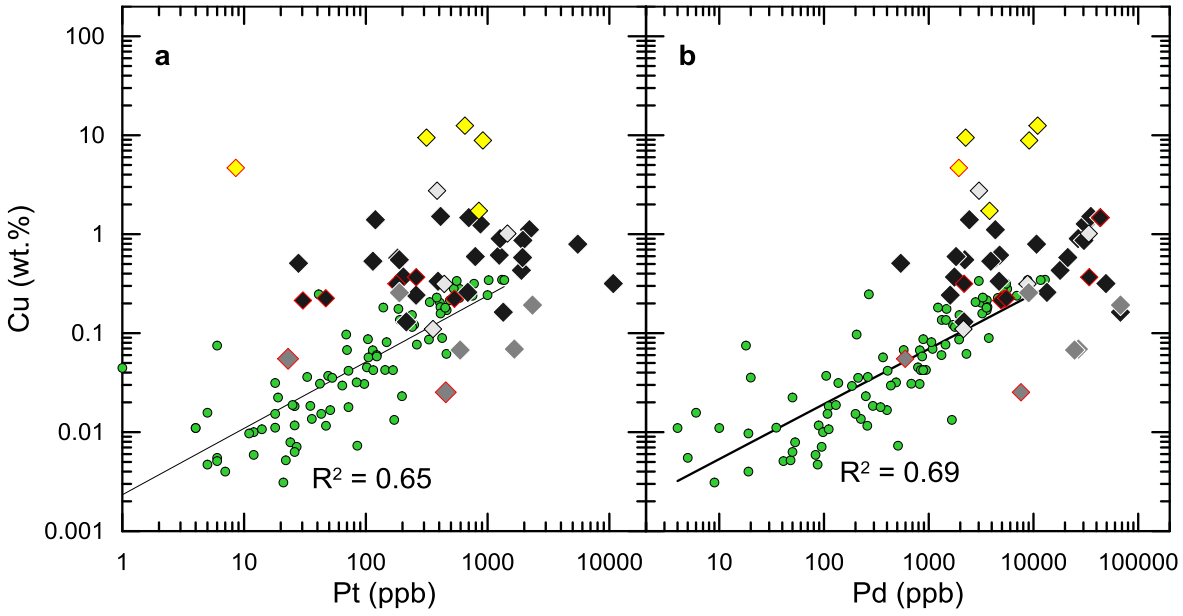

Figure 2.14 Binary diagrams of (a) Pt; and (b) Pd versus Cu. Note that there is no correlation for the sulfide-rich pods indicating that chalcopyrite-rich samples are not enriched in Pt and Pd as there should have been if the Cu-rich samples represented a fractionated liquid. In contrast there is a relatively strong degree of correlation for the disseminated sulfides indicating that they represent sulfide liquid compositions. See Fig. 7 for legend.

2.6.3.3 PRIMITIVE MANTLE NORMALIZED PATTERNS

Assuming that Ni, Cu and PGE have not been mobilized, we plotted on figure 2.15 all our samples recalculated to 100% sulfides using the equation proposed by Barnes and Lightfoot (2005). Based on the degree of fractionation between IPGE + Rh and Pt + Pd, two populations of MSS may be characterized. First, we identified primitive MSS, having higher IPGE values, negative Pt anomalies typical of early MSS accumulation (Barnes and Naldrett 1986; Barnes et al. 1988; Barnes 2004) and lower Pd values. Secondly, we identified evolved MSS, having lower IPGE values, no Pt anomaly, and higher Pd values. Primitive mantle normalized multi-element diagrams of Ccp-rich samples interpreted to represent cumulus ISS show a similar shape except for Cu and Ni values. Even though we would expect that cumulus ISS should be depleted in IPGE compared with cumulus MSS, similar values are observed (Fig. 2.15), for reasons not clearly understood.

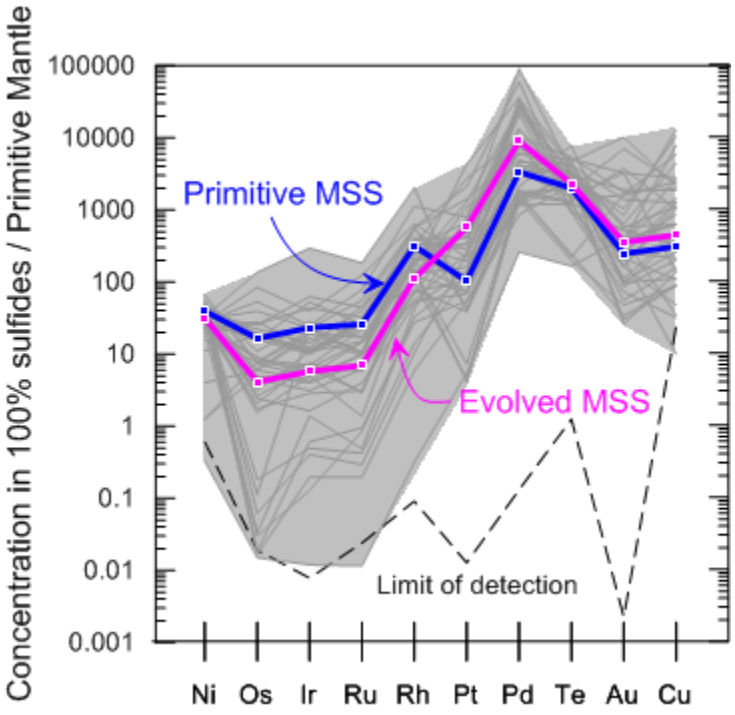

Figure 2.15 Primitive mantle normalized metal patterns of sulfide-rich pods. Primitve-mantle values are from Lyubetskaya and Korenaga (2007). Data are recalculated to 100% sulfides using the equation from Barnes and Lightfoot (2005). Note that primitive MSS signature is characterized by Pt negative anomaly and higher IPGE+Rh and lower Pt and Pd values relative to evolved MSS.

2.7 DISCUSSION

In the light of the results presented in sections 2.6.1–2.6.3, any model for the formation of sulfide-rich pods at LDI should consider the following evidence: (1) the location of the pods within the intrusion along co-magmatic structures and their textural features; (2) the cumulus MSS geochemical signature of rocks with more than 5 wt. % whole-rock S; (3) the presence of primary igneous assemblage and associated textures overprinted by Py; and (4) the lack of correlation between the geochemistry and the degree of alteration.

Although the location of the pods and the presence of altered assemblages may suggest hydrothermal processes at first glance, our investigation indicates a magmatic origin for the sulfide-rich pods. Prior to proposing a genetic model for the origin of the sulfide-rich pods we discuss how it might be possible for denser high-temperature immiscible sulfide liquids to be accumulated across the stratigraphy. We also consider the processes that influenced the composition of the sulfide liquids. We then assess the effects of alteration and the role of fluids during late-magmatic evolution. Based on PGE geochemistry, we model MSS fractionation from sulfide liquids and we attempt to explain the origin of PGE fractionation. Then we compare our results to other Ni-Cu-PGE deposits. Lastly, following our model we propose some suggestions for exploration at LDI and in potential LDI-like deposits.

2.7.1 EMPLACEMENT OF SULFIDES

It is commonly accepted that sulfide-rich mineralization associated with mafic and ultramafic intrusions does not result from equilibrium cotectic precipitation from silicate magma, and it therefore requires transportation and/or mechanical accumulation of sulfides (Barnes 2007). Depending on the processes leading to their final deposition, sulfides acquire particular textures and chemical compositions. Considering these criteria, several models have been proposed for the origin of sulfide-rich mineralization over a wide variety of Ni-Cu-PGE ore deposits.

Sulfide liquids may be collected by gravity due to their high density (4200 to 4500 kg/m^3; Dobson et al. 2000) compared with mafic silicate liquids. In this case they should be present towards the base of the intrusion, consisting of Po–Pn–Ccp and having compositions in equilibrium with a mafic silicate liquid. If the intrusion was deformed during emplacement, then the sulfide liquids could have been mobilized to low pressure zones in the intrusion and across the stratigraphy. If the intrusion underwent deformation after cooling, the sulfides could have undergone ductile plastic flow (Duuring et al. 2007; Collins et al. 2012; Mukwakwami et al. 2013). During post-magmatic evolution, the sulfides could have undergone metamorphic sulfide anatexis (Frost et al. 2002; Tomkins et al. 2006) or hydrothermal mobilization (Keays and Jowitt 2013).

Based on our investigation, sulfide liquid mobilization during co-magmatic deformation seems to be the most likely scenario at LDI. Though the possibility that a denser sulfide

liquid may migrate over significant distances through a relatively viscous mafic magma might seem unreasonable at first, several factor lead us to consider it probable. First, sulfide liquids have lower viscosities (around 0.01 Pa/s; Dobson et al. 2000) and lower solidus temperatures (Dutrizac 1976) than mafic silicate liquids. Second, when the silicate rocks were almost consolidated, sulfides could represent a non-negligible proportion of the total liquid phases present (Mungall 2002). This is supported by the fact that solidus temperatures of mineral assemblages similar to those of the Mine Block Intrusion might be around 950–1150°C (Yoder and Tilley 1962), whereas an evolved sulfide liquid enriched in Cu does not completely consolidate until ~880°C (Dutrizac 1976). Additionally, increase of Cu content in sulfide liquids during crystal fractionation decreases viscosity and surface tension of sulfide liquids which may promote their mobility (Ebel and Naldrett 1996).

Presence of volatiles in silicate magmas (e.g., H_2O; Hamilton et al. 1964) and in sulfide liquids as well (e.g., halogens; Mungall and Brenan 2003; Wykes and Mavrogenes 2005) lowers the solidus temperatures of both mafic silicate liquids and sulfide liquids but more importantly it lowers their respective viscosities and therefore facilitates their mobility. There is evidence for the presence of volatiles in LDI magmas (Barnes and Gomwe 2011; Hanley and Gladney 2011; Sisha et al. 2014), and we may infer that sulfide liquids derived from LDI magmas may have hosted some dissolved volatiles.

The weight of the overlying cumulates could also have provided a powerful force to displace both the remaining interstitial silicate liquid and any sulfide liquid present, as compaction and liquid extraction continued (Mungall 2002). The presence of adcumulate

textures in fresh LDI rocks observed by Gomwe (2008), and the 10–12 km depth of intrusion estimated by Hanley and Gladney (2011) attest to the efficiency with which interstitial silicate liquid was expelled during compaction. Thus, compaction combined with co-magmatic deformation would have allowed efficient sulfide liquid mobility into zones of lower stress such as fractures, faults, shear zones, embayments and all dilation zones across the stratigraphy (Fig. 2.16).

Once the lower stress areas within the silicate magma solidified, sulfide liquid was trapped and accumulated into the different lithological units. The presence of patches of interconnected sulfides and net-textured sulfides indicates that the intrusion solidified prior to complete accumulation of sulfide liquids. The position of the sulfide-rich samples along major structures and in rocks that formed at different stages of magma differentiation is consistent with sulfide-rich pods having been emplaced as liquid while the Mine Block Intrusion was deformed. The evidence of high-temperature deformation within silicate minerals and the lack of features from ductile plastic flow further support this idea.

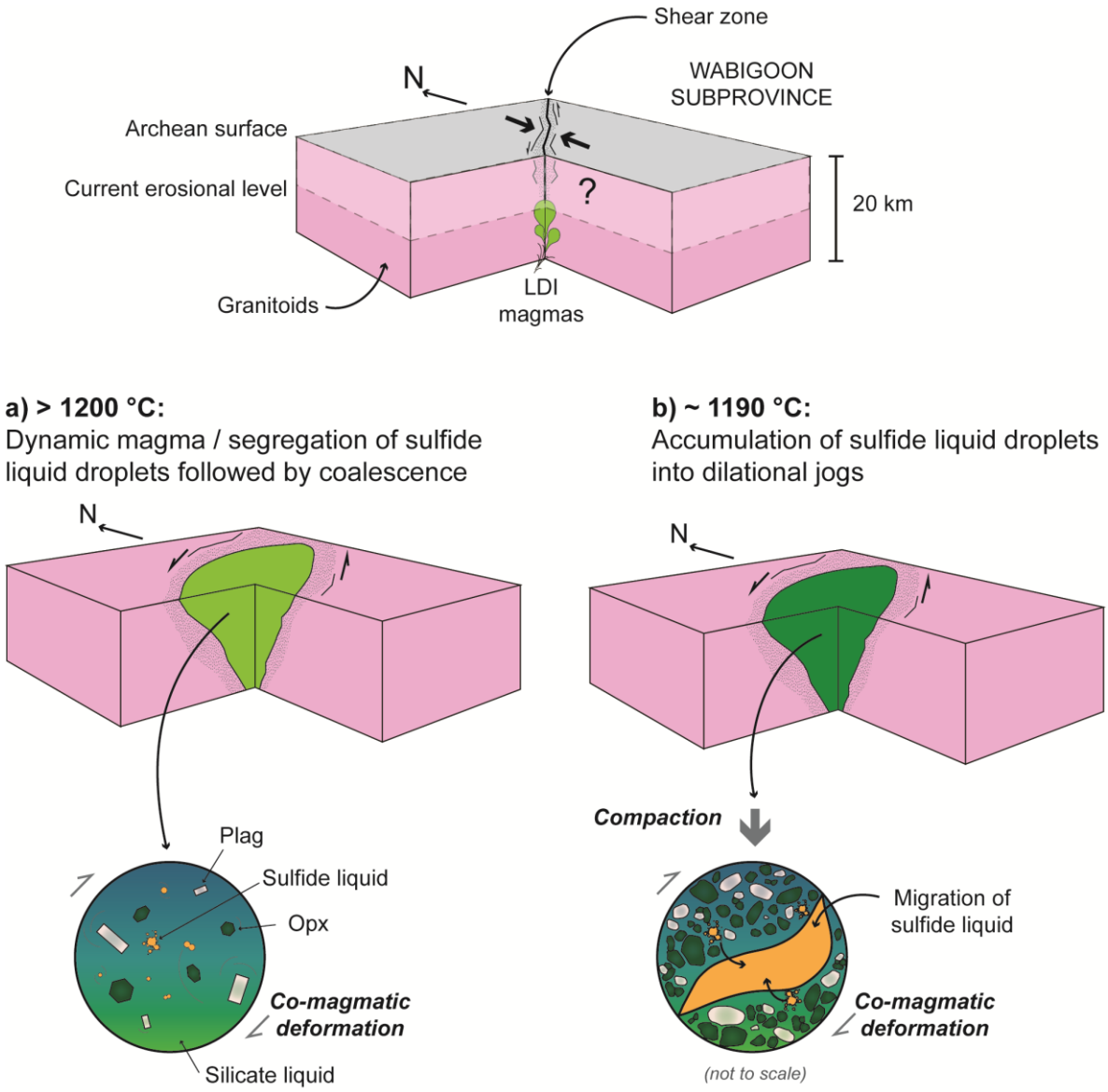

Figure 2.16 Schematic model of the emplacement history of Lac des Iles sulfide-rich pods. (a) Segregation of sulfide liquid droplets from silicate liquid. Dynamic environment leads to scavenging of chalcophile elements by sulfide liquids and coalescence of the droplets. (b) Migration of the sulfide liquid a high temperatures in the presence of stress differences results in its accumulation into zones of lower pressure.

2.7.2 CRYSTAL FRACTIONATION OF SULFIDE LIQUID

Experimental work (Fleet et al. 1993; Li et al. 1996; Barnes et al. 1997b; Mungall et al. 2005, Lui and Brenan, 2012) indicates that Fe, IPGE, Rh, Mo, and Re partition into the first mineral to crystallize from a magmatic sulfide liquid (MSS). At high temperature, Ni and Co are slightly incompatible with MSS but as the temperature falls they become slightly compatible and concentrate into MSS. Copper, Pt, Pd, Au, Ag and most of the semi metals partition into the liquid. Once ISS crystallizes from the liquid, Cu, Ag, Zn and Cd partition into the ISS whereas Pt, Pd, Au and the semi-metals remain in the liquid. Thus, in the ultimate stages of sulfide liquid fractionation the residual liquid is enriched in Pt, Pd, Au and semi-metals, which may have a very low solidus temperature and be capable of migrating away from cumulus ISS (Hanley 2007; Helmy et al. 2007, 2013; Tomkins 2010; Dare et al. 2014).

High Ni/Cu ratios owing to Po-Pn assemblages and equal distribution of IPGE and Rh reflect MSS crystallization from fractionating sulfide liquids. The Ccp-rich samples found at the edges of some pods are not enriched in Pd and Pt relative to Po-Pn-rich assemblages: this lack of enrichment strongly suggests the migration of residual liquids during accumulation of ISS. The presence of cumulus ISS provides further evidence of sulfide liquid crystal fractionation. Thus, crystallization of sulfide-rich pods is consistent with a model of crystal fractionation of sulfide liquids (Fig. 2.17). Nonetheless this model does not

account for the excess of Py and Mgt observed in some pods, and it requires post-cumulus modifications of the igneous assemblage.

a) ~ 1190 °C:

Zonation of the pods by sulfide liquid crystal fractionation
Oxygen diffusion out of sulfide liquid and early crystallization of MSS

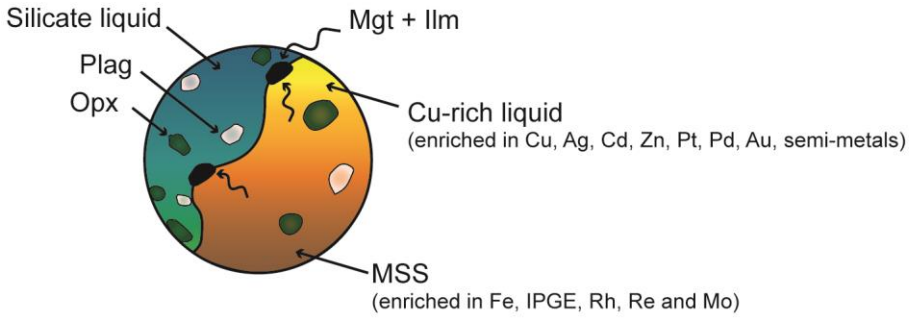

b) ~ 880 °C:

Late crystallization of ISS from Cu-rich liquid and partitioning of Pt, Pd, Au and semi-metals in residual liquid

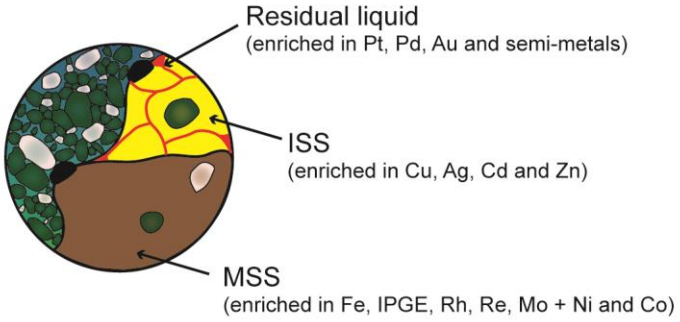

c) < 880 °C:

Residual liquid squeezed out of the sulfide-rich pods

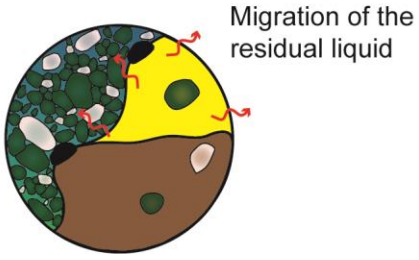

Figure 2.17 Schematic model of the crystallization history of Lac des Iles sulfide-rich pods. (a) Crystallization of MSS enriched in Fe, IPGE, Rh, Re and Mo from sulfide liquids and formation of Cu-rich liquid enriched in Ag, Cd, Zn, Pt, Pd, Au and semi-metals. Oxygen diffuses out of the sulfide liquid and reacts with the silicate liquid to form magnetite + ilmenite. (b) Crystallization of ISS from Cu-rich liquid and formation of residual liquids enriched in Pt, Pd, Au and semi-metals. Nickel and Co partition into MSS. (c) Migration of residual liquids away from sulfide cumulates. The residual sulfide liquid is expelled because the already crystallised material is compacted.

2.7.3 REPLACEMENT OF IGNEOUS ASSEMBLAGE

Although a sulfide liquid may crystallize up to several percent of Py and Mgt (Craig and Kullerud 1969; Naldrett 1969; Kress et al. 2008), the large amounts of Py and Mgt observed in many samples cannot be explained solely by crystallization from an immiscible magmatic sulfide liquid. The primary sulfide assemblage in PGE deposits associated with mafic and ultramafic rocks consists predominantly of Po–Pn–Ccp with minor Py and Mgt (Naldrett 2004 and references therein), whereas assemblages containing mainly Py, other sulfide species or Mgt are attributed to late-magmatic processes such as metamorphism and deuteric/hydrothermal alteration (Craig 1973; Konnunaho et al. 2013). At LDI, there is evidence for considerable late-magmatic modifications of the sulfide-rich pods, as indicated by the predominance of Py and the preservation of primary Po–Pn–Ccp assemblage displaying igneous textures in some samples.

Several sulfide assemblages have also been described in the disseminated ore at LDI (Talkington and Watkinson 1984; Hinchey and Hattori 2005; Djon and Barnes 2012). A typical primary igneous assemblage composed of Po–Pn–Ccp ± Py has been observed in the least altered rocks whereas secondary assemblages composed of Ccp–Py–Pn and Ccp–Py–millerite (Mil) have been identified in the more altered rocks. Secondary assemblages that display disequilibrium textures with silicate minerals have been attributed to mineralogical changes in the primary assemblage by Djon and Barnes (2012). Because of the negligible amounts of Mgt in the altered assemblages, the secondary assemblages were

interpreted to have formed by Fe loss from Po and Po+Pn to surrounding silicates, respectively promoting the formation of Py and Py+Mil.

Generally, disseminated sulfides are more susceptible to modification than massive sulfides (Konnunaho et al. 2013) even though enrichment of massive sulfides in secondary Py has been documented in other localities (Seccombe et al. 1981; Collins et al. 2012). This susceptibility arises because disseminated sulfides are more likely to be externally buffered, due to higher surface area-to-volume ratios subject to re-equilibration with circulating fluids. In sulfide-rich pods we did not observe millerite or other Ni-rich sulfides such as vaesite or violarite. The ubiquity of Pn and the absence of Ni-rich sulfides attest that mineral transformation in sulfide-rich pods was not complete and did not affect Pn.

Pentlandite may exsolve from MSS at temperature as low as 230°C, however, coarse Pn requires higher temperature to grow and is more likely to have formed at around 600°C (Kelly and Vaughan 1983), at which temperature we infer Po started to form. The maximum depth of emplacement estimated at 3.2 kbars by Hanley and Gladney (2011) suggests a stability for Py only below 750°C (Craig and Kullerud 1969). According to Naldrett et al. (1967) MSS starts to crystallize at 1190°C. Therefore, Py could either have replaced MSS if replacement began above 600°C (Fig. 2.18a), or Po ± Pn if replacement occurred below 600°C (Fig. 2.18b). The process whereby Py replaced MSS or Po appears to have been by S addition in the Baker Zone but by Fe loss in the Roby Zone and Offset Zone.

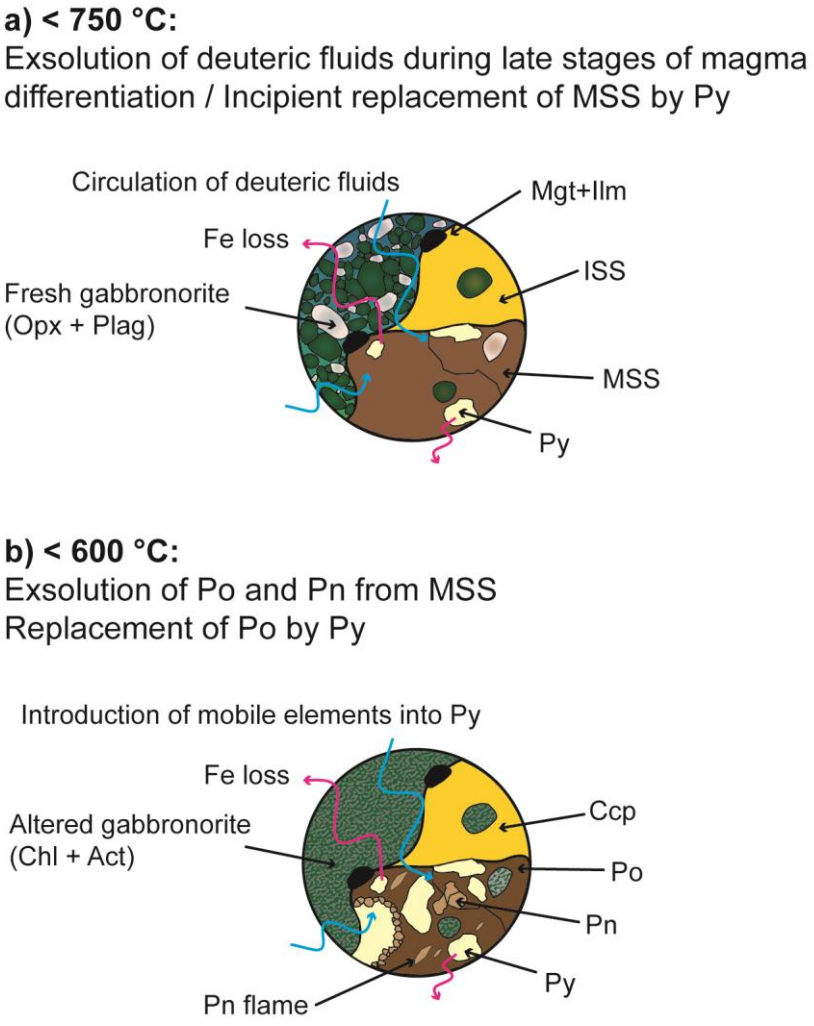

Figure 2.18 Schematic model of the replacement history of the igneous assemblage from Lac des Iles sulfide-rich pods. (a) Deuteric fluids exsolve from silicate magmas during late stages of differentiation and Fe diffuses out of MSS (in Baker Zone S is added). Pyrite starts to replace MSS. (b) MSS exsolves to form pyrrhotite and pentlandite and Fe diffuses out of pyrrhotite (in Baker Zone S is added). Pyrrhotite is replaced by pyrite. Circulating fluids introduce mobile elements such as As and Bi into Py during its replacement of Po.

2.7.4 ROLE OF THE FLUIDS

At LDI, there is evidence for volatile-rich fluid activity as indicated by: the predominance of altered rocks; the presence of varitextured and pegmatitic rocks; the presence of igneous hornblende and biotite in fresh rocks; and the fluid inclusions and halogen geochemistry of apatites (Watkinson et al. 2002; Somarin et al. 2009; Hanley and Gladney 2011; Boudreau et al., 2014; Schisa et al. 2014). The similar compositions of fresh and altered rocks suggests that alteration was most likely promoted by exsolution of deuteric fluids from fractionating water-rich magmas (Barnes and Gomwe 2011). Additionally Hinchey and Hattori (2005) and Djon and Barnes (2012) noticed that Py abundance at LDI increases with the degree of alteration of silicate minerals, suggesting that the sulfide mineralogy was affected by such fluids (Fig. 2.18). Therefore, the destabilization of the silicate-mineral assemblage may have promoted a disequilibrium between sulfides and silicates. This may have promoted Fe diffusion from sulfides towards silicates as a process of re-equilibration. The presence of fluids may have facilitated this reaction.

Given the evidence of such intense fluid activity, one might argue that Pd was introduced by fluids, as Pd is the most soluble PGE (Wood 2002; Barnes and Liu 2012). Therefore, Pd-enrichment compared with other PGE would be a reasonable expectation. However, we did not observe any relationship between Pd-enrichment and the degree of alteration. If Pd was introduced or upgraded in the sulfide-rich pods by fluids, then the most altered samples should be richer in Pd, but this is not the case. Consequently, we suggest that the fluids

possibly responsible for the mineralogical alteration did not contribute to the ore-forming processes. However, mineral replacement reactions could lead to local PGE redistribution, resulting in the presence of PGE in Py (Duran et al. in prep) as well as discrete PGM associated with a secondary assemblage (e.g., Py, chlorite and actinolite).

2.7.5 MODELING OF MSS CRYSTAL FRACTIONATION

To model crystal fractionation of sulfide liquid and sulfide accumulation, some estimate of the compositions of initial sulfide liquids is necessary. In contrast to sulfide-rich pods interpreted as sulfide cumulates, disseminated sulfides from the LDI ore zones more likely represent initial liquids as evidenced by the sub-equal amounts of Po, Pn and Ccp in fresh rocks and Ni/Cu ratios close to unity (Gomwe 2008). Thus, we may compare the median composition recalculated to 100% sulfides of disseminated sulfides and sulfide-rich pods on a primitive mantle normalized basis (Fig. 2.19). However, as outlined in section 2.6.3, disseminated sulfides have experienced some S loss. To allow for the possible S loss from the disseminated sulfides, we corrected their S content based on Se to have S/Se ratios of 3000. Selenium, S and all the PGE were available for eight samples from Gomwe (2008) re-analyzed for PGE by Djon and Barnes (2012), and we used these to calculate the median of disseminated sulfides. Sulfide-rich pods display lower Pt and Pd values than disseminated sulfides, which is consistent with our interpretation of sulfide-rich pods representing cumulates and disseminated sulfides representing initial liquids. However,

sulfide-rich pods display IPGE and Rh values similar to those of the disseminated sulfides. It would be expected that initial liquids display lower IPGE and Rh values. However, Barnes and Lightfoot (2005) show that disseminated sulfides at many deposits have higher PGE concentrations than massive sulfides, possibly due to a greater interaction between the magma and the sulfide droplets that form disseminated ore (i.e., disseminated sulfides have a higher sulfide to silicate ratio: R-factor; Campbell and Naldrett 1979).

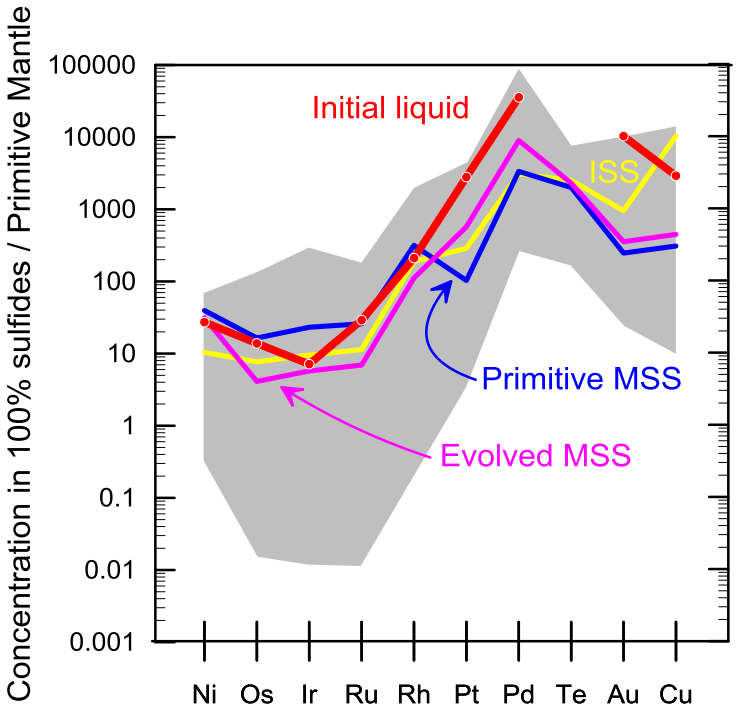

Figure 2.19 Primitive mantle normalized metal patterns of Lac des Iles sulfide-rich pods and initial liquid. Primitve-mantle values are from Lyubetskaya and Korenaga (2007). Data are recalculated to 100% sulfides using the equation from Barnes and Lightfoot (2005). Relative to the liquid, sulfide-rich pods are depleted in Pt, Pd and Au.

To consider the relationship between the various types of sulfides in Ni-Cu deposits, Barnes et al. (1997a) developed a plot of Pd in 100 % sulfides versus Ir in 100% sulfides. In view of the possible S mobility at LDI we used Pd/Se versus Ir/Se. Disseminated sulfides from the ore zones exhibit a fairly high degree of correlation on a plot of Pd/Se versus Ir/Se (Fig. 2.20). This trend may represent the range of initial sulfide liquid compositions. Compositions of the inferred liquids may be modelled by varying the R-factor. Sulfides with low Pd/Se and Ir/Se ratios formed at low R-factor, whereas sulfides with high Pd/Se and Ir/Se ratios formed at high R-factor. Most of the sulfide-rich pods plot below the trend representing the initial liquid compositions with Ir being enriched relative to Pd, suggesting that they formed by accumulation of MSS from the initial liquids. Only one sample plots above the trend where Pd is enriched relative to Ir and that could represent the fractionated liquid. Therefore, the fractionated liquid may have been relocated elsewhere.

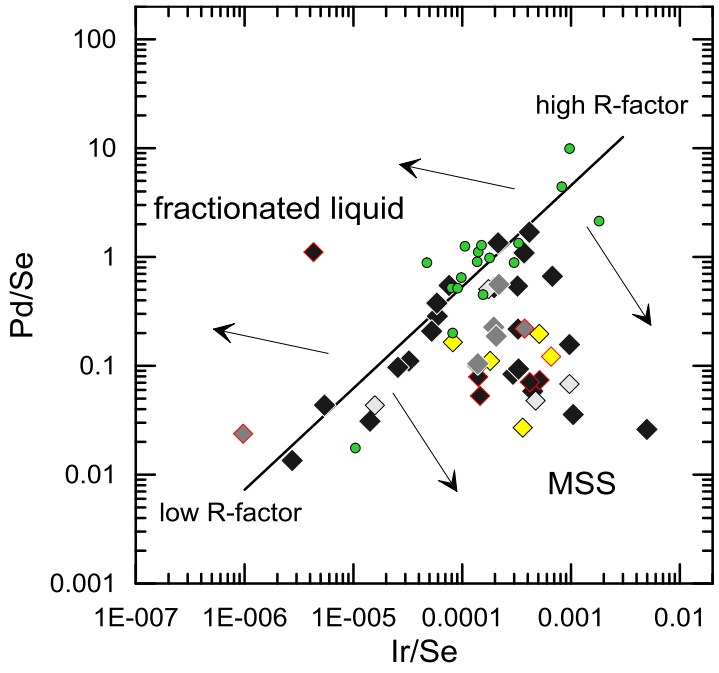

Figure 2.20 Binary diagram of Pd/Se versus Ir/Se. The composition of disseminated sulfides represents the composition of the initial liquids and can be modelled by varying the R factor. The composition of sulfide-rich pods can be modelled by crystal fractionation of MSS from the initial liquids. See Fig. 7 for legend.

2.7.6 ORIGIN OF PGE FRACTIONATION

In recent years, pioneering ideas arose from similar observations of fractionation of Pt-Pd from IPGE-Rh. These ideas related to: formation of Pt-Fe alloys in the mantle (Kepezhinskas and Defant 2001); melting conditions of the mantle (Maier and Barnes 2004; Mungall and Brenan 2014); crystallization of IPGE alloys (Peck et al. 1992) or Pt-Fe alloys (Park et al. 2013) from magmas; partitioning of IPGE into chromite (Pagé et al. 2012; Park et al. 2012) or olivine (Holwell et al. 2011); early crystallization of sperrylite in As-rich system (Hanley 2007; Dare et al. 2010; Helmy et al. 2010); crystal fractionation of MSS (Barnes and Naldrett 1986; Barnes et al. 1988; Barnes 2004); and post-magmatic modifications by fluids (Su and Lesher 2012; Boudreau et al. 2014).

Formation of alloys prior to S saturation of magmas would drastically decrease the budget of PGE available for scavenging by sulfide liquids, which should be reflected in the composition of initial liquids. Partitioning of IPGE into chromite or olivine could explain the high Pd/Ir ratios but not the high Pd/Pt ratios. Early crystallization of sperrylite does not apply at LDI owing to the low content of As. Post-magmatic modifications would imply a difference in composition between the most and the least altered samples, which we do not observe. Further, post-magmatic modifications alone cannot explain the differences between disseminated sulfides and sulfide-rich pods. A likely explanation might be that the initial sulfide liquids were evolved liquids slightly depleted in Ir and strongly enriched in Pd and to some extent enriched in Pt. Given these considerations, sulfide cumulates may

have inherited this signature from their parental sulfide liquids. This explanation might be supported by evidence that several steps of MSS removal from the liquid would generate depletion in Ir and enrichement in Pd + Pt (Ebel and Naldrett 1997).

The fact that we observe a range of MSS signatures, from primitive to evolved, is consistent with a multistage model of MSS removal, and could imply the presence of more primitive cumulates at depth as is proposed by Barnes and Gomwe (2011). To avoid the influence of R-factor and to model evolution of MSS we used a plot of Pd/Ir versus Rh/Pt (Fig. 2.21). Sulfide-rich pods show a relatively strong degree of correlation with sulfides having high Rh/Pt and low Pd/Ir ratios representing primitive accumulation, and sulfides having low Rh/Pt and high Pd/Ir ratios representing evolved accumulation.

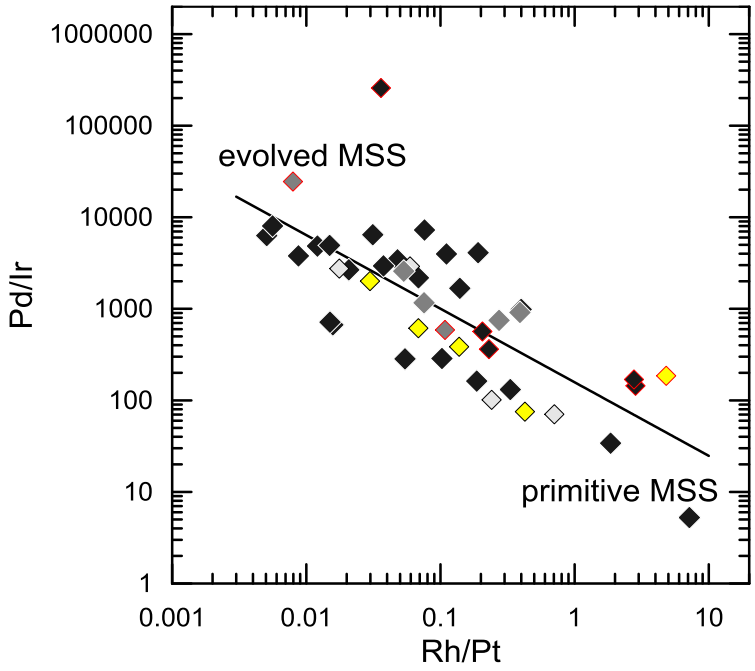

Figure 2.21 Binary diagram of Pd/Ir versus Rh/Pt. The composition of sulfide-rich pods represents the evolution of MSS. Primitive MSS has high Rh/Pt and low Pd/Ir ratios whereas more evolved MSS has low Rh/Pt and high Pd/Ir ratios. See Fig. 7 for legend.

2.7.7 COMPARISON WITH MASSIVE SULFIDES FROM OTHER PGE DEPOSITS

Although LDI differs in many ways from other Ni-Cu-PGE deposits, we compared median compositions of primitive and evolved MSS with some better-known sulfide-rich mineralization from Ni-Cu-PGE deposits that display similar aspects. These deposits include: the Portimo Complex (Finland) which has rocks with similar textures to LDI, i.e., varitextured rocks (Iljina 1994); Aguablanca (Spain) which is emplaced in an arc setting and hosts subvertical semi-massive ore within the intrusion (Piña et al. 2008); and Noril'sk (Russia) which has Pd-rich sulfides (Zientek et al. 1994). The primitive mantle normalized metal patterns in figure 2.22 show the median compositions of MSS from Portimo, Aguablanca and Noril'sk, and the Cu-rich liquid from Noril'sk. The sulfide-rich pods from LDI resemble Portimo, Aguablanca and Noril'sk MSS in terms of Ni, IPGE, Pt, and Au patterns, with a similar but smaller Pd peak. The Pd and Te concentrations of the LDI sulfide-rich pods MSS most closely resemble Noril'sk Cu-rich deposits. The similarities between LDI sulfide-rich pods and other massive sulfides from magmatic Ni-Cu-PGE deposits are consistent with our interpretation.

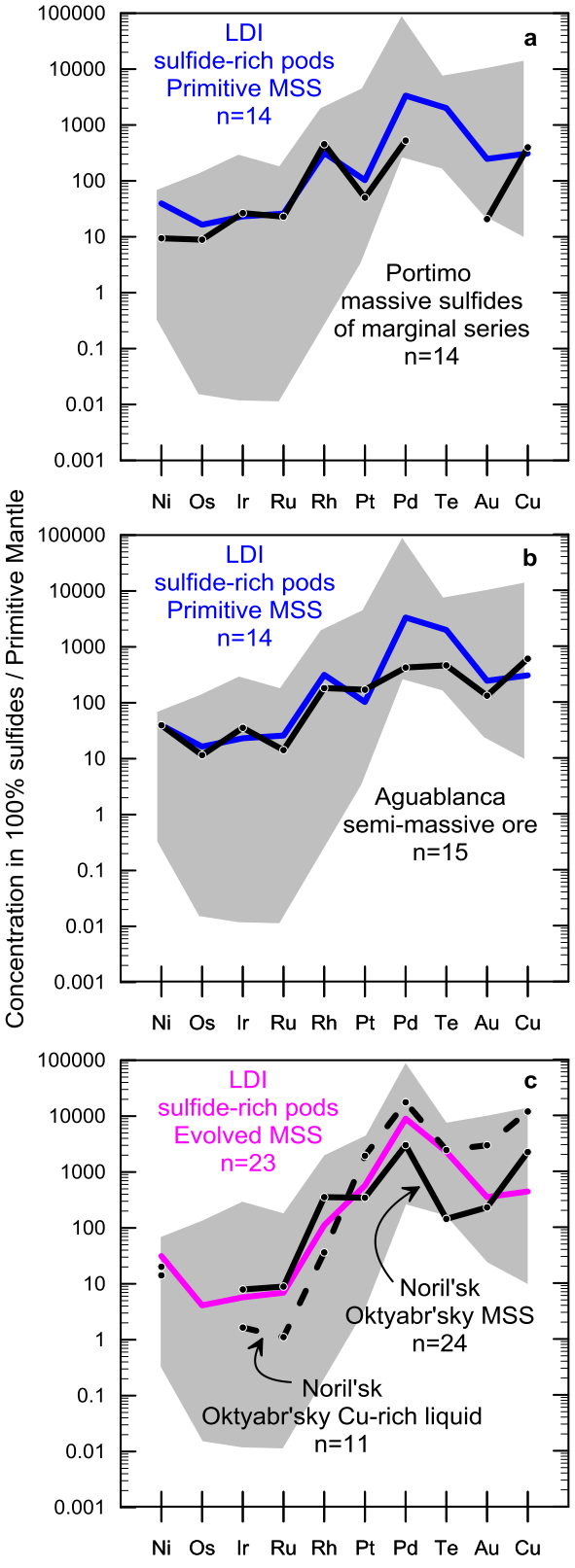
Concentration in 100% sulfides / Primitive Mantle
100000
10000
1000
100
10
1
0.1
0.01
0.001
Ni Os Ir Ru Rh Pt Pd Te Au Cu
a
LDI
sulfide-rich pods
Primitive MSS
n=14
Portimo
massive sulfides
of marginal series
n=14
b
LDI
sulfide-rich pods
Primitive MSS
n=14
Aguablanca
semi-massive ore
n=15
c
LDI
sulfide-rich pods
Evolved MSS
n=23
Noril'sk
Oktyabr'sky MSS
n=24
Noril'sk
Oktyabr'sky Cu-rich liquid
n=11

Figure 2.22 Primitive mantle normalized metal patterns of Lac des Iles sulfide-rich pods compared to (a) Massive sulfides of the marginal series from the Portimo Complex (Iljina 1994); (b) Semi-massive ore from Aguablanca (Piña et al. 2008); and (c) Massive sulfides from Noril'sk Oktyabr'sky mine (Zientek et al. 1994). Primitve-mantle values are from Lyubetskaya and Korenaga (2007). Data are recalculated to 100% sulfides using the equation from Barnes and Lightfoot (2005).

2.7.8 EXPLORATION CONSIDERATIONS

Sulfide-rich pods at LDI represent a style of mineralization ignored in previous work. These pods may have a genetic relationship with the currently mined disseminated ore. Characterisation of these pods provides a better understanding of ore-forming processes. Although present in minor proportions at the scale of the Mine Block Intrusion, we have shown that sulfide-rich pods are PGE-rich, and therefore they should not be neglected from mining operations and exploration targeting.

Our contribution highlights sulfide liquid mobility over significant distances during co-magmatic movements of the intrusion. Sulfide accumulation into footwall rocks, as observed in the Platreef and Sudbury (Li et al. 1992; Holwell et al. 2006; Dare et al. 2014), might be considered as potential exploration targets. We suggest that the products of fractionated liquids enriched in Pt-Pd and more primitive cumulates could be present elsewhere in the intrusion.

Our work shows that although late-magmatic alteration did affect the mineralogy it may not have changed the PGE content of the sulfides. Therefore the fluids that triggered mineralogical changes may not have played a role in ore-forming processes. Several authors (Mulja and Mitchell, 1991; Hanley 2007; Helmy et al. 2007; Tomkins 2010; Dare et al. 2014) suggest that the most fractionated liquids enriched in Pd, Pt and semi-metals should still be liquid under 700°C. Interaction of these liquids with residual magmas or magmatic fluids in late crystallization stages may have led to metals redistribution. In

volatile-rich environments and under the extant co-magmatic stress regime such at LDI, the most fractionated liquid may have efficiently separated from its parental sulfides and interacted with volatiles. Ultimately, the genesis of sulfide-rich pods at LDI required a sequence of complex processes, which we have partially illuminated with the present evidence.

2.8 CONCLUDING REMARKS

Our study delineates the origin of sulfide-rich pods from the Mine Block Intrusion of the LDI Complex. The combined approach of field observations, petrographic investigation, whole-rock geochemistry and S isotope compositions allow us to propose a realistic model for the genesis of sulfide-rich pods at LDI, which can be summarized as follows:

1. Location of sulfide-rich pods across the stratigraphy is intimately associated with high temperature deformation. Sulfides accumulated as liquids throughout the intrusion in response to the opening of dilation zones. This interpretation is consistent with the presence of net-textured sulfides and the lack of evidence of ductile deformation.

2. Geochemical compositions of sulfide-rich pods are consistent with crystal fractionation of sulfide liquids. The studied sulfide-rich pods represent cumulus MSS and a few of them are associated with cumulus ISS. This is further supported by the preservation of igneous assemblages and textures.

3. Disseminated sulfides in ore zones could represent initial liquids from which sulfide-rich pods accumulated because they have sulfide liquid compositions and are enriched in Pd relative to sulfide-rich pods.

4. Sulfide cumulates are no longer associated with their complementary residual liquids enriched in Pd, Pt, Au and semi-metals and thus may have migrated away from the pods. Understanding of the effective separation of residual liquids from a fractionating sulfide liquid under high temperature stress has strong economic implications.

5. High Pd/Ir and Pd/Pt ratios are ascribed to the composition of evolved sulfide liquids, which suggests a model whereby multistage MSS removal depleted the liquid in IPGE and Rh and enriched it in Pd and Pt. Variable signatures of MSS attest to the evolution of the parental sulfide liquids.

6. Overprint of Py in the sulfide-rich pods is the result of local Fe redistribution from MSS/Po to surrounding silicates in the Roby Zone and of S addition in the Baker Zone. This did not play a role in ore-forming processes.

2.9 ACKNOWLEDGEMENTS

This study was completed by the first author as part of his PhD research project at UQAC. We are grateful to North American Palladium for providing financial support to Sarah-Jane Barnes' Canada Research Chair in Magmatic Ore Deposits, for allowing access to the mine

property and publication of this paper, and for hiring the first author as exploration geologist during field seasons. We would like also to thank the entire North American Palladium Exploration Team over the years for technical support in the field and with modeling software. Dany Savard and Sadia Mehdi are thanked for their assistance with whole-rock geochemical analyses at LabMaTer, UQAC. This study largely benefited from intellectual inputs from Philippe Pagé, Sarah Dare and Ed Sawyer of UQAC and from Lionnel Djon, Arnaud Tchalikian and Skylar Schmidt of North American Palladium. Finally, anonymous reviewers are thanked for their time and for thorough revision and improvement of this manuscript.

2.10 REFERENCES

Auclair G, Fouquet Y, Bohn M (1987) Distribution of Se in high temperature hydrothermal sulfides at 13° north, East Pacific Rise. Can Min 25:577–587

Barnes S-J, Naldrett AJ (1986) Variations in platinum group element concentrations in the Alexo mine komatiite, Abitibi greenstone belt, northern Ontario. Geol Mag 123:515–524

Barnes S-J et al (1988) The use of mantle normalisation and metal ratios in discriminating between the effects of partial melting, crystal fractionation and sulphide segregation on platinum group metals, gold, nickel and copper: examples from Norway. In: Prichard HM, Potts PJ, Bowles JFW, Cribbs SJ (eds) Geo-Platinum ’87. Elsevier, London, pp 113–139

Barnes S-J, Zientek ML, Severson MJ (1997a) Ni, Cu, Au, and platinum-group elements contents of sulphides associated with intraplate magmatism: a synthesis. Can J Earth Sci 34: 337–351

Barnes S-J, Makovicky E, Karup-Moller S, Makovicky M, Rose-Hanson J (1997b) Partition coefficients for Ni, Cu, Pd, Pt, Rh and Ir between monosulfide solid solution and sulfide liquid and the implications for the formation of compositionally zoned Ni–Cu sulfide bodies by fractional crystallization of sulfide liquid. Can J Earth Sci 34:366–374

Barnes S-J, Lightfoot PC (2005) Formation of magmatic nickel sulfide ore deposits and processes affecting their copper and platinum group element contents. Economic Geology 100th Anniversary Volume, pp 179–213

Barnes S-J, Gomwe TS (2010) Composition of the Lac des Iles magma and implications for the origin of the ore. In: 11th international platinum symposium, program abstracts, Ontario Geological Survey, miscellaneous release-data 269 (abstract)

Barnes S-J, Gomwe TS (2011) The Pd Deposits of the Lac des Iles Complex, Northwestern Ontario. Rev Econ Geol 17:351–370

Barnes SJ (2004) Komatiites and nickel sulfide ores of the Black Swan area, Yilgarn Craton, Western Australia. 4. Platinum group element distribution in the ores, and genetic implications. Miner Deposita 39:752–765

Barnes SJ (2007) Cotectic precipitation of olivine and sulfide liquid from komatiite magma and the origin of komatiite-hosted disseminated nickel sulfide mineralization at Mount Keith and Yakabindie, Western Australia. Econ Geol 102:299–304

Barnes SJ and Liu W (2012) Pt and Pd mobility in hydrothermal fluids: Evidence from komatiites and from thermodynamic modelling. Ore Geol Rev 44:49–58

Bedard LP, Savard DD, Barnes S-J (2008) Total sulphur concentration in geological reference materials by elemental infrared analyzer. Geostand Newsl 32:203–208

Boudreau A, Djon L, Tchalikian A, Corkery J (2014) The Lac Des Iles palladium deposit, Ontario, Canada. Part I. The effect of variable alteration on the Offset Zone. Miner Deposita 49:625–654

Brügmann GE, Naldrett AJ, Macdonald AJ (1989) Magma mixing and constitutional zone-refining in the Lac des Iles Complex, Ontario—genesis of platinum-group element mineralization. Econ Geol 84:1557–1573

Brügmann GE, Reischrnann T, Naldrett AJ, Sutcliffe RH (1997) Roots of an Archean volcanic arc complex; the Lac des Iles area in Ontario, Canada. Precambrian Res 81:223–239

Cabri LJ (1973) New data on phase relations in the Cu-Fe-S system. Econ Geol 68:443–454

Campbell IH, Naldrett AJ (1979) The influence of silicate: sulphide ratios on the geochemistry of magmatic sulphides. Econ Geol74:503–1505

Collins JE, Barnes SJ, Hagemann SG, McCuaig CT, Frost KM (2012) Post magmatic Variability in Ore Composition and Mineralogy in the T4 and T5 Ore Shoots at the High-Grade Flying Fox Ni-Cu-PGE Deposit, YilgarnCraton, Western Australia. Econ Geol 107:859–879

Craig JR (1973) Pyrite-pentlandite assemblages and other low temperature relations in the Fe–Ni–S systems. Am J Sci 273A:496–510

Craig JR, Kullerud G (1969) Phase relations in the Cu–Fe–Ni–S system and their application to magmatic ore deposits. Econ Geol Monogr 4:344–358

Dare SAS, Barnes S-J, Prichard HM, Fisher PC (2014) Mineralogy and Geochemistry of Cu-Rich Ores from the McCreedy East Ni-Cu-PGE Deposit (Sudbury, Canada): Implications for the Behavior of Platinum Group and Chalcophile Elements at the End of Crystallization of a Sulfide Liquid. Econ Geol 109:343–366

Djon MLN, Barnes S-J (2012) Changes in sulphides and platinum-group minerals with the degree of alteration in the Roby, Twilight, and High Grade Zones of the Lac des Iles Complex, Ontario, Canada. Miner Deposita 47:875–896

Dobson DP, Crichton WA, Vočadlo L, Jones AP, Wang Y, Uchida T, Rivers M, Sutton S, Brodholt J (2000) In situ measurement of viscosity of liquids in the Fe-FeS system at high pressures and temperatures. Ame Min 85:1838–1842

Dutrizac JE (1976) Reactions in cubanite and chalcopyrite. Can Min 14:172–181

Duuring P, Bleeker W, Beresford SW (2007) Structural modification of the komatiite-associated Harmony nickel sulfide deposit, Leinster, Western Australia. Econ Geol 102:277–297

Ebel DS, Naldrett AJ (1996) Fractional crystallization of sulfide ore liquids at high temperature. Econ Geol 91:607–621

Ebel DS, Naldrett AJ (1997) Crystallization of sulfide liquids and the interpretation of ore composition. Can J Earth Sci 34:352–365

Eckstrand OR, Hulbert LJ (1987) Selenium and the source of sulfur in magmatic nickel and platinum deposits. In: Geological Association of Canada-Mineralogical Association Canada, program abstracts, volume 12, pp 40 (abstract)

Fleet ME, Chryssoulis SL, Stone WE, Weisener CG (1993) Partitioning of platinum-group elements and Au in the Fe–Ni–Cu–S system: experiments on the fractional crystallization of sulfide melt. Contrib Mineral Petrol 115:36–44

Fonseca ROC, Campbell AH, O'Neill HSC, Fitzgerald JD (2008) Oxygen solubility and speciation in sulphide-rich mattes. Geochim Cosmochim Acta 72:2619–2635

Frost BR, Mavrogenes JA, Tomkins AG (2002) Partial melting of sulfide ore deposits during medium- and high-grade metamorphism. Can Min 40:1–18

Gomwe TS (2008) The formation of the palladium-rich Roby, Twilight and High Grade Zones of the Lac des Iles Complex. Unpublished PhD thesis, Université du Québec à Chicoutimi, Canada, p 296

Gupta VK, Sutcliffe RH (1990) Mafic-ultramafic intrusives and their gravity field: Lac des Iles area, northern Ontario. Geol Soc of Ame Bull 102: 1471–1483

Hamilton DL, Burnham WC, Osborn EF (1964) The solubility of water and effects of oxygen fugacity and water content on crystallization in mafic magmas. J Petrol 5:21–39

Hanley JJ (2007) The role of arsenic-rich melts and mineral phases in the development of high-grade Pt-Pd mineralization within komatiite-associated magmatic Ni-Cu sulfide horizons at Dundonald Beach South, Abitibi subprovince, Ontario, Canada. Econ Geol 102:305–317

Hanley JJ, Gladney ER (2011) The presence of carbonic-dominant volatiles during the crystallization of sulfide-bearing mafic pegmatites in the North Roby Zone, Lac des Iles Complex, Ontario. Econ Geol 106:33–54

Hauck SA, Severson MJ, Zanko L, Barnes S-J, Morton P, AlminasH, Foord EE, Dahlberg EH (1997) An overview of the geology and oxide, sulfide, and platinum-group element mineralization along the western and northern contacts of the Duluth Complex. Geol Soc of Ame Spe Pap 312:137–185

Helmy HM, Ballhaus C, Berndt J, Bockrath C, Wohlgemuth-Ueberwasser C (2007) Formation of Pt, Pd and Ni tellurides; experiments in sulfide-telluride systems. Contrib Mineral Petrol 153:577–591

Hinchey JG, Hattori KH (2005) Magmatic mineralization and hydrothermal enrichment of the High Grade Zone at the Lac des Iles palladium mine, northern Ontario, Canada. Miner Deposita 40: 13–23

Hinchey JG, Hattori KH, Lavigne MJ (2005) Geology, petrology, and controls on PGE mineralization of the southern Roby and Twilight zones, Lac des Iles mine, Canada. Econ Geol 100:43–61

Holwell DA, McDonald I (2006) Petrology, geochemistry and the mechanisms determining the distribution of platinum-group element and base metal sulfide mineralization in the Platreef at Overysel, northern Bushveld Complex, South Africa. Miner Deposita 41:575–598

Holwell DA, McDonald I (2010) A review of the behaviour of platinum group elements within natural magmatic sulfide ore systems: the importance of semimetals in governing partitioning behaviour. Platinum Metals Review 54:26–36

Holwell DA, Abraham-James TH, Keays RR, Boyce AJ (2011) The nature and genesis of marginal Cu- PGE-Au sulphide mineralisation in Palaeogene Macrodykes of the Kangerlussuaq region, east Greenland. Mineral Deposita 47:3–21

Iljina M (1994) The Portimo layered igneous Complex – With emphasis on diverse sulphide and platinum-group element deposists. Department of geology University of Oulu Finland PhD thesises. University of Oulu Finland Acta Universitatis Ouluensis A Scientiae Rerum Naturalium 258, p 158

Keays RR, Jowitt SM (2013) The Avebury Ni deposit, Tasmania: A case study of an unconventional nickel deposit. Ore Geol Rev 52:4–17

Kelly DP, Vaughan DJ (1983) Pyrrhotine-pentlandite ore textures: a mechanistic approach. Mineral Mag 47:453–463

Kepezhinskas P, Defant MJ (2001) Nonchondritic Pt/Pd ratios in arc mantle xenoliths: Evidence for platinum enrichment in depleted island-arc mantle sources. Geology 29:851–854

Konnunaho JP, Hanski EJ, Bekker A, Halkoaho TAA, Hiebert RS, Wing BA (2013) The Archean komatiite-hosted, PGE-bearing Ni–Cu sulfide deposit at Vaara, eastern Finland: evidence for assimilation of external sulfur and post-depositional desulfurization. Miner Deposita 48:967–989

Kress V, Greene LE, Ortiz MD, Mioduszewski L (2008) Thermochemistry of sulfide liquids IV: density measurements and the thermodynamics of O-S-Fe-Ni-Cu liquids a low to moderate pressures. Contrib Mineral Petrol 156:785–797

Lavigne MJ, Michaud MJ (2001) Geology of North American Palladium Ltd'.s Roby Zone Deposit, Lac des Iles. Explor Min Geol 10:1–17

Li C, Naldrett AJ, Coats CJA, Johannessen P (1992) Platinum, palladium, gold, and copper-rich stringers at the Strathcona mine, Sudbury: their enrichment by fractionation of a sulfide liquid. Econ Geol 87:1584–1598

Li C, Barnes S-J, Makovicky E, Rose-Hansen J, Makovicky M (1996) Partitioning of Ni, Cu, Ir, Rh, Pt and Pd between monosulfide solid solution and sulfide liquid: effects of composition and temperature. Geochim Cosmochim Acta 60:1231–1238

Liu Y-N, Brenan JM (2012) Experimental measurement of PGE and semi-metal partitioning during sulfide melt crystallization at controlled fO2-fS2 conditions. In: 12th international Ni-Cu-PGE symposium, program abstracts, State Key Laboratory of Ore Deposit Geochemistry, Institute of Geochemistry, Chinese Academy of Sciences, pp 36–39 (abstract)

Lyubetskaya T, Korenaga J (2007) Chemical composition of Earth’s primitive mantle and its variance: 1.Method and results. J Geophys Res 112:B03211. doi:10.1029/2005JB004223

Macdonald AJ (1988) Platinum-group element mineralization and the relative importance of magmatic and deuteric processes: Field evidence from the Lac des Iles deposit,

Ontario, Canada. In: Prichard HM, Potts PJ, Bowles JFW, Cribb SJ (eds) Geo-Platinum ’87. Elsevier, Amsterdam, pp 215–236

Maier WD, Barnes S-J (2004) Pt/Pd and Pd/Ir ratios in mantle-derived magmas: possible role for mantle metasomatism. S Afr J Geol 107:333–340

Mulja T, Mitchell RH (1991) The Geordie Lake Intrusion, Coldwell Complex, Ontario: A palladium- and tellurium-rich disseminated sulfide occurrence derived from an evolved tholeiitic magma. Econ Geol 86:1050–1069

Mungall JE (2002) Late-Stage Sulfide Liquid Mobility in the Main Mass of the Sudbury Igneous Complex: Examples from the Victor Deep, McCreedy East, and Trillabelle Deposits. Econ Geol 97:1563–1576

Mungall JE, Brenan JM (2003) Experimental evidence for the chalcophile behavior of the halogens. Can Min 41:207–220

Mungall JE, Andrews R, Cabri LJ, Sylvester PJ, Tubrett M (2005) Partitioning of Cu, Ni, An, and platinum-group elements between monosulfide solid solution and sulfide melt under controlled oxygen and sulfur fugacities. Geochim Cosmochim Acta 69:4349–4360

Mungall JE, Brenan JM (2014) Partitioning of platinum-group elements and Au between sulfide liquid and basalt and the origins of mantle-crust fractionation of the chalcophile elements. Geochim Cosmochim Acta 125:265–289

Mukwakwami J, Lafrance, B, Lesher MC, Tinkham DK, Rayner NM, Ames DE (2014) Deformation, metamorphism, and mobilization of Ni-Cu-PGE sulfide ores at Garson Mine, Sudbury. Miner Deposita 49:17–198

Naldrett AJ, Craig JR, Kullerud G (1967) The central portion of the Fe-Ni-S system and its bearing on pentlandite exsolution in iron-nickel sulfide ores. Econ Geol 62:826–847

Naldrett AJ (1969) A portion of the system Fe–S–O between 900 and 1080 °C and its application to sulfide ore magmas. J Petrol 10:171–201

Naldrett AJ (2004) Magmatic sulfide deposits: geology, geochemistry and exploration. Springer, Berlin, 727 pp

Pagé P, Barnes S-J, Bédard JH, Zientek ML (2012) In situ determination of Os, Ir, and Ru in chromites formed from komatiite, tholeiite and boninite magmas: implications for chromite control of Os, Ir and Ru during partial melting and crystal fractionation. Chem Geol 302:3–15

Park J-W, Campbell IH, Eggins SM (2012) Enrichment of Rh, Ru, Ir and Os in Cr spinels from oxidized magmas: Evidence from the Ambae volcano, Vanuatu. Geochim Cosmochim Acta 78:28–50

Park J-W, Campbell IH, Arculus RJ (2013) Platinum alloy and sulfur saturation in an arc-related basalt to rhyolite suite: Evidence from the Pual Ridge lavas, the Eastern Manus Basin. Geochim Cosmochim Acta 101:76–95

Peck DC, Keays RR, Ford RJ (1992) Direct crystallization of refractory platinum-group element alloys from boninitic magmas: evidence from western Tasmania. Aus J Earth Sci 39:373–387

Percival JA, Williams HR (1989) Late Archean Quetico accretionary complex, Superior province Canada. Geology 17: 23–25

Queffurus M, Barnes S-J (2014) Selenium and sulfur concentrations in country rocks from the Duluth Complex, Minnesota, USA: Implications for formation of the Cu-Ni-PGE sulfides. Econ Geol 109:785–794

Rankin LR (2013) Structural controls on emplacement and deformation of PGE-mineralised mafic-ultramafic intrusions – LDI district, NW Ontario. North American Palladium technical report, 115 pp

Ripley EM, Li C (2003) Sulfur isotope exchange and metal enrichment in the formation of magmatic Cu–Ni–(PGE) deposits. Econ Geol 98:635–641

Somarin AK, Kissin SA, Heerema DD, Bihari DJ (2009) Hydrothermal alteration, fluid inclusion and stable isotope studies of the north Roby Zone, Lac des Iles PGE mine, Ontario, Canada. Resour Geol 59:107–120

Savard D, Barnes S-J, Meiseil T (2010) Comparison between nickel sulfur fire-assay Te co-precipitation and isotopic-dilution with high pressure asher techniques for determination of platinum group elements, rhenium and gold. Geostand Newsl 34:281–291

Savard D, Bédard LP, Barnes S-J (2006) TCF selenium preconcentration in geological materials for determination at sub-μgg-1 with INAA (Se/TCF-INAA). Talanta 70:566–571

Schisa P, Boudreau A, Djon L, Tchalikian A, Corkery J (2014) The Lac Des Iles palladium deposit, Ontario, Canada. Part II. Halogen variations in apatite. Miner Deposita doi:10.1007/s00126-014-0541-4

Seccombe BK, Groves DI, Marston RJ, Barrett FM (1981) Sulfide paragenesis and sulfur mobility in Fe–Ni–Cu sulfide ore at Lunnon and Juan Main shoots, Kambalda: textural and sulfur isotope evidence. Econ Geol 76:1675–1685

Stone D, Lavigne MJ, Schnieders B, Scott J, Wagner D (2003) Regional geology of the Lac des Iles area. Ontario Geol Surv Open File Rep 6120:15-1–15-25

Su S, Lesher CM (2012) Genesis of PGE mineralization in the Wengeqi mafic-ultramafic complex, Guyang County, Inner Mongolia, China. Mineral Deposita 47:197–207

Sutcliffe RH, Sweeny JM, Edgar AD (1989) The Lac des Iles Complex, Ontario: petrology and platinum-group-elements mineralization in an Archean mafic intrusion. Can J Earth Sci 26:1408–1427

Sutcliffe RH (1989) Magma mixing in late Archean tonalitic and mafic rocks of the Lac Des Iles Area, Western Superior Province. Precambrian Res 44:81–101

Talkington RW, Watkinson DH (1984) Trends in the distribution of the precious metals in the Lac-Des-Iles Complex, Northwestern Ontario. Can Min 22:125–136

Tomkins AG, Pattison DRM, Frost RB (2007) On the initiation of metamorphic sulfide anatexis. J Petrol 48:511–535

Tomkins AG (2010) Wetting facilitates late-stage segregation of precious metal-enriched sulfosalt melt in magmatic sulfide systems. Geology 38:951–954

Watkinson DH, Dunning GR (1979) Geology and platinum-group mineralization, Lac des Iles complex, northwestern Ontario. Can Min 17:453–462

Watkinson DH, Lavigne MJ, Fox PE (2002) Magmatic-hydrothermal Cu and Pd-rich deposits in gabbroic rocks from North America. In: Cabri LJ (ed) The geology,

geochemistry, mineralogy and mineral beneficiation of platinum-group elements. Can Inst Min Metall 54, pp 299–320

Wood SA (2002) The aqueous geochemistry of the platinum group elements with applications to ore deposits. In: Cabri LJ (ed) The geology, geochemistry, mineralogy and mineral beneficiation of platinum-group elements. Can Inst Min Metall 54, pp 211–249

Wykes JL, Mavrogenes JA (2005) Hydrous sulfide melting: Experimental evidence for the solubility of H2O in sulfide melts. Econ Geol 100:157–164

Yoder HS, Tilley CE (1962) Origin of basaltic magmas: Experimental study of natural and synthetic rock systems. J Petrol 3:342–532

Zientek ML, Likhachev AP, Kunilov VE, Barnes S-J, Meier AL, Carlson RR, Briggs PH, Fries TL, Adrian BM (1994) Cumulus processes and the composition of magmatic ore deposits: examples from the Talnakh District, Russia. In: Lightfoot PC, Naldrett AJ (eds) Proceedings of the Sudbury-Noril'sk symposium, Ontario Geological Survey, special publication issue 5. Ontario Geological Survey, Greater Sudbury, pp 373–392

CHAPITRE 3

CHALCOPHILE AND PLATINUM-GROUP ELEMENT DISTRIBUTION AMONG THE PRIMARY SULFIDES AND FE-TI OXIDES IN SULFIDE-RICH PODS FROM THE LAC DES ILES PALLADIUM DEPOSITS (WESTERN ONTARIO, CANADA): CONSTRAINTS ON PROCESSES CONTROLLING THE COMPOSITION OF THE ORE

CHARLEY J. DURAN[1], SARAH-JANE BARNES[1], JOHN T. CORKERY[2]

[1] UNIVERSITE DU QUEBEC À CHICOUTIMI

[2] NORTH AMERICAN PALLADIUM

MINERALOGICAL MAGAZINE, SUBMITTED DECEMBER 9, 2014

3.1 RÉSUMÉ

Nous démontrons que la distribution des éléments du groupe du platine (EGP) et chalcophiles parmis les sulfures de métaux de base (SMB) primaires et les oxydes de Fe-Ti des lentilles riches en sulfures des gisements et de la mine de Pd du Lac des Iles (Canada) est consistente avec la cristallisation fractionnée de liquides sulfurés. En utilisant le couplage ablation laser / spectrométrie de masse (LA-ICP-MS), nous avons caractérisé les concentrations de 22 et 24 éléments traces trouvés respectivement dans les SMB et les oxydes de Fe-Ti associés. Nous proposons un nouveau diagramme multi-éléments pour les sulfures. Ce diagramme est normalisé à la composition du manteau primitif et conçu pour souligner le comportement de partage des éléments traces entre la solution solide monosulfurée (MSS) et les liquides fractionnés. La pyrrhotite (Po) et la pentlandite (Pn) contrôlent le budget roche totale du Co, Ni et EGPI (Os, Ir, Ru). Le Re et le Mo sont présents en solution solide dans la Po et la Pn. Cependant, des inclusions contenant Re-Mo ont été trouvées dans certains grains de Po. La Pn contient aussi des quantités considérables de Rh, Pd et Ag. La chalcopyrite (Ccp) contrôle la totalité du Cu et une large proportion d'Ag, Cd et Zn. Aucun SMB ne montre des quantités significatives de Pt, Au ou semi-métaux. De plus, la Ccp a exsolvé à partir de solution solide intermédiaire (ISS). La plupart du Pt, Au et semi-métaux est suspectée de résider principalement dans des minéraux isolés, qui ont pu cristalliser à partir des derniers liquides fractionnés. La distribution irrégulière d'Ag, Bi et Pb dans la Po et la Pn indique que les lentilles riches en sulfures ont été affectées par la déformation, mais cela n'a pas affecté les EGP. En plus des SMB, de la

magnetite (Mgt) et de l'ilménite (Ilm) sont présentes dans les lentilles riches en sulfures. La Mgt est appauvrie en Si, Ca, Y, HFSE, Ti et certains éléments chalcophiles (Mo et Cu) relativement au V, Ni et Cr. L'Ilm est enrichie en HFSE et d'une moindre mesure en V, Ni et Cr. La composition de la Mgt est consistente avec une origine magmatique et indique qu'elle a cristallisé après les sulfures. Les variations en Cr et V suggèrent que la Mgt a enregistré la cristallisation fractionnée des liquides sulfurés. La co-cristallisation d'Ilm avec la Mgt suggère que la plupart des oxydes de Fe-Ti se sont formés lorsque l'oxigène a diffusé hors des liquides sulfurés et a réagit avec les magmas silicatés.

3.2 ABSTRACT

We demonstrate that the distribution of chalcophile and platinum-group elements (PGE) among primary base metal sulfides (BMS) and Fe-Ti oxides from sulfide-rich pods of the Lac des Iles Pd mine and deposits (Canada) is consistent with crystal fractionation of sulfide liquids. Using laser ablation inductively coupled plasma mass spectrometry (LA-ICP-MS), we characterized the concentrations of 22 and 24 trace elements, respectively, found in the BMS and the associated Fe-Ti oxides. We propose a new multi-element diagram for sulfides. This diagram is normalized to the primitive mantle composition and designed to emphasize the partitioning behavior of trace elements between monosulfide solid solution (MSS) and fractionated liquids. Pyrrhotite (Po) and pentlandite (Pn) control the whole-rock budget of Co, Ni and IPGE (Os, Ir, Ru). Rhenium and Mo are present in

solid solution within Po and Pn. However, Re-Mo-bearing inclusions were found in some Po grains. The Pn also contains considerable amounts of Rh, Pd and Ag. Chalcopyrite (Ccp) controls the bulk of the Cu and a large proportion of Ag, Cd and Zn. No BMS exhibited significant amounts of Pt, Au or semi-metals. All of these observations suggest that Po, Pn and some discrete minerals exsolved from MSS. Furthermore, Ccp exsolved from intermediate solid solution (ISS). Most of the Pt, Au and semi-metals are suspected to primarily reside within discrete minerals, which may have crystallized from the late fractionated liquids. The irregular distribution of Ag, Bi and Pb within Po and Pn indicates that the sulfide-rich pods have been affected by deformation, but this did not affect the PGE. In addition to the BMS, magnetite (Mgt) and ilmenite (Ilm) are present in the sulfide-rich pods. The Mgt is impoverished in Si, Ca, Y, HFSE, Ti and some chalcophile elements (Mo and Cu) relative to V, Ni, and Cr. Ilm is enriched in HFSE and to a lesser extent V, Ni and Cr. The composition of the Mgt is consistent with a magmatic origin and indicates that it crystallized after the sulfides. Variations in Cr and V suggest that Mgt records the crystal fractionation of sulfide liquids. The co-crystallization of Ilm, along with Mgt, suggests that most of the Fe-Ti oxides formed as the oxygen diffused out of the sulfide liquids and reacted with silicate magmas.

3.3 INTRODUCTION

The Pd deposits of the Lac des Iles (LDI) Complex in Western Ontario, Canada, occur as zones of finely disseminated sulfides in varitextured meta-gabbronorites and chlorite-actinolite schist (Lavigne and Michaud, 2001; Barnes and Gomwe, 2011). The deposits form fairly wide (50-400 m) zones (which are referred to as the Roby, Offset, Twilight and High-grade zones), in which the mineralization occur as disseminated base metal sulfides (BMS) and platinum-group minerals (PGM). The deposits have undergone alteration that could have affected the initial composition of the ore (Hinchey and Hattory, 2005; Somarin et al., 2009; Barnes and Gomwe, 2011; Hanley and Gladney, 2011; Djon and Barnes, 2012; Boudreau et al., 2014), particularly in the High-grade Zone, which consists of chlorite-actinolite schist (Barnes and Gomwe, 2011). This possibility has led to a debate regarding whether the sulfide minerals crystallized from magmatic sulfide liquids and were subsequently altered (Hinchey et al., 2005; Barnes and Gomwe, 2011; Djon and Barnes, 2012; Duran et al., submitted) or crystallized directly from aqueous magmatic fluids that percolated through the magma pile (Boudreau et al., 2014; Schisa et al., 2014).

In addition to the disseminated mineralization, sulfide-rich pods have been identified throughout the intrusion (Duran et al., submitted). Both the disseminated sulfides and sulfide-rich pods have been interpreted by Duran et al. (submitted) as a result of crystal fractionation of sulfide liquids, with the disseminated sulfides representing in situ crystallization of initial liquids and the sulfide-rich pods representing cumulates. Such a relationship between disseminated and sulfide-rich mineralization has also been proposed

for some Ni-Cu sulfide deposits, e.g., Aguablanca, Spain (Piña et al., 2012) and Jinchuan, China (Chen et al., 2014).

Since the advent of laser ablation inductively coupled plasma mass spectrometry (LA-ICP-MS), the PGE and chalcophile element geochemistry of BMS has been investigated in a variety of PGE reefs and Ni-Cu sulfide deposits (Huminicki et al., 2005; Barnes et al., 2006, 2008; Holwell and McDonald, 2007; Godel et al., 2007, 2008, 2012; Hutchinson and McDonald, 2008; Dare et al., 2010, 2011; Piña et al., 2012; Osbahr et al., 2013, 2014; Smith et al., 2014; Chen et al., 2014), including the disseminated mineralization of LDI (Djon and Barnes, 2012). The approach in that was to assess the influence of crystal fractionation of sulfide liquids on the distribution of the elements among the BMS. Owing to the presence of secondary accessory minerals, e.g., pyrite and millerite, in some deposits (Dare et al., 2011; Djon et al., 2012; Piña et al., 2013; Osbahr et al., 2013, 2014; Smith et al., 2014) this approach has also been useful for highlighting the redistribution of some elements during post-magmatic processes. In addition, the geochemistry of magnetite has been used as an indicator of provenance and petrogenesis (Dare et al., 2012, 2014b; Nadoll et al. 2014; Boutroy et al., 2014) as the magnetite records the composition of the magmatic liquid/hydrothermal fluid from which it crystallizes.

Sulfide-rich pods from LDI exhibit the typical BMS assemblage observed in magmatic Ni-Cu-PGE deposits (i.e., pyrrhotite, pentlandite and chalcopyrite) but many of them contain variable amounts of pyrite and magnetite. The presence of pyrite, which is the dominant mineral in some pods, has been attributed to post-cumulus alteration of the pods (Duran et

al., submitted). In this study, we focus on the primary ore-mineral assemblage by using LA-ICP-MS analyses in order to: 1) determine the composition of the primary ore-mineral assemblage, 2) consider the origin of magnetite and 3) assess the processes whereby the primary ore-mineral assemblage reached its present composition. The influence of post-cumulus processes will be considered in a future study.

3.4 GEOLOGICAL BACKGROUND

An overall description of the geology of the LDI Complex, including the Pd mine and deposits, has been presented in Duran et al. (submitted) and references therein, and only a brief overview is presented here. The complex is located in Western Ontario, approximately 80 km north of Thunder Bay, near the boundary between the Wabigoon and Quetico subprovinces of the Superior province. The LDI Complex (2689 ± 1 Ma; Stone et al. 2003) forms a suite of mafic to ultramafic intrusions emplaced in granitoids. The Pd mine and deposits occur within the central intrusion of the complex, i.e., the Mine Block Intrusion (Fig. 3.1). Based on the estimate of the liquid composition of the rocks from the Mine Block Intrusion, Barnes and Gomwe (2010) suggested that the parental magmas of these rocks most closely resembled andesites, which most likely formed in a continental arc setting (Brügmann et al., 1997).

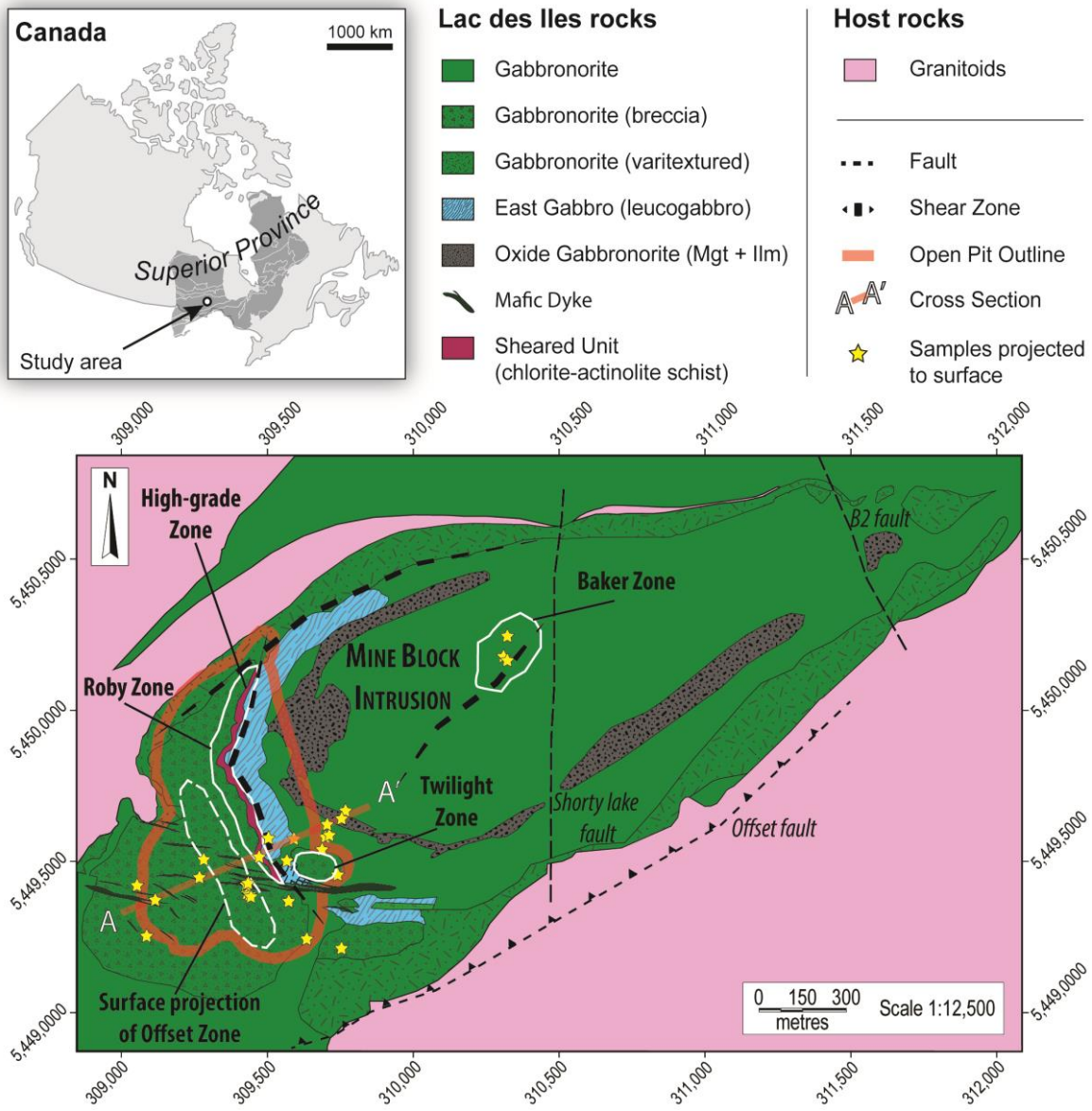

Figure 3.1 Simplified geological map of the Mine Block Intrusion of the Lac des Iles Complex (Modified from North American Palladium). Sulfide-rich samples are projected to the surface and follow a SW-NE orientation.

At the surface, the Mine Block Intrusion appears as an oval, funnel-shaped body (Figs 3.1 and 3.2). The intrusion is elongated along a SW–NE trend similar to regional faults (Gupta and Sutcliffe, 1990), and is affected by many syn- and post-magmatic shear zones and faults. This has been related to a continual deformation history while the Mine Block Intrusion was emplaced (Rankin, 2013).

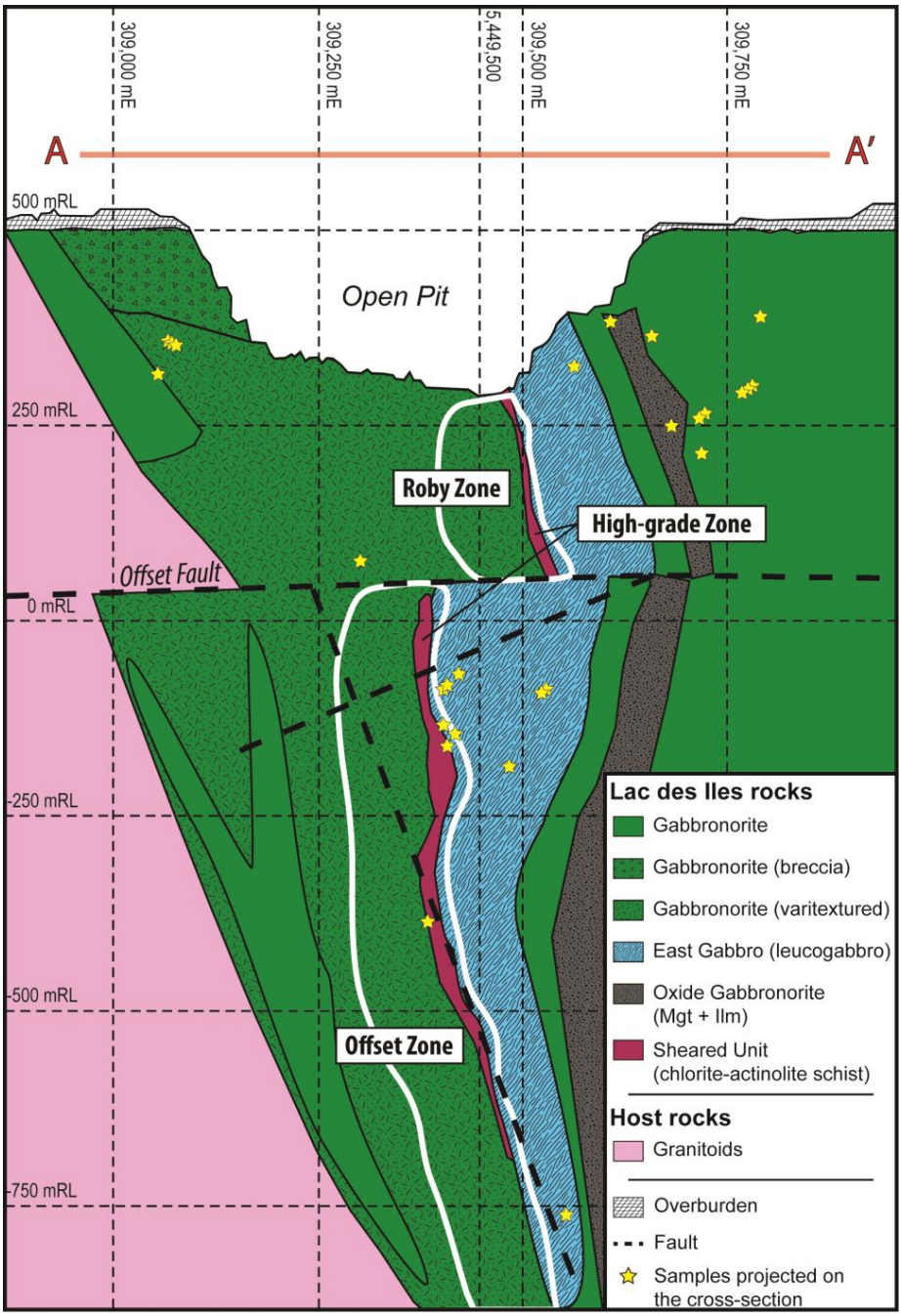

Figure 3.2 Idealized cross-section of the Mine Block Intrusion of the Lac des Iles Complex (Modified from North American Palladium), with projected locations of sulfide-rich samples from drill cores. Note that sulfides-rich pods sampled from the open pit and from the Baker Zone are not plotted on the cross-section.

The different lithological units of the Mine Block Intrusion display a radial stratigraphy, which suggests that the intrusion crystallized inwards (Schisa et al., 2014). The rocks mainly consist of noritic to gabbronoritic adcumulates with extremely variable textures (e.g., magmatic breccias, varitextured and pegmatitic rocks). Despite the variable textures, these rocks have similar incompatible element ratios (Barnes and Gomwe, 2011), which indicates that the rocks have a co-magmatic affinity. Barnes and Gomwe (2011) suggested that the variability in the rock textures was induced by recrystallization once the magmas became saturated in volatile-rich fluids. Based on the halogen geochemistry of apatite and previous work by Somarin et al. (2009) and Hanley and Gladney (2011), Schisa et al. (2014) identified three stages of fluid activity: (1) early degassing of Cl-rich CO_2-H_2O vapor from residual silicate liquid at high temperature; (2) late degassing of Cl-poor CO_2-H_2O vapor from residual silicate liquid at lower temperature, becoming enriched in CO_2 after dehydration during amphibole stabilization; and (3) mixing of country rock fluids of meteoric composition with late vapor under greenschist conditions.

Further evidence of fluid activity is highlighted by most of the rocks being altered to greenschist and lower amphibolite facies (Boudreau et al., 2014). Adcumulate textures were considerably altered to form a secondary mineral assemblage due to deuteric alteration and/or low-grade metamorphism. Plagioclase was variably altered to form sericite, epidote–group minerals, chlorite and carbonates. Orthopyroxene was more significantly altered to form actinolite and chlorite, being locally completely replaced (Barnes and Gomwe, 2011; Boudreau et al., 2014).

The main zone of mineralization (i.e., Roby Zone) occur in the western part of the Mine Block Intrusion, where it has been described at the surface (Lavigne and Michaud, 2001). The Roby Zone includes a 15-30 m wide sheared unit composed of chlorite-actinolite schist and known as the High-grade Zone. Further, the Roby Zone extends to the depth at which it is cut off by the Offset Fault. Below the Offset Fault, the mineralization is known as the Offset Zone, which is a fault offset that was displaced approximately 250 m to the west of the overlying Roby Zone.

In addition to the disseminated mineralization, sulfide-rich pods are present throughout the intrusion. These sulfide-rich pods cross-cut the stratigraphy and occur along major structures (Figs. 3.1 and 3.2; Duran et al., submitted). They range from net-textured to massive sulfides. Although their host rocks have been altered to greenschist and lower amphibolite facies, as have been most of the rocks in the intrusion, no alteration halos have been observed proximal to the pods. Duran et al. (submitted) proposed that sulfide liquids concentrated in the pods due to the opening of dilation zones.

3.5 PETROGRAPHY OF SULFIDE-RICH PODS

The petrography of LDI sulfide-rich pods has been previously presented in detail by Duran et al. (submitted), and only a brief overview is presented here.

Pyrrhotite forms large anhedral grains and is associated with pentlandite which forms polycrystalline aggregates around, or oriented exsolution flames within, pyrrhotite (Figs. 3.3a, b). In some pods, pyrrhotite and pentlandite are the predominant BMS. The remainder consists of pyrite chalcopyrite and Fe-Ti oxides (i.e., magnetite and ilmenite). Chalcopyrite is the least abundant BMS and it forms small anhedral grains that are randomly dispersed (Fig. 3.3c). In a few cases, chalcopyrite has been found to be the most abundant BMS, forming large anhedral polycrystalline aggregates along the edges of the pods. The magnetite and ilmenite form small anhedral grains within pyrrhotite or at sulfide-silicate grain boundaries (Fig. 3.3d). In some cases, magnetite has been observed to form large anhedral patches (Fig. 3.3e) that are associated with large anhedral grains of ilmenite. The pyrite forms primarily small euhedral grains, small and large anhedral grains, and polycrystalline aggregates. The amount of Py within the pods is extremely variable, with pyrite ranging from being nearly absent to being the predominant BMS.

The pyrrhotite, pentlandite and chalcopyrite display a textural relationship that is commonly observed in magmatic Ni-Cu-PGE deposits. They have been interpreted as crystallization products of sulfide liquids (Duran et al. submitted). The excess of pyrite in many pods has been attributed to post-cumulus processes (Duran et al. submitted), which are not the focus of the current investigation and will be presented in another study (Duran et al. in prep).

Based on our petrographic investigation, three origins for the oxides are possible. First, they could have crystallized from silicate liquid. The association of magnetite with ilmenite is a

common feature of magmatic Fe-Ti-V and Fe-Ti-P deposits found in layered intrusions (Von Gruenewaldt et al., 1985; Tollari et al., 2008). However, most of the silicate host rocks contain very low amounts of Fe-Ti oxides. Second, the magnetite and pyrite could have formed by oxidation of pyrrhotite through the following reaction: $4FeS + 2O_2 = 2FeS_2 + Fe_3O_4$. However, in some samples the magnetite does not occur in association with pyrite (Figs. 3.3d-f). Furthermore, the oxidation model does not account for the presence of ilmenite. Finally, the oxides could have crystallized from the BMS liquids. Natural BMS liquids contain 1-10% oxygen (Kress et al., 2008) and therefore can crystallize magnetite. To account for the ilmenite we propose that as the crystallization of sulfide minerals occurred, oxygen diffused out of the sulfide liquids and reacted with the silicate liquids (Fonseca et al., 2008). Petrographic observation alone is not sufficient to arrive at this conclusion. Rather, the observations must be combined with an analysis of the composition of the oxides, which will be discussed below.

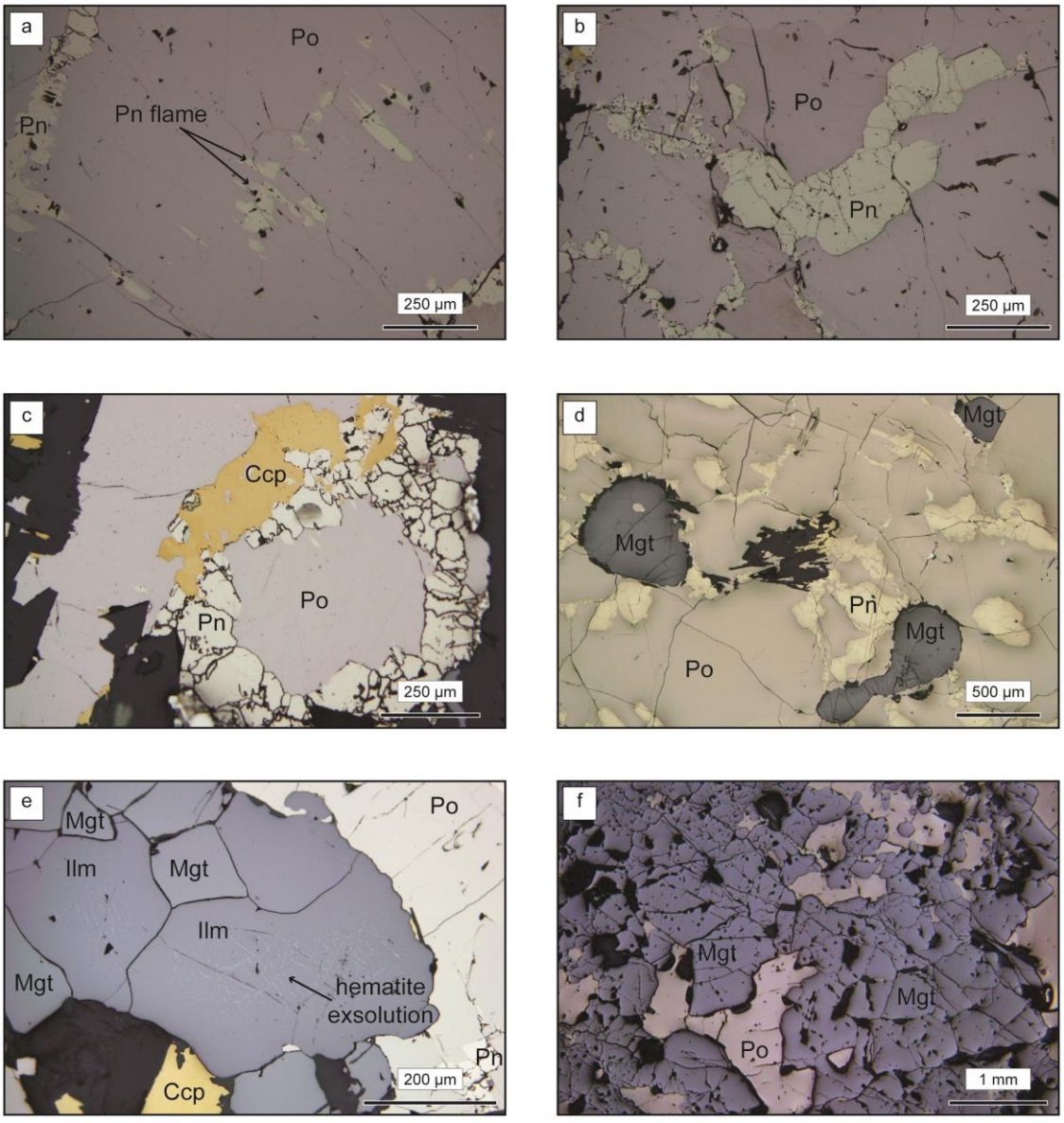

Figure 3.3 Photomicrographs in reflected light of the primary base metal sulfides and Fe-Ti oxides observed in the sulfide-rich pods; (a) pyrrhotite with oriented pentlandite exsolution flames; (b) pyrrhotite with coarse pentlandite; (c) pyrrhotite, pentlandite and chalcopyrite; (d) pyrrhotite–pentlandite assemblage with small rounded anhedral magnetite; (e) magnetite and ilmenite associated with sulfides and silicates. Note that hematite exsolutions are present within ilmenite; (f) large patch of magnetite with pyrrhotite.

3.6 ANALYTICAL METHOD

A total of 15 sulfide-rich pod samples from Duran et al. (submitted) were selected and used to determine in situ composition of BMS, Fe-Ti oxides, or both. Sulfide and oxide minerals were identified and described using an OLYMPUS DP71 optical microscope coupled with a digital camera at the Université du Québec à Chicoutimi (UQAC). LA-ICP-MS analysis was performed at LabMaTer (UQAC) using an Excimer 193 nm Resonetics Resolution M-50 laser ablation system coupled with an Agilent 7700x mass spectrometer. A range of beam sizes from 43 to 75 μm, a range of speeds from 2.5 to 5 μm/s, a range of laser frequencies from 10 to 15 Hz and a range of power from 4 to5 mJ/pulse were used to analyze the minerals. For large grains a traverse across the grain was made, and for small grains spot analyses were performed. The gas blank was measured for 30 s before switching on the laser for at least 60 s. The ablated material was then carried into the ICP-MS by an argon–helium gas mix. Data reduction was carried out using the Iolite package for Igor Pro software (Paton et al., 2011). Internal standardization was based on ^{57}Fe using the stoichiometric iron values of each mineral species.

For sulfides, counts of the following isotopes were monitored: ^{29}Si, ^{33}S, ^{34}S, ^{57}Fe, ^{59}Co, ^{61}Ni, ^{63}Cu, ^{65}Cu, ^{66}Zn, ^{75}As, ^{77}Se, ^{82}Se, ^{95}Mo, ^{99}Ru, ^{101}Ru, ^{103}Rh, ^{105}Pd, ^{108}Pd, ^{109}Ag, ^{111}Cd, ^{118}Sn, ^{121}Sb, ^{128}Te, ^{130}Te, ^{185}Re, ^{189}Os, ^{193}Ir, ^{194}Pt, ^{195}Pt, ^{197}Au, ^{208}Pb and ^{209}Bi. Silicon was monitored to ensure that the measured signal represented pure sulfide. Three certified reference materials were used for external calibration: Laflamme Po727, which is a

synthetic FeS doped with 40 ppm PGE and Au that was supplied by the Memorial University of Newfoundland, was used to calibrate for PGE and Au; MASS-1, which is a ZnCuFeS pressed powder pellet doped with 50–70 ppm Ag, As, Bi, Pb, Re, Sb, Se, Sn and Te that was supplied by the United States Geological Survey (USGS), was used to calibrate for Ag, As, Bi, Cd, Co, Cu, Mo, Pb, Sb, Se, Sn and Te; JB-MSS5, which is a synthetic FeS sulfide that contain approximately 50–70 ppm of most chalcophile elements and was supplied by Prof. James Brenan was used to calibrate for Ni and Re. In addition, JB-MSS5 was used as an in-house reference material to monitor the calibrations of both Laflamme Po727 and MASS-1. Interference of ^{101}Ru with $^{61}Ni^{40}Ar$ was corrected using a NiS blank run at the beginning and end of each analytical session. Internal standardization was based on ^{34}S because the NiS blank does not contain Fe. Interference of ^{103}Rh with $^{63}Cu^{40}Ar$ was corrected using ^{103}Rh measured in MASS-1, which contains 13.4 % ^{63}Cu but no ^{103}Rh. For chalcopyrite this interference made it impossible to accurately determine the Rh concentrations. Interference of ^{108}Pd with ^{108}Cd was corrected by monitoring ^{111}Cd, and Pd^{108} was used to measure Pd.

Maps of the element distribution were made when the LA-ICP-MS signal revealed variations in the element distribution, especially within pentlandite grains. A range of beam sizes from 15 to 25 μm, a range of speeds from 10 to 20 μm/s, a laser frequency of 15 Hz and a power of 5 mJ/pulse were used to map the grains in their entirety. The maps were generated using the Iolite software package on the basis of the time-resolved composition

of each element. The maps indicate the relative concentration of the elements and are semi-quantitative.

For oxides, counts of the following isotopes were monitored: ^{25}Mg, ^{27}Al, ^{29}Si, ^{34}S, ^{44}Ca, ^{45}Sc, ^{47}Ti, ^{49}Ti, ^{51}V, ^{52}Cr, ^{53}Cr, ^{55}Mn, ^{57}Fe, ^{59}Co, ^{60}Ni, ^{63}Cu, ^{65}Cu, ^{66}Zn, ^{69}Ga, ^{71}Ga, ^{74}Ge ^{75}As, ^{89}Y, ^{90}Zr, ^{92}Zr, 93Nb, ^{95}Mo, ^{107}Ag, ^{111}Cd, ^{118}Sn, ^{121}Sb, ^{178}Hf, ^{181}Ta, ^{182}W, and ^{208}Pb. Silicon and sulfur were monitored to ensure that the measured signal represented pure oxide. Three certified reference materials were used for external calibration of the LA-ICP-MS data: GSE-1g, which is a synthetic glass that was supplied by the USGS, was used to calibrate for all elements; GSD-1g, which is also a synthetic glass that was supplied by the USGC, and BC28, which is a pure natural magnetite from the lowermost layer of the Bushveld Complex, were both used as in-house reference materials to monitor the calibration of GSE-1g. According to Dare et al. (2012), interferences of ^{90}Zr with ^{50}Ti^{40}Ar, ^{50}V^{40}Ar and ^{50}Cr^{40}Ar; ^{92}Zr with ^{52}Cr^{40}Ar; and ^{93}Nb with ^{53}Cr^{40}Ar are negligible, thus corrections were not required.

The results of the monitors for both sulfides and oxides are generally within 10% analytical error of the working values and relative standard deviation (RSD) is typically < 10%. The results of the monitors for both sulfides and oxides are presented in the online supplementary material.

3.7 RESULTS AND INTERPRETATION

The first phase to crystallize from a magmatic sulfide liquid is monosulfide solid solution (MSS). Iron oxide crystallizes next, and intermediate solid solution (ISS) crystallizes last. As the temperature decreases, all three minerals undergo exsolution. Monosulfide solid solution exsolves to form pyrrhotite (Po) and pentlandite (Pn) ± minor pyrite. Iron oxide exsolves to magnetite (Mgt) and ilmenite (Ilm) and ISS exsolves into chalcopyrite (Ccp) or cubanite ± Py. The composition of the phases that crystallize from the fractionating sulfide liquids depends on the following factors: (1) the composition of the initial sulfide liquid from which they crystallize; (2) the partition coefficients of the elements into the crystallizing phases; and (3) the processes whereby the elements can be redistributed (e.g., exsolution).

3.7.1 PYRRHOTITE, PENTLANDITE AND CHALCOPYRITE

In the past, the compositions of BMS have been plotted on primitive mantle normalized patterns of PGE and a limited number of other metals to investigate the processes that control the PGE distribution (Barnes et al., 2006; Chen et al., 2014). Because of advancements in the capabilities of LA-ICP-MS, a wider range of elements may now be considered. To incorporate these elements, we have developed a new multi-element diagram that present the elements in decreasing order of compatibility in MSS. Compatibility in MSS was chosen because based on the whole-rock geochemistry we

believe that most of the rocks are cumulus MSS (Duran et al. submitted). To preserve the shape of the PGE patterns, these elements have been kept together, although they are not exactly positioned in order of compatibility in MSS.

The median composition of each BMS is presented in Table 3.1, along with the minimum and maximum values. The full dataset is presented in the online supplementary material. Within the BMS, most elements are homogeneously distributed as indicated by the time-signal diagrams (Fig. 3.4). Thus, the median compositions are considered to be representative for most elements. Silver, Bi and Pb are exceptions to this in most Pn and in some Po (Figs. 3.4b, d). Additionally, Re- and Mo-bearing inclusions have been intersected in some Po grains. Given these considerations, we shall now assess the role of MSS in controlling the distribution of the elements among the BMS on the multi-element diagram.

Element		Isotope	Pyrrhotite F=0.77 ; n=37			Pentlandite F=0.18 ; n=55			Chalcopyrite F=0.05 ; n=20		
			Median	Min	Max	Median	Min	Max	Median	Min	Max
Co	(ppm)	^{59}Co	156	21.7	353	6720	137	16736	5.52	0.279	5538
Ni	(ppm)	^{61}Ni	7099	3048	10671	246805	192104	280342	2042	420	22823
Cu	(ppm)	^{65}Cu	0.262	0.061	636	1.42	0.326	4689	345381	253482	351162
As	(ppm)	^{75}As	0.773	≤0.455	2.05	0.762	≤0.455	7.91	0.771	≤0.455	8.12
Se	(ppm)	^{82}Se	125	65.4	341	79.1	37.6	1931	153	42.7	239
Mo	(ppm)	^{95}Mo	0.181	0.108	0.297	0.086	0.039	2.96	0.099	0.052	0.660
Ru	(ppm)	^{101}Ru*	0.026	≤0.017	0.303	0.080	≤0.017	0.679	0.125	0.018	0.260
Rh	(ppm)	^{103}Rh*	0.014	≤0.003	0.095	0.058	0.013	1.41	n.a.	n.a.	n.a.
Pd	(ppm)	^{108}Pd*	0.025	≤0.010	0.307	18.3	0.401	785	1.26	0.033	141
Ag	(ppm)	^{109}Ag	0.335	0.139	1.16	2.60	0.208	70.3	33.6	1.126	83.3
Cd	(ppm)	^{111}Cd	≤0.054	≤0.054	0.374	≤0.054	≤0.054	2.21	0.843	0.067	7.36
Sn	(ppm)	^{118}Sn	0.126	0.069	56.1	0.080	≤0.032	22.5	0.152	≤0.032	1.64
Sb	(ppm)	^{121}Sb	0.025	≤0.012	0.056	0.016	≤0.012	0.326	0.017	≤0.012	0.049
Te	(ppm)	^{128}Te	0.299	≤0.194	0.841	0.287	≤0.194	5.14	0.262	≤0.194	4.84
Re	(ppm)	^{185}Re	0.016	≤0.006	0.324	0.012	≤0.006	25.7	0.009	≤0.006	0.286
Os	(ppm)	^{189}Os	0.023	≤0.016	0.175	≤0.016	≤0.016	0.414	≤0.016	≤0.016	0.049
Ir	(ppm)	^{193}Ir	0.016	≤0.004	0.070	0.009	≤0.004	0.029	≤0.004	≤0.004	0.027
Pt	(ppm)	^{195}Pt	≤0.014	≤0.014	0.056	0.015	≤0.014	0.485	≤0.014	≤0.014	0.520
Au	(ppm)	^{197}Au	0.011	≤0.008	0.050	0.012	≤0.008	0.133	0.012	≤0.008	0.075
Pb	(ppm)	^{208}Pb	0.430	0.075	6.79	2.62	0.083	234	3.38	1.50	42.0
Bi	(ppm)	^{209}Bi	0.050	0.004	1.47	0.088	≤0.003	2.784	0.117	0.010	4.72

*Table 3.1 Compositions of base metal sulfides from Lac des Iles sulfide-rich pods as determined by LA-ICP-MS analysis. F = weight fraction; n = number of analysis; min = minimum value; max = maximum value; n.a. = not available; * = values corrected for interference.*

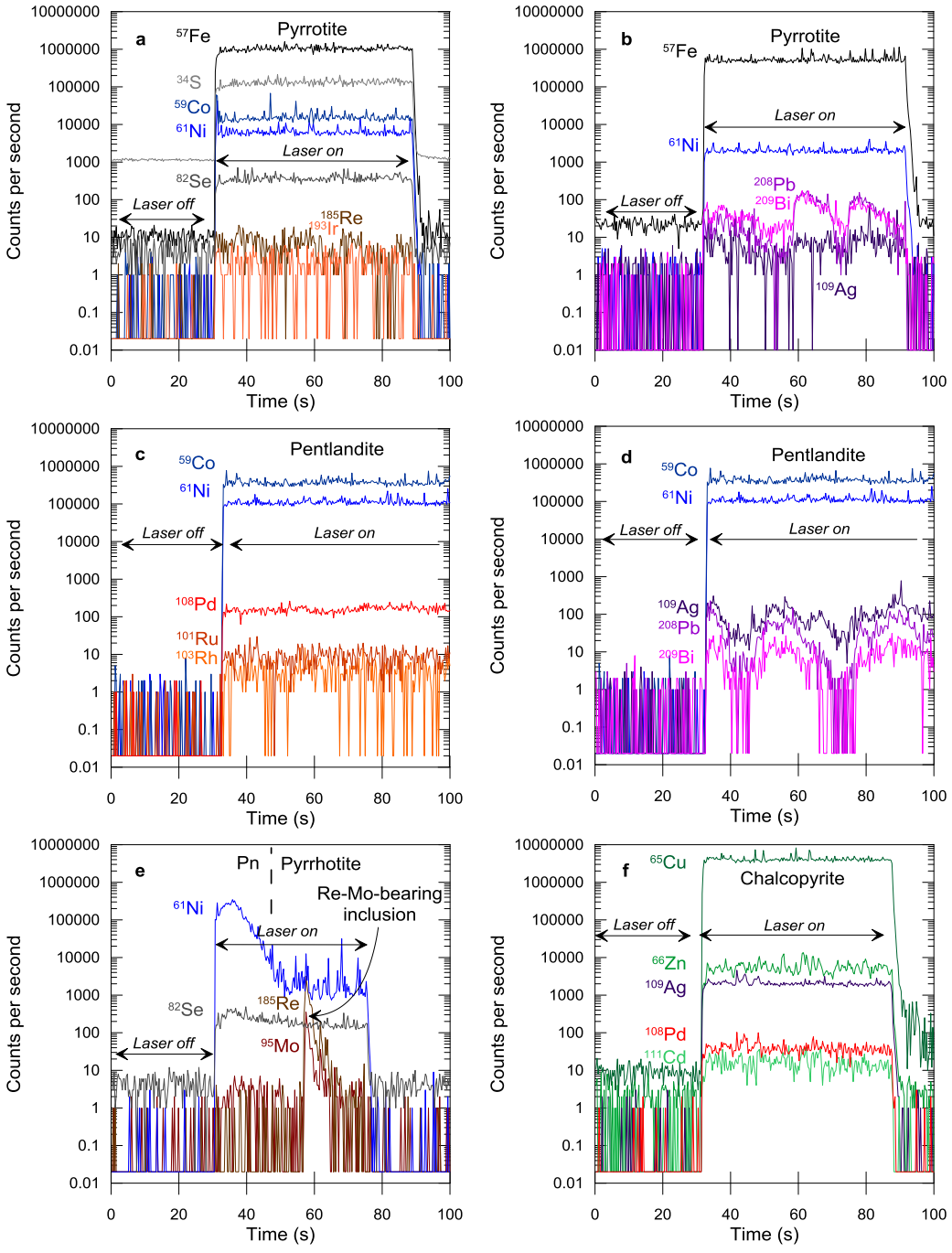

Figure 3.4 Examples of time-signal diagrams of base metal sulfides; (a-b) pyrrhotite; (c-d) pentlandite; (e) pyrrhotie + pentlandite with Re-Mo-bearing inclusion; (f) chalcopyrite.

Each BMS mineral has its own distinctive normalized trace element pattern, as can be seen from Figure 3.5 and in this section we assess why that is. To test whether the variation in the geochemistry is controlled by MSS crystal fractionation, we may assess the distribution of the elements among the BMS with respect to their compatibility in MSS, proceeding from the left hand side of the diagram to the right. For instance, the partition coefficient for Se into MSS is slightly less than 1, and slightly more than 1 into ISS (Helmy et al., 2010; Liu and Brenan, 2012). Thus, Se is expected to concentrate in similar proportions in Po, Pn and Ccp. Indeed, all three BMS have Se concentrations of approximately 100 ppm, and plot on the same level on the diagram (Fig. 3.5).

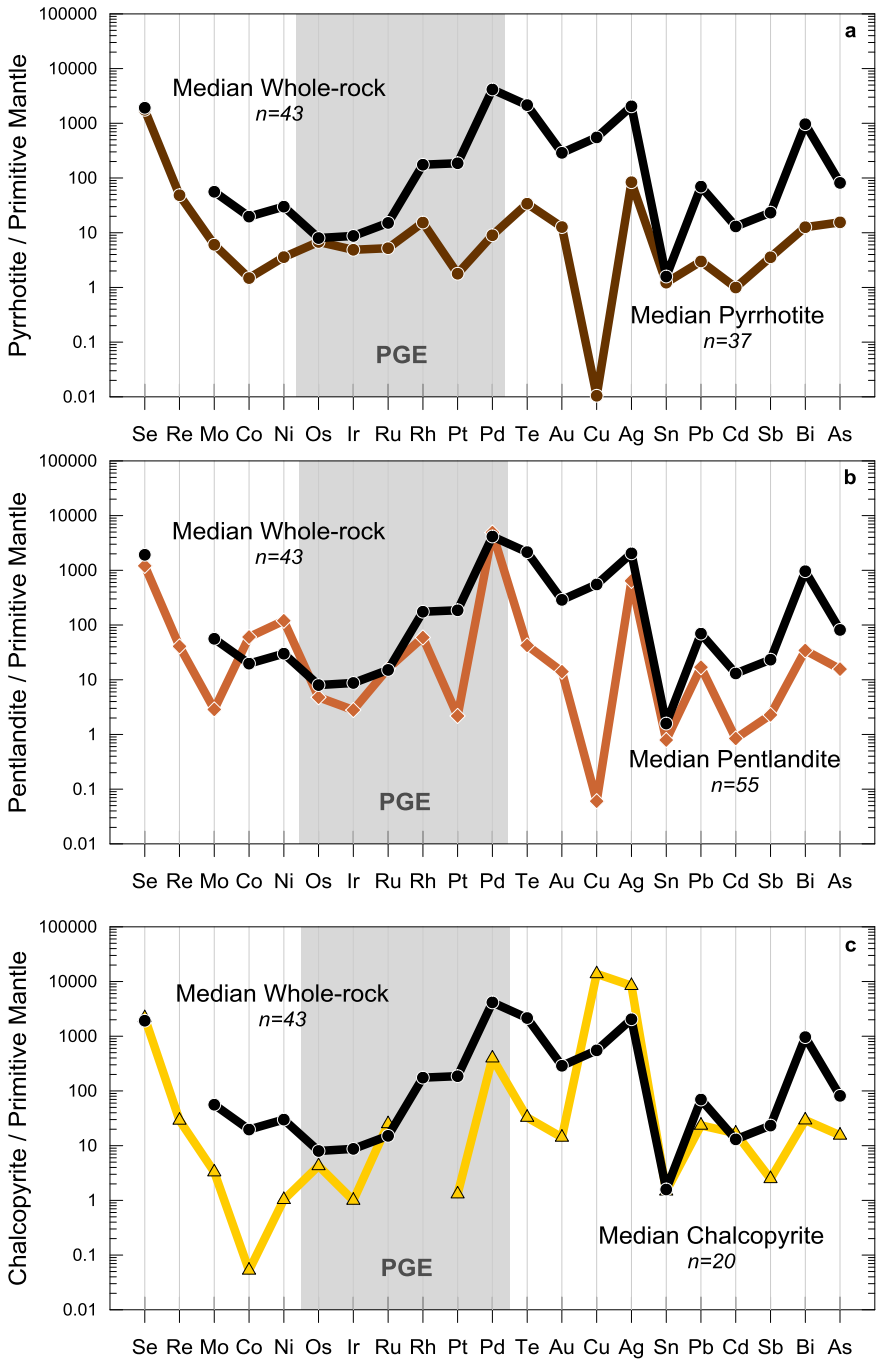

Figure 3.5 Primitive mantle normalized multi-element diagrams of sulfides from Lac des Iles sulfide-rich pods compared with whole-rock: (a) pyrrhotite; (b) pentlandite; (c) chalcopyrite. The whole-rock data are from Duran et al. (submitted). The normalization values are from Lyubetskaya and Korenaga (2007).

Rhenium and Mo values are slightly higher in Po (from ≤0.006 to 0.324 and from 0.108 to 0.297 ppm, respectively) and Pn (from ≤0.006 to 25.7 and from 0.039 to 2.96 ppm, respectively) than in Ccp (from ≤0.006 to 0.286 and from 0.052 to 0.660 ppm, respectively). These elements have similar levels on the BMS patterns (Fig. 3.5). However, Re and Mo are not compatible with ISS and are expected to concentrate in MSS (Brenan, 2008; calculated from Li and Audétat, 2012; Liu and Brenan, 2012). The low abundance of these elements in Po and Pn and the lack of correlations with other compatible elements may reflect the presence of Re-bearing minerals (Fig 3.4).

Cobalt and Ni display different behavior on the three BMS patterns. Pentlandite has Co and Ni concentrations that are approximately 100 times those of the primitive mantle. Pyrrothite has intermediate values that are 2 to 4 times those of the primitive mantle. Chalcopyrite has a Co concentration that is approximately 0.005 times that of the primitive mantle. At high temperature, Co and Ni are slightly incompatible in MSS, but upon cooling, they become compatible and partition into MSS (Li et al., 1996; Mungall et al., 2005). The higher concentrations of these elements in Pn and Po relative to Ccp (Fig. 3.5) reflects their partitioning into MSS during crystal fractionation. This type of correlation can be readily noticed on a plot of Co versus Ni (Fig. 3.6), in which Po and Pn exhibit a relatively strong correlation, whereas Ccp does not. Furthermore, Co and Ni are preferentially concentrated in Pn with values of up to 16736 ppm for Co. This result reflects the preference of these elements for Pn over Po during exsolution of MSS.

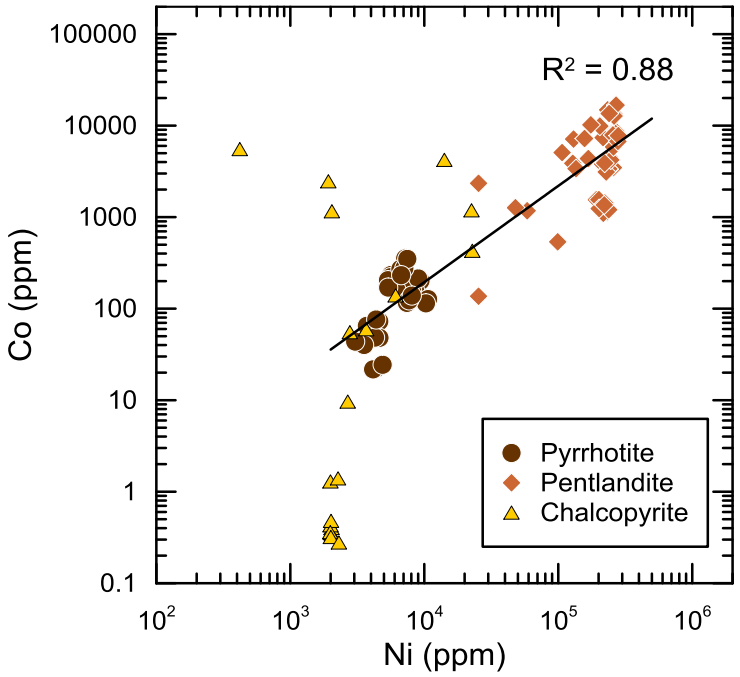

Figure 3.6 Binary diagram of Co versus Ni. Note the strong degree of correlation for pyrrhotite and pentlandite.

As in the case of Ni and Co, IPGE and Rh are compatible in MSS. Pyrrhotite displays a relatively flat pattern from Os to Ru, with a slight increase toward Rh, and Pn displays a strong increase from Ir to Rh (Fig. 3.5). In contrast, Ccp exhibits a negative Ir anomaly. On a plot of Os versus Ir (Fig. 3.7a), all the BMS exhibit a relatively strong positive correlation and fall close to the 1:1 line, indicating that these elements are sub-equally distributed, albeit Os is slightly enriched relative to Ir as observed in whole-rock. Pyrrhotite has the highest concentrations of Os and Ir followed by Pn. Chalcopyrite has Os and Ir concentrations close to or below the limit of detection. On a plot of Rh versus Ru (Fig. 3.7b), Po and Pn exhibit a relatively strong positive correlation and fall close to the 1:1 line, similar to the whole-rock, which indicates that these elements are sub-equally distributed. Pentlandite has the highest concentrations of Ru and Rh. The preference of IPGE and Rh for Po and Pn is reflecting their compatibility during MSS crystallization. During MSS exsolution it appears that Os and Ir prefer Po over Pn and Ru and Rh prefer Pn over Po.

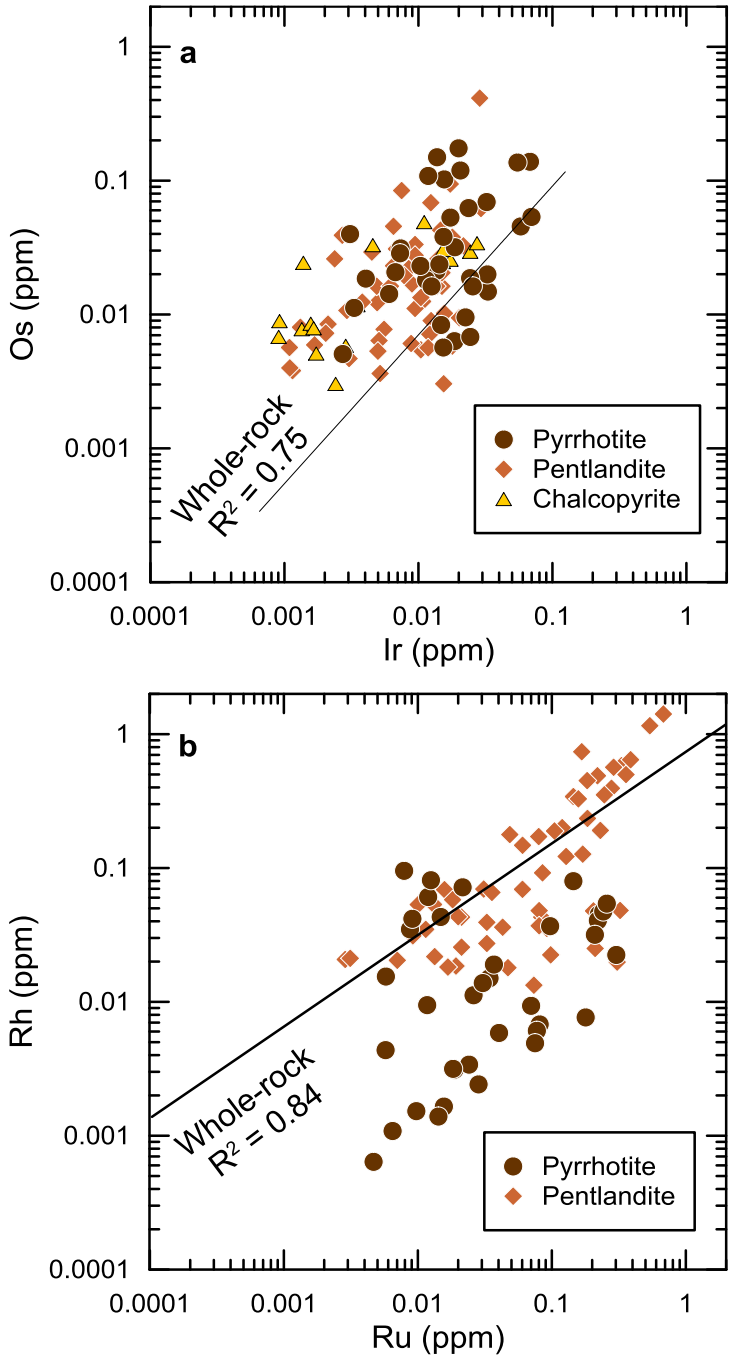

Figure 3.7 Binary diagrams: (a) Os versus Ir; and (b) Rh versus Ru. Note the strong degree of correlation for sulfides, which follow the whole-rock trend on both diagrams. Chalcopyrite analyses are not plotted in panel b because of excessive interference between 63Cu and 103Rh.

Although Pd is not compatible in MSS and ISS during crystal fractionation of sulfide liquids (Barnes and Lightfoot, 2005 and references therein; Mungall et al., 2005; Brenan, 2008; calculated from Li and Audétat, 2012), its partition coefficient is not 0 and some Pd is present in the MSS. This has been ascribed to the subsolidus diffusion of Pd from MSS and fractionated liquids into Pn (Barnes et al., 2006; Dare et al., 2010). As observed elsewhere (e.g., J-M Reef, Stillwater Complex, Godel and Barnes, 2008; Platreef, Bushveld Complex, Holwell and McDonald, 2007; Medvezky Creek Mine, Noril'sk, and Merensky Reef, Bushveld Complex, Barnes et al., 2008; McCreedy deposit, Sudbury, Dare et al., 2011; Rosie Nickel Prospect, Yilgarn Craton, Godel et al., 2012; Aguablanca, Piña et al., 2012; Grasvally Norite-Pyroxenite-Anorthosite (GNPA) member, Bushveld Complex, Smith et al., 2014; Jinchuan, Chen et al., 2014), the Pn pattern displays a high positive Pd peak. On plots of Pd versus Rh and Pd versus Ru (Figs. 3.8a, b), Pn exhibits strong correlations, and Pd is enriched by 3 orders of magnitude relative to Rh and Ru. This correlation reflects the diffusion of Pd into Pn during its exsolution from MSS. In contrast, Po and Ccp do not exhibit any correlation.

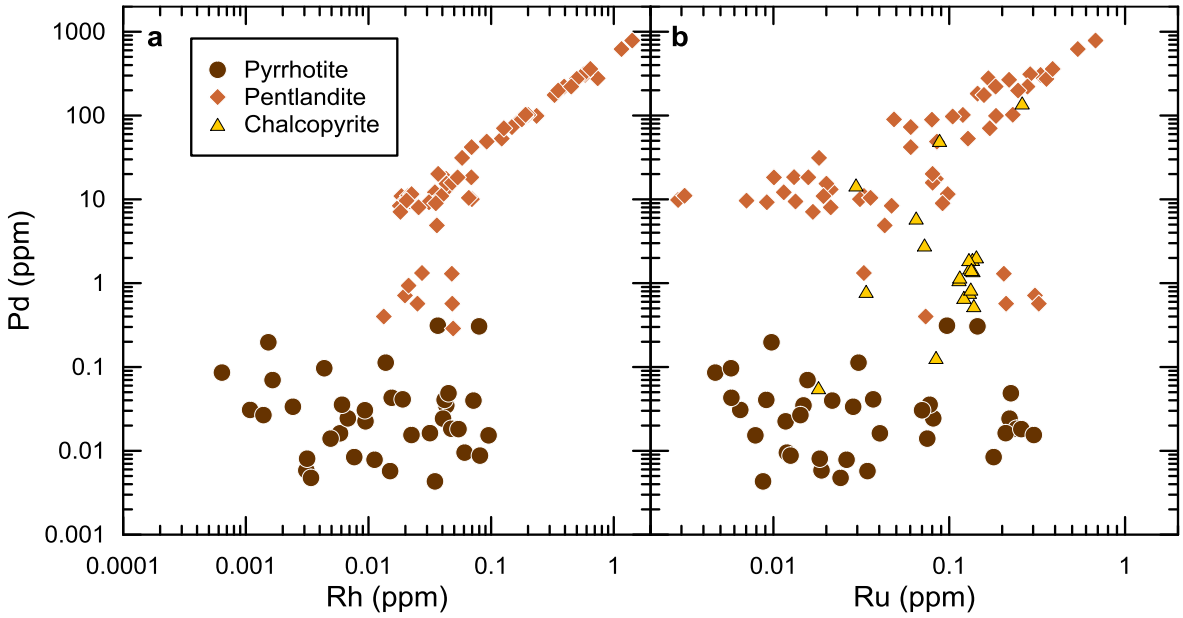

Figure 3.8 Binary diagrams: (a) Pd versus Rh; and (b) Pd versus Ru. Note the strong degree of correlation for pentlandite on both diagrams. As in Fig. 7b chalcopyrite analyses are not plotted in panel (a) because of interference between 63Cu and 103Rh.

Unlike Pd, Pt and Au are not commonly found in BMS. They are expected to remain in the late fractionated liquids with the semi-metals (Barnes and Lightfoot, 2005 and references therein; Mungall et al., 2005; Brenan, 2008; calculated from Li and Audétat, 2012; Liu and Brenan, 2012). For all the BMS of LDI sulfide-rich pods, Pt and Au are close to or below detection limits and do not correlate with any elements or with each other. We assume that these elements are present as distinct discrete minerals, e.g., PGM or electrum.

When MSS crystallizes, Cu, Ag, Cd and Zn partition into the fractionated liquid because they are not compatible in MSS. Upon cooling, these elements partition into ISS, and they are usually found in Ccp (Barnes et al., 2006; Barnes et al., 2008). Chalcopyrite exhibits a strong enrichment for Cu and Ag, at around 10000 times their concentration in the primitive mantle. In contrast, Po and Pn exhibit a negative Cu anomaly and have lower Ag values. On plots of Ag versus Cd and Zn (Figs. 3.9a, b), the BMS do not show a clear correlation, but in general Ag, Cd and Zn are concentrated in Ccp. Silver concentrations in Pn are quite high (up to 70.3 ppm) and variable, which may be explained by the heterogeneous distribution of Ag.

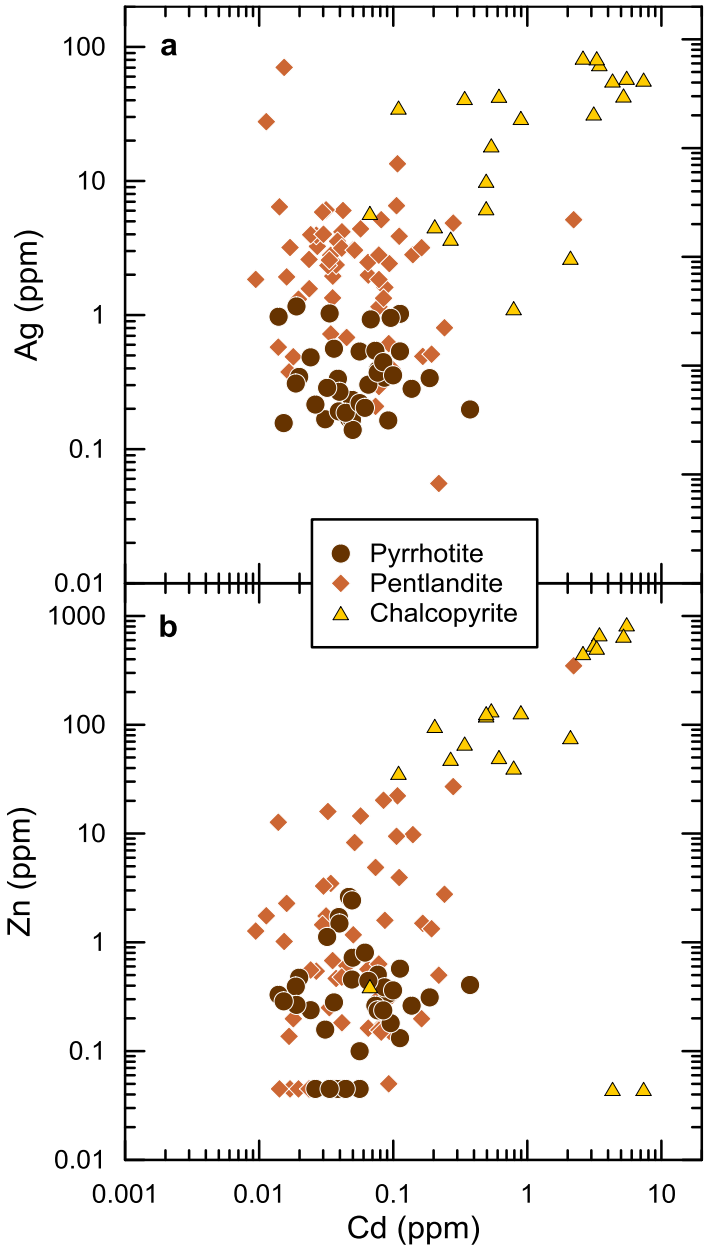

Figure 3.9 Binary diagrams: (a) Ag versus Cd; and (b) Zn versus Cd. Note that chalcopyrite is generally enriched in these elements relative to pyrrhotite and pentlandite.

As in the case of Pt and Au, semi-metals are not compatible in MSS and ISS (Helmy et al., 2010; Liu and Brenan, 2012). The three BMS contain very low concentrations of semi-metals relative to the whole-rock. Pyrrhotite displays a smoothly increasing pattern from Sn to As. Pentlandite is characterized by small positive Pb and Bi peaks similar to the whole-rock pattern. The Ccp patterns resemble the Pn pattern except for Cd which is highly enriched in Ccp as mentioned previously.

To investigate the role of crystal fractionation in controlling the whole-rock composition, we may test whether the composition of the primary BMS assemblage reproduces that of the whole-rock. In addition to the compositions of the whole-rock and each BMS, this calculation requires the modal proportions of all three BMS. To estimate the modal proportions of each BMS, some assumptions have to be made. Namely, we assume that Pn controls the total amount of Ni, and Ccp controls the total amount of Cu. Thus, we may estimate the Pn and Ccp proportions in 100% sulfides using the equation from Godel and Barnes (2008). Because Fe is controlled by Po, Py and Fe-Ti oxides, it is not possible to perform the same exercise for Po. Assuming that Py is a secondary product (Duran et al., submitted) we may infer the initial Po proportion based on the Pn and Ccp proportions. In 100% sulfides, the median whole-rock (Duran et al. submitted) contain 18% Pn, 5% Ccp and 77% Po.

The sum of the three BMS for Se, Ni, Os and Cu accounts for $\geq$ 80 % of the whole-rock composition, thereby indicating that these elements are controlled by the BMS assemblage

(Fig. 3.10). For Co, Ir, Ru and Sn the BMS assemblage accounts for 40-80 % of the whole-rock composition. This result indicates that these elements are mainly controlled by BMS, but a small amount is hosted by other phases (e.g., Py, Mgt or PGM). The BMS assemblage also accounts for significant amounts of the Mo, Rh, Pd, Ag, Cd, Sb, and As whole-rock composition (10-30%; Fig. 3.10). This result suggests that these elements are significantly present in BMS but that a greater amount is hosted by other phases, e.g., PGM. Because of the lack of whole-rock analyses for Re, it is not possible to determine whether BMS control this element in LDI sulfide-rich pods. However, we suspect that Re is not significantly controlled by BMS because Re-inclusions have been observed. For Pt, Au, Te, Bi and Pb the sum of the three BMS accounts for less than 10% of the whole-rock composition (Fig. 3.10), thereby suggesting that these elements are not significantly present in BMS. Whereas the concentrations of Se, Ni, Co, IPGE, Cu, Ag and Sn may be explained by MSS-ISS crystallization, the distribution of the other elements requires further explanation.

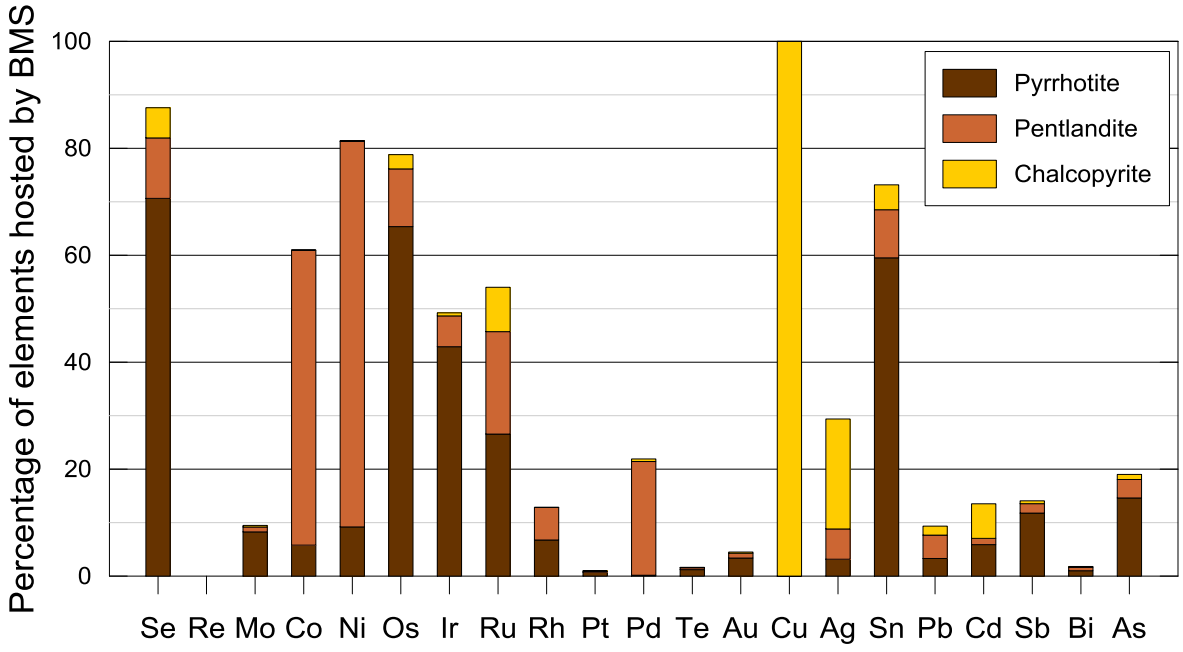

Figure 3.10 Mass balance of chalcophile and platinum-group elements in primary base metal sulfides from the Lac des Iles sulfide-rich pods. The graph is plotted as the median proportion (percent) of each element in pyrrhotite, pentlandite and chalcopyrite. See the text for details.

The presence of Re and Mo in solid solution within Po and Pn, and the presence of Re-Mo-bearing inclusions within Po grains, suggests that Re and Mo were initially concentrated into MSS prior to exsolution of Po and Pn. A similar interpretation has been proposed by Godel and Barnes (2008) and Dare et al. (2010) for Stillwater and Sudbury, respectively. Similarly, Rh could have exsolved as PGM from MSS because it has a compatible behavior. However, we did not observe such minerals, and further investigation is required. Along with Pn, the Pd- and Pt- tellurides, bismuthtellurides and sulfides observed by Duran et al. (submitted), that exhibit exsolution textures could be a consequence of exsolution processes as well. Euhedral PGM could have crystallized from the residual liquids. Furthermore, arsenides and antimonides have been observed in the LDI disseminated sulfides (Djon and Barnes, 2012) and they could be present in sulfide-rich pods. These general observations suggest that the elements that are not primarily controlled by BMS were initially concentrated in sulfides prior to exsolution as discrete minerals from MSS, and they appear to have also crystallized from the residual liquids.

3.7.2 MAGNETITE AND ILMENITE

Magnetite may form in a variety of environments, ranging from high-temperature magmatic to low-temperature hydrothermal environments. As mentioned above, the composition of Mgt depends on the composition of the liquid/fluid from which it crystallizes and the partition coefficient of the elements in Mgt. In addition, its composition depends on the

competition between co-crystallizing phases such as Ilm and sulfides for the elements. On this basis, Dare et al. (2014b) developed a multi-element diagram to identify the signatures of Mgt from various environments, with elements plotted from left to right in order of compatibility in Mgt. In the subsequent treatment of the data we present the elements in increasing order of compatibility in Mgt (Fig. 3.11).

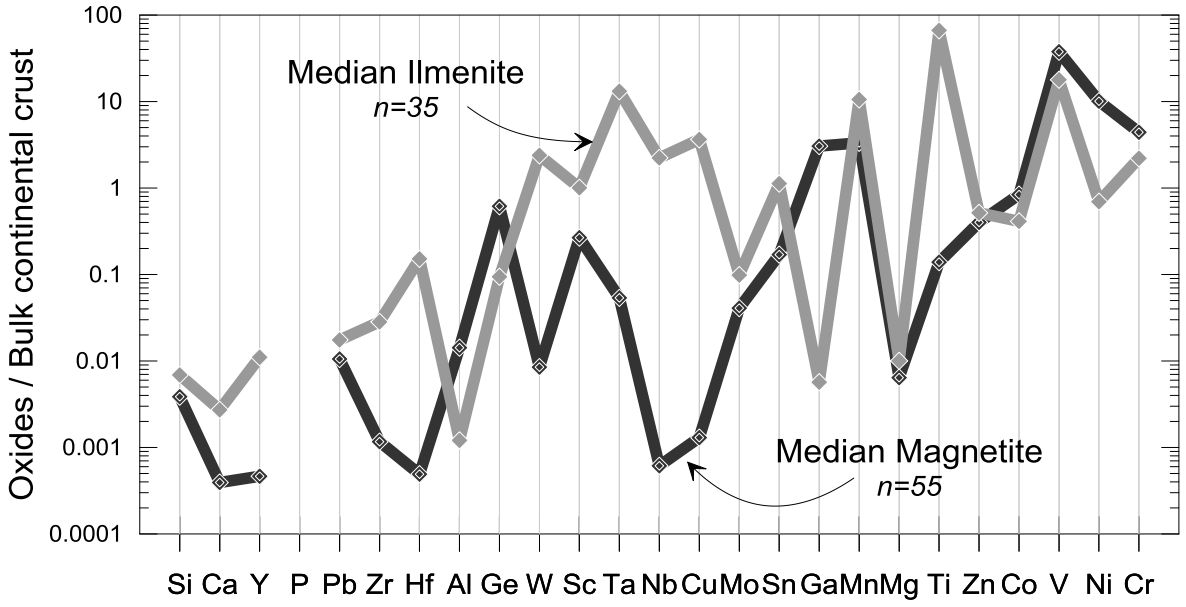

Figure 3.11 Bulk continental crust normalized multi-element diagrams of magnetite and ilmenite. The normalization values are from Rudnick and Gao (2003).

The median composition of each Fe-Ti oxide is presented in Table 3.2, along with the minimum and maximum values. The full dataset is presented in the online supplementary material. Typical time-signal diagrams for the Fe-Ti oxides are presented in Figure 3.12 and they indicate that the lithophile and chalcophile elements are present in solid solution. In Ilm, the elements are homogeneously distributed (Fig. 3.12). Hematite exsolutions in Ilm are not apparent on the time-signal diagrams owing to their size, which is smaller than the size of the laser beam. In Mgt, most of the elements are homogeneously distributed except for Mg and Al (Fig. 3.12), which are preferentially concentrated in spinel exsolutions too small to be visible in thin section.

Element		Isotope	Magnetite n=55			Ilmenite n=25		
			Median	Min	Max	Median	Min	Max
Mg	(ppm)	^{25}Mg	182	46.3	2930	284	68.2	1731
Al	(ppm)	^{27}Al	1196	518	6768	101	18.6	1046
Si	(ppm)	^{29}Si	1094	≤648	8856	1957	766	4505
Ca	(ppm)	^{44}Ca	18.0	≤12.3	744	125	15.9	2130
Sc	(ppm)	^{45}Sc	1.18	0.403	3.67	288	44.7	332
Ti	(ppm)	^{47}Ti	506	96.4	3305	273921	230140	294189
V	(ppm)	51V	5200	27.8	21800	2467	566.1	6238
Cr	(ppm)	^{52}Cr	596	5.04	13530	298	4.51	1852
Mn	(ppm)	^{55}Mn	2583	222	2987	8189	5177	17043
Co	(ppm)	^{59}Co	22.3	7.34	166	11.0	1.22	182
Ni	(ppm)	^{60}Ni	596	237	1145	41.0	11.7	1322
Cu	(ppm)	^{63}Cu	1.10	0.083	1901	2.66	1.68	1689
Zn	(ppm)	^{66}Zn	28.9	9.28	1305	37.2	19.0	169
Ga	(ppm)	^{71}Ga	48.9	18.2	125	0.825	0.454	3.79
Ge	(ppm)	^{74}Ge	0.799	0.443	1.29	≤0.125	≤0.125	0.445
Y	(ppm)	^{89}Y	≤0.013	≤0.013	0.288	0.221	0.068	1.36
Zr	(ppm)	^{90}Zr	0.028	≤0.015	0.375	6.57	0.610	176
Nb	(ppm)	^{93}Nb	≤0.018	≤0.018	1.41	29.2	9.93	125
Mo	(ppm)	^{95}Mo	≤0.143	≤0.143	0.471	0.899	0.318	2.12
Sn	(ppm)	^{118}Sn	0.454	0.080	11.6	1.71	0.211	32.56
Hf	(ppm)	^{178}Hf	≤0.015	≤0.015	0.028	0.562	0.041	6.28
Ta	(ppm)	^{181}Ta	≤0.006	≤0.006	0.174	1.56	0.185	8.06
W	(ppm)	^{182}W	≤0.015	≤0.015	1.07	2.39	0.180	25.7
Pb	(ppm)	^{208}Pb	0.116	0.020	5.76	0.192	≤0.011	0.913

Table 3.2 Compositions of Fe-Ti oxides from Lac des Iles sulfide-rich pods as determined by LA-ICP-MS analysis. n = number of analysis; min = minimum value; max = maximum value.

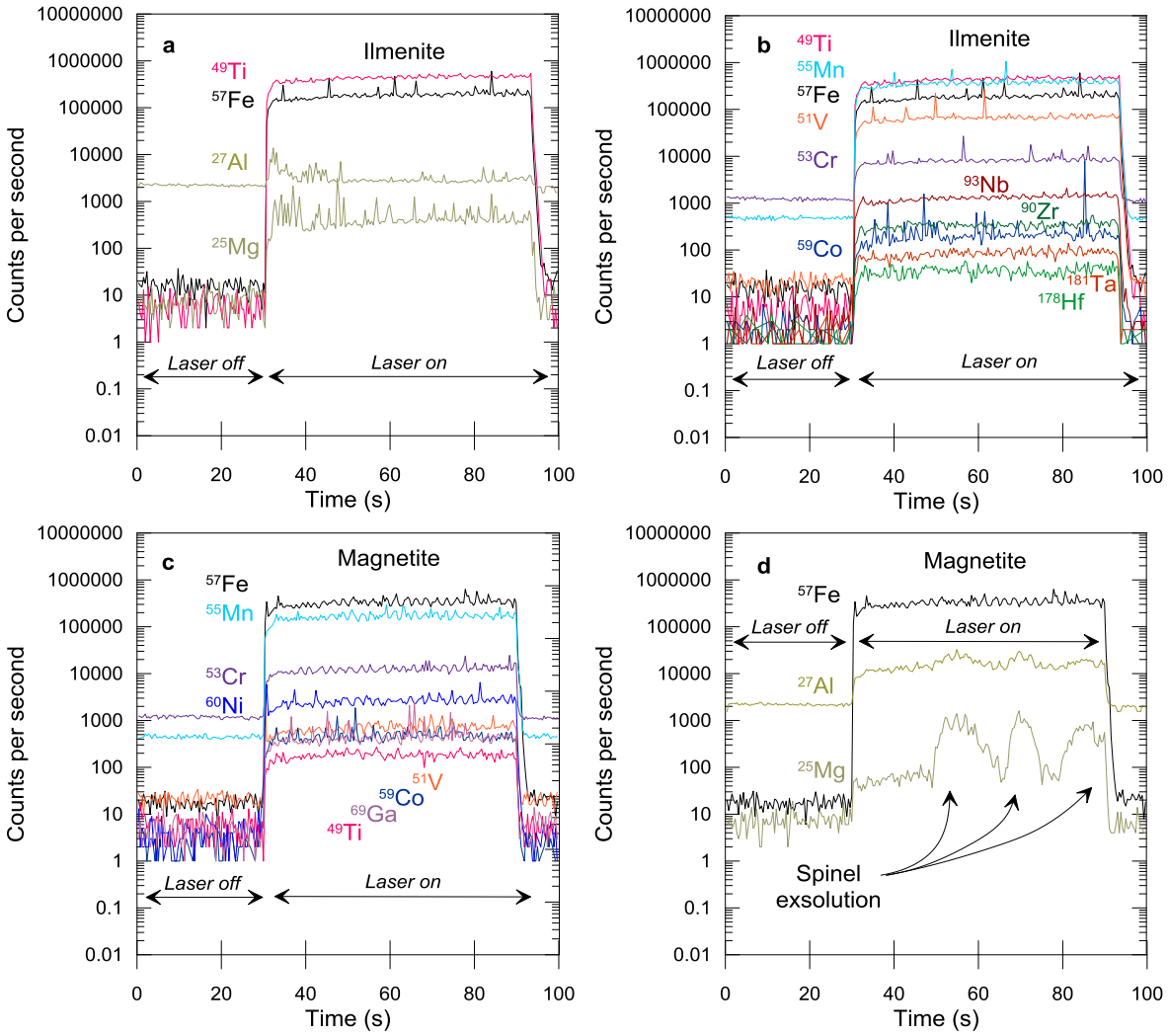

Figure 3.12 Examples of time-signal diagrams of Fe-Ti oxides: (a-b) ilmenite; (c-d) magnetite.

Considering the multi-element patterns from incompatible to compatible elements, we note an increasing slope. Typically, magmatic Mgt is relatively depleted in the least compatible elements, such as Si and Ca, which are present when Mgt forms from hydrothermal fluids (Dare et al., 2014b; Nadoll et al., 2014). In Mgt that are present in the LDI sulfide-rich pods, the Si and Ca concentrations are close to or below the detection limit. Similarly, Si concentrations in Ilm are close to the detection limit, but Ca concentrations are in the range of 15.9 to 2130 ppm with most values < 1000 ppm. Both observations suggest that the Mgt and Ilm from LDI sulfide-rich pods did not form from a fluid.

In contrast, magmatic Mgt is relatively enriched in Al, Mn, high field strength elements (HFSE; Zr, Hf, Ta and Nb), Sc, W and Ti (Dare et al., 2014b). These elements are considered relatively immobile and are depleted in hydrothermal Mgt (Nadoll et al., 2014). In Mgt that are present in the LDI sulfide-rich pods, the Al and Mn concentrations are quite high, in the range of 222 to 6768 ppm, but the concentrations of Ti are low, < 1 wt.%. The concentrations of HFSE, Sc and W are also low (< 1 ppm). The low Ti, HFSE, Sc and W values are especially apparent on the multi-element patterns (Fig. 3.11), which show Hf, W and Nb negative anomalies. These low values contradict the interpretation, based on Si, Mn, Al, and Mn, that the Mgt is igneous. This contradiction may be resolved by considering the presence of Ilm. In the Sept-Iles layered intrusion and in the Lac St Jean anorthosite it has been demonstrated that, during co-crystallization of both Fe-Ti oxides, Ilm preferentially includes HFSE, Sc and W, whereas Mgt preferentially accommodates Al, Ga, Mg, Ni, and Cr (Méric, 2011; Néron, 2012). The Fe-Ti oxides from the LDI sulfide-

rich pods exhibit a similar behavior, with Mgt being depleted in HFSE, Sc and W whereas Ilm exhibits an enrichment in these elements. Conversely Mgt is enriched in Al, Ga, Ni and Cr, and Ilm is depleted in these elements (Fig. 3.11).

Magmatic Mgt may also be fairly enriched in some chalcophile elements, such as Pb, Cu, Mo, Sn, Zn and Co (Dare et al., 2012, 2014b). However, just as co-crystallization of Ilm impoverishes Mgt in Ti, HFSE, Sc and W, sulfide segregation prior to crystallization of oxides affects the chalcophile element composition of the oxides. The concentrations of Pb, Cu, Mo, Sn, Zn and Co are relatively low in both Mgt and Ilm (Fig. 3.11). Cobalt and Zn are the only elements for which the concentrations may exceed hundreds of ppm. The other elements have concentrations of < 33 ppm. The low overall abundance of these chalcophile elements in oxides may reflect their partitioning into sulfides in preference to oxides. However, Sn concentrations in sulfides are not much higher than in oxides. This has also been noticed at Sudbury (Dare et al. 2012) and suggests that Sn is sub-equally distributed between oxides and sulfides.

Vanadium, Ni and Cr are usually the most enriched elements in magmatic Mgt whereas they are depleted in hydrothermal Mgt (Dare et al., 2014b; Nadoll et al., 2014). In Mgt from LDI sulfide-rich pods, the Cr and V concentrations are extremely variable ranging from 5.04 ppm to 2.18 wt.%. Nickel concentrations are less variable, staying in the ranges of 237 to 1145 ppm for Mgt and 11.7 to 1322 ppm for Ilm. On the multi-element diagram of Mgt, the median values of V, Ni and Cr are greater than 10 times the value of the bulk continental crust, which indicates strong enrichment of these elements (Fig. 3.11). The Ilm

pattern for V, Ni and Cr is similarly shaped but lower, which indicates the preference of these elements for Mgt over Ilm. On a plot of Cr versus V (Fig. 3.13), a relatively strong positive correlation between these elements for both Mgt and Ilm is noticeable. This trend has been observed at other localities (e.g., Sudbury, Voisey's Bay and Noril'sk) and has been interpreted to result from sulfide liquid fractionation (Dare et al., 2012; Boutroy et al., 2014). Vanadium and Cr are compatible elements in Mgt and are fairly incompatible in sulfides. Therefore, the minor amounts of these elements that are present in sulfide liquids are concentrated in Mgt that crystallizes early, thus depleting the fractionated liquids. Consequently, late-crystallizing Mgt is impoverished in these elements relative to early-crystallizing Mgt. In contrast, Ni is slightly incompatible in MSS at high temperature, and some Ni partitions into early-crystallizing Mgt. Nickel is incompatible in ISS upon cooling, consequently, some of the Ni partitions into late-crystallizing Mgt. Thus, the Ni concentrations remain fairly constant during crystal fractionation. The variable Cr and V concentrations and the constant Ni level suggest to us that Fe-Ti oxide compositions changed with the crystal fractionation of sulfide liquids.

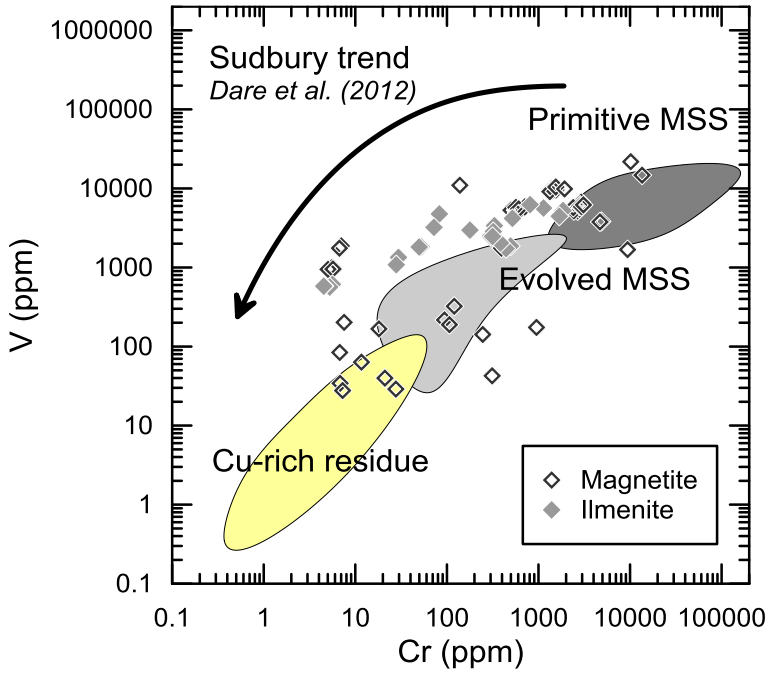

Figure 3.13 Binary diagrams of V versus Cr. Note that the data set follows the trend of sulfide fractionation defined by Dare et al. (2012).

The Mgt with low concentrations of V and Cr could be interpreted as having a hydrothermal signature rather than being the product of crystallization from evolved sulfide liquids. The plot of Ni+Cr versus Si+Mg developed by Dupuis and Beaudoin (2011) may be used to discriminate Mgt from magmatic Ni-Cu-PGE deposits and hydrothermal deposits (Dare et al., 2012; Boutroy et al., 2014). This plot shows that, although the Mgt from LDI sulfide-rich pods show variable degrees of fractionation and depletion in some compatible elements, most of them do not plot outside of the field of Ni-Cu-PGE deposits, thus confirming the magmatic origin of the Mgt (Fig. 3.14).

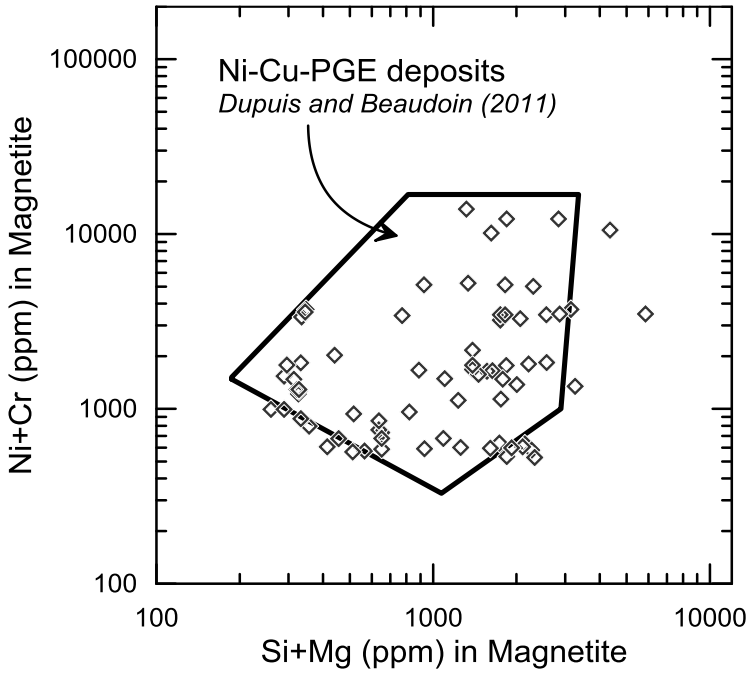

Figure 3.14 Binary diagrams of Ni + Cr versus Si + Mg in magnetite. Note that the data set plots within the field of Ni-Cu-PGE deposits defined by Dupuis and Beaudoin (2011).

3.8 DISCUSSION

Processes that could have affected the PGE and chalcophile element distribution of primary ore-mineral assemblage from Ni-Cu-PGE deposits have been highlighted by several authors. The determining factors include the following: (1) the nature of the parental magma; (2) crystal fractionation of sulfide liquids; (3) crystallization of Fe-Ti oxides; (4) exsolution of MSS; and (5) deformation. To consider the influence of each of these processes on the composition of the primary ore-mineral assemblage of the LDI sulfide-rich pods, we compared our results with those for well-characterized Ni-Cu-PGE deposits.

3.8.1 PARENTAL MAGMA

In mafic-ultramafic igneous systems, the PGE and chalcophile elements are commonly assumed to be scavenged from silicate magmas by sulfide liquids, which occurs when the silicate magmas reach sulfur saturation (e.g., Naldrett, 2004). Given this consideration, the amounts of PGE and chalcophile elements collected by sulfide liquids are controlled by two parameters: (1) the concentrations of the PGE and chalcophile elements in the silicate magma; and (2) the sulfide to silicate ratio, or R-factor.

The amounts of PGE and chalcophile elements that are available in the parental magma are directly related to the nature of the magma. Sulfides derived from similar magmas should have similar patterns on primitive mantle normalized metal diagrams. However, sulfides

derived from similar magmas but with different R-factors will not have the same composition, especially for PGE. Barnes and Lightfoot (2005) demonstrated that massive sulfides at many localities have lower PGE concentrations than disseminated sulfides, possibly because of a lower R-factor. This difference arises because PGE have the highest partition coefficients for sulfides. Nonetheless, because they have similar partition coefficients (Barnes and Lightfoot, 2005 and references therein; Mungall et al., 2005; Brenan, 2008; calculated from Li and Audétat, 2012) the PGE will be enriched in the same proportions regardless of the R-factor.

For example, when comparing Po and Pn from LDI sulfide-rich pods with Po and Pn from LDI disseminated mineralization (Djon and Barnes, 2012), similar patterns are found (Fig. 3.15). However, the minerals from the disseminated mineralization are slightly enriched in all the elements than those from the sulfide-rich pods, most likely because of a higher R-factor. This observation supports the idea proposed by Duran et al. (submitted) that sulfide-rich pods and disseminated mineralization have a genetic relationship. Moreover, this result demonstrates that sulfides from sulfide-rich pods and those from disseminated sulfides come from the same parental magma.

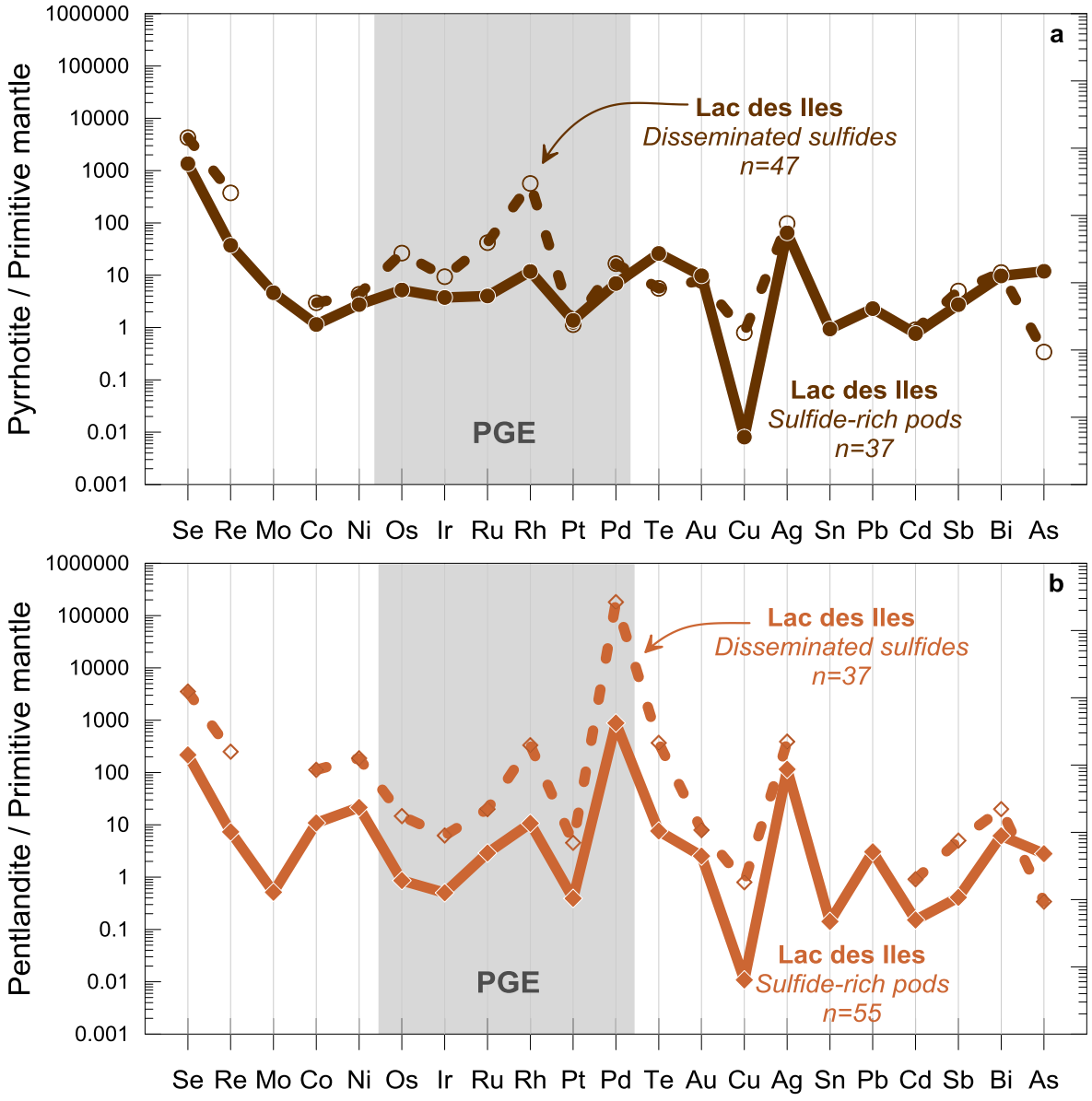

Figure 3.15 Primitive mantle normalized multi-element diagrams of (a) pyrrhotite and (b) pentlandite from Lac des Iles sulfide-rich pods compared with Lac des Iles disseminated sulfides (dashed lines). The data for disseminated sulfides are from Djon and Barnes (2012). The normalization values are from Lyubetskaya and Korenaga (2007).

According to Barnes and Gomwe (2010) LDI parental magma most closely resembles andesite (i.e., evolved magma) and may have been emplaced in a continental arc (Brügmann et al., 1997). To test this idea we plot our Po and Pn and compared them with those derived from evolved magmas, e.g., Sudbury (Dare et al., 2011) and Aguablanca (Piña et al., 2012). Sudbury magmas formed when a meteorite impact flash-melted the bulk continental crust (Golightly, 1994), and they represent an average andesite composition (Rudnick and Gao, 2003). In contrast, Aguablanca magmas formed in an arc setting. Both of these deposits originated from evolved magmas, and the concentrations of PGE and chalcophile elements in our Po and Pn are close to the values of Po and Pn from these deposits (Fig. 3.16a, b; Fig. 3.17a, b). This observation is consistent with LDI parental magma having been of andesitic affinity.

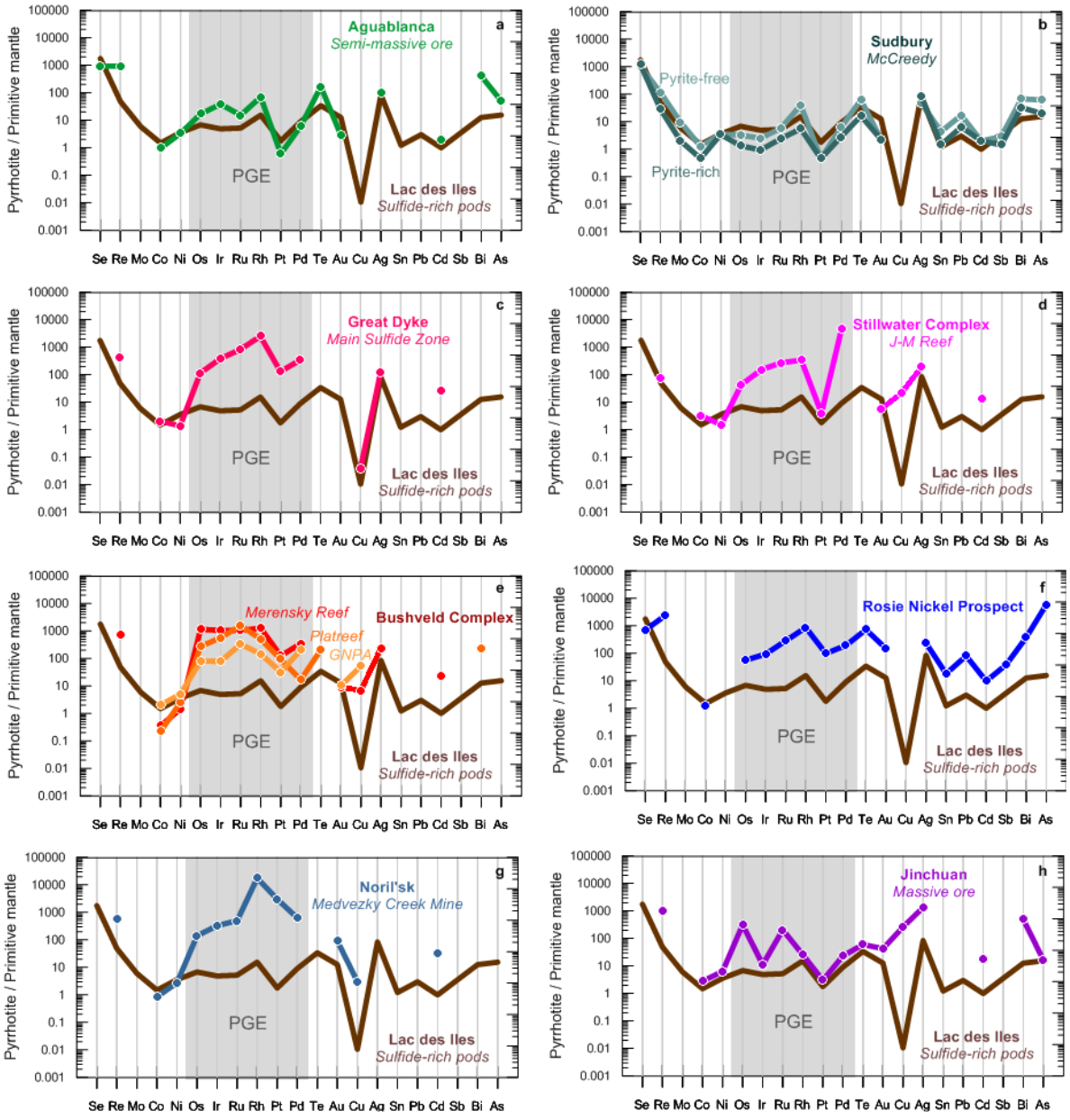
a
Aguablanca
Semi-massive ore
b
Sudbury
McCreedy
Pyrite-free
Pyrite-rich
c
Great Dyke
Main Sulfide Zone
d
Stillwater Complex
J-M Reef
e
Merensky Reef
Platreef
GNPA
Bushveld Complex
f
Rosie Nickel Prospect
g
Noril'sk
Medvezky Creek Mine
h
Jinchuan
Massive ore
PGE
Lac des Iles
Sulfide-rich pods
Pyrrhotite / Primitive mantle
100000
10000
1000
100
10
1
0.1
0.01
0.001
Se Re Mo Co Ni Os Ir Ru Rh Pt Pd Te Au Cu Ag Sn Pb Cd Sb Bi As

Figure 3.16 Primitive mantle multi-element diagrams of pyrrhotite from Lac des Iles sulfide-rich pods compared with pyrrhotite from (a) Aguablanca, semi-massive ore (Piña et al., 2012); (b) Sudbury, McCreedy Deposit (Dare et al., 2010); (c) Great Dyke, Main Sulfide Zone, (Barnes et al., 2008); (d) Stillwater Complex, J-M Reef (Godel and Barnes, 2008); (e) Merensky Reef (Barnes et al., 2008), Platreef (Holwell and McDonald, 2007) and GNPA (Smith et al., 2014) from the Bushveld Complex; (f) Rosie Nickel Prospect (Godel et al., 2012); (g) Noril'sk, Medvezky Creek Mine (Barnes et al., 2008); (h) Jinchuan, massive ore (Chen et al., 2014). The normalization values are from Lyubetskaya and Korenaga (2007).

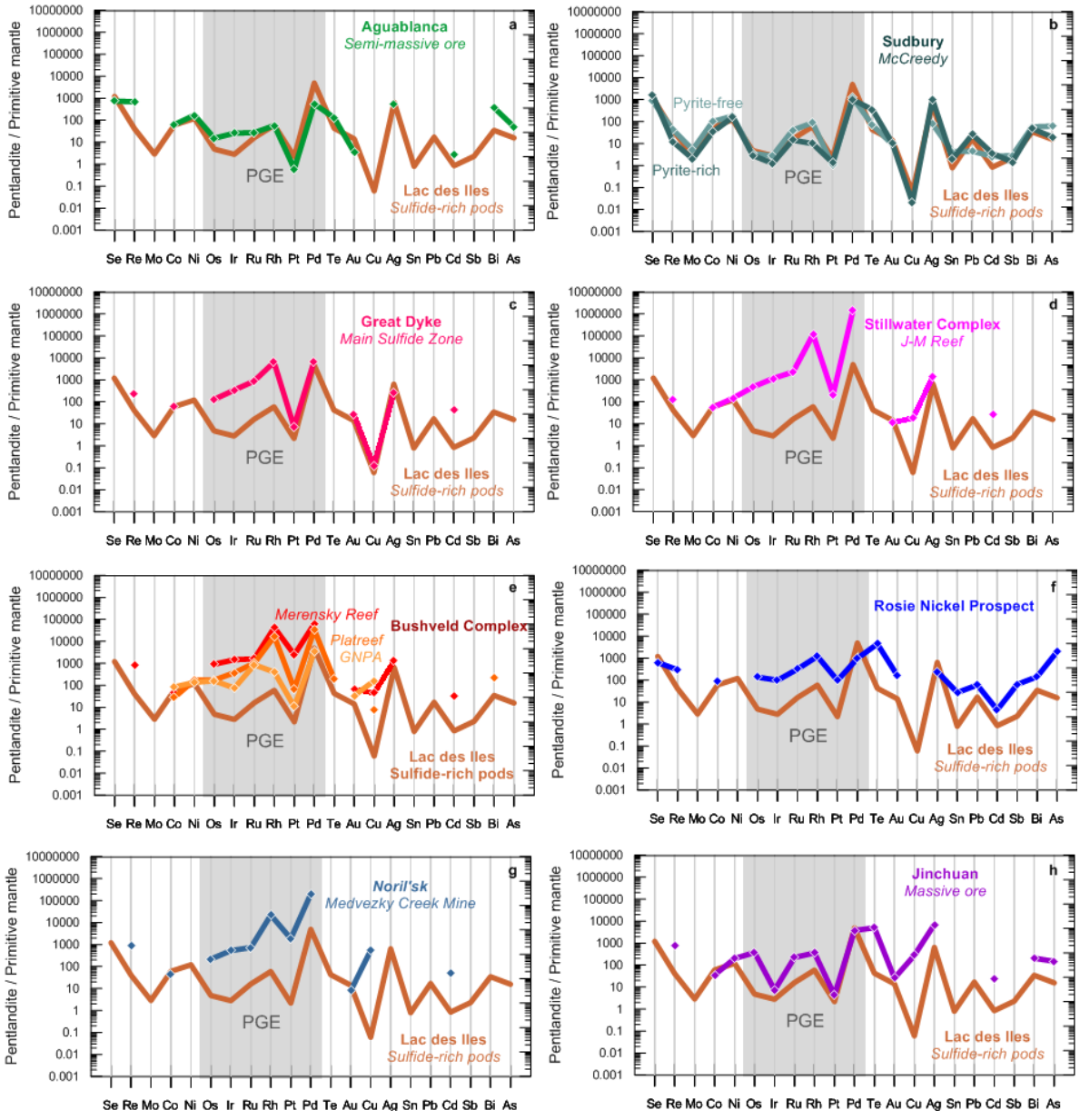
a
Aguablanca
Semi-massive ore
b
Sudbury
McCreedy
Pyrite-free
Pyrite-rich
c
Great Dyke
Main Sulfide Zone
d
Stillwater Complex
J-M Reef
e
Merensky Reef
Bushveld Complex
Platreef
GNPA
f
Rosie Nickel Prospect
g
Noril'sk
Medvezky Creek Mine
h
Jinchuan
Massive ore
PGE
Lac des Iles
Sulfide-rich pods
Pentlandite / Primitive mantle
Se Re Mo Co Ni Os Ir Ru Rh Pt Pd Te Au Cu Ag Sn Pb Cd Sb Bi As

Figure 3.17 Primitive mantle multi-element diagrams of pentlandite from Lac des Iles sulfide-rich pods compared with pentlandite from (a) Aguablanca, semi-massive ore (Piña et al., 2012); (b) Sudbury, McCreedy Deposit (Dare et al., 2010); (c) Great Dyke, Main Sulfide Zone, (Oberthür et al., 1997; Barnes et al., 2008); (d) Stillwater Complex, J-M Reef (Godel and Barnes, 2008); (e) Merensky Reef (Barnes et al., 2008), Platreef (Holwell and McDonald, 2007) and GNPA (Smith et al., 2014) from the Bushveld Complex; (f) Rosie Nickel Prospect (Godel et al., 2012); (g) Noril'sk, Medvezky Creek Mine (Barnes et al., 2008); (h) Jinchuan, massive ore (Chen et al., 2014). The normalization values are from Lyubetskaya and Korenaga (2007).

In contrast, the Po and Pn from LDI sulfide-rich pods do not resemble Po and Pn derived from more primitive magmas (e.g., layered intrusions, ultramafic intrusions, komatiites and flood basalts) in that they are much poorer in most of the elements, particularly in PGE (Fig. 3.16c-h; Fig. 3.17c-h). In addition, the Pn from LDI has a higher Pd/Ir ratio, which supports the idea that the MSS formed from a fractionated magma because fractionated magmas have high Pd/Ir ratios, whereas primitive ones do not (Fig. 3.17).

3.8.2 CRYSTAL FRACTIONATION OF SULFIDE LIQUIDS

Based on the geological setting, petrography and whole-rock geochemistry of LDI sulfide-rich pods, Duran et al. (submitted) argued that the sulfide-rich pods originated from accumulation of magmatic sulfide liquids that subsequently experienced crystal fractionation. This idea is further supported by the enrichment in Ni, Co, Re, IPGE and Rh and the depletion in Cu, Ag, Cd and Zn in Po-Pn relative to Ccp. The distribution of these elements among the BMS, suggests that Ni, Co, Re, IPGE and Rh were concentrated in MSS whereas Ag, Cd and Zn were excluded along with Cu in fractionated liquids, as observed in the experiments of Liu and Brenan (2012). A similar partitioning behavior of these elements has been observed at many places, at which crystal fractionation of sulfide liquids is believed to have occurred (Li et al., 1992; Dare et al., 2014a).

The low concentrations of Pt, Pd, Au and semi-metals in the Ccp along with the presence of PGM, likely resulted from formation of ISS and residual liquids enriched in Pt, Pd, Au and semi-metals (Helmy et al., 2010; Liu and Brenan, 2012). Therefore, in the late stages of crystal fractionation, the late liquid enriched in Pt, Pd, Au and semi-metals may have crystallized as discrete PGM and electrum. These observations are consistent with sulfide liquids having experienced crystal fractionation.

In addition to the BMS assemblage, Mgt crystallization from sulfide liquids is also known to record the crystal fractionation process in its chemistry (Dare et al., 2012). Where the record of crystal fractionation by Mgt prevails, Mgt exhibits a typical trend on a V versus Cr plot (Dare et al., 2012; Boutroy et al., 2014). Because the Mgt associated with LDI sulfide-rich pods exhibits this type of trend (Fig. 3.13), we believe that the Mgt recorded the crystal fractionation experienced by the sulfides. Furthermore, Mgt associated with LDI sulfide-rich pods shows a similar pattern to Mgt from Sudbury on a bulk continental crust multi-element diagram (Fig. 3.18), particularly to Mgt derived from the more evolved part of Sudbury (i.e., McCreedy). This similarity may suggest a common origin for both Mgt from LDI and McCreedy.

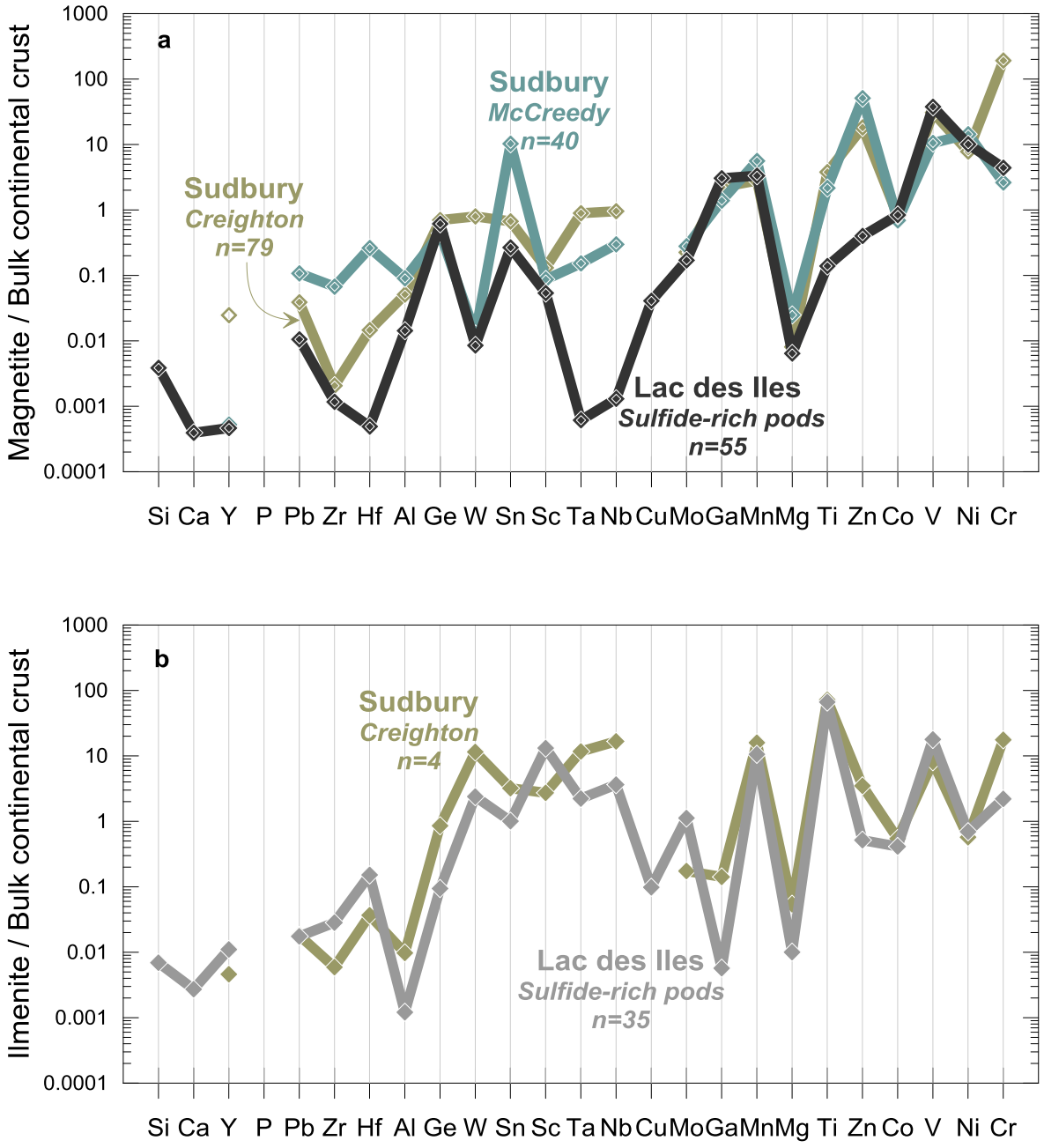

Figure 3.18 Bulk continental crust normalized multi-element diagrams of (a) magnetite and (b) ilmenite from Lac des Iles sulfide-rich pods and Sudbury. The data from Sudbury are from Dare et al. (2012). The normalization values are from Rudnick and Gao (2003).

3.8.3 ORIGIN OF FE-TI OXIDES

The recording of crystal fractionation in the composition of Mgt suggests that Mgt crystallized after the sulfide liquids formed. This interpretation can be supported by normalizing the composition of our Mgt to the composition of Mgt crystallized from andesitic magmas that did not reach S saturation (Dare et al., 2014b). The Mgt associated with LDI sulfide-rich pods is depleted in all of the chalcophile elements relative to Mgt from andesites that contain no sulfides (Fig. 3.19), thereby suggesting that Mgt associated with sulfide-rich pods crystallized after the magmas reached S saturation.

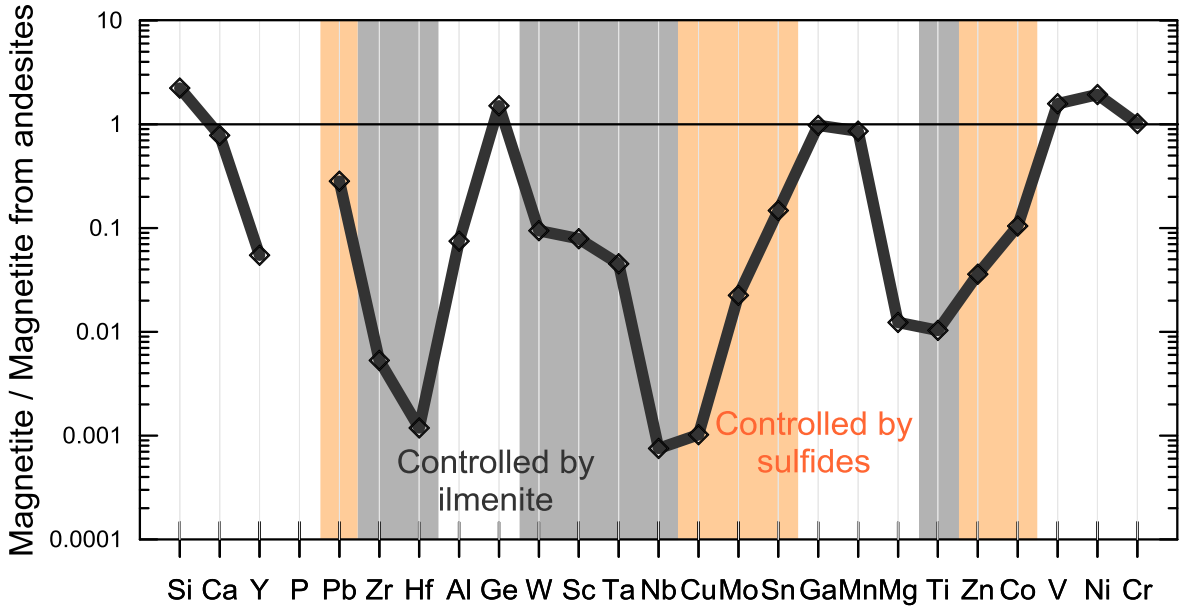

Figure 3.19. Multi-element diagrams of magnetite from Lac des Iles sulfide-rich pods normalized to magnetite from andesites (values from Dare et al., 2014b). Note that magnetite from Lac des Iles sulfide-rich pods is depleted in chalcophile elements (light-red field) and HFSE (light-grey field) relative to magnetite from andesites.

In contrast with Mgt associated with LDI sulfide-rich pods, Mgt from andesites analyzed by Dare et al. (2014b) did not co-crystallize with Ilm. Our results demonstrate that Mgt is relatively depleted in Ti and HFSE (Fig. 3.19). However, Ti is not a chalcophile element, and relatively few occurrences of Ilm associated with sulfides have been reported (Tomkins et al., 2012; Dare et al., 2012). Although the sulfide liquids that formed the sulfide-rich pods may have crystallized some Mgt, it is unlikely that the Ilm directly crystallized from sulfide liquids. An alternative idea is that the Ilm and some Mgt formed by the reaction of oxygen with silicate liquids as it diffused out of the sulfide liquids (Fig. 3.20), as proposed by Fonseca et al. (2008).

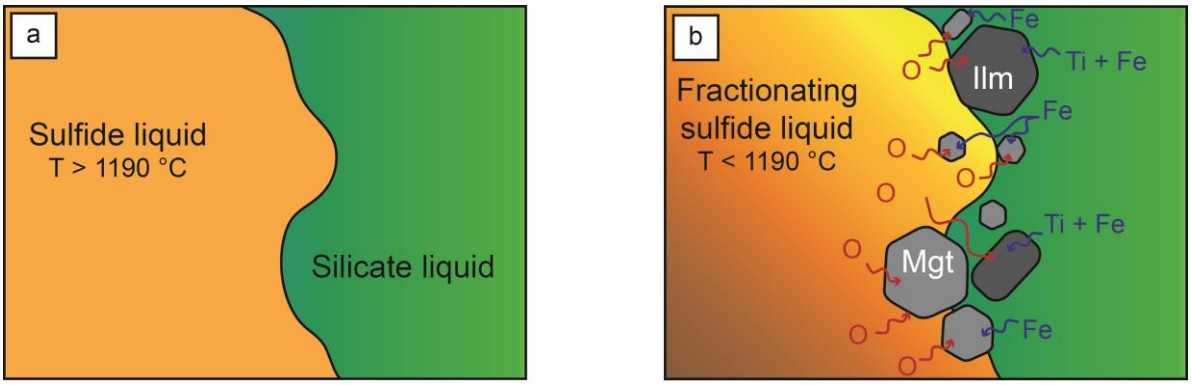

Figure 3.20 Schematic model of the formation of Fe-Ti oxides. (a) The sulfide liquid containing dissolved oxygen is in contact with silicate liquid at temperature higher than 1190 °C. (b) As the temperature decreases, the sulfide liquid experiences crystal fractionation. The amount of dissolved oxygen increases in the fractionated liquid and reacts with Fe and Ti diffusing out of the silicate liquid, thereby forming Fe-Ti oxides.

3.8.4 EXSOLUTION OF MSS

In magmatic Ni-Cu-PGE deposits Po and Pn represent exsolution products of MSS that form during cooling (Naldrett, 1969; Craig, 1973). Numerous studies have demonstrated that Po and Pn usually account for between 40% and 80% of the whole-rock IPGE composition and that Pn usually contains significant amounts of Pd in Ni–Cu–PGE deposits (i.e., Aguablanca, Piña et al., 2012; McCreedy deposit, Sudbury, Dare et al., 2011; Main Sulfide Zone, Great Dyke, Oberthür et al., 1997 and Barnes et al., 2008; J-M Reef, Stillwater Complex, Godel and Barnes, 2008; Merensky Reef, Platreef, and GNPA, all of which are part of the Bushveld Complex, Barnes et al., 2008, Holwell and McDonald, 2007, Smith et al., 2014, respectively; Rosie Nickel Prospect, Yilgarn Craton, Godel et al., 2012; Medvezky Creek Mine, Noril'sk, Barnes et al., 2008; Jinchuan, Chen et al., 2014). The distributions of Ni, Co, IPGE and Pd between Po and Pn from LDI sulfide-rich pods are fairly similar, which supports the idea of Po and Pn having exsolved from MSS.

To test whether exsolution of Po and Pn from MSS would redistribute PGE in the same manner in various environments, we have plotted the composition of each PGE in Po versus the composition in Pn for some Ni-Cu-PGE deposits (Fig. 3.21). On a plot of Ir in Po versus Ir in Pn we notice that LDI sulfide-rich pods lie close to the 1:1 line, as do most of the other Ni-Cu-PGE deposits. Osmium and Ru exhibit trends that are similar to that of Ir (Figs. 3.21a-c). This result indicates that, during the development of Po and Pn, the IPGE are sub-equally distributed. The only exception is the J-M Reef of the Stillwater Complex,

in which Pn tends to be enriched in IPGE relative to Po by a factor of 10. In contrast with IPGE, Rh shows variable distributions between Po and Pn, depending on the deposits (Fig. 3.21d). Most deposits plot close to the 1:1 line, but Platreef and Merensky Reef of the Bushveld Complex and J-M Reef of the Stillwater Complex show a 10:1 enrichment of Rh in Pn. Although Pt does not reside primarily within Po and Pn, some of the available data indicate a variable distribution. Indeed, the Medvezky Creek Mine of Noril'sk, the Platreef and GNPA of the Bushveld Complex and the Great Dyke lie below the 1:1 line, whereas the other deposits lie above the line (Fig. 3.21e). This difference may arise from the cooling rates of the deposits. Because the deposits at which the Po is enriched in Pt relative to Pn are those that have cooled faster, we suspect that the cooling rate influences the diffusion of the small amount of Pt incorporated within the MSS because rapid cooling limits the distance that diffusion can accomplish. Diffusion can attain greater distances with slow cooling. However, the use of the median and the analytical uncertainties due to the low levels of Pt in both Po and Pn might be misleading and care should be taken when comparing these data. Palladium is systematically enriched in Pn relative to Po, but the primary PGE producers (LDI, Stillwater, Great Dyke and Bushveld) are enriched by a factor of approximately 100, whereas the Ni-Cu deposits (Sudbury, Aguablanca and Rosie) are enriched by a factor of approximately 10 (Fig. 3.21f). This difference likely arises from the larger amount of Pd collected by sulfides in the PGE deposits.

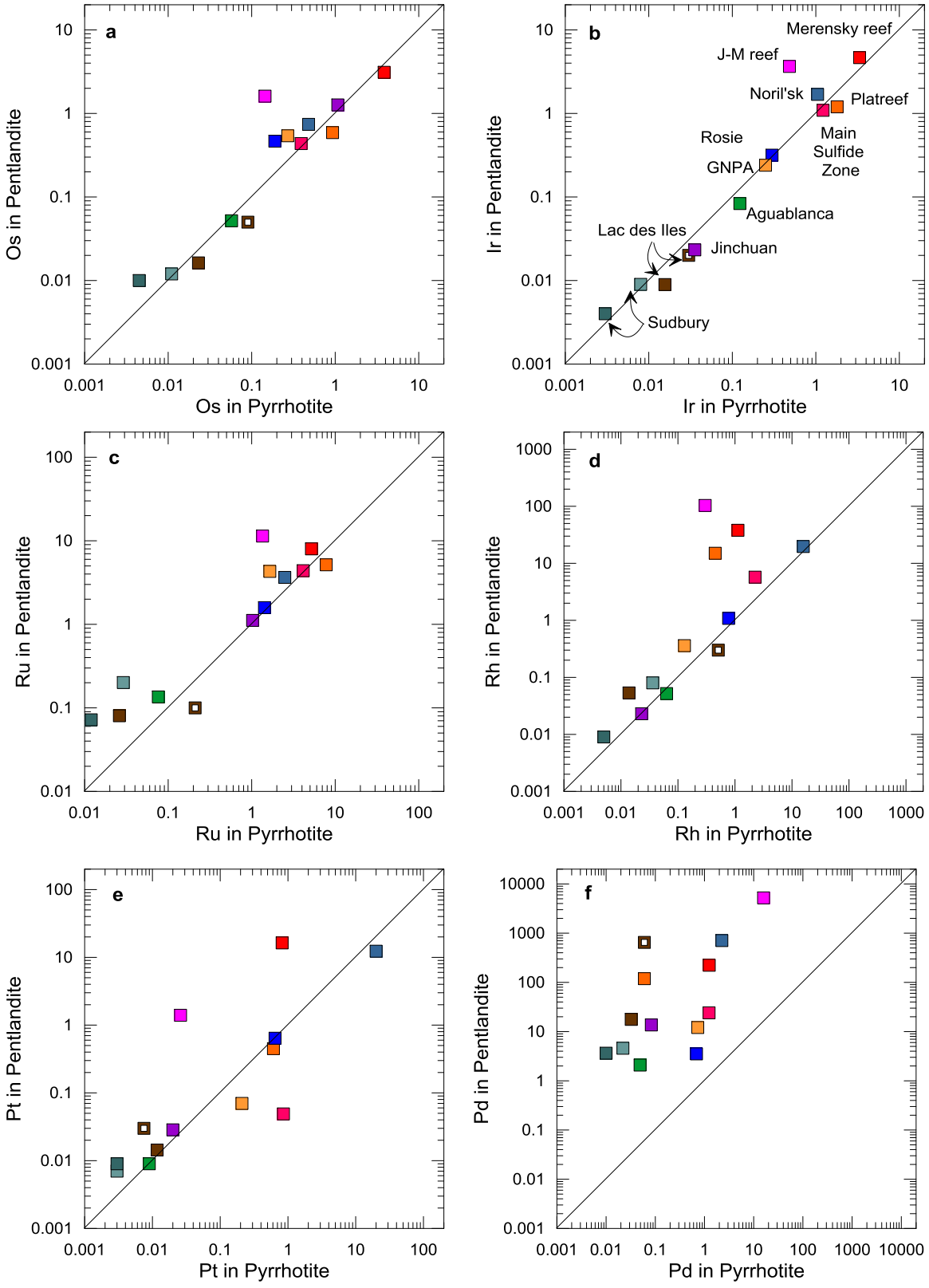
a
Os in Pentlandite
Os in Pyrrhotite
b
Ir in Pentlandite
Ir in Pyrrhotite
Merensky reef
J-M reef
Noril'sk
Platreef
Rosie
Main
Sulfide
Zone
GNPA
Aguablanca
Lac des Iles
Jinchuan
Sudbury
c
Ru in Pentlandite
Ru in Pyrrhotite
d
Rh in Pentlandite
Rh in Pyrrhotite
e
Pt in Pentlandite
Pt in Pyrrhotite
f
Pd in Pentlandite
Pd in Pyrrhotite

Figure 3.21 Binary diagrams of PGE in pentlandite versus PGE in pyrrhotite. (a) Os in pentlandite versus Os in pyrrhotite; (b) Ir in pentlandite versus Ir in pyrrhotite; (c) Ru in pentlandite versus Ru in pyrrhotite; (d) Rh in pentlandite versus Rh in pyrrhotite; (e) Pt in pentlandite versus Pt in pyrrhotite; (f) Pd in pentlandite versus Pd in pyrrhotite. The data sources for other Ni-Cu-PGE deposits are: Holwell and McDonald (2007), Godel and Barnes (2008), Barnes et al. (2008), Dare et al. (2010), Djon and Barnes (2012), Piña et al. (2012), Godel et al. (2012), Smith et al. (2014), and Chen et al. (2014).

Although Ag is incompatible in MSS, we also noticed that, in our Pn and in those from other deposits (i.e., Aguablanca, Piña et al., 2012; McCreedy Deposit, Sudbury, Dare et al., 2011; Main Sulfide Zone, Great Dyke, Barnes et al., 2008; J-M Reef, Stillwater Complex, Godel and Barnes, 2008; Merensky Reef, Bushveld Complex, Barnes et al., 2008; Rosie Nickel Prospect, Yilgarn Craton, Godel et al., 2012; Jinchuan, Chen et al., 2014), Ag is present in significant amounts. Furthermore, Ag is enriched in Pn relative to Po by a factor of 10 (Fig. 3.22). This could be a consequence of Ag diffusion during exsolution of Pn from MSS in the same manner as Ni, Co and Pd.

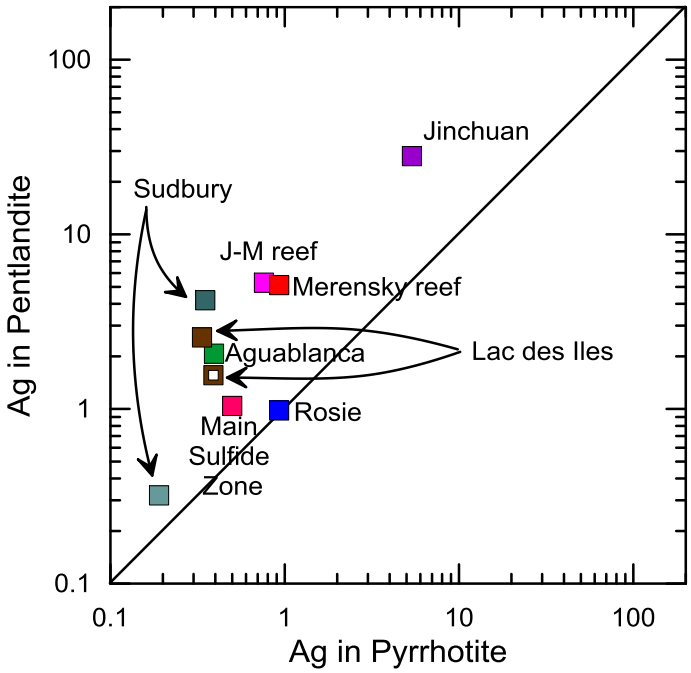

Figure 3.22 Binary diagram of Ag in pentlandite versus Ag in pyrrhotite. The data sources for other Ni-Cu-PGE deposits are: Godel and Barnes (2008), Barnes et al. (2008), Dare et al. (2010), Djon and Barnes (2012), Piña et al. (2012), Godel et al. (2012), Chen et al. (2014).

The presence of Re-Mo-bearing minerals within Po grains, Pd-bearing PGM displaying exsolution textures together with Pn (Duran et al., submitted) and possibly Rh-bearing minerals suggests that discrete minerals have exsolved from MSS along with Po and Pn. This interpretation has also been proposed in a number of previous studies (Godel and Barnes, 2008; Dare et al., 2010; Chen et al., 2014).

3.8.5 DEFORMATION

Only a few studies have paid attention to the role of deformation in redistributing certain elements at the grain scale. These include studies of metamorphosed sulfides from Penikat (Barnes et al., 2008), Raglan (Misson et al., 2014), and some komatiites from the Yilgarn Craton (Vukmanovic et al., 2014).

Metamorphism is believed to promote diffusion of some elements when the sulfides recrystallize. Whereas IPGE are mainly hosted by Po and Pn in unmetamorphosed Ni-Cu-PGE deposits, Barnes et al. (2008) noticed that the IPGE concentrations of Po and Pn from the PV Reef of the Penikat Intrusion, which has undergone greenschist facies metamorphism, only account for a small amount of the mass balance. Moreover, they observed that PGM composed of IPGE were more abundant than in unmetamorphosed deposits. In contrast, we did not observe PGM composed of IPGE in BMS from the LDI

sulfide-rich pods. Instead, Po and Pn account for the majority of the IPGE. Therefore, metamorphism is unlikely to have affected the IPGE distribution in the sulfide-rich pods.

Similarly, Pd and Rh are systematically homogeneously distributed in Pn, as indicated by the time-signal diagrams in Figure 3.4. Given this consideration, we may argue that deformation did not contribute to redistributing the Pd and Rh at LDI.

However, Vukmanovic et al. (2014) demonstrated that the concentrations of some elements such as Ag, Bi, and Pb, increase along certain grain boundaries, low-angle boundaries, and twin boundaries within Po grains. This observation was limited to the elements with large ionic radii, which might have been redistributed more easily. Vukmanovic et al. (2014) suggested that deformation-controlled diffusion could occur at temperatures as low as 350°C, which is consistent with greenschist facies conditions. Similarly, we observed heterogeneous distribution of these elements within some Po and in much of the Pn (Fig. 3.4). This is especially apparent on the chemical maps (Fig. 3.23), where Ag and Pb are more concentrated along cracks and grain boundaries. Furthermore, a heterogeneous distribution of these elements is observed within coarse Pn, which is likely to have formed at approximately 600°C. Given these considerations, the initial distribution of Ag, Bi and Pb in Pn may have been modified during deformation under greenschist conditions. Alternatively, these metals could have been introduced by fluids as Ag and Pb can form stable complexes with HS- and Cl- in magmatic-hydrothermal systems (e.g., Pokrovski et al., 2013). Circulation of fluids along the deformation planes in the sulfides could have allowed incorporation of these metals along cracks and grain boundaries.

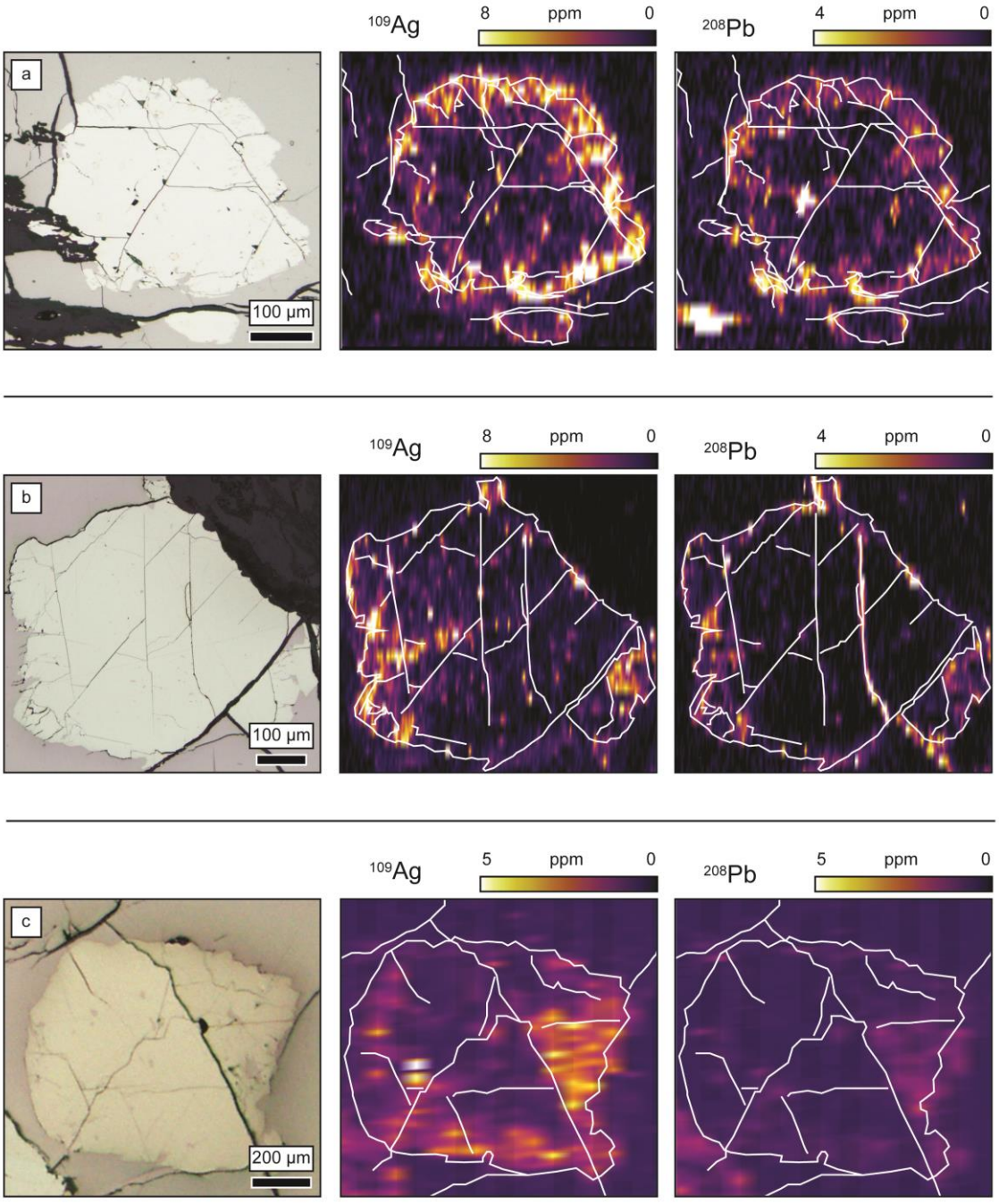

Figure 3.23 Distribution of Ag and Pb in coarse grained pentlandite showing that: (a) Ag and Pb are concentrated along the grain boundaries; (b-c) Ag and Pb are concentrated along cracks and grain boundaries. Note that grain boundaries and cracks are outlined in white.

3.8.6 EXPLORATION CONSIDERATIONS

Lac des Iles represents an enigmatic Pd deposit. It is the only example of such deposits that is known to date and exploration targeting has failed to identify these rock types as being fertile for PGE. Therefore, there is a significant need to refine exploration models and develop new geochemical tools that can be used for exploration. The multi-element diagram that we have developed can be used to fingerprint the origin of sulfides as either being derived from primitive or evolved magmas. In a greenfields setting, this criterion can be of key importance for adapting exploration strategies.

One interesting observation is that Pn contains much of the Pd and Rh present in sulfides, and this has potential for use in discriminating between primary PGE producers and Ni-Cu sulfide deposits during exploration. For instance a plot of Pd in Pn versus Rh in Pn (Fig. 3.24) can be used to determine the provenance of Pn. In unconsolidated detritus such as glacial till, Pn may be present in the heavy mineral fraction. The use of Pn geochemistry to fingerprint Ni-Cu-PGE could represent a powerful exploration tool that is becoming more practical because of the increasing availability of LA-ICP-MS analysis.

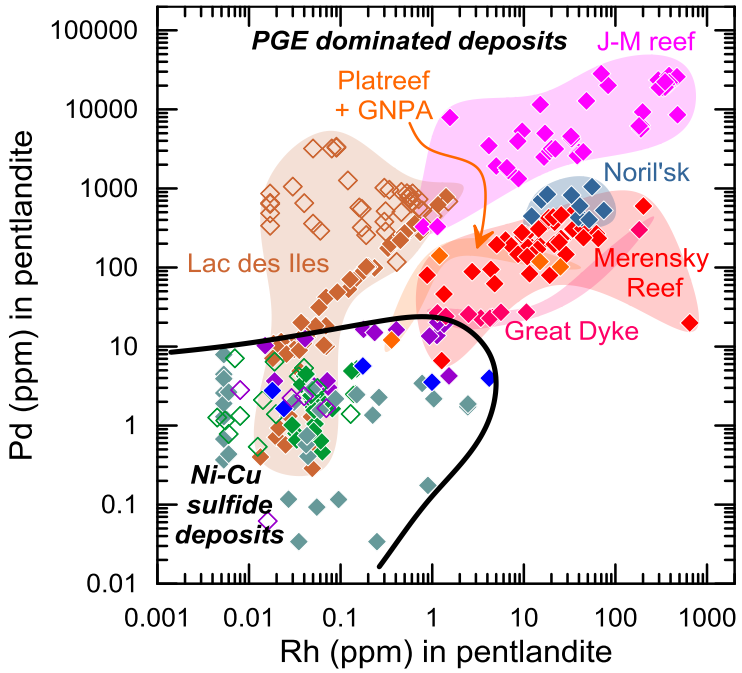

Figure 3.24 Binary diagram of Pd in pentlandite versus Rh in pentlandite. Note that pentlandites from PGE dominated deposits can be discriminated from pentlandites from Ni-Cu sulfide deposits on the basis of their Pd and Rh concentrations. The data sources are: Holwell and McDonald (2007), Godel et al. (2007), Barnes et al. (2008) and Smith et al. (2014) for the Bushveld Complex (Merensky Reef, Platreef and GNPA), Barnes et al. (2008) and Oberthür et al. (1997) for the Great Dyke, Godel and Barnes (2008) for the J-M Reef of the Stillwater Complex, Barnes et al. (2008) for Noril'sk, Djon and Barnes (2012) and this study for Lac des Iles (open diamonds = disseminated ore; closed diamonds = sulfide-rich pods), Dare et al. (2010) for Sudbury (grey diamonds), Piña et al. (2012) for Aguablanca (open green diamonds = disseminated ore; closed green diamonds = semi-massive ore, Godel et al. (2012) for Rosie Nickel Prospect (blue diamonds), and Chen et al. (2014) for Jinchuan (open purple diamonds = disseminated ore; closed purple diamonds = massive and semi-massive ore).

3.9 CONCLUDING REMARKS

This LA-ICP-MS study has highlighted (1) the distribution of PGE and chalcophile elements among primary BMS and the associated Fe-Ti oxides of the LDI sulfide-rich pods and (2) the processes that influence this distribution. Our findings may be summarized as follows:

(1) The sulfide mineral compositions of LDI sulfide-rich pods exhibit similarities to sulfide minerals derived from evolved magmas (e.g., Sudbury and Aguablanca) and do not resemble sulfide minerals derived from primitive magmas. The sulfide liquids from which the sulfide minerals at LDI formed were, therefore, derived from evolved magmas, most likely of andesitic composition.

(2) The similarity between the sulfide mineral composition in the massive pods and the disseminated sulfides suggests a common origin for both types of mineralization.

(3) The distribution of PGE and chalcophile elements among the primary BMS at LDI was initially governed by their partitioning behavior during the crystal fractionation of MSS.

(4) Magnetite crystallized after the sulfides and recorded the signature of crystal fractionation of sulfide liquids. Because Mgt co-crystallized with Ilm, we believe that most Fe-Ti oxides associated with the sulfide-rich pods were formed by reaction of oxygen with silicate liquids as it diffused out of the sulfide liquids.

(5) Pyrrhotite and Pn account for most of the whole-rock Co and IPGE in solid solution. The Pn hosts significant amounts of Rh and Pd. Palladium also occurs as Pd-bearing PGM displaying exsolution textures together with Pn, and Re-Mo-bearing inclusions are present within Po grains. These observations suggest that elements that were initially concentrated in MSS have been redistributed by exsolution of Po, Pn and some discrete minerals.

(6) The Ccp is enriched in Ag, Cd and Zn relative to Po and Pn but is depleted in Pd, Pt, Au and semi-metals. This result indicates that Ccp has exsolved from ISS and does not represent the Cu-rich liquid.

(7) The Pt, Au and semi-metals are not present in significant concentrations in BMS, but are suspected to be present as discrete PGM and electrum. Crystallization of the late fractionated liquids, enriched in Pt, Pd, Au and semi-metals, appears to be an explanation for this observation.

(8) The heterogeneous distributions of Ag, Bi and Pb within the Pn and some of the Po suggest that the sulfide-rich pods have undergone some deformation-induced metal diffusion. However, the distribution of the PGE has not been influenced by this deformation.

3.10 ACKNOWLEDGMENTS

This study was completed by the first author as part of his PhD research project at UQAC. We are grateful to North American Palladium for providing financial support for the Sarah-Jane Barnes' Canada Research Chair in Magmatic Ore Deposits, for allowing access to the mine property and publication of this paper, and for hiring the first author as an exploration geologist during field seasons. We would also like to thank the entire North American Palladium Exploration Team for technical support in the field over the years. Dany Savard and Sadia Mehdi are thanked for their assistance with the LA-ICP-MS facilities at LabMaTer, UQAC. This study largely benefited from intellectual input from Philippe Pagé and Ed Sawyer of UQAC, Sarah Dare of University of Ottawa, and Lionnel Djon, Arnaud Tchalikian, and Skylar Schmidt of North American Palladium. Finally, the anonymous reviewers are thanked for their time and for thorough revision and improvement of this manuscript.

3.11 REFERENCES

Barnes, S-J. and Lightfoot, P.C. (2005) Formation of magmatic nickel sulfide ore deposits and processes affecting their copper and platinum group element contents. Economic Geology 100th Anniversary Volume, pp 179–213.

Barnes, S-J. and Gomwe, T.S. (2010) Composition of the Lac des Iles magma and implications for the origin of the ore. In: 11th international platinum symposium, program abstracts, Ontario Geological Survey, miscellaneous release-data 269 (abstract).

Barnes, S-J. and Gomwe, T.S. (2011) The Pd Deposits of the Lac des Iles Complex, Northwestern Ontario. Reviews in Economic Geology, 17, 351–370.

Barnes, S-J., Cox, R.A. and Zientek, M.L. (2006) Platinum-group element, gold, silver and base metal distribution in compositionally zoned sulfide droplets from the Medvezky Creek Mine, Noril'sk, Russia. Contribution to Mineralogy and Petrology, 152, 187–200.

Barnes, S-J., Prichard, H.M., Cox, R.A., Fisher, P.C. and Godel, B. (2008) The location of the chalcophile and siderophile elements in platinum group element ore deposits (a textural, microbeam and whole rock geochemical study): implications for the formation of the deposits. Chemical Geology, 248, 295–317.

Boudreau, A., Djon, L., Tchalikian, A. and Corkery, J. (2014) The Lac des Iles palladium deposit, Ontario, Canada. Part I. The effect of variable alteration on the Offset Zone. Mineralium Deposita, 49, 625–654.

Boutroy, E., Dare, S.A.S., Beaudoin, G., Barnes, S-J. and Lightfoot, P.C. (2014) Magnetite composition in Ni-Cu-PGE worldwide: application to mineral exploration. Journal of Geochemical Exploration, 145, 64–81.

Brenan, J.M. (2008) Re–Os fractionation by sulfide melt–silicate melt partitioning: A new spin. Chemical Geology, 248, 140–165.

Brügmann, G.E., Reischrnann, T., Naldrett, A.J. and Sutcliffe, R.H. (1997) Roots of an Archean volcanic arc complex; the Lac des Iles area in Ontario, Canada. Precambrian Research, 81, 223–239.

Chen, L-M., Song, X-Y., Danyushevsky L.V., Wang, Y-S., Tian, Y-L. and Xiao, J-F. (2014) A laser ablation ICP-MS study of platinum-group and chalcophile elements in base metal sulfide minerals of the Jinchuan Ni–Cu sulfide deposit, NW China. Ore Geology Reviews, http://dx.doi.org/10.1016/j.oregeorev.2014.07.011

Craig, J.R. (1973) Pyrite-pentlandite assemblages and other low temperature relations in the Fe–Ni–S systems. American Journal of Sciences, 273A, 496–510.

Dare, S.A.S., Barnes, S-J. and Prichard, H.M. (2010) The distribution of platinum group elements and other chalcophile elements among sulfides from the Creighton Ni–Cu–PGE sulfide deposit, Sudbury, Canada, and the origin of Pd in pentlandite. Mineralium Deposita, 45, 765–793.

Dare, S.A.S., Barnes, S-J., Prichard, H.M. and Fisher, P.C. (2011) Chalcophile and platinum-group element (PGE) concentrations in the sulfide minerals from the McCreedy East deposit, Sudbury, Canada, and the origin of PGE in pyrite. Mineralium Deposita, 46, 381–407.

Dare, S.A.S., Barnes, S-J. and Beaudoin, G. (2012) Variation in trace element content of magnetite crystallized from a fractionating sulfide liquid, Sudbury, Canada: Implications for provenance discrimination. Geochimica and Cosmochimica Acta, 88, 27–50.

Dare, S.A.S., Barnes, S-J., Prichard, H.M. and Fisher, P.C. (2014a) Mineralogy and geochemistry of Cu-rich ores from the McCreedy East Ni-Cu-PGE Deposit (Sudbury,

Canada): Implications for the behavior of platinum group and chalcophile elements at the end of crystallization of a sulfide liquid. Economic Geology, 109, 343–366.

Dare, S.A.S., Barnes, S-J., Beaudoin, G., Méric, J., Boutroy, E. and Potvin-Doucet, C. (2014b) Trace elements in magnetite as petrogenetic indicators. Mineralium Deposita, 49, 785–796.

Djon, M.L.N. and Barnes, S-J. (2012) Changes in sulphides and platinum-group minerals with the degree of alteration in the Roby, Twilight, and High Grade Zones of the Lac des Iles Complex, Ontario, Canada. Mineralium Deposita, 47, 875–896.

Dupuis, C. and Beaudoin, G. (2011) Discriminant diagrams for iron oxide trace element fingerprinting of mineral deposit types. Mineralium Deposita, 46, 319–335.

Fonseca, R.O.C., Campbell, A.H., O'Neill, H.S.C. and Fitzgerald, J.D. (2008) Oxygen solubility and speciation in sulphide-rich mattes. Geochimica and Cosmochimica Acta, 72, 2619–2635.

Godel, B. and Barnes, S-J. (2008) Platinum-group elements in sulfide minerals and the whole rocks of the J-M Reef (Stillwater Complex): Implication for the formation of the reef. Chemical Geology, 248, 272–294.

Godel, B., Barnes, S-J. and Maier, W.M. (2007) Platinum-group elements in sulfide minerals, platinum-group minerals, and whole-rocks of the Merensky Reef (Bushveld Complex, South Africa): Implications for the formation of the reef. Journal of Petrology, 48, 1569–1604.

Godel, B., González-Álvarez, I., Barnes, S.J., Barnes, S-J., Parker, P. and Day J. (2012) Sulfides and sulfarsenides from the Rosie Nickel Prospect, Duketon greenstone belt, Western Australia. Economic Geology, 107, 275–294.

Golightly, P.J. (1994) The Sudbury igneous complex as an impact melt: Evolution and ore genesis. In: Proceedings of the Sudbury-Noril'sk Symposium (eds. P.C. Lightfoot and A.J. Naldrett), Ontario Ministry of Northern Development and Mines, Ontario Geological Survey, 105–118 pp.

Gupta, V.K. and Sutcliffe, R.H. (1990) Mafic-ultramafic intrusives and their gravity field: Lac des Iles area, northern Ontario. Geological Society of America Bulletin, 102, 1471–1483.

Hanley, J.J. and Gladney, E.R. (2011) The presence of carbonic-dominant volatiles during the crystallization of sulfide-bearing mafic pegmatites in the North Roby Zone, Lac des Iles Complex, Ontario. Economic Geology, 106, 33–54.

Helmy, H.M., Ballhaus, C., Wohlgemuth-Ueberwasser, C., Fonseca, R.O.C. and Laurenz, V. (2010) Partitioning of Se, As, Sb, Te and Bi between monosulfide solid solution and sulfide melt – Application to magmatic sulfide deposits. Geochimica et Cosmochimica Acta, 74, 6174–6179.

Hinchey, J.G. and Hattori, K.H. (2005) Magmatic mineralization and hydrothermal enrichment of the High Grade Zone at the Lac des Iles palladium mine, northern Ontario, Canada. Mineralium Deposita, 40, 13–23.

Hinchey, J.G., Hattori, K.H. and Lavigne, M.J. (2005) Geology, petrology, and controls on PGE mineralization of the southern Roby and Twilight zones, Lac des Iles mine, Canada. Economic Geology, 100, 43–61.

Holwell, D.A. and McDonald, I. (2007) Distributions of platinum-group elements in the Platreef at Overysel, northern Busveld Complex: A combined PGM and LA-ICP-MS study. Contribution to Mineralogy and Petrology, 154, 171–190.

Huminicki, M.A.E., Sylvester, P.J., Cabri, L.J., Lesher, M.C. and Tubrett, M. (2005) Quantitative mass balance of platinum-group elements in the Kelly Lake Ni-Cu-PGE deposit, Copper Cliff Offset, Sudbury. Economic Geology, 100, 1631–1646.

Hutchinson, D. and McDonald, I. (2008) Laser ablation ICP-MS study of platinum-group elements in sulphides from the Platreef at Turfspruit, northern limb of the Bushveld Complex, South Africa. Mineralium Deposita, 43, 695–711.

Kress, V., Greene, L.E., Ortiz, M.D. and Mioduszewski, L. (2008) Thermochemistry of sulfide liquids IV: density measurements and the thermodynamics of O-S-Fe-Ni-Cu liquids a low to moderate pressures. Contribution to Mineralogy and Petrology, 156, 785–797.

Lavigne, M.J. and Michaud, M.J. (2001) Geology of North American Palladium Ltd'.s Roby Zone Deposit, Lac des Iles. Exploration and Mining Geology, 10, 1–17.

Li, C., Naldrett, A.J., Coats, C.J.A. and Johannessen, P. (1992) Platinum, palladium, gold, and copper-rich stringers at the Strathcona mine, Sudbury: their enrichment by fractionation of a sulfide liquid. Economic Geology, 87, 1584–1598.

Li, C., Barnes, S-J., Makovicky, E., Rose-Hansen, J. and Makovicky, M. (1996) Partitioning of Ni, Cu, Ir, Rh, Pt and Pd between monosulfide solid solution and sulfide liquid: effects of composition and temperature. Geochimica et Cosmochimica Acta, 60, 1231–1238.

Li, Y. and Audétat, A. (2012) Partitioning of V, Mn, Co, Ni, Cu, Zn, As, Mo, Ag, Sn, Sb, W, Au, Pb, and Bi between sulfide phases and hydrous basanite melt at upper mantle conditions. Earth and Planetary Science Letters, 355–356, 327–340.

Liu, Y-N. and Brenan, J.M. (2012) Experimental measurement of PGE and semi-metal partitioning during sulfide melt crystallization at controlled fO2-fS2 conditions. In: 12th international Ni-Cu-PGE symposium, program abstracts, State Key Laboratory of Ore Deposit Geochemistry, Institute of Geochemistry, Chinese Academy of Sciences, 36–39 pp.

Lyubetskaya, T. and Korenaga, J. (2007) Chemical composition of Earth's primitive mantle and its variance: 1.Method and results. Journal of Geophysical Research, 112, B03211. doi:10.1029/2005JB004223

Méric, J. (2011) Caractérisation géochimiques des magnétites de la zone critique de l'intrusion magmatique de Sept-Iles (Québec, Canada) et intégration a une base de données utilisant la signature géochimique des oxydes de fer comme outil d'exploration. Université du Québec à Chicoutimi - Université Montpellier 2, Honors Thesis, 48 pp.

Misson, P-J., Barnes, S-J. and Pagé, P. (2013) What happened during the metamorphism of Ni-Cu-PGE deposit: The example of the Delta deposit (Raglan area, Northern Quebec). In: GAC-MAC joint annual meeting, abstract volume, 37, 192 pp.

Mungall, J.E., Andrews, D.R.A., Cabri, L.J., Sylvester, P. and Tubrett, M. (2005) Partitioning of Cu, Ni, Au, and platinum-group elements between monosulfide solid solution and sulfide melt under controlled oxygen and sulfur fugacities. Geochimica et Cosmochimica Acta, 69, 4349–4360.

Nadoll, P., Angerer, T., Mauk, J.L., French, D. and Walshe, J. (2014) The chemistry of hydrothermal magnetite: A review. Ore Geology Reviews, 61, 1–32.

Naldrett, A.J. (1969) A portion of the system Fe–S–O between 900 and 1080 °C and its application to sulfide ore magmas. Journal of Petrology, 10, 171–201.

Naldrett, A.J. (2004) Magmatic sulfide deposits: geology, geochemistry and exploration. Springer, Berlin, 727 pp.

Néron, A. (2012) Caractérisation géochimiques des oxydes de Fe-Ti dans un dépôt de Fe-Ti-P associe à la suite anorthositique de Lac Saint Jean, Québec, Canada (secteur Lac à Paul) et intégration des données du secteur Lac à La Mine. Université du Québec à Chicoutimi, Honors Thesis, 39 pp.

Oberthür, T., Cabri, L.J., Weiser, T.W., McMahon, G. and Müller P. (1997) Pt, Pd and other trace elements in sulfides of the Main Sulfide Zone, Great Dyke, Zimbabwe: A reconnaissance study. Canadian Mineralogist, 35, 597–609.

Osbahr, I., Klemd, R., Oberthür, T., Brätz, H. and Schouwstra, R. (2013) Platinum-group element distribution in base-metal sulfides of the Merensky Reef from the eastern and western Bushveld Complex, South Africa. Mineralium Deposita, 48, 211–232.

Osbahr, I., Oberthür, T., Klemd, R. and Josties, A. (2014) Platinum-group element distribution in base-metal sulfides of the UG2 chromitite, Bushveld Complex, South Africa — a reconnaissance study. Mineralium Deposita, 49, 655–665.

Paton, C., Hellstrom, J., Paul, B., Woodhead, J. and Hergt, J. (2011) Iolite: freeware for the visualisation and processing of mass spectrometric data. Journal of. Analytical Atomic Spectrometry, 26, 2508–2518.

Piña, R., Gervilla, F., Barnes, S-J., Ortega, L. and Lunar, R. (2012) Distribution of platinum-group and chalcophile elements in the Aguablanca Ni–Cu sulfide deposit (SW Spain): Evidence from a LA-ICP-MS study. Chemical Geology, 302–303, 61–75.

Piña, R., Gervilla, F., Barnes, S-J., Ortega, L. and Lunar, R. (2013) Platinum-group elements-bearing pyrite from the Aguablanca Ni-Cu sulphide deposit (SW Spain): a LA-ICP-MS study. European Journal of Mineralogy, 25, 241–252.

Pokrovski, G.S., Borisova, A.Y. and Bychkov, A.Y. (2013) Speciation and transport of metals and metalloids in geological vapors. Reviews in Mineralogy and Geochemistry, 76, 165–218.

Rankin, L.R. (2013) Structural controls on emplacement and deformation of PGE-mineralised mafic-ultramafic intrusions – LDI district, NW Ontario. North American Palladium technical report, 115 pp.

Rudnick, R.L. and Gao, S. (2003) Composition of the continental crust. In: Treatise on Geochemistry, (eds. H.D. Holland and K.K. Turekian), Elsevier, Oxford, 3, 1–64 pp.

Schisa, P., Boudreau, A., Djon, L., Tchalikian, A. and Corkery, J. (2014) The Lac des Iles palladium deposit, Ontario, Canada. Part II. Halogen variations in apatite. Mineralium Deposita, doi10.1007/s00126-014-0541-4

Smith, J.W., Holwell, D.A. and McDonald, I. (2014) Precious and base metal geochemistry and mineralogy of the Grasvally Norite-Pyroxenite-Anorthosite (GNPA) member, northern Bushveld Complex, South Africa: implications for a multistage emplacement. Mineralium Deposita, 49, 667–692.

Somarin, A.K., Kissin, S.A., Heerema, D.D. and Bihari, D.J. (2009) Hydrothermal alteration, fluid inclusion and stable isotope studies of the north Roby Zone, Lac des Iles PGE mine, Ontario, Canada. Resource Geology, 59, 107–120.

Stone, D., Lavigne, M.J., Schnieders, B., Scott, J. and Wagner, D. (2003) Regional geology of the Lac des Iles Area. Ontario Geological Survey Open File Report 6120, 15-1, 15-25 pp.

Tollari, N., Barnes, S-J., Cox, R. and Nabil, H. (2008) Trace element concentrations in apatites from the Sept-Îles Intrusive Suite, Canada—implications for the genesis of nelsonites. Chemical Geology, 252, 180–190.

Tomkins, A.G., Rebryna, K.C., Weinberg, R.F. and Schaefer, F. (2012) Magmatic sulfide formation by reduction of oxidized arc basalt. Journal of Petrology, 53, 1537–1567.

Von Gruenewaldt, G., Klemm, D.D., Henckel, J. and Dehm, R.M. (1985) Exsolution features in titanomagnetites from massive magnetite layers and their host rocks of the Upper Zone, Eastern Bushveld Complex. Economic Geology, 80, 1049–1061.

Vukmanovic, Z., Reddy, S.M., Godel, B., Barnes, S.J., Fiorentini, M.L., Barnes, S-J. and Kilburn, M.R. (2014) Relationship between microstructures and grain-scale trace element distribution in komatiite-hosted magmatic sulphide ores. Lithos, 302–303, 42–61.

CHAPITRE 4

CHALCOPHILE AND PLATINUM-GROUP ELEMENT DISTRIBUTION IN PYRITES FROM THE SULFIDE-RICH PODS OF THE LAC DES ILES PD DEPOSITS, WESTERN ONTARIO, CANADA: IMPLICATIONS FOR POST-CUMULUS RE-EQUILIBRATION OF THE ORE AND THE USE OF PYRITE COMPOSITIONS IN EXPLORATION

CHARLEY J. DURAN[1], SARAH-JANE BARNES[1], JOHN T. CORKERY[2]

[1] UNIVERSITE DU QUEBEC À CHICOUTIMI

[2] NORTH AMERICAN PALLADIUM

JOURNAL OF GEOCHEMICAL EXPLORATION, SUBMITTED JANUARY 7, 2015

4.1 RÉSUMÉ

Le Lac des Iles occupe une position unique dans le développement de modèles pour la formation de gisements d'éléments du groupe du platine (EGP). C'est parce que les gisements ne ressemblent pas à un gisement d'EGP classique de plusieurs façons : la minéralisation a des ratios Pd/Ir et Pd/Pt très élevés; la plupart des roches qui contiennent les gisements ne présentent plus de minéralogie primaire et sont constituées d'amphibole, chlorite et séricite; les textures des roches des zones minéralisées sont extrêmement variables; l'intrusion a une faible superficie en surface et est zonée concentriquement. Par conséquences, le rôle de fluides magmatiques tardifs a été considéré important dans la formation des gisements. Les sulfures disséminés ne sont pas la seule forme de minéralisation. Il y a des lentilles riches en sulfures, qui recoupent la stratigraphie. Les textures et les proportions des sulfures dans les lentilles varient de ceux qui sont essentiellement magmatiques à ceux qui consistent principalement de pyrite. La pyrite pourrait avoir été déposée à partir de fluides hydrothermaux ou elle pourrait avoir été formée par l'altération de l'assemblage magmatique. Afin de faire la différence entre ces deux origines, le contenu en EGP et éléments chalcophiles des pyrites a été investigué. Il a été trouvé que la pyrite contient Os, Ir, Ru et Rh. Ces éléments se concentrent aussi dans les sulfures magmatiques pyrrhotite et pentlandite. Leur présence dans la pyrite pourrait être expliquée par la redistribution de Fe depuis la pyrrhotite vers les silicates intersticiels, possiblement au cours du refroidissement. Les cartes de distribution des éléments montrent qu'il y a une zonation des éléments. Les EGPI-Rh sont présents vers le cœur des pyrites

avec l'As, tandis que le Co et Se sont présents vers les bordures. Les éléments mobiles tels que le Pb, Bi et Ag sont présents dans de fines surcroissances sur les bordures des pyrites et dans quelques cas, le Pt, Te et Sn sont aussi présents dans les surcroissances. La comparaison de la composition et de la distribution des éléments avec des pyrites provenant d'autres contextes ignés (Sudbury et Aguablanca), montre que les éléments ont une distribution similaire, tandis que les pyrites provenant de gisements hydrothermaux de basse température ont des compositions différentes. Un graphique de Co/Se vs Sb/As s'avère être efficace pour distinguer les pyrites ignées des pyrites provenant d'autres contextes, et pourrait possiblement être utilisé en exploration.

4.2 ABSTRACT

The Lac des Iles Pd-deposit occupies a unique position in the development of models for the formation of platinum-group element (PGE) deposits. This is because the deposits do not resemble a classical PGE deposit in a number of ways: the ores have very high Pd/Ir and Pd/Pt ratios; most of the host rocks to the deposits no longer have a primary mineralogy and consist largely of amphibole, chlorite and sericite; the textures of the rocks from the ore zones are extremely variable; the intrusion is small and concentrically zoned. Consequently the role of late magmatic fluids has been considered important in the formation of the deposits. The disseminated sulfides are not the only form of mineralization. There are sulfide-rich pods present, which cross-cut the stratigraphy. The sulfide minerals textures

and proportions within the pods vary from those which are essentially magmatic to those which consist predominantly of pyrite. The pyrite could have been deposited from hydrothermal fluids or it could have formed by alteration of magmatic sulfides. In order to distinguish between these two origins, the PGE and chalcophile element contents of the pyrite were investigated. It was found that the pyrite contains Os, Ir, Ru and Rh. These elements also concentrate in the magmatic sulfides pyrrhotite and pentlandite. Their presence in the pyrite could be explained by redistribution of Fe from the pyrrhotite to interstitial silicates possibly during cooling. Maps of the distribution of the elements show that there is zoning of the elements. The IPGE-Rh are present towards the cores of pyrite along with As whereas Co and Se are present towards the rims. Mobile elements such as Pb, Bi and Ag are present in thin overgrowths at the edges of pyrite and in a few cases, Pt, Te and Sn are also present in the overgrowths. Comparison of the composition of pyrite and element distribution with pyrites from other igneous settings (Sudbury and Aguablanca), shows that the elements have a similar distribution, whereas pyrites from low-temperature hydrothermal deposits have different compositions. A plot of Co/Se vs Sb/As appears to be effective at separating the igneous pyrites from pyrites found in other settings and could possibly be used in exploration.

4.3 INTRODUCTION

Pyrite (Py) is the most abundant sulfide mineral on the Earth's surface (Vaughan, 2006 and references therein) and occurs as a common accessory mineral in many igneous, metamorphic, and sedimentary rocks. The conditions at which Py may form range from exsolution of S-rich monosulfide solid solution (MSS) at temperatures as high as 750°C (Kullerud and Yoder, 1959), down to reaction of detrital Fe-minerals with H2S resulting from sulfate reduction by bacteria during shallow burial of sediments (Berner, 1970). Furthermore, Py may remain stable under the highest grades of metamorphism owing to its high temperature stability and physical strength (Craig and Vokes, 1993). During its formation, Py can incorporate a large number of minor and trace elements (Abraitis, 2004) that in some cases show compositional zoning (Craig et al., 1998; Craig and Solberg, 1999; Chouinard et al., 2005; Large et al., 2009; Thomas et al., 2011; Piña et al., 2013). The compositional and textural features of Py are closely related to the processes whereby Py formed. Consequently, these features could be used as petrogenetic indicators.

Pyrite is also widespread in a variety of ore deposits, particularly in hydrothermal deposits such as volcanogenic-hosted massive sulfides (VHMS), orogenic gold deposits, and Cu-porphyries (Large et al. 2009; Maslennikov et al., 2009; Thomas et al., 2011; Reich et al., 2013; Revan et al., 2014). In contrast, the presence of Py in magmatic Ni-Cu-PGE deposits is less common. However, recent studies have demonstrated that Py in these types of deposits contain PGE (Oberthür et al. 1997; Barkov et al. 1997; Dare et al. 2011; Djon and Barnes 2012; Piña et al., 2012, 2013; Osbahr et al., 2013, 2014; Smith et al. 2014).

However, because Py is not abundant, very little attention has been paid to the processes that control the distribution of PGE in Py. In magmatic Ni-Cu-PGE deposits, four possible processes may be invoked for the formation of Py: (1) exsolution from S-rich MSS; (2) S addition to the MSS components (i.e., pyrrhotite and pentlandite) during post-cumulus re-equilibration; (3) Fe loss from the MSS components during post-cumulus re-equilibration and (4) precipitation from hydrothermal fluids.

The Mine Block Intrusion of the Lac des Iles (LDI) Complex hosts the LDI Pd mine and deposits. The LDI Pd deposits consist of fairly wide zones (50-400 m) of finely disseminated sulfides (Lavigne and Michaud, 2001; Hinchey et al., 2005; Barnes and Gomwe, 2011; Djon and Barnes, 2012; Boudreau et al., 2014). In addition, sulfide-rich pods have been discovered within the Mine Block Intrusion (Duran et al., submitted). Although some of these sulfide-rich pods are composed of a pyrrhotite-pentlandite assemblage that exhibits igneous textures, many of them are extensively enriched in Py (Duran et al. submitted). In a few sulfide-rich pod samples, Py has even been found to be the predominant sulfide mineral. Based on whole-rock geochemistry, this transition from pyrrhotite-pentlandite to Py has been ascribed to post-cumulus Fe redistribution from the pyrrhotite and pentlandite to the interstitial silicates (Duran et al. submitted). Therefore, Py from the LDI sulfide-rich pods represent an ideal opportunity to investigate how PGE and chalcophile elements behave during the post-cumulus re-equilibration of MSS.

In this study we have investigated the trace element concentrations and the compositional trace element zoning of Py from the LDI sulfide-rich pods using laser ablation inductively

coupled plasma mass spectrometry (LA-ICP-MS). One of the major aims of this study was to address whether Py originated from the replacement of the MSS component of the sulfides as expected from our previous study (Duran et al., submitted) or was of hydrothermal origin. As a result of investigating Py compositions from igneous settings and comparing these with Py of other origin, we have observed that Py from igneous settings are richer in Co and Se and poorer in Sb and As. We have used this observation to develop a discrimination diagram for Py that could be used for exploration in glacial terrains.

4.4 ANALYTICAL METHOD

Twelve of the 15 sulfide-rich pod samples documented in Duran et al. (submitted) were also used to study Py. Pyrite was identified and described using an OLYMPUS DP71 optical microscope at Université du Québec à Chicoutimi (UQAC). Analyses by LA-ICP-MS were performed at LabMaTer (UQAC) using an Excimer 193 nm Resonetics Resolution M-50 laser ablation system coupled with an Agilent 7700x mass spectrometer. A range of beam sizes from 43 to 75 μm, a range of stage speeds from 2.5 to 5 μm/s, a range of laser frequencies from 10 to 15 Hz and a range of power from 4 to 5 mJ/pulse were used to analyze the Py grains. For large grains, a line scan across the grain was made, and for small grains spot analyses were performed. The gas blank was measured for 30 s before switching on the laser for at least 60 s. The ablated material was then carried into the ICP-MS by an argon–helium gas mix. Data reduction was carried out using Iolite package

for Igor Pro software (Paton et al., 2011). Internal standardization was based on ^{57}Fe using stoichiometric iron values of Py.

Counts of the following isotopes were monitored: ^{29}Si, ^{33}S, ^{34}S, ^{57}Fe, ^{59}Co, ^{61}Ni, ^{63}Cu, ^{65}Cu, ^{66}Zn, ^{75}As, ^{77}Se, ^{82}Se, ^{95}Mo, ^{99}Ru, ^{101}Ru, ^{103}Rh, ^{105}Pd, ^{108}Pd, ^{109}Ag, ^{111}Cd, ^{118}Sn, ^{121}Sb, ^{128}Te, ^{130}Te, ^{185}Re, ^{189}Os, ^{193}Ir, ^{194}Pt, ^{195}Pt, ^{197}Au, ^{208}Pb and ^{209}Bi. Silicon was monitored to ensure that the measured signal represented pure sulfide. Three certified reference materials were used for external calibration: Laflamme Po727, which is a synthetic FeS doped with 40 ppm PGE and Au supplied by Memorial University of Newfoundland, was used to calibrate for PGE and Au; MASS-1, which is a ZnCuFeS pressed powder pellet doped with 50–70 ppm Ag, As, Bi, Pb, Re, Sb, Se, Sn and Te supplied by the United States Geological Survey (USGS), was used to calibrate for Ag, As, Bi, Cd, Co, Cu, Mo, Pb, Sb, Se, Sn and Te; JB-MSS5, which is a synthetic FeS sulfide containing approximately 50–70 ppm of most chalcophile elements supplied by Prof. James Brenan of University of Toronto was used to calibrate for Ni and Re. In addition, JB-MSS5 and GSE were used as in-house reference materials to monitor calibrations of both Laflamme Po727 and MASS-1. The results of the monitors are generally within 10% analytical error of the working values and relative standard deviation (RSD) is typically < 10%. The results of the monitors are presented in the electronic supplementary material.

Interference by ^{61}Ni^{40}Ar on ^{101}Ru was corrected using a NiS blank run at the beginning and end of each analytical session. Interference by ^{63}Cu^{40}Ar on ^{103}Rh was corrected using ^{103}Rh measured in MASS-1, which contain 13.4 % ^{63}Cu but no ^{103}Rh. Because Py contains very

little Cu or Ni, neither of these interferences were significant. Interference of ^{108}Cd on ^{108}Pd was corrected by monitoring ^{111}Cd.

Maps of the element distribution were made on Py where preliminary line scans showed variations in the element distribution. The beam size (15 to 25 μm) and the speed of the stage movement (10 to 20 μm/s) were vaired based on a compromise between the grain size and the resolution. A laser frequency of 15 Hz and a power of 5 mJ/pulse were used to map the Py grains in their entirety. The maps were generated using the Iolite software package on the basis of the time-resolved count rate-concentration relationships of each element. The maps indicate the relative concentration of the elements and are semi-quantitative.

4.5 GEOLOGICAL BACKGROUND

The 2689 ± 1 Ma (Stone et al., 2003) LDI Complex is located in Western Ontario, approximately 80 km north of Thunder Bay, near the boundary between the Wabigoon and Quetico subprovinces in the Superior province. The complex forms a suite of mafic to ultramafic intrusions emplaced in granitoids, along major SW–NE trending crustal structures (Gupta and Sutcliffe, 1990). The LDI Pd mine and deposits are hosted by the central intrusion of the Complex, the Mine Block Intrusion (Fig. 4.1).

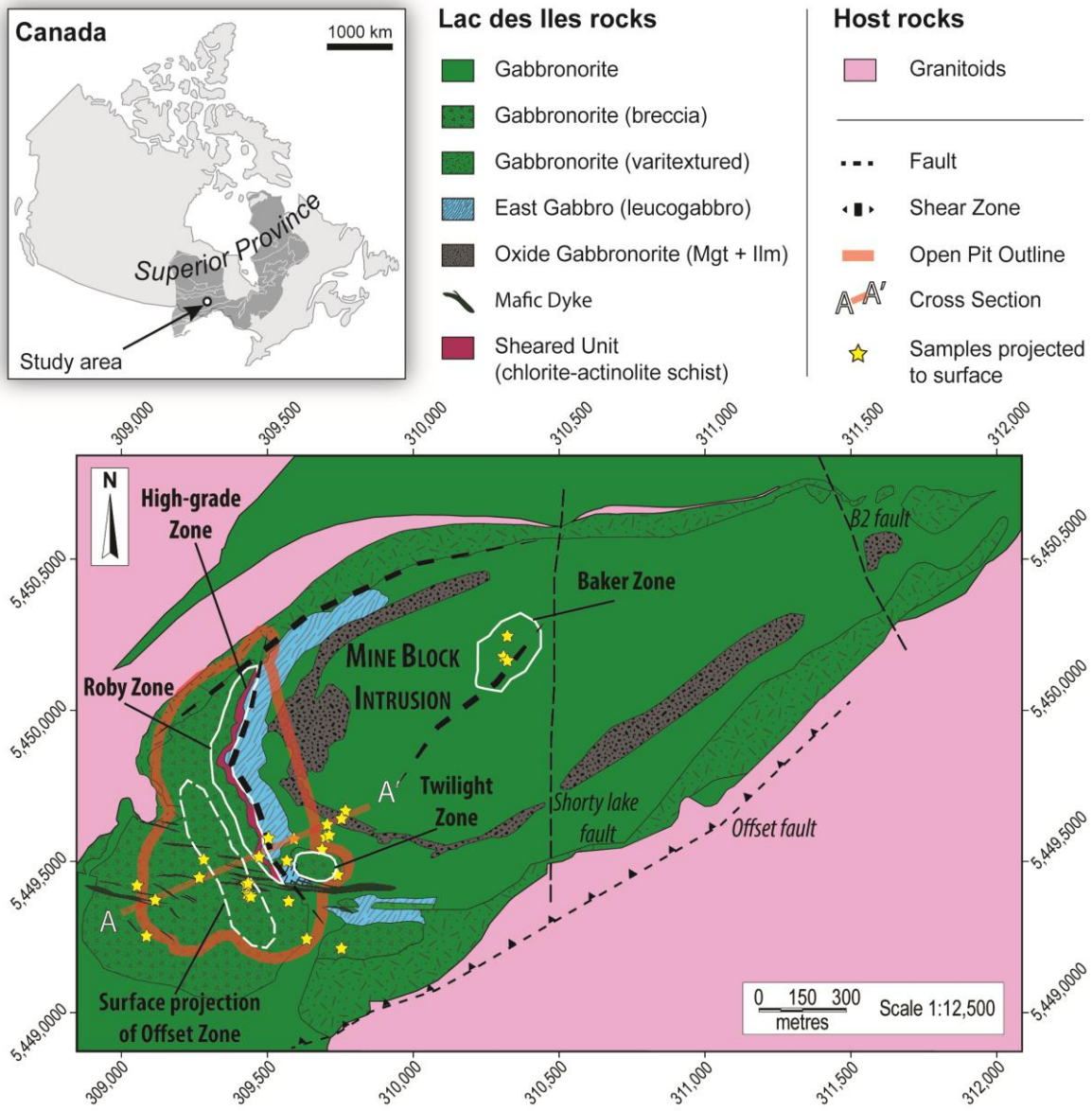

Figure 4.1. Simplified geological map of the Mine Block Intrusion of the Lac des Iles Complex (Modified from North American Palladium). Sulfide-rich samples are projected to the surface and follow a SW-NE orientation.

This intrusion is believed to have formed from multiple pulses of magmas (Lavigne and Michaud, 2001). Furthermore, the Mine Block Intrusion has been affected by many syn-magmatic ductile shear zones and post-magmatic brittle faults (Rankin, 2013), indicating that the intrusion has been deformed during its emplacement/crystallization and subsequently. The main lithological units (i.e., the varitextured rim, East Gabbro, and oxide-gabbronorite) display a weakly concentric stratigraphy. The rocks of the Mine Block Intrusion mainly consist of noritic to gabbronoritic adcumulates with extremely variable textures (e.g., magmatic breccias, varitextured and pegmatitic rocks). These rocks are interpreted to have a co-magmatic affinity owing to their similar incompatible elements ratios (Barnes and Gomwe, 2011). The texture variability of these rocks was probably induced by recrystallization, which likely occurred when the magmas became saturated in volatile-rich fluids. Elevated abundances of dissolved, and exsolution of, magmatic volatiles is supported by the presence of magmatic hornblende and biotite (Watkinson et al., 2002), apatite (Schisa et al., 2014) and fluid inclusions in quartz (Hanley and Gladney, 2011).

Further evidence of fluid activity is highlighted by most of the rocks being altered to greenschist and lower amphibolite facies (Boudreau et al., 2014). Adcumulate textures were largely obliterated by a secondary mineral assemblage. Plagioclase was variably altered to form sericite, epidote-group minerals, chlorite and carbonates. Orthopyroxene was more significantly altered to form actinolite and chlorite. Locally, orthopyroxene has been completely replaced (Barnes and Gomwe, 2011; Boudreau et al., 2014).

The main zone of mineralization (i.e., Roby Zone) occur in the western part of the intrusion. The Roby Zone consists of a fairly wide zone (50-400 m) of finely disseminated sulfides and platinum-group minerals (PGM) in metanorites. Furthermore, the Roby Zone includes a 15-30 m wide sheared unit composed of chlorite-actinolite schist and known as the High-grade Zone. The Roby Zone extends at depth where it is cut off by the Offset Fault. Below the Offset Fault the mineralization is known as the Offset Zone which is a fault offset that is displaced approximately 250 m west of the overlying Roby Zone (Fig. 4.2).

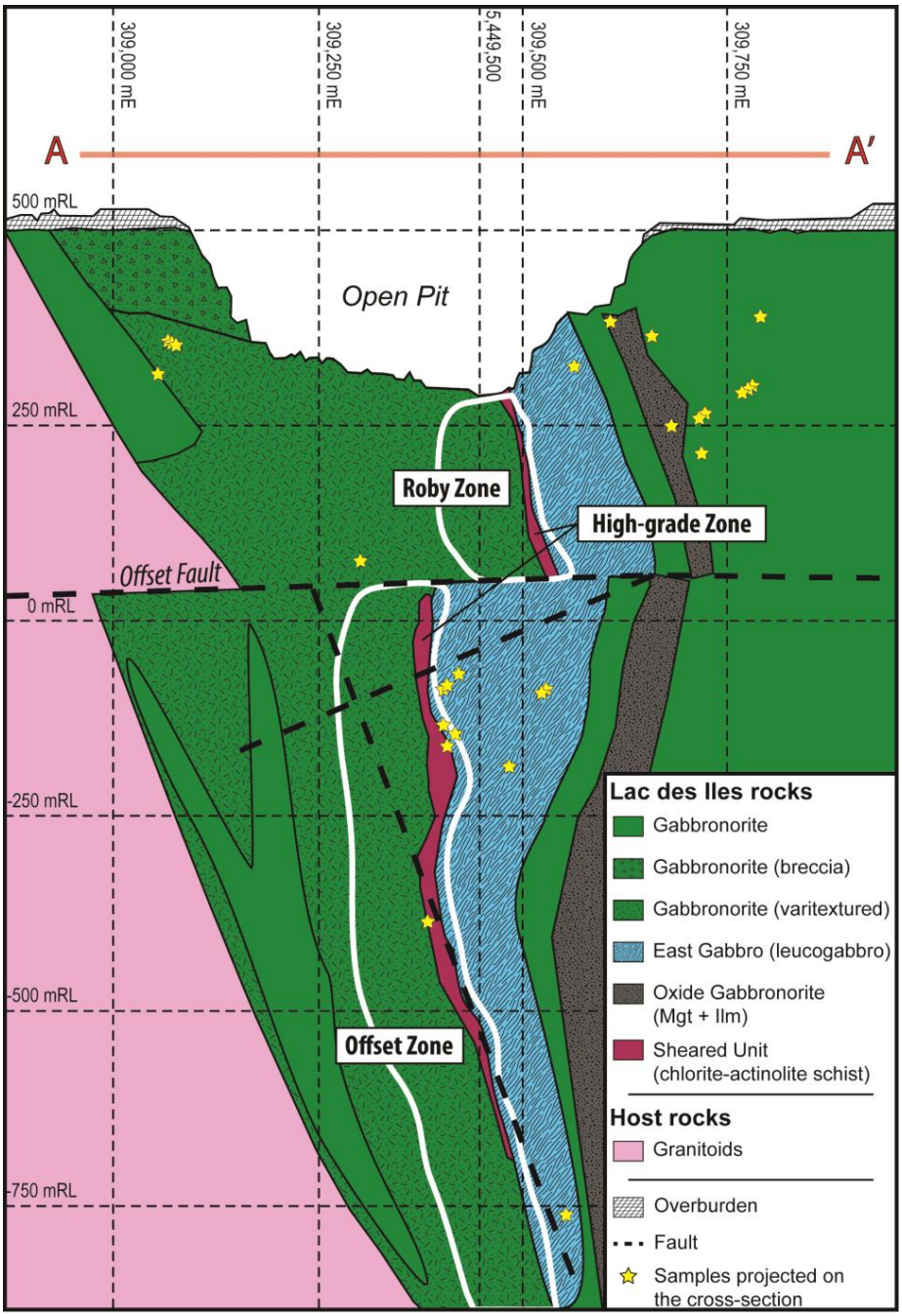

Figure 4.2. Idealized cross-section of the Mine Block Intrusion of the Lac des Iles Complex (Modified from North American Palladium), with projected locations of sulfide-rich samples from drill cores. Note that sulfides-rich pods sampled from the open pit and from the Baker Zone are not plotted on the cross-section.

As in the case of silicate minerals, the primary sulfide assemblage has been altered. Alteration of pyrrhotite, pentlandite and chalcopyrite gave rise to Py, millerite and other secondary sulfide minerals (Hinchey and Hattori, 2005; Djon and Barnes, 2012). A change in the platinum-group element mineralogy has also been observed with the change of sulfide mineralogy (Djon and Barnes, 2012). The positive correlation between S and PGE in the Roby Zone is consistent with the mineralization having been formed by magmatic sulfide liquids. However, the lack of correlation between S and PGE, and the higher Pd/Ir and Pd/Pt ratios observed in the High-grade Zone rocks, indicate that S has been lost and Pd has been upgraded in this zone (Hinchey and Hattori, 2005; Djon and Barnes, 2012; Barnes and Gomwe, 2011). Given these considerations, Barnes and Gomwe (2011) suggested that Pd was scavenged from magmatic sulfides at depth by late-magmatic fluids, which were in turn concentrated in the shear zone as the rocks were converted to schist and sulfides were modified.

4.6 SULFIDE-RICH PODS

In addition to the disseminated mineralization, sulfide-rich pods are present throughout the intrusion. These sulfide-rich pods cross-cut the stratigraphy and occur along major structures (Figs. 4.1, 4.2; Duran et al., submitted). An overall description of the LDI sulfide-rich pods has been presented in Duran et al. (submitted). Sulfide-rich pods contain net-textured to massive sulfides. Although their host rocks have been altered to greenschist

and lower amphibolite facies, no alteration halos have been observed proximal to the pods. Moreover the sulfides do not appear to have been structurally emplaced because no evidence of ductile plastic flow has been identified. Consequently, we proposed (Duran et al., submitted) that sulfide liquids concentrated in the pods due to the opening of dilation zones when the intrusion was being emplaced and deformed.

The sulfide assemblage consists of pyrrhotite-pentlandite-Py ± chalcopyrite. Pyrrhotite (Po) and pentlandite (Pn) exhibit typical igneous exsolution textures. Two trends were identified from this Po-Pn assemblage (Duran et al., submitted). The first trend is a zonation toward a chalcopyrite-dominated assemblage that occurs along the edge of some pods. The whole-rock geochemical analyses have shown a decoupling of Cu from Ni. The second trend is a transition toward a Py-dominated assemblage that occurs from one pod to another. Molar proportions of base metals and S show a trend of Py development to a typical primary magmatic composition. The PGE show strong correlations between Os, Ir, Ru and Rh, and poor correlations between Pd-Pt and Cu, regardless of the amount of Py. These overall data were interpreted to reflect the accumulation of MSS from fractionating sulfide liquids. LA-ICP-MS analysis of Po, Pn, and chalcopyrite (Duran et al., submitted) further supported this interpretation. Consequently, it has been proposed that Py replaced MSS/Po during subsequent alteration processes.

4.7 PETROGRAPHY OF PYRITES

Pyrite has been observed in all the studied sulfide-rich pod samples from Duran et al. (submitted). However, Py modal proportions widely vary from one sample to another, ranging from almost none (Fig. 4.3a) to being the predominant (> 50%) sulfide mineral (Fig. 4.3b-d). In most cases, Py forms small (a few microns) to large (several millimeters) anhedral grains (Figs. 4.3a, b), and is associated with Po. Pyrite is also commonly associated with Pn (Fig. 3c) and occasionnaly associated with chalcopyrite (Fig. 4.3d). Pyrite also forms polycrystalline aggregates having ribbon-like textures (Fig. 4.3e) similar to those observed at Aguablanca (Piña et al., 2013). In some cases, Py forms small euhedral grains in which zoning can be observed (Fig. 4.3f). In a few cases, Py occurs as irregular grains with a spongy texture associated with silicate minerals and as small veins cross-cutting Po or magnetite. These types of Py are minor in abundance and have not been further studied.

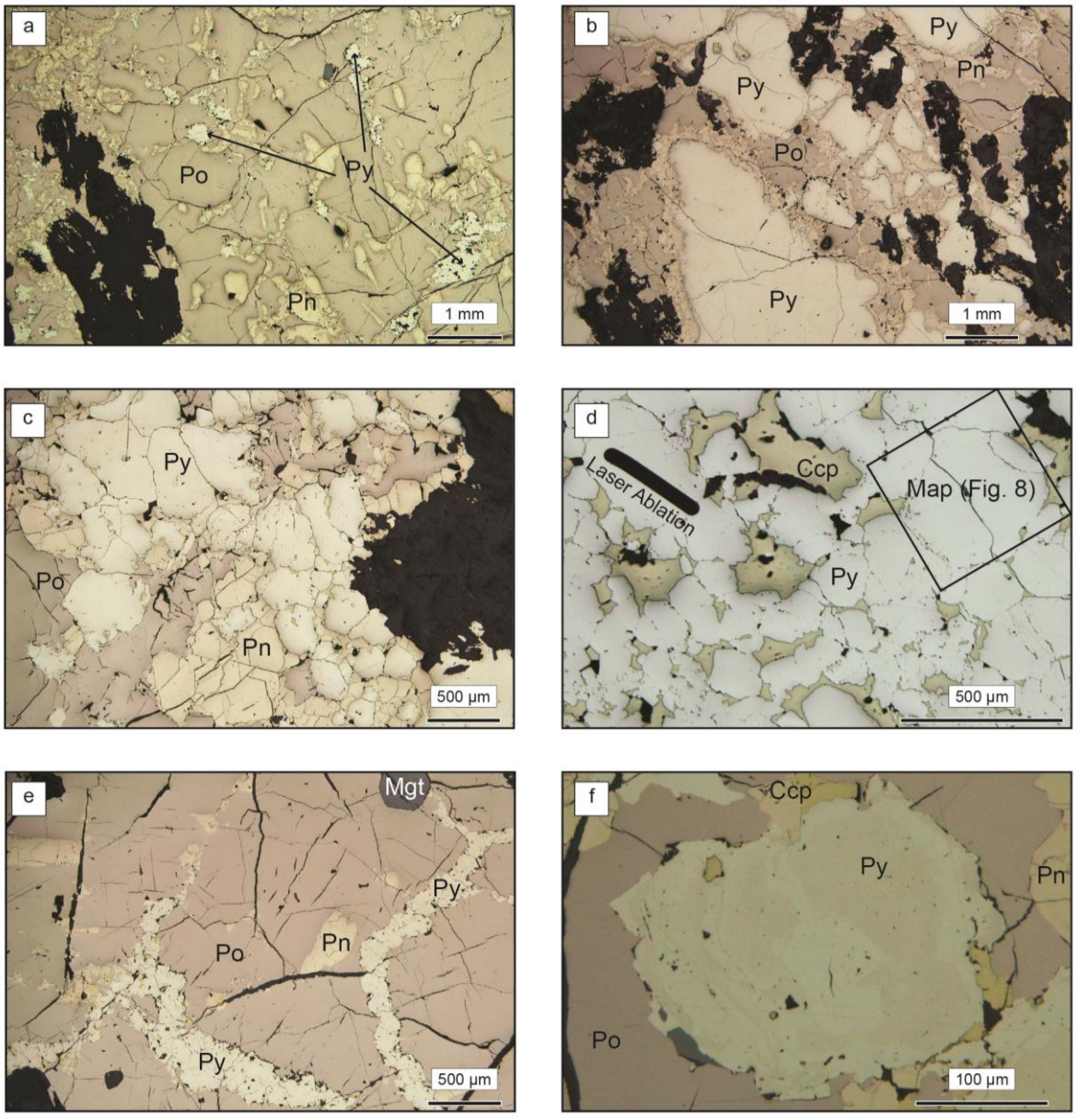

Figure 4.3. Photomicrographs in reflected light of typical pyrites observed in sulfide-rich pods: (a) small anhedral pyrites associated with pyrrhotite and pentlandite; (b) large anheral pyrites surrounded by polycrystalline veinlets of pentlandite; (c) anhedral pyrites associated with pyrrhotite and pentlandite; (d) anhedral pyrite associated with chalcopyrite; (e) ribbon-like pyrites associated with pyrrhotite and pentlandite; (f) small anhedral pyrite exhibiting a zoning.

4.8 RESULTS AND INTERPRETATION

The first phase to crystallize from a magmatic sulfide liquid is monosulfide solid solution (MSS). Upon cooling, MSS exsolves to form Po and Pn ± minor Py (Naldrett et al., 1967). However, the large amount of Py observed in many of the sulfide-rich pods at LDI are not consistent with Py having exsolved from MSS along with Po and Pn (Craig, 1973). Based on whole-rock geochemistry of sulfide-rich pods, Duran et al. (submitted) suggested that Py replaced MSS or Po. The molar ratios of [Fe+Ni+Cu+Co]/[S] of the whole-rocks are close to 1 (as would be expected for a magmatic sulfide), which suggests that S has not been added nor Fe lost from the rocks (Duran et al., submitted). Djon and Barnes (2012) found that Py could have formed as a consequence of Fe redistribution from Po and Pn to the interstitial silicates in the disseminated sulfides, and Duran et al. (submitted) applied a similar model to the massive sulfides. In the case of massive sulfides, the Pn has been preserved and the re-equilibration affected only the MSS/Po. In order to develop this idea, we investigated the composition and distribution of trace elements within Py, and we plot the Py composition on the multi-element diagram developed by Duran et al. (submitted) along with the composition of Po and Pn.

4.8.1 MINOR AND TRACE ELEMENTS IN PYRITE: COMPOSITION AND DISTRIBUTION

Pyrite from the LDI sulfide-rich pods exhibits a wide range of compositions between and within samples. This variation is much wider than the variations observed in each of the co-existing sulfide minerals (i.e., Po, Pn and chalcopyrite; see Duran et al., submitted). Furthermore, the global variations in Py compositions does not appear to be related to their surrounding mineral assemblage, texture and/or sample provenance. The median composition of Py is presented in Table 4.1 with the minimum and maximum values. The full dataset is presented in the electronic supplementary material.

Element		Isotope	Pyrite n=57		
			Median	Min	Max
Co	(ppm)	^{59}Co	5912	60.9	13779
Ni	(ppm)	^{61}Ni	591	61.1	48878
Cu	(ppm)	^{65}Cu	111	0.344	25603
Zn	(ppm)	^{66}Zn	59.6	<0.090	1569
As	(ppm)	^{75}As	62.8	<0.456	242
Se	(ppm)	^{82}Se	88.3	18.8	655
Mo	(ppm)	^{95}Mo	0.191	<0.028	3.17
Ru	(ppm)	^{101}Ru*	0.075	<0.017	5.26
Rh	(ppm)	^{103}Rh*	0.107	<0.003	13.1
Pd	(ppm)	^{108}Pd*	0.113	<0.010	131
Ag	(ppm)	^{109}Ag	1.49	<0.012	9.26
Cd	(ppm)	^{111}Cd	3.12	<0.054	33.5
Sn	(ppm)	^{118}Sn	0.433	<0.032	6.24
Sb	(ppm)	^{121}Sb	0.661	<0.012	6.89
Te	(ppm)	^{130}Te	1.66	<0.194	15.9
Re	(ppm)	^{185}Re	0.033	<0.006	0.242
Os	(ppm)	^{189}Os	0.039	<0.016	0.745
Ir	(ppm)	^{193}Ir	0.034	<0.004	0.466
Pt	(ppm)	^{194}Pt	0.066	<0.014	4.05
Au	(ppm)	^{197}Au	0.072	<0.008	0.354
Pb	(ppm)	^{208}Pb	6.24	0.016	1220
Bi	(ppm)	^{209}Bi	2.51	0.003	18.2

*Table 4.1. Compositions of pyrites from Lac des Iles sulfide-rich pods as determined by LA-ICP-MS analysis. n = number of analysis; min = minimum value; max = maximum value; * = values corrected for interference.*

Within Py, most elements are heterogeneously distributed, as indicated by the time-signal diagrams (Fig. 4.4). This heterogeneous distribution could account for the wide range of measured compositions. To highlight the heterogeneous distribution of the elements within Py grains (i.e., zoning), elemental mapping has been carried out using LA-ICP-MS.

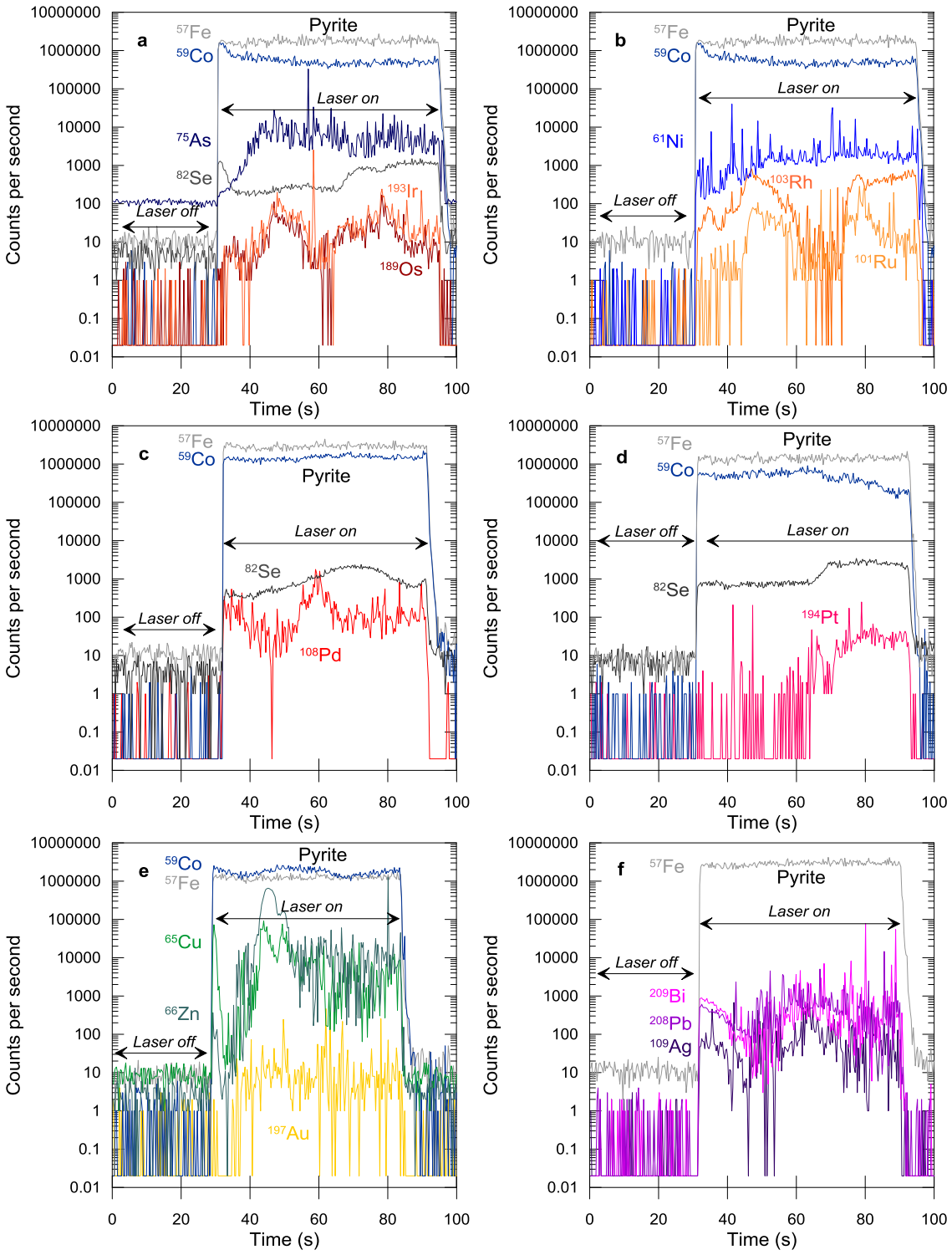

Figure 4.4. Examples of time-signal diagrams of pyrites.

Most of the Py that have been mapped are zoned with respect to the IPGE, Rh, Co, Se and As (Figs. 4.5-8). The LA-ICP-MS maps show concentric, oscillatory zoning sub-parallel to crystal faces with respect to these elements, except for one small Py (Fig. 4.9) in which no zoning of IPGE and Rh has been observed. In the larger Py, IPGE, Rh and As are present in or near the cores of the Py, forming thin layers (Figs. 4.5-8). Cobalt and Se form antithetical layers outward the grains and are much enriched in the rims, in which they form thicker layers (Figs. 4.5-7). This type of zoning has also been observed in Py from Sudbury (Dare et al., 2011; Adibpour et al., 2014) and Aguablanca (Piña et al., 2013). Despite their heterogeneous distribution, IPGE show a strong degree of correlation between one another and are sub-equally distributed. This type of correlation is especially apparent on plots of Ru vs Ir and Os vs Ir (Figs. 4.10a, b). The IPGE also show a fairly strong degree of correlation with Rh (Fig. 4.11). However, Rh appears to have been preferentially concentrated over IPGE as Rh plots above the 1:1 line for Py (Fig. 4.11). The IPGE and Rh do not correlate with As, and Co does not correlate with Se, even though these elements are associated within Py. We suggest that this is because IPGE, Rh and Co substitute for Fe and As substitutes for S in the Py structure (Abraitis, 2004 and references therein).

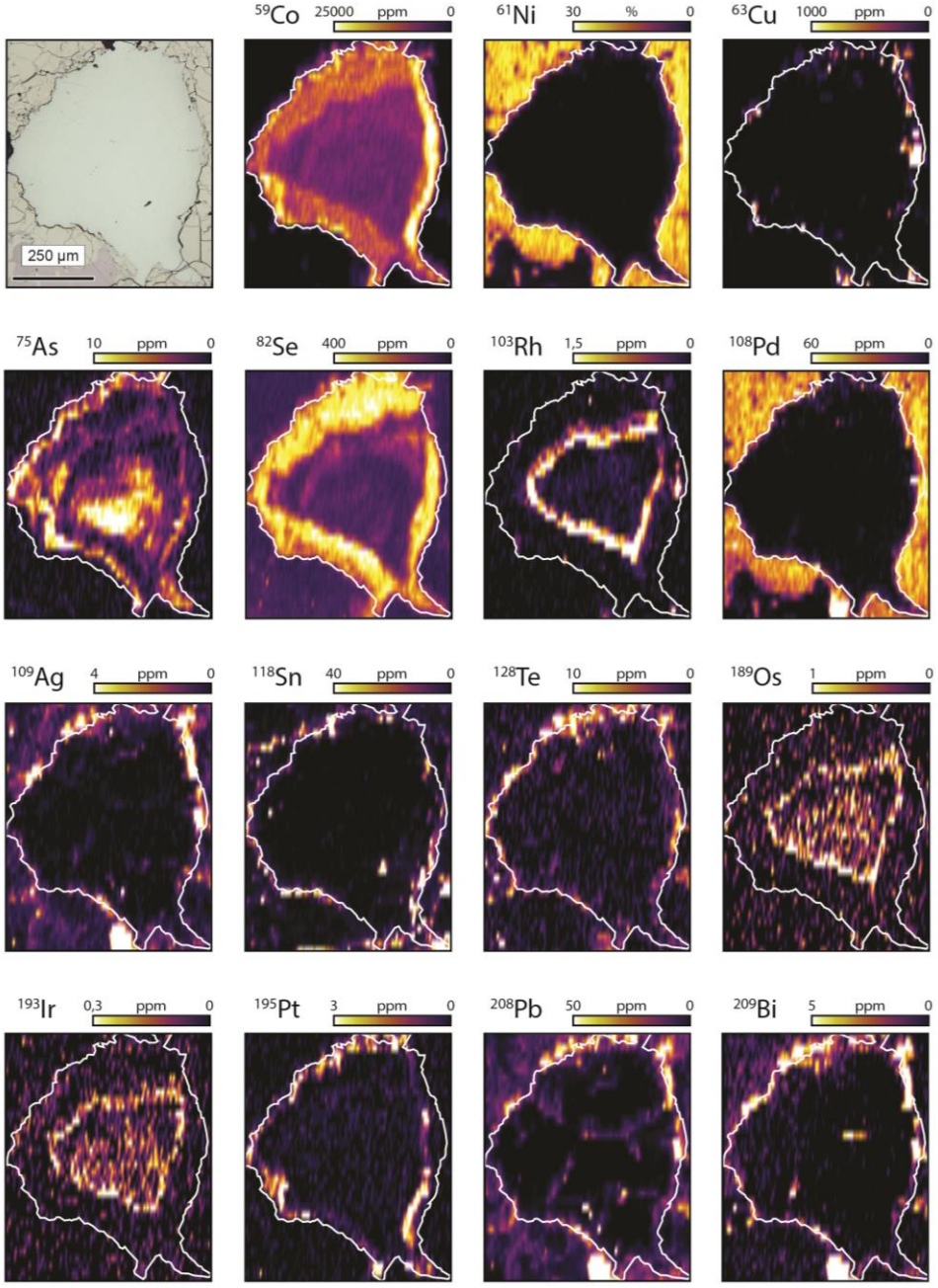

Figure 4.5. LA-ICP-MS elemental map of a pyrite grain from sample CD-RP010. Note that IPGE, Rh and As are present in the center of the grain and form antithetical zones with Co and Se. Cobalt and Se are concentrated towards the rim of the grain. Note also the presence of Ag, Sn, Te, Pt, Pb and Bi in a thin overgrowth surrounding the grain. White line show the grain outlines.

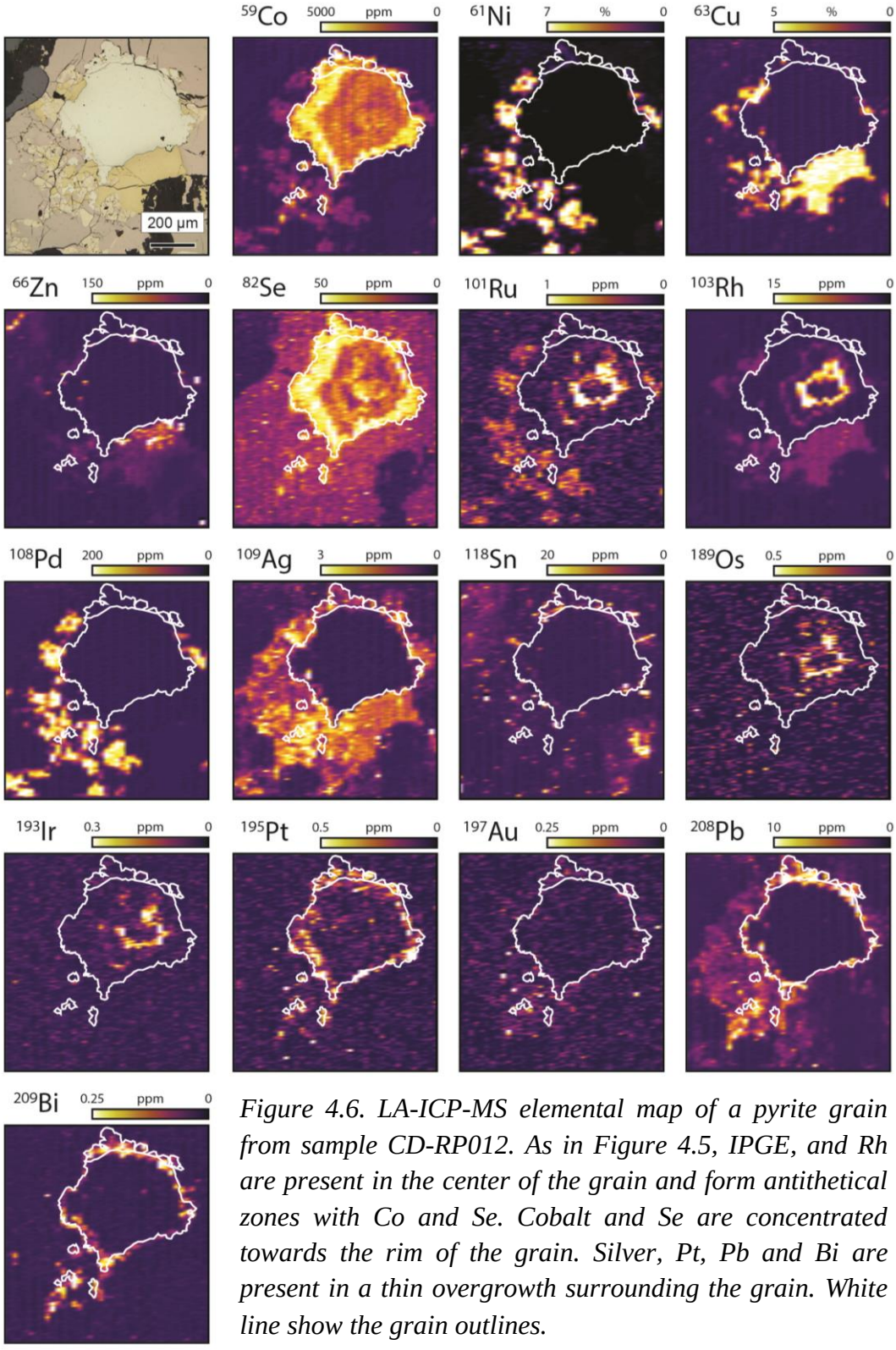

Figure 4.6. LA-ICP-MS elemental map of a pyrite grain from sample CD-RP012. As in Figure 4.5, IPGE, and Rh are present in the center of the grain and form antithetical zones with Co and Se. Cobalt and Se are concentrated towards the rim of the grain. Silver, Pt, Pb and Bi are present in a thin overgrowth surrounding the grain. White line show the grain outlines.

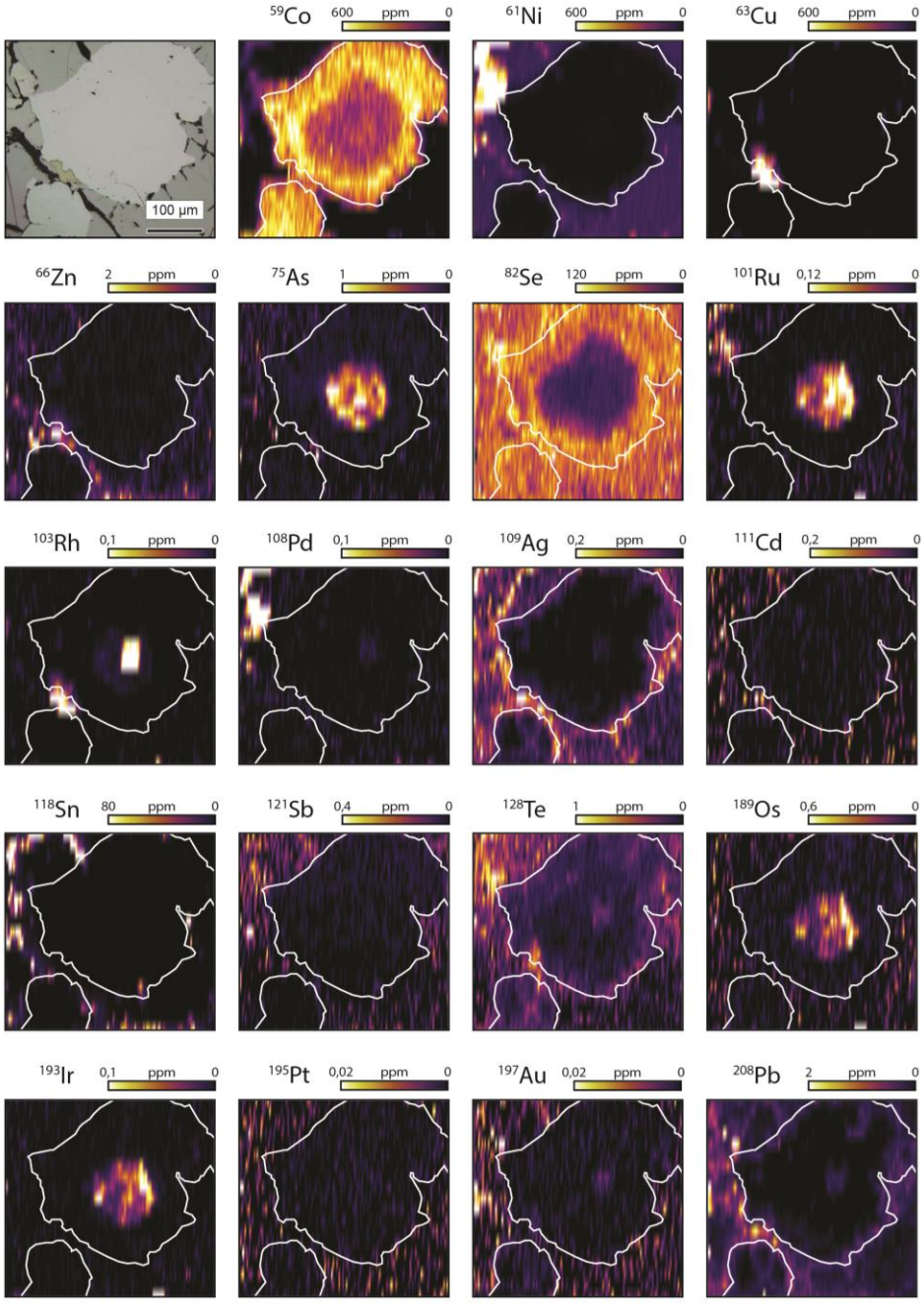

Figure 4.7. LA-ICP-MS elemental map of a pyrite grain from sample CD-10603. As in Figures 4.5, IPGE, Rh and As are present in the center of the grain whereas Co and Se are concentrated towards the rim of the grain. Note that Rh in the center of the grain forms a euhedral shape. Tin appears to be present in the cracks but there is no overgrowth surrounding the grain. White line show the grain outlines.

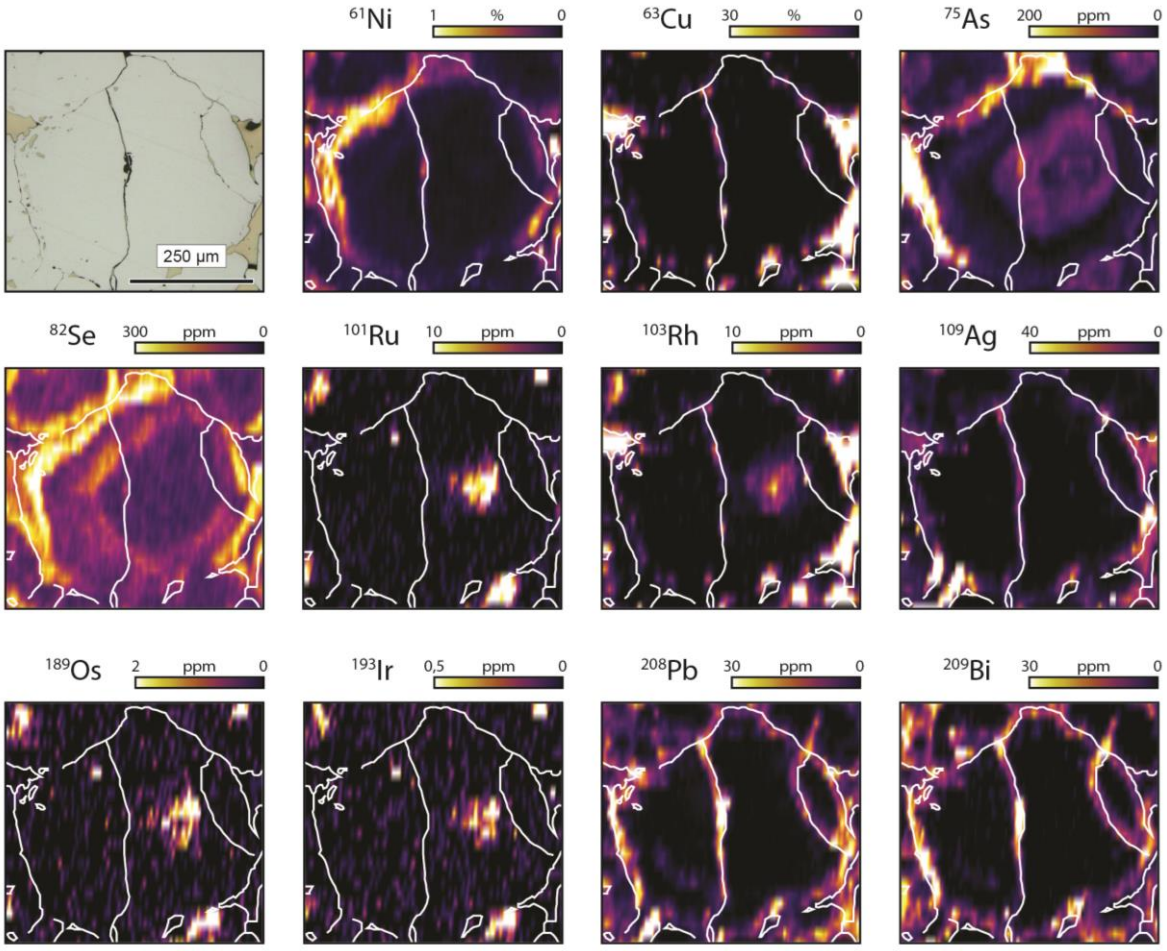

Figure 4.8. LA-ICP-MS elemental map of a pyrite grain from sample CD-11054. Note that IPGE, Rh and As are present in the center of the pyrite grains (in the middle of the image, in the right and left top corners, and in the right bottom corner). Arsenic also appears to be present between the boundaries of the pyrite grains. Selenium is present in the rims of the grains. Silver,Pb and Bi are present in thin overgrowths and in the fractures. White lines show the grain outlines and the fractures.

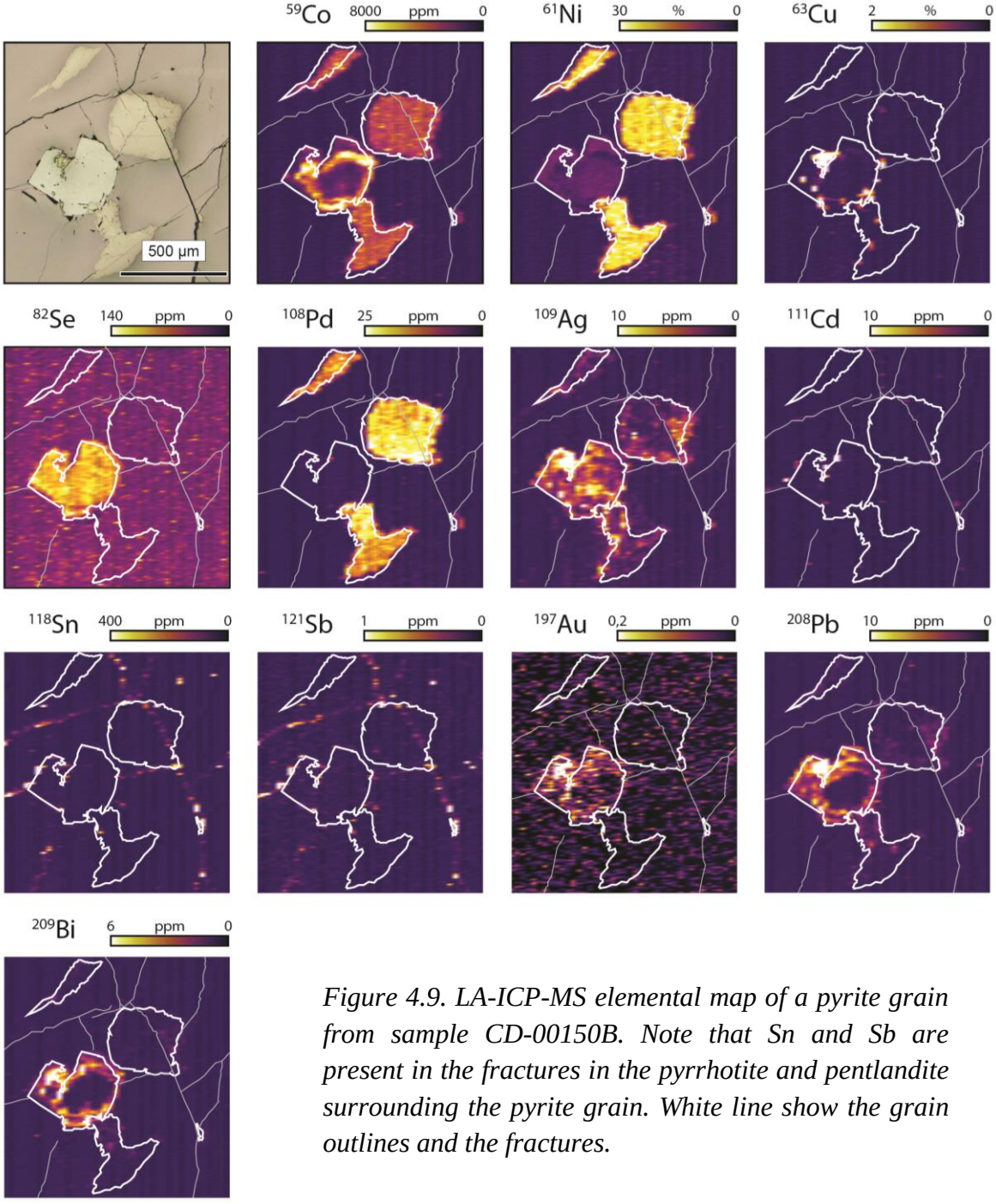

Figure 4.9. LA-ICP-MS elemental map of a pyrite grain from sample CD-00150B. Note that Sn and Sb are present in the fractures in the pyrrhotite and pentlandite surrounding the pyrite grain. White line show the grain outlines and the fractures.

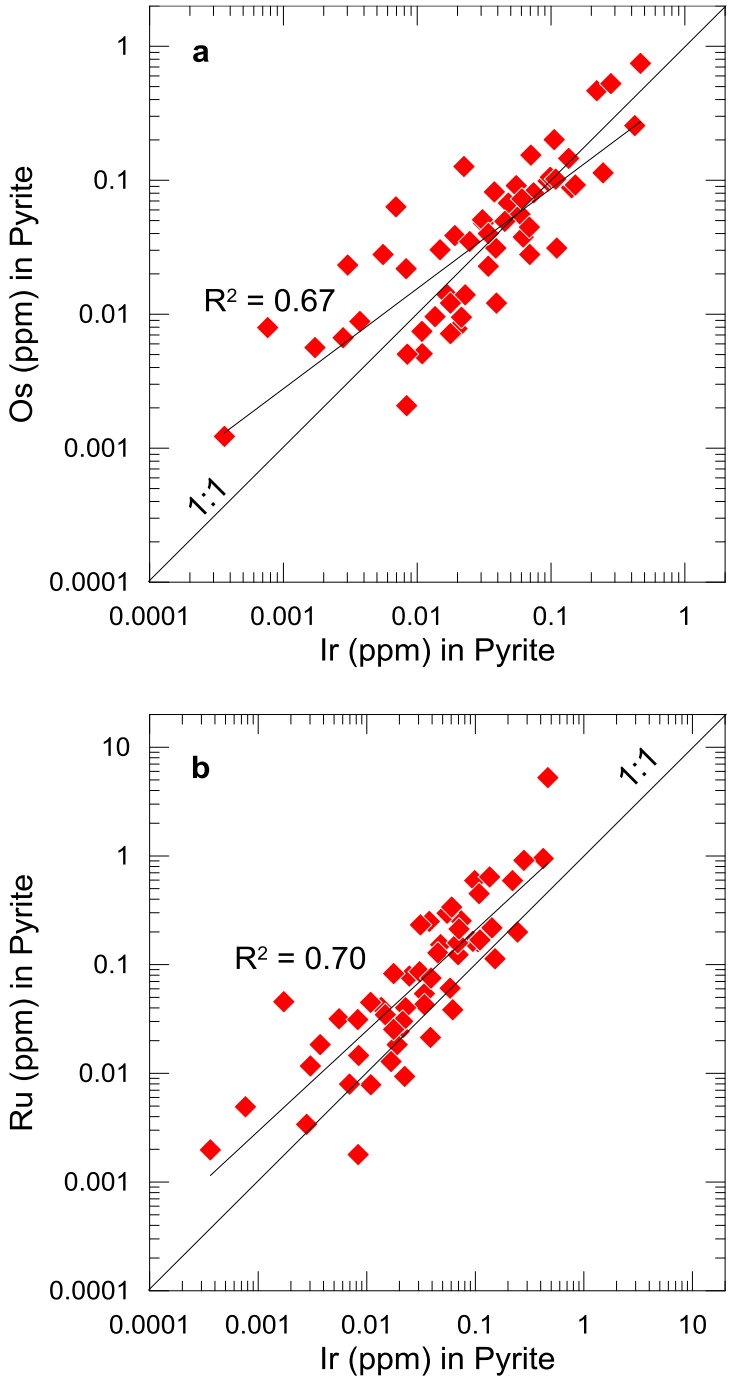

Figure 4.10. Binary diagrams: (a) Ir versus Os; and (b) Ir versus Ru. Note the relatively strong degree of correlation between these elements. The pyrite trend follows the 1:1 line indicating a similar distribution of the IPGE.

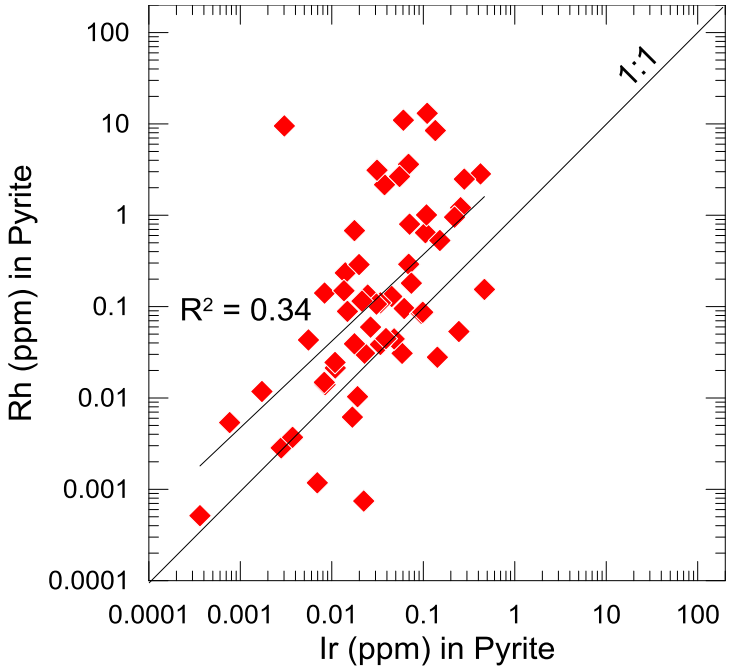

Figure 4.11. Binary diagrams of Ir versus Rh. Note that the degree of correlation between Ir and Rh is lower than between Ir and the other IPGE. The pyrites appears to be richer in Rh than in IPGE.

In all of the maps, we observed a concentric zoning with respect to Ag, Bi, and Pb. These elements are considerably enriched in the Py rims, in which they form a thin overgrowth (Figs. 4.5-9), on the thicker layer that is enriched in Co and Se. In Figure 8, Ag, Bi, and Pb are also observed along fractures within the Py grain. On plots of Ag vs Bi and Ag vs Pb (Figs. 4.12a, b), relatively strong degrees of correlation can be observed. However, neither of Ag, Bi and Pb correlate with Co nor Se.

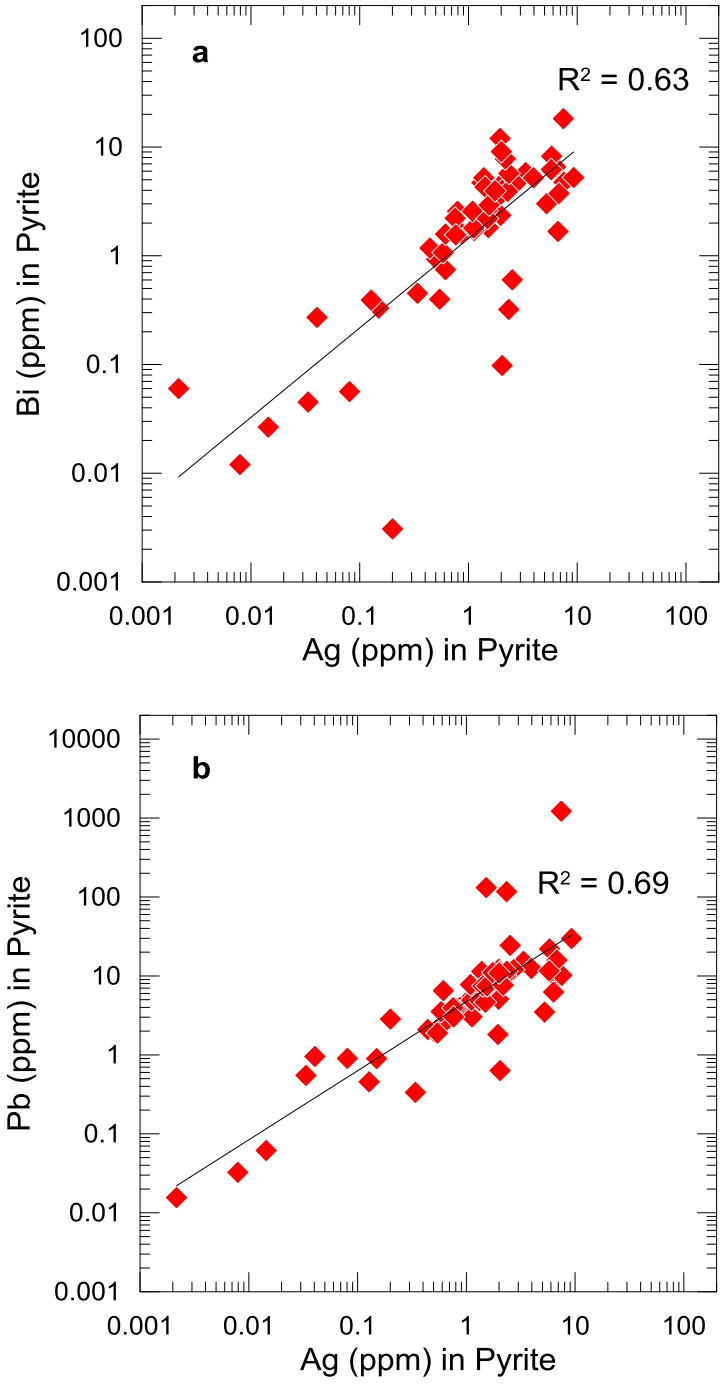

Figure 4.12. Binary diagrams: (a) Ag versus Bi; and (b) Ag versus Pb. Note the relatively strong degree of correlation between these elements.

In two maps (Figs. 4.5, 4.6) we observed similar zoning for Pt, forming a thin overgrowth along with Ag, Bi, Pb and in one case (Fig. 4.6) with Te and Sn. However, we did not observe any correlation of Pt with other elements. Platinum zoning and/or overgrowth have also been observed at Aguablanca and Sudbury by Piña et al. (2013), and Dare et al. (2011) and Adibpour et al. (2014), respectively. In the other Py, Pt concentrations were too low and no zoning has been observed. In Figure 4.7, Pt and Au concentrations are higher in the surrounding Po than in the Py.

In Figure 4.9, Sn and Sb are present along fractures and in Figure 6, Sn is present within a silicate mineral. Cadmium has not been observed forming any zoning or being present along the fractures. However, Cd exhibits a strong degree of correlation with Sb (Fig. 4.13).

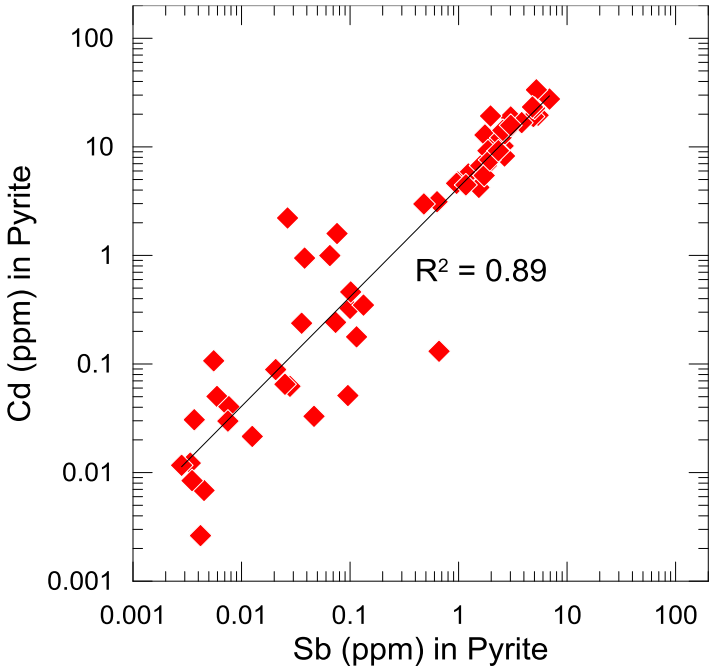

Figure 4.13. Binary diagrams of Sb versus Cd. Note the strong degree of correlation between these elements.

Most of the Py do not contain significant concentrations of Ni. Nickel zoning has only been observed in the small Py (Fig. 4.9). In this case, Ni has been found to form oscillatory zoning antithetical to Co. In the other Py, Ni concentrations were low and no zoning has been observed. Similarly Re, Mo, Pd and Cu concentrations are low and the grains do not show zoning.

4.8.2 INCORPORATION OF CHALCOPHILE AND PLATINUM-GROUP ELEMENTS IN PYRITE

Pyrite in magmatic sulfides has been interpreted as having formed by either exsolution from S rich MSS (Dare et al., 2011) or replacement of Po and possibly Pn (Piña et al., 2013; Smith et al. 2014). At LDI the quantity of Py present is too great for the former explanation. An alternative hypothesis is that Py formed by replacement of Po and possibly Pn. In order to consider this idea we can compare the median Py with those of Po and Pn on primitive mantle normalized multi-element plots. (Fig. 4.14). Overall the patterns for all three minerals are similar for most elements, approximately flat at 1 to 100 times the primitive mantle values. Exceptions to this are the large negative Cu anomalies for all three minerals and positive Pd anomaly for Pn. The Py pattern is similar in shape to the Po and Pn patterns except that it has negative Ni anomalies. If the Py formed from Po and Pn, Ni appears to have been lost from the system along with Fe as proposed by Boudreau et al. (2014).

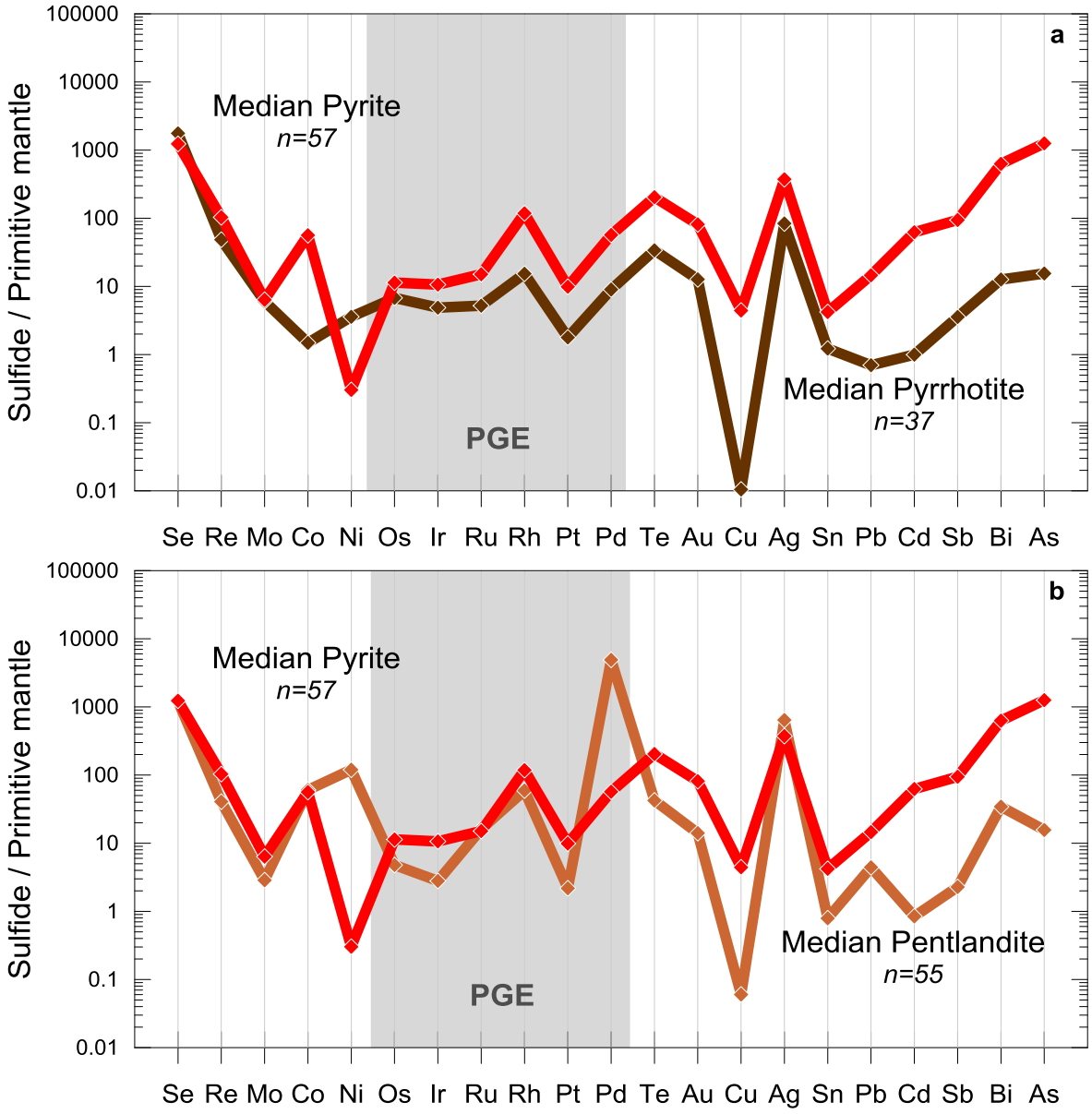

Figure 4.14. Primitive mantle normalized multi-element diagrams of pyrite compared with (a) pyrrhotite; and (b) pentlandite. The normalization values are from Lyubetskaya and Korenaga (2007).

Although the shape of the three mineral patterns show similarities, Py exhibits an increasing degree of enrichment in the elements with incompatibility in MSS. Thus Se, Mo, Re and Os are present at similar levels in all three minerals, but elements such as Bi and As show an enrichment in Py by a factor of approximately 100 relative to the Po and Pn. If the elements had been enriched in Py by mass loss when Po lost Fe, then it would be expected that they would be enriched by a factor of ~1.4. The factor of 1.4 arises because Po, which is composed of 62.33% Fe, must release 40 % of its Fe budget in order to reach 46.55% Fe to form Py. It is possible that Py-rich samples were originally richer in the trace elements and thus the enrichment in Py is simply because the Po and Pn from which they formed were trace element rich. To test this idea we have plotted Ir and Rh in Py vs Ir and Rh in Po and Pn for individual samples (Fig. 4.15). Here it is clear that the Py is enriched in both Ir and Rh relative to the Po and Pn.

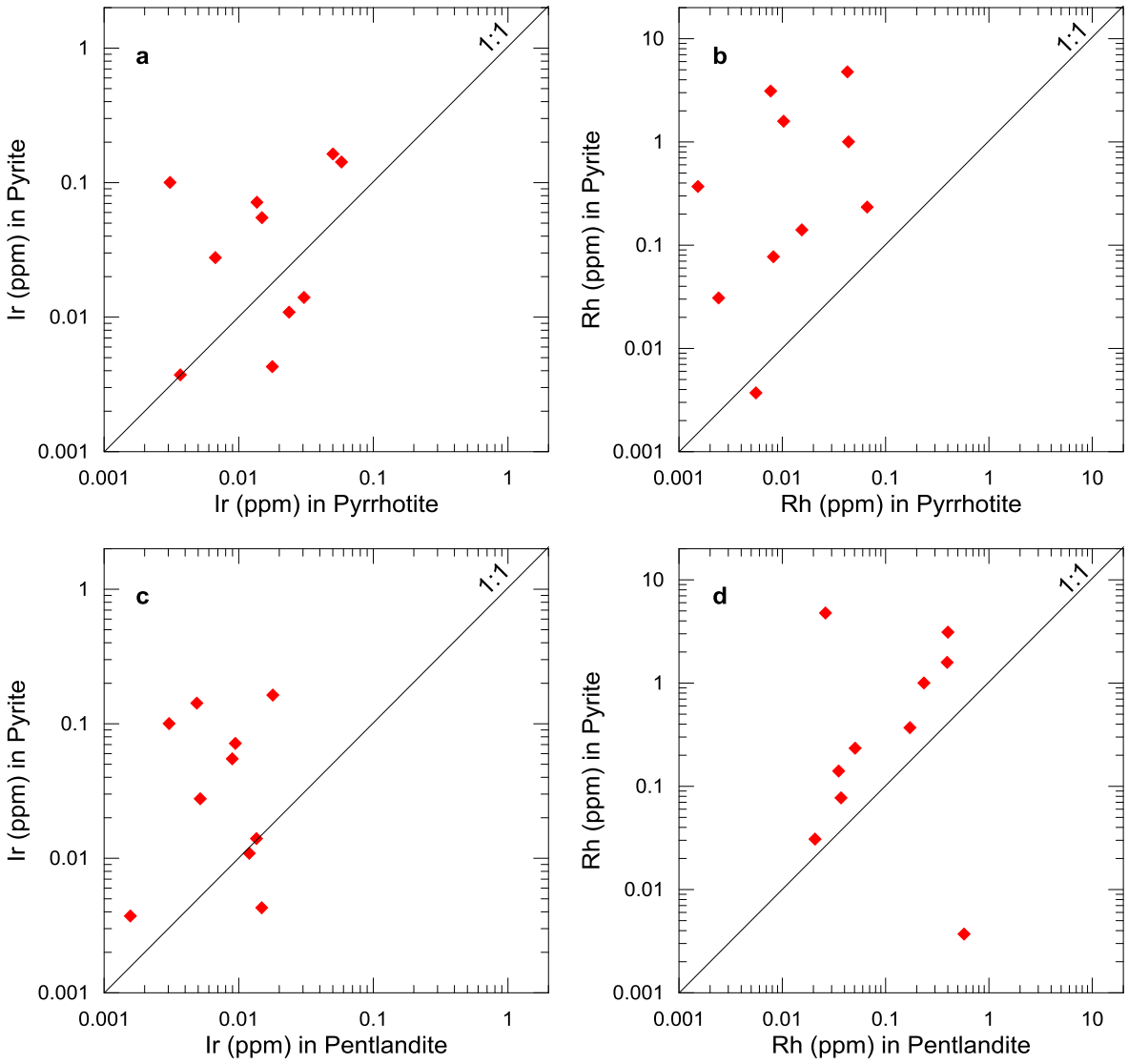

Figure 4.15. Binary diagrams: (a) Ir in pyrite versus Ir in pyrrhotite, (b) Rh in pyrite versus Rh in pyrrhotite; (c) Ir in pyrite versus Ir in pentlandite; (d) Rh in pyrite versus Rh in pentlandite. Data represent the median of individual samples. Note that pyrite is enriched in Ir and Rh relative to pyrrhotite and pentlandite.

Although the elements show a zonation in the Py with the IPGE, Rh and As in the centre and Co and Se at the margins, most elements appear to fit into the Py structure. However some elements such as Ag, Bi, Pb, Pt, Te, Sn and Sb appear to be located along fractures or thin overgrowths on the Py. For those elements which appear to be part of the Py structure and which are strongly enriched in the Py, we suggest that as the Py formed it inherited the trace elements from the Po, but in addition elements diffused from the surrounding sulfides into the Py because they fit better into the Py structure than the Po or Pn. This interpretation is consistent with the compatibility of IPGE, Rh, Co and Se with MSS (Barnes and Lightfoot, 2005 and references therein; Mungall et al., 2005; Brenan, 2008; calculated from Li and Audétat, 2012), and is further supported by the results of Brenan et al. (2000) that show that Os can diffuse into Py. However, this interpretation is inconsistent for As because it is not significantly contained by Po and Pn due to its incompatibility with MSS (Helmy et al., 2010; Liu and Brenan, 2012). A possible explanation could be that As has been added to the rocks by fluids. This hypothesis is in agreement with our previous observation that Py-rich samples are enriched in As relative to other samples (Duran et al., submitted). The elements found along fractures and thin overgrowths are also incompatible with MSS and may have been added by fluids.

4.8.3 ORIGIN OF ZONING IN PYRITE

Piña et al. (2013) proposed that this type of zoning could be the result of boundary layer effect during fluid-assisted solid-state replacement of MSS/Po. A similar origin can be proposed for the Py of the LDI sulfide-rich pods. Figure 4.16 illustrates how Py may have formed. During the development of Py, IPGE, Rh and As were preferentially incorporated into Py leaving the surrounding MSS/Po relatively depleted in IPGE. The As was possibly introduced by fluids, that may have assisted the diffusion of IPGE from the surrounding MSS/Po and Rh from Pn. The strong affinity of IPGE and Rh for As (Piña et al., 2013) would account for the association of these elements within the Py structure. Moreover, Barkov et al. (2004) have shown that As could exert a structural control over the incorporation of IPGE and Rh in PGE sulfides with a Py-like structure. The presence of small PGM composed of IPGE would have provided ideal sites of nucleation for Py and would be consistent with the presence of IPGE and Rh in the centre of the grains.

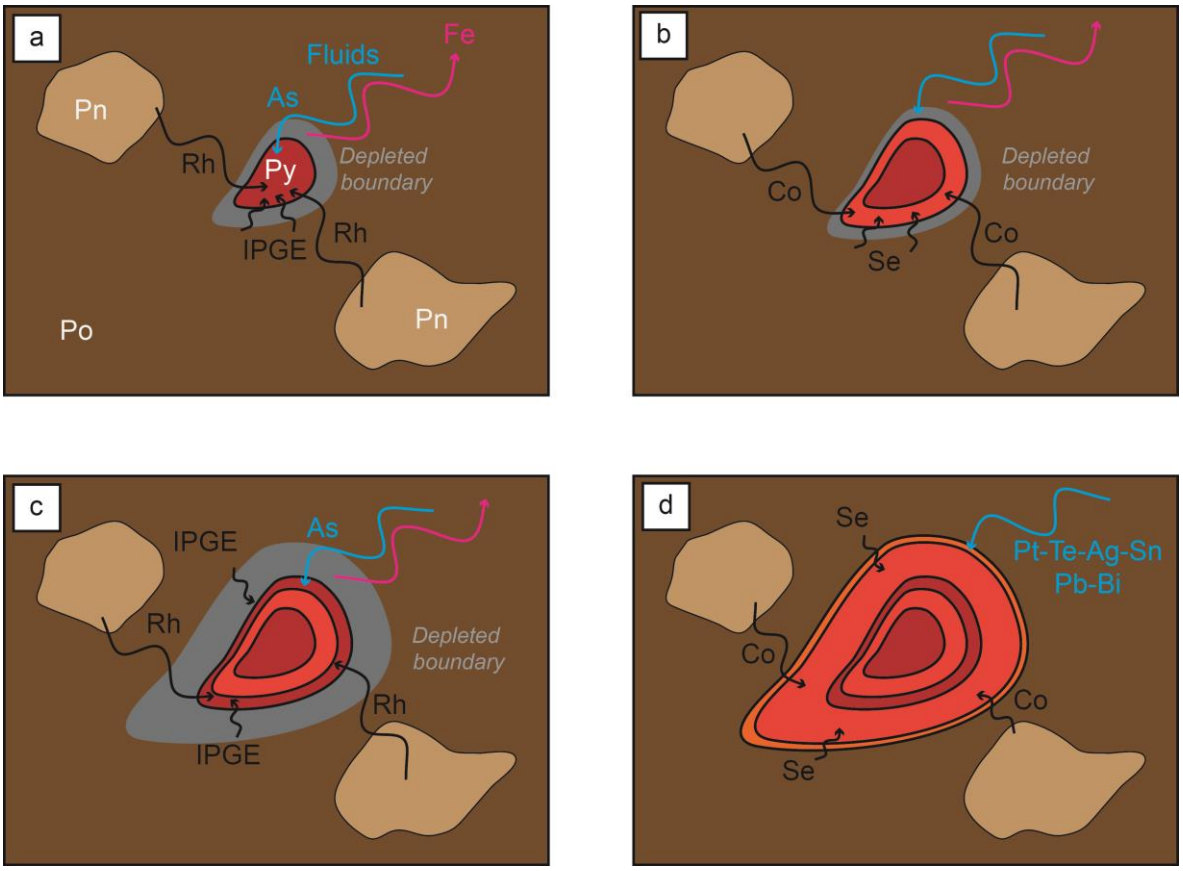

Figure 4.16. Schematic model of the formation of pyrite (See text for details). (a) Redistribution of Fe out of the sulfides and introduction of As by fluids plus diffusion of IPGE-Rh from MSS/Po and Pn into Py, which leaves a boundary depleted in IPGE-Rh; (b) Diffusion of Co and Se from MSS/Po and Pn into Py when Py grows over the boundary depleted in IPGE-Rh, which leaves a new boundary depleted in Co and Se; (c) Reiteration of (a) and (b) leading to concentric zoning sub-parallel to crystal faces; (d) Introduction of mobile elements into Py by fluids, which ultimately forms a thin overgrowth.

Because the diffusion of IPGE and Rh was probably slower than the Py growth, the next layer of Py to grow formed from IPGE-Rh depleted MSS/Po and incorporated Co and Se instead of IPGE, Rh and As. Furthermore, the experiments of Brenan et al. (2000) show that the diffusion of Os in Py is limited to near surface and that the uptake of Os in Py only occurs when grain growth exists. Cobalt may have diffused from surrounding Pn as MSS/Po is not a significant source of Co. Eventually, several iterations of this process gave rise to the oscillatory concentric zoning observed within Py. In the ultimate stages of Py growth, fluids may have introduced the most mobile elements such as Te, Cu, Ag, Sn, Pb, Cd, Sb and Bi, thus forming a thin overgrowth in the Py rims. This suggestion is further supported by the presence of some of these elements along fractures and the Py-rich samples being enriched in Bi (Duran et al., submitted). Locally, PGM composed of Pt may have been dissolved by these fluids and Pt was incorporated in the last overgrowth of some Py.

However, the lack of IPGE-Rh zoning in the small Py (Fig. 9) could be interpreted otherwise, i.e., as a different type of Py. Alternatively this observation could be a consequence of the sample cut (Jugo, personal communication). Because the IPGE-Rh zoning appear to be present toward the core of the Py, the grains that would have been cut on the edges and not in the center would not exhibit the IPGE-Rh zoning. Therefore, care should be taken when interpreting observations based on a 2D representation. We suggest that the small Py that lack IPGE-Rh zoning represents the edges of the grain and has not been cut through its center.

4.9 DISCUSSION

4.9.1 COMPARISON WITH PYRITE FROM THE DISSEMINATED SULFIDES

Duran et al. (submitted) have demonstrated that Po and Pn from the sulfide-rich pods were less enriched in all the PGE and chalcophile elements relative to Po and Pn from disseminated sulfides, possibly due to the sulfide liquids having lower R-factor. Therefore, it could be expected that Py replacing disseminated sulfides would be enriched in PGE and chalcophile elements relative to Py replacing sulfide-rich pods. This hypothesis is consistent in the case of Se, Co and Pd (Fig. 4.17). However, an interesting feature rising from this study is that Py from sulfide-rich pods is more enriched in IPGE (10 to 15 times the primitive mantle values; Fig. 4.17) relative to Py from disseminated sulfides (2 to 8 times the primitive mantle values; Fig. 4.17). In addition, both Py from sulfide-rich pods and disseminated sulfides have similar Rh values. This observation could be explained by the larger volume of sulfides and the higher weight fractions of Po and Pn in sulfide-rich pods (77 and 18 %, respectively) relative to disseminated sulfides (54 and 12 %, respectively; Djon and Barnes, 2012). This would provide more IPGE and Rh to diffuse during the formation of Py within sulfide-rich pods.

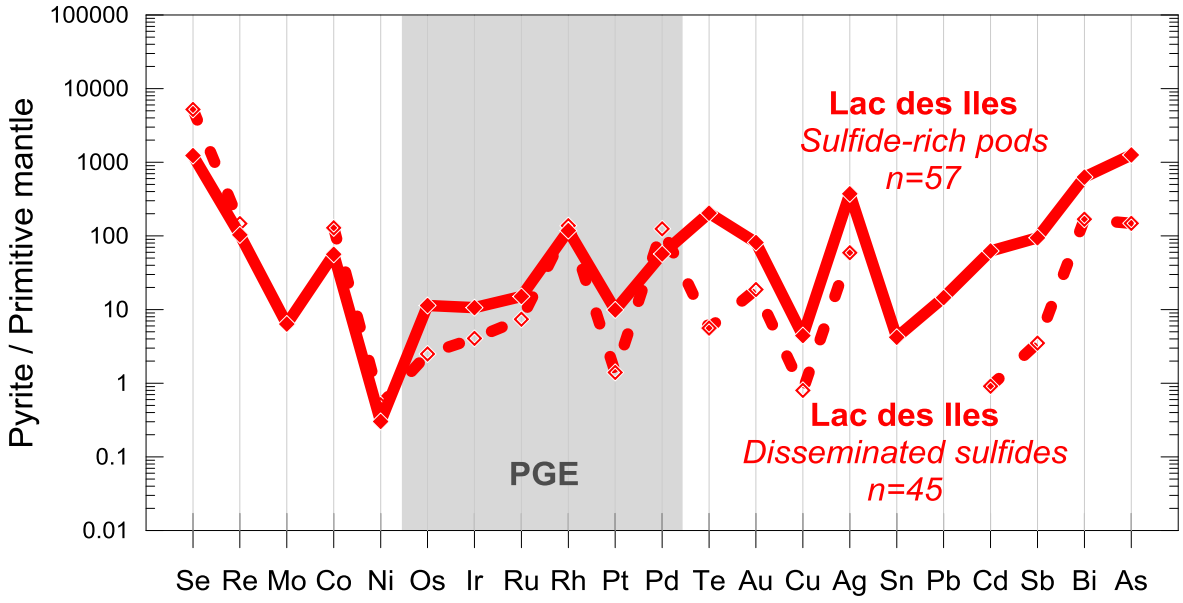

Figure 4.17. Primitive mantle multi-element diagrams of pyrite from Lac des Iles sulfide-rich pods compared with pyrite from Lac des Iles disseminated sulfides (dashed line). Note that the pyrite from the sulfide-rich pods is richer in IPGE, Te, Au, Cu, Ag, Cd, Sb, Bi and As than the pyrite from the disseminated sulfides. The data for disseminated sulfides are from Djon and Barnes (2012). The normalization values are from Lyubetskaya and Korenaga (2007).

Platinum, Te, Au, Cu, Ag and semi-metals are also enriched in Py from sulfide-rich pods relative to Py from disseminated sulfides (Fig. 4.17). In contrast, to IPGE and Rh, these elements are not significantly present in the Po and Pn of the LDI sulfide-rich pods (Duran et al., submitted). Therefore, the larger volume of sulfides and the higher weight fractions of Po and Pn would not provide significant amounts of Pt, Te, Au, Cu, Ag and semi-metals to incorporate into Py within sulfide-rich pods. An alternative possibility could be that the larger volume of sulfides are associated by larger volume of PGM.

4.9.2 COMPARISON WITH PYRITE FROM OTHER NI-CU-PGE DEPOSITS

In comparing the trace element composition and distribution of Py across the Ni-Cu-PGE deposits where Py has been studied (i.e, Sudbury, Aguablanca, Bushveld), there are some common features. First, the Py from LDI, Aguablanca (Piña et al., 2013), Sudbury (Dare et al., 2011) and the Grasvally Norite-Pyroxenite-Anorthosite (GNPA) member of the Bushveld Complex (Smith et al., 2014) exhibit similar patterns on the multi-element diagram that is normalized to primitive mantle (Fig. 4.18). Second, all Py are significantly enriched in Co (thousands of ppm) and IPGE-Rh (a few ppm). Third, in cases Py has been mapped using LA-ICP-MS (Dare, unpublished data; Piña et al., 2013; Adibpour et al., 2014) it revealed similar concentric oscillatory zoning with respect to Co, Se, IPGE-Rh and As (Fig. 4.19). Furthermore, the concentrations of Co, Se, Rh and As are in similar ranges as indicated in Figure 4.20. The distribution of most of the trace elements among Py and

co-existing Po and Pn is also highly similar (Fig. 4.21). When Py has not been mapped (Djon and Barnes, 2012; Osbahr et al., 2013, 2014; Smith et al., 2014), Py shows a wide range of compositions. This observation could be the result of concentric oscillatory zoning. Ultimately, in all Ni-Cu-PGE deposits some Pt- and/or Pd-bearing Py have been documented, but this was not a systematic observation in contrast to IPGE and Rh. In addition, the few available data for semi-metals suggest that these elements are also enriched into Py.

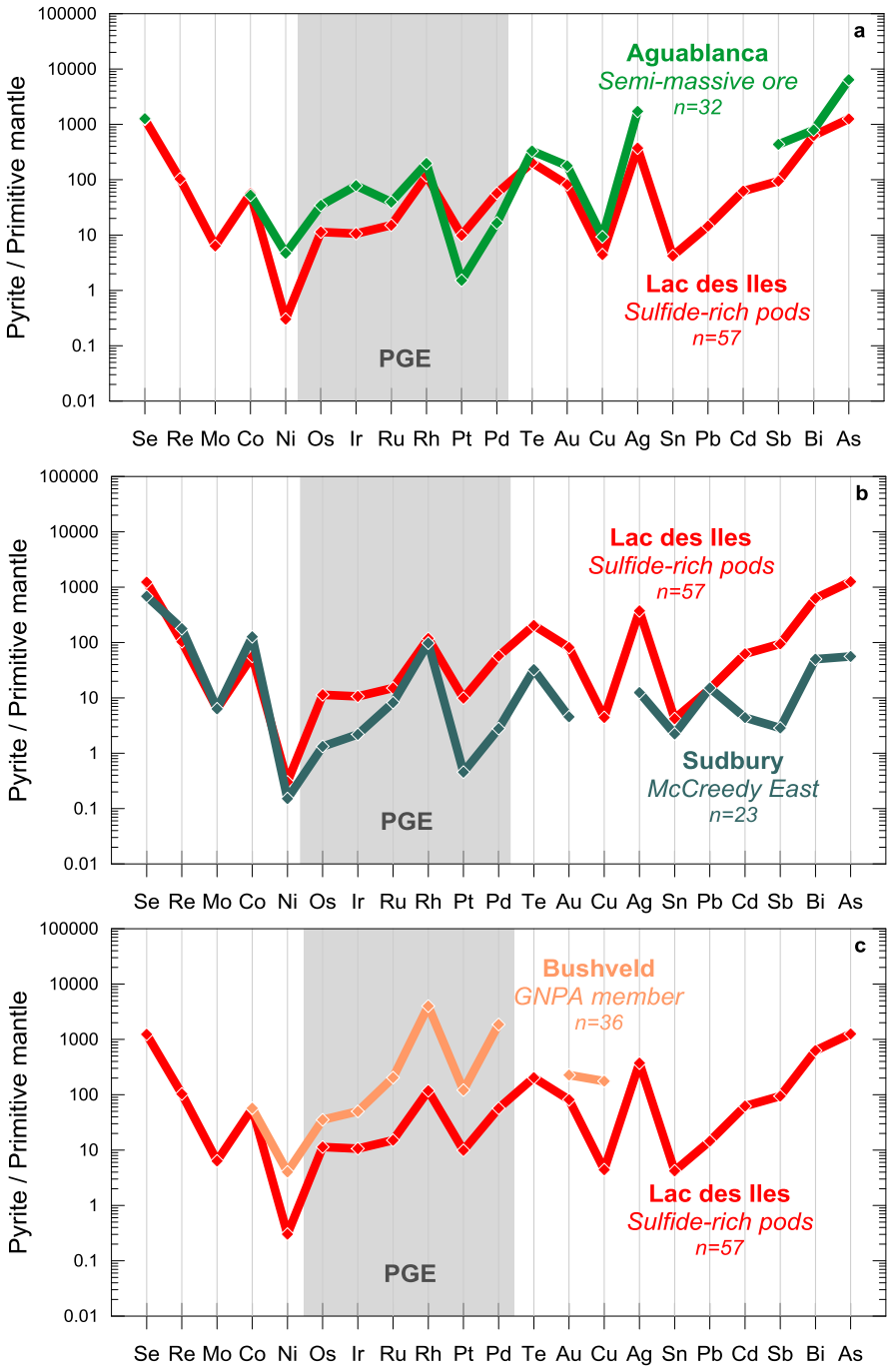

Figure 4.18. Primitive mantle multi-element diagrams of pyrite from Lac des Iles sulfide-rich pods compared with pyrite from (a) Aguablanca, semi-massive ore (Piña et al., 2013); (b) Sudbury, McCreedy Deposit (Dare et al., 2011); Bushveld Complex, GNPA (Smith et al., 2014) The normalization values are from Lyubetskaya and Korenaga (2007).

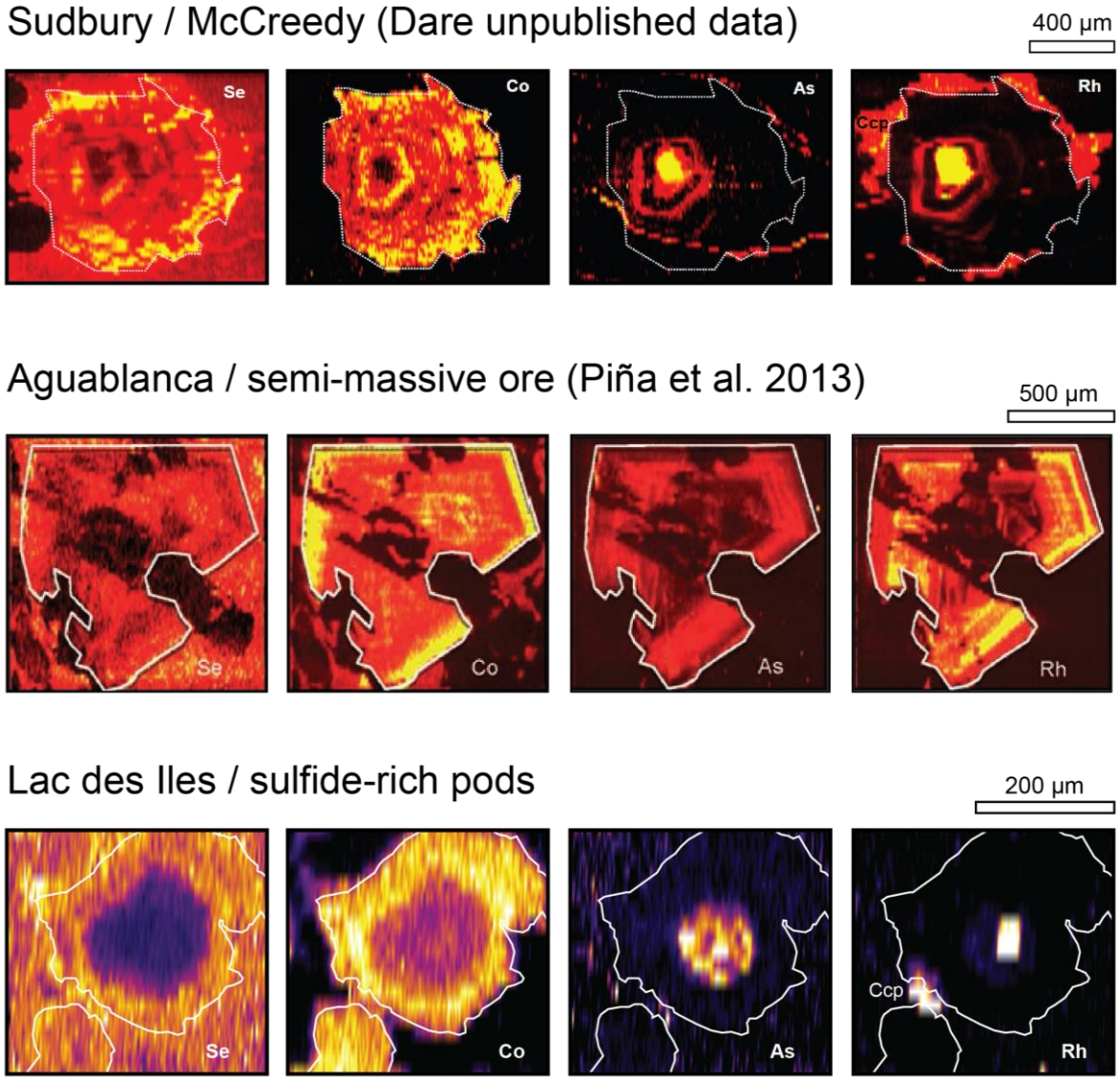

Figure 4.19. LA-ICP-MS elemental maps of pyrites from Sudbury, McCreedy Deposit (Dare, unpublished data) Aguablanca, semi-massive ore (Piña et al., 2013) and Lac des Iles, sulfide-rich pods. Note the similar compositional distribution of the elements (Co, Se, Rh and As). White lines show the grain outlines.

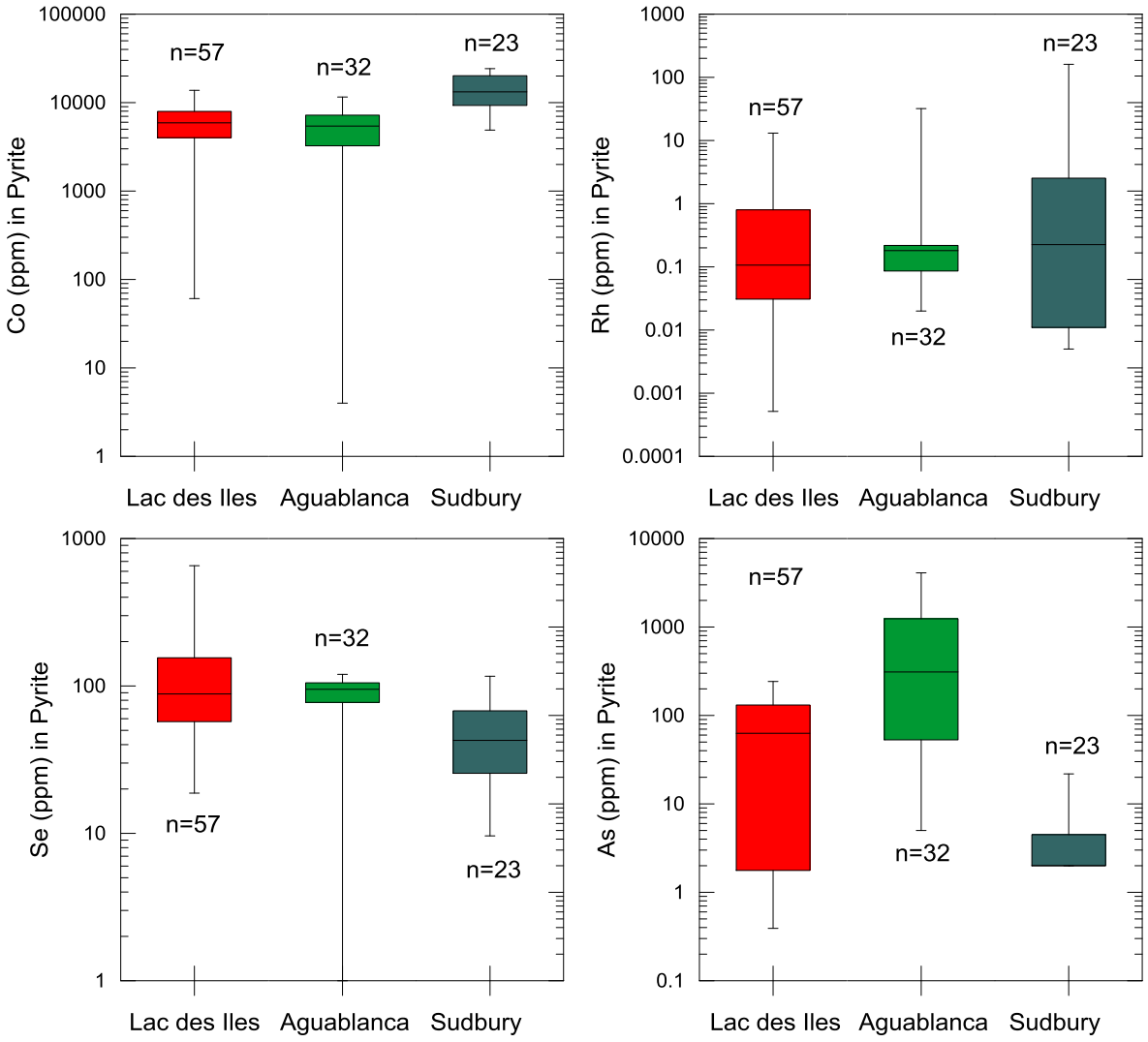

Figure 4.20. Box and whisker plots (median, first and third quartile ranges, and minimum and maximum values) of the Co, Se, Rh and As concentrations of pyrites from Lac des Iles sulfide-rich pods, Aguablanca semi-massive ore (Piña et al., 2013) and Sudbury McCreedy Deposit (Dare et al., 2011).

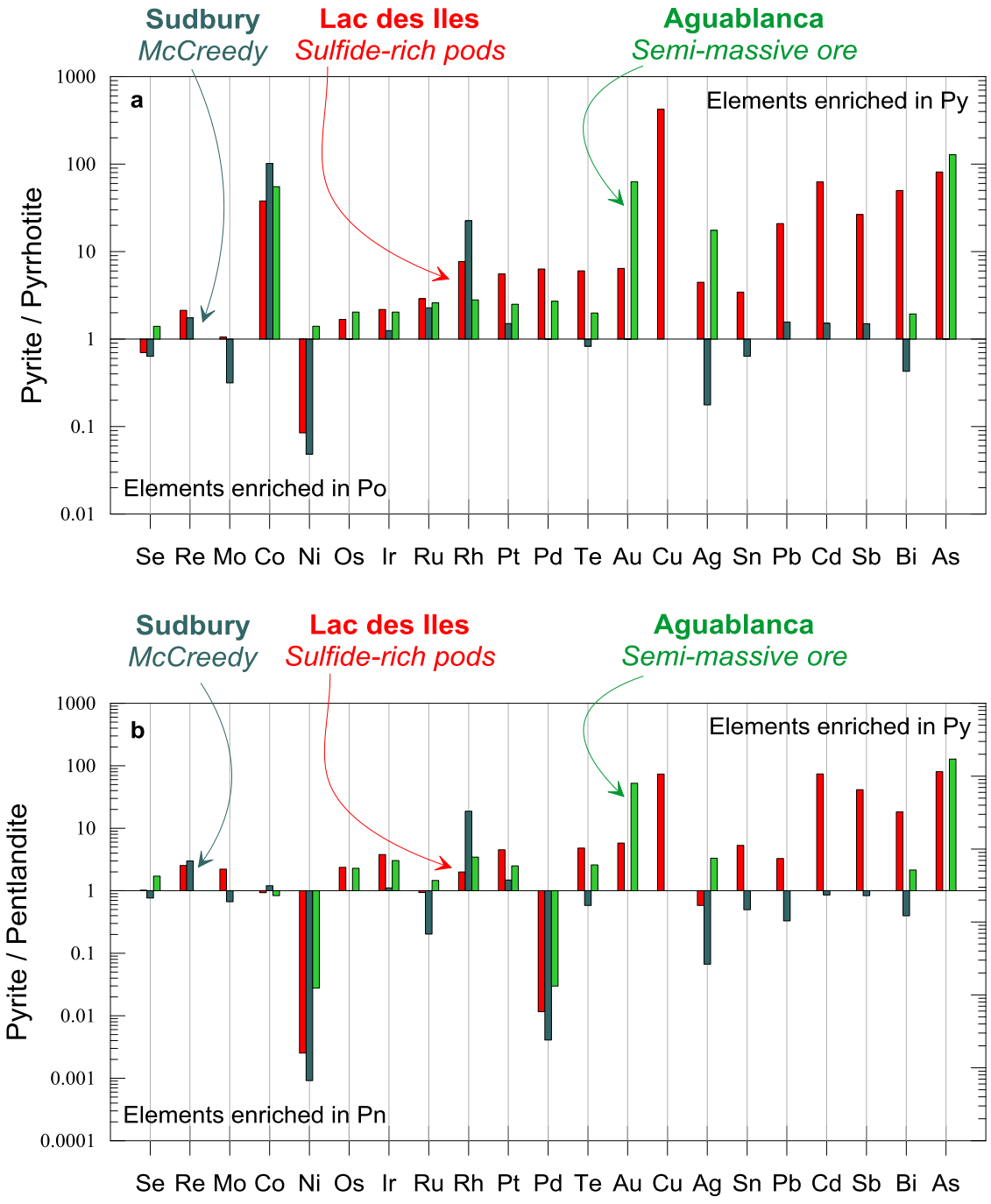

Figure 4.21. Histograms of pyrite compositions from Lac des Iles sulfides-rich pods, Sudbury McCreedy (Dare et al., 2011) and Aguablanca semi-massive ore (Piña et al., 2013) normalized to co-existing (a) pyrrhotite and (b) pentlandite.

One interesting feature rising from this comparison is that Py from the different Ni-Cu-PGE deposits is considered as the result of ore-modifying processes. Therefore, the similarities observed in Py across the Ni-Cu-PGE deposits studied so far indicate that common ore-modifying processes have occurred during Py formation.

4.9.3 EXPLORATION CONSIDERATIONS

Pyrites from Ni-Cu-PGE deposits studied so far consist of the replacement product of the primary ore and, therefore, inherit the original ore features. Consequently, when exploring for magmatic Ni-Cu-PGE deposits using stream sediments or glacial deposits, the presence of Py should not be neglected. The study of Py could reveal the presence of primary Ni-Cu-PGE mineralization obliterated by alteration.

One interesting feature is that Py from Ni-Cu-PGE deposits contains significant amounts of Co and Se. In contrast, Py from hydrothermal deposits have generally low values of Co and Se and are much enriched in As and Sb. This result has a strong potential for use in discriminating between Ni-Cu-PGE and hydrothermal deposits in exploration. In detrital sedimentary rocks such as glacial tills, Py may be present in the heavy mineral fraction. A plot of Co/Sb versus Se/As may be used to discriminate the provenance of Py (Fig. 4.22). Clearly, Py from Ni-Cu-PGE deposits have high Co/Sb and Se/As ratios whereas Py from low-temperature hydrothermal (i.e., orogenic gold deposits, volcanogenic-hosted massive

sulfides) and sedimentary deposits (Large et al. 2009; Maslennikov et al., 2009; Thomas et al., 2011; Revan et al., 2014) have low Co/Sb and Se/As ratios.

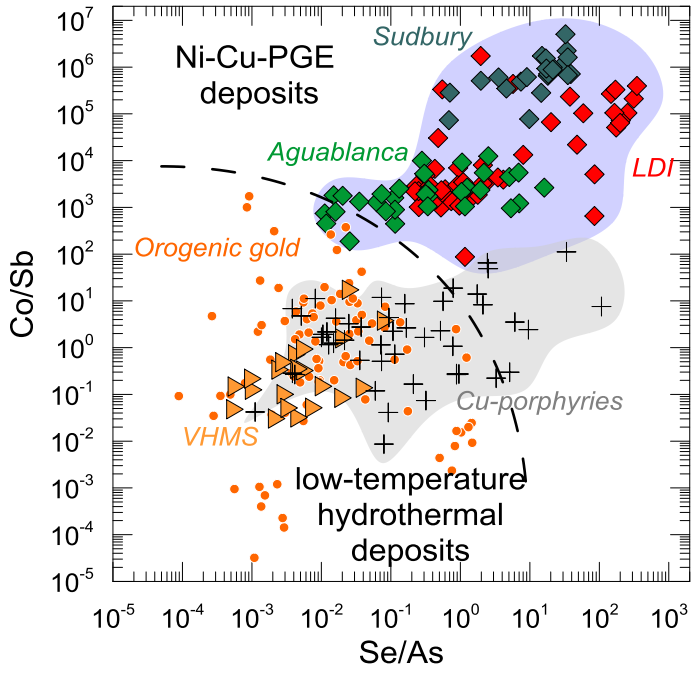

Figure 4.22. Binary diagram of the Co/Sb ratio in pyrite versus the Se/As ratio in pyrite. Note that pyrites from magmatic Ni-Cu-PGE deposits can be discriminated from pyrites from hydrothermal deposits on the basis of the Co, Sb, Se and As concentrations. The data sources for other deposits are: Large et al. (2009), Maslennikov et al. (2009), Thomas et al. (2011), Dare et al. (2011), Piña et al. (2013), Reich et al. (2013), Revan et al. (2014).

However, Py from Cu-porphyries deposits have intermediate Co/Sb and Se/As ratios (Reich et al., 2013), and may overlap with the field of Ni-Cu-PGE deposits (Fig. 4.22). Moreover, high Pd and Pt concentrations in Py from alkaline porphyries have been reported (Hanley et al., 2010; Serafimovski et al., 2013), which might be confusing when trying to discriminate the provenance of Py. In this case, IPGE geochemistry can be used, because Py from Ni-Cu-PGE deposits generally have high concentrations in these elements whereas Py from porphyries deposits do not.

4.10 CONCLUDING REMARKS

This LA-ICP-MS study reveals the compositional and textural features of Py from the sulfide-rich pods of the LDI Pd deposits. Furthermore, this study provides an insight on the processes whereby MSS can be affected during alteration. Our findings may be summarized as follows:

1. Pyrites host considerable amounts of Co, IPGE, Rh and semi-metals.
2. Pyrites show typical concentric oscillatory zoning. The IPGE, Rh and As form thin bands towards the core of Py whereas Co and Se form larger bands towards the rims. Thin overgrowths comprising Pb, Ag and Bi were commonly observed. Occasionally, these overgrowths contain Pt, Te and Sn.

3. Some mobile elements were observed to be present along the fractures within or proximal to Py.
4. The primitive mantle normalized pattern of Py has a shape highly similar to that of Po. In addition Py has similar concentrations in Co and Rh to Pn.
5. These features are interpreted as a consequence of mineral replacement reactions, whereby Po has been converted to Py. The enrichment of Py in Co, Rh ± IPGE could be explained by a process of fluid-assisted solid-state diffusion from surrounding Pn ± Po. The enrichment in semi-metals likely resulted from the incorporation by circulating fluids. Local Pt incorporation may have resulted from PGM dissolution.
6. The lower concentration of PGE and chalcophile elements in Py from the disseminated sulfides is consistent with this interpretation. The larger volume of sulfide and the higher weigh fraction of Po and Pn in sulfide-rich pods would provide a more important source of PGE and chalcophile elements available for diffusion.
7. The similarities in composition and textures with Py from other Ni-Cu-PGE deposits suggest a common ore-modifying process.
8. The Co/Sb and Se/As ratios of Py from Ni-Cu-PGE deposits strongly differs from that of Py from low-temperature hydrothermal deposits. Therefore, the use of the plot of Co/Sb versus Se/As in Py has a strong potential in exploration to discriminate between the possible origins of Py in detrital materials such as tills.

4.11 ACKNOWLEDGMENTS

This study was completed by the first author as part of his PhD research project at UQAC. We are grateful to North American Palladium for providing financial support to Sarah-Jane Barnes' Canada Research Chair in Magmatic Ore Deposits, for allowing access to the mine property and publication of this paper, and for hiring the first author as an exploration geologist during field seasons. We would like to thank the entire North American Palladium Exploration Team for technical support in the field over the years. Dany Savard and Sadia Mehdi are thanked for their assistance with LA-ICP-MS facilities at LabMaTer, UQAC. This study largely benefited from intellectual input from Rubén Piña of Universidad Complutense (Madrid) and Sarah Dare of University of Ottawa who both also provided with the LA-ICP-MS maps used in Figure 17. We also thank Philippe Pagé, Ed Sawyer, Jerôme Augustin and Dominique Genna of UQAC, and Lionnel Djon, Arnaud Tchalikian, and Skylar Schmidt of North American Palladium for great discussions. Finally, anonymous reviewers are thanked for their time and for thorough revision and improvement of this manuscript.

4.12 REFERENCES

Abraitis, P.K., Pattrick, R.A.D., Vaughan, D.J., 2004. Variations in the compositional, textural and electrical properties of natural pyrite: a review. International Journal of Mineral Processing 74, 41–59.

Adibpour, M., Jugo, P.J., Ames, D.E., 2014. Trace element distribution in pyrite from the Levack mine (Sudbury, Canada): Insight into the processes affecting PGE. In: 12th International Platinum Symposium, 11–14 August 2014 Yekaterinburg, Russia, Program Abstracts, pp 241–242.

Barkov, A.Y., Halkoaho, T.A.A., Laajoki, K.V.O., Alapietti, T.T., Peura, R.A., 1997. Ruthenian pyrite and nickeloan malanite from the imandra layered complex, Northwestern Russia. Can. Mineral. 35, 887–897.

Barkov, A.Y., Fleet, M.E., Martin, R.F., Alapietti, T.T., 2004. Zoned sulfides and sulfarsenides of the platinum-group elements from the Penikat layered complex, Finland. Can. Mineral. 42, 515–537.

Barnes, S-J., Lightfoot, P.C., 2005. Formation of magmatic nickel sulfide ore deposits and processes affecting their copper and platinum group element contents. Econ. Geol. 100th Anniversary Volume, pp 179–213.

Barnes, S-J., Gomwe, T.S., 2011. The Pd Deposits of the Lac des Iles Complex, Northwestern Ontario. Rev. Econ. Geol. 17, 351–370.

Berner, R.A., 1970. Sedimentary pyrite formation. Ame. J. Science 268, 1–23.

Boudreau, A., Djon, L., Tchalikian, A., Corkery, J., 2014. The Lac des Iles palladium deposit, Ontario, Canada. Part I. The effect of variable alteration on the Offset Zone. Mineral. Deposita 49, 625–654.

Brenan, J.M., 2008. Re–Os fractionation by sulfide melt–silicate melt partitioning: A new spin. Chem. Geol. 248, 140–165.

Brenan, J.M., Cherniak, D.J., Rose, L.A., 2000. Diffusion of osmium in pyrrhotite and pyrite: implications for closure of the Re–Os isotopic system. Earth Planet. Sci. Lett. 180, 399-413.

Brügmann, G.E., Reischrnann, T., Naldrett, A.J., Sutcliffe, R.H., 1997. Roots of an Archean volcanic arc complex; the Lac des Iles area in Ontario, Canada. Precamb. Res. 81, 223–239.

Chouinard, A., Paquette, J. Williams-Jones, A.E., 2005. Crystallographic controls on trace-element incorporation in auriferous pyrite from the Pascua epithermal high-sulfidation deposit, Chile-Argentina. Can. Mineral. 43, 951–963.

Craig, J.R., 1973. Pyrite-pentlandite assemblages and other low temperature relations in the Fe–Ni–S systems. Ame. J. Sci. 273A, 496–510.

Craig, J.R., Vokes, F.M., 1993. The metamorphism of pyrite and pyritic ores: an overview. Mineral. Mag. 57, 3–18.

Craig, J.R., Vokes, F.M., Solberg, T.M., 1998. Pyrite: physical and chemical textures. Mineral. Deposita 34, 82–101.

Craig, J.R., Solberg, T.M., 1999. Compositional zoning in ore minerals at the Craig mine, Sudbury, Ontario, Canada. Can. Mineral. 37, 1163 – 1176.

Dare, S.A.S., Barnes, S-J., Prichard, H.M., Fisher, P.C., 2011. Chalcophile and platinum-group element (PGE) concentrations in the sulfide minerals from the McCreedy East deposit, Sudbury, Canada, and the origin of PGE in pyrite. Mineral. Deposita 46, 381–407.

Djon, M.L.N., Barnes, S-J., 2012. Changes in sulphides and platinum-group minerals with the degree of alteration in the Roby, Twilight, and High Grade Zones of the Lac des Iles Complex, Ontario, Canada. Mineral. Deposita 47, 875–896.

Gupta, V.K., Sutcliffe, R.H., 1990. Mafic-ultramafic intrusives and their gravity field: Lac des Iles area, northern Ontario. Geol. Soc. Amer. Bull. 102, 1471–1483.

Hanley, J.J., MacKenzie, M.K., Warren, M.R., Guillong, M., 2010. Distribution and origin of platinum-group elements in alkali porphyry Cu–Au and low sulfidation epithermal Au deposits in the Canadian Cordillera. In: 11th International Platinum Symposium, 21–24 June 2010 Sudbury, Canada, Program Abstracts, miscellaneous release-data 269.

Hanley, J.J., Gladney, E.R., 2011. The presence of carbonic-dominant volatiles during the crystallization of sulfide-bearing mafic pegmatites in the North Roby Zone, Lac des Iles Complex, Ontario. Econ. Geol. 106, 33–54.

Helmy, H.M., Ballhaus, C., Wohlgemuth-Ueberwasser, C., Fonseca, R.O.C., Laurenz, V., 2010. Partitioning of Se, As, Sb, Te and Bi between monosulfide solid solution and sulfide melt – Application to magmatic sulfide deposits. Geochim. Cosmochim. Acta 74, 6174–6179.

Hinchey, J.G., Hattori, K.H., 2005. Magmatic mineralization and hydrothermal enrichment of the High Grade Zone at the Lac des Iles palladium mine, northern Ontario, Canada. Mineral. Deposita 40, 13–23.

Hinchey, J.G., Hattori, K.H., Lavigne, M.J., 2005. Geology, petrology, and controls on PGE mineralization of the southern Roby and Twilight zones, Lac des Iles mine, Canada. Econ. Geol. 100, 43–61.

Kullerud, G., Yoder, H.S., 1959. Pyrite stability relations in the Fe–S system. Econ. Geol. 54, 533–572.

Large, R.R., Danyushevsky, L., Hollit, C., Maslennikov, V., Meffre, S., Gilbert, S., Bull, S., Scott, R., Emsbo, P., Thomas, H., Singh, B., Foster, J., 2009. Gold and trace element zonation in pyrite using a laser imaging technique: implications for the timing of gold in orogenic and carlin-style sediment-hosted deposits. Econ. Geol. 104, 635–668.

Lavigne, M.J., Michaud, M.J., 2001. Geology of North American Palladium Ltd'.s Roby Zone Deposit, Lac des Iles. Explo Mining Geol. 10, 1–17.

Li, Y., Audétat, A., 2012. Partitioning of V, Mn, Co, Ni, Cu, Zn, As, Mo, Ag, Sn, Sb, W, Au, Pb, and Bi between sulfide phases and hydrous basanite melt at upper mantle conditions. Earth Planet. Sci. Lett. 355–356, 327–340.

Liu, Y-N., Brenan, J.M., 2012. Experimental measurement of PGE and semi-metal partitioning during sulfide melt crystallization at controlled fO2-fS2 conditions. In: 12th international Ni-Cu-PGE symposium, program abstracts, State Key Laboratory of Ore Deposit Geochemistry, Institute of Geochemistry, Chinese Academy of Sciences, 36–39 pp.

Lyubetskaya, T., Korenaga, J., 2007. Chemical composition of Earth's primitive mantle and its variance: 1.Method and results. J. Geophys. Res. 112, B03211. doi:10.1029/2005JB004223

Maslennikov, V.V., Maslennikova, S.P., Large, R.R., Danyushevsky, L.V., 2009. Study of trace element zonation in vent chimneys from the Silurian Yaman-Kasy volcanic-hosted massive sulfide deposit (Southern Urals, Russia) using laser ablation-inductively coupled plasma mass spectrometry (LA-ICPMS). Econ. Geol. 104, 1111–1141.

Mungall, J.E., Andrews, D.R.A., Cabri, L.J., Sylvester, P., Tubrett, M., 2005. Partitioning of Cu, Ni, Au, and platinum-group elements between monosulfide solid solution and sulfide melt under controlled oxygen and sulfur fugacities. Geochim. Cosmochim. Acta 69, 4349–4360.

Naldrett, A.J., Craig, J.R., Kullerud, G., 1967. The central portion of the Fe-Ni-S system and its bearing on pentlandite exsolution in iron-nickel sulfide ores. Econ. Geol. 62, 826–847.

Naldrett, A.J., 2004. Magmatic sulfide deposits: geology, geochemistry and exploration. Springer, Berlin, 727 pp.

Oberthür, T., Cabri, L.J., Weiser, T.W., McMahon, G., Müller P., 1997. Pt, Pd and other trace elements in sulfides of the Main Sulfide Zone, Great Dyke, Zimbabwe: A reconnaissance study. Can. Mineral. 35, 597–609.

Osbahr, I., Klemd, R., Oberthür, T., Brätz, H., Schouwstra, R., 2013. Platinum-group element distribution in base-metal sulfides of the Merensky Reef from the eastern and western Bushveld Complex, South Africa. Mineral. Deposita 48, 211–232.

Osbahr, I., Oberthür, T., Klemd, R., Josties, A., 2014. Platinum-group element distribution in base-metal sulfides of the UG2 chromitite, Bushveld Complex, South Africa — a reconnaissance study. Mineral. Deposita 49, 655–665.

Paton, C., Hellstrom, J., Paul, B., Woodhead, J., Hergt, J., 2011. Iolite: freeware for the visualisation and processing of mass spectrometric data. J. Anal. Atom. Spectro. 26, 2508–2518.

Piña, R., Gervilla, F., Barnes, S-J., Ortega, L., Lunar, R., 2012. Distribution of platinum-group and chalcophile elements in the Aguablanca Ni–Cu sulfide deposit (SW Spain): Evidence from a LA-ICP-MS study. Chem. Geol. 302–303, 61–75.

Piña, R., Gervilla, F., Barnes, S-J., Ortega, L., Lunar, R., 2013. Platinum-group elements-bearing pyrite from the Aguablanca Ni-Cu sulphide deposit (SW Spain): a LA-ICP-MS study. Eur. J. Mineral. 25, 241–252.

Piña, R., Gervilla, F., Barnes, S-J., Ortega, L., Lunar, R., 2013. Partition coefficients of platinum group and chalcophile elements between arsenide and sulfide phases as determined in the Beni Bousera Cr-Ni mineralization (North Morocco). Econ. Geol. 108, 935–951.

Rankin, L.R., 2013. Structural controls on emplacement and deformation of PGE-mineralised mafic-ultramafic intrusions – LDI district, NW Ontario. North American Palladium technical report, 115 pp.

Reich, M., Deditius, A., Chryssoulis, S., Li, J-W., Ma, C-Q., Parada, M.A., Barra, F., Mittermayr, F., 2013. Pyrite as a record of hydrothermal fluid evolution in a porphyry

copper system: A SIMS/EMPA trace element study. Geochim. Cosmochim. Acta 104, 42–62.

Revan, M.K., Genç, Y., Maslennikov, V.V., Maslennikova, S.P., Large, R.R., Danyushevsky, L.V., 2014. Mineralogy and trace-element geochemistry of sulfide minerals in hydrothermal chimneys from the Upper-Cretaceous VMS deposits of the eastern Pontide orogenic belt (NE Turkey). Ore Geol. Rev. 63, 129–149.

Schisa, P., Boudreau, A., Djon, L., Tchalikian, A., Corkery, J., 2014. The Lac des Iles palladium deposit, Ontario, Canada. Part II. Halogen variations in apatite. Mineral. Deposita doi:10.1007/s00126-014-0541-4.

Smith, J.W., Holwell, D.A., McDonald, I., 2014. Precious and base metal geochemistry and mineralogy of the Grasvally Norite-Pyroxenite-Anorthosite (GNPA) member, northern Bushveld Complex, South Africa: implications for a multistage emplacement. Mineral. Deposita 49, 667–692.

Somarin, A.K., Kissin, S.A., Heerema, D.D., Bihari, D.J., 2009. Hydrothermal alteration, fluid inclusion and stable isotope studies of the north Roby Zone, Lac des Iles PGE mine, Ontario, Canada. Res. Geol. 59, 107–120.

Stone, D., Lavigne, M.J., Schnieders, B., Scott, J., Wagner, D., 2003. Regional geology of the Lac des Iles Area. Ontario Geological Survey Open File Report 6120, 15-1, 15-25 pp.

Serafimovski, T., Blažev, K., Tasev, G., Pockov, K., 2013. Au-Pd bearing pyrites and chalcopyrites from the Buchim porphyry copper deposit, Eastern Macedonia. In: Mineral deposit research for a high-tech world. Proceedings of the 12th Biennial SGA

Meeting, 12–15 August 2013, Uppsala, Sweden. ISBN 978-91-7403-207-9, 876-879 pp (extended abstract).

Thomas, H. V., Large, R.R., Bull, S.W., Maslennikov, V., Berry, R.F., Fraser, R., Froud, S., Moye, R., 2011. Pyrite and pyrrhotite textures and composition in sediments, laminated quartz veins, and reefs at Bendigo gold mine, Australia: insights for ore genesis. Econ. Geol. 106, 1–31.

Vaughan, D.J., 2006. Sulfide mineralogy and geochemistry: introduction and overview. Rev. Mineral. Geochem. 61, 1–5.

Watkinson, D.H, Lavigne, M.J., Fox, P.E., 2002. Magmatic-hydrothermal Cu and Pd-rich deposits in gabbroic rocks from North America. In: Cabri L.J. (ed) The geology, geochemistry, mineralogy and mineral beneficiation of platinum-group elements. Can. Inst. Min. Metall. 54, pp 299–320.

CHAPITRE 5

SYNTHÈSE ET CONCLUSION

5.1 INTRODUCTION

Ce chapitre synthétise les principales conclusions et les contributions de la thèse. Il est organisé en trois parties. La première parite récapitule les contributions basées sur nos constats et nos interprétations, et présente les éléments de réponse relatifs à la problématique. La seconde partie souligne les implications proposées. Cette partie met l'emphase sur les processus qui ont pu affecter les lentilles riches en sulfures du Lac des Iles et pouvant s'appliquer dans un contexte plus général. Enfin la troisième partie résume les apports de la thèse au débat actuel.

5.2 LENTILLES RICHES EN SULFURES

5.2.1 ÉVIDENCES D'UNE ORIGINE MAGMATIQUE

Les observations pétrographiques suggèrent que les lentilles riches en sulfures se sont formées à partir de liquides sulfurés. La transition de sulfures matriciels à sulfures massifs indique la migration des sulfures à l'état liquide qui se sont concentrés dans des zones de dilatation. La pésence d'un assemblage constitué de pyrrhotite et de pentlandite, avec des textures d'exsolution, évoluant vers un assemblage de chalcopyrite peut être interprétée comme une évidence de cristallisation fractionnée de liquides sulfurés. La prédominance de pyrrhotite et de pentlandite et les faibles proportions de chalcopyrite réprésentent la formation de cumulats de MSS. Cette interprétation est supportée par les analyses

géochimiques roche totale montrant un découplage du Cu à partir du Ni et un fractionnement des EGP. La distribution des EGP et des éléments chalcophile parmis la pyrrhotite, la pentlandite et la chalcopyrite est également consistente avec cette interprétation. Des caractéristiques similaires ont été observées dans des sulfures massifs provenant de gisements magmatiques (e.g., Portimo, Aguablanca, Noril'sk, Sudbury). Par ailleurs, les signatures de la magnétite et de l'ilménite des lentilles riches en sulfures du Lac des Iles sont similaires à celles des gisements de Sudbury et attestent de l'origine magmatique des oxides de Fe-Ti. La possibilité que les oxides de Fe-Ti associés avec les sulfures des lentilles soient un produit d'oxidation des sulfures a été réfutée. Aucune évidence d'origine hydrothermale n'a été identifiée. Cependant, nous avons mis en évidence la modification de l'assemblage magmatique au cours de l'altération.

5.2.2 MODIFICATIONS POST-MAGMATIQUES

Les analyses géochimiques roche totale et LA-ICP-MS montrent que la pyrite n'a pas précipité à partir de fluides mais s'est formé par remplacement de la MSS ou de ses constituents. Les proportions molaires de S et des métaux de bases montrent une tendance de développement de pyrite au détriment de l'assemblage magmatique primaire. La plupart des échantillons n'ont pas eu leur contenu en S modifié comme indiqué par les ratios S/Se et les isotopes du S. Ainsi il a été proposé que la pyrite se soit formée par redistribution du Fe ± Ni de l'assemblage magmatique. Les pyrites contiennent des quantités significatives

d'EGPI, Rh et Co, et leur signature est similaire à celles des pyrrhotites et pentlandites co-existentes. La concentration d'EGPI, Rh et Co qui sont initialement concentrés dans la pyrrhotite et la pentlandite est consistente avec la redistribution de Fe ± Ni à partir de la pyrrhotite vers les silicates intersticiels, possiblement au cours du refroidissement. L'enrichissement en As et Bi des échantillons riches en pyrite et l'observation d'éléments mobiles tels que Sn, Sb, Pb et Ag dans les fractures adjacentes de certaines pyrites impliquent que ces éléments ont été ajoutés aux roches par des fluides. Ces fluides ont pu interagir avec les sulfures et faciliter la redistribution du Fe ± Ni, mais sans remobiliser les EGP.

5.2.3 RELATIONS AVEC LES SULFURES DISSÉMINÉS

Les analyses LA-ICP-MS révélent que les compositions des pyrrhotites et pentlandites des lentilles riches en sulfures sont similaires à celles des sulfures disséminés. Cette observation indique que ces deux types de minéralisation sont dérivées du même magma parent. À l'inverse des lentilles riches en sulfures ayant des compositions de cumulats de MSS, les sulfures disséminés ont des compositions de liquides. Cette interprétation est supportée par les proportions sub-égales de pentlandite et de chalcopyrite, les ratios Ni/Cu proche de l'unité, et des teneurs à 100% sulfures de Pd et Pt plus élevées. Une modélisation numérique utilisant les ratios Pd/Se et Ir/Se des sulfures disséminés et des lentilles riches en

sulfures, montre que les lentilles riches en sulfures ont pu se former par accumulation de MSS à partir des liquides sulfurés qui ont formé les sulfures disséminés.

5.3 IMPLICATIONS

5.3.1 MAGMA PARENT

Les signatures géochimiques de pyrrhotite et de pentlandite des lentilles riches en sulfures du Lac des Iles sont différentes de celles de sulfures dérivés de magmas primitifs qui se trouvent dans les intrusions litées (Bushveld, Stillwater et Great Dykes), dans les intrusions et coulées ultramafiques (Jinchuan et Rosie Nickel prospect) et dans les basaltes en plateau (Noril'sk). En revanche, les signatures sont similaires à celles de sulfures dérivés de magmas évolués tels que ceux de Sudbury et Aguablanca. Ces observations supportent les interprétations de Barnes et Gomwe (2010) qui suggèrent un magma évolué, probablement d'origine andésitique, comme magma parent du Lac des Iles. Notre étude révèle donc que la signature géochimique des sulfures peut fournir des indices sur la nature du magma duquel ils sont dérivés.

5.3.2 RETRAIT DE MSS EN PLUSIEURS ÉTAPES

Les analyses géochimiques roche totale montrent que les lentilles riches en sulfures du Lac des Iles sont non seulement des cumulats de MSS évolués, mais que ceux-ci ont des degrés de fractionnement différents. En effet, des cumulats plus primitifs avec des teneurs en EGPI plus élevées, des teneurs en Pd plus faibles et des anomalies négatives en Pt, et des cumulats plus évolués avec des teneurs en EGPI plus faibles, des teneurs en Pd plus élevées et aucune anomalie négative en Pt ont été identifiés. Cette tendance est bien illustrée par les ratios Pd/Ir et Rh/Pt qui montrent l'évolution du degré de fractionnement des cumulats. Une telle différence de fractionnement peut être expliquée par la formation précoce de cumulats de MSS appauvrissant en EGPI et enrichissant en Pd et Pt les liquides sulfurés. Éventuellement, la formation de cumulats de MSS à partir de liquides sulfurés de plus en plus évolués à pu être répétée.

5.3.3 DIFFUSION D'OXIGÈNE

Les travaux expérimentaux de Fonseca et al. (2008) ont montré que les liquides sulfurés pouvaient contenir des quantités significatives d'oxygène dissout. La diffusion d'oxygène hors du liquide sulfuré au cours de la cristallisation de ce dernier vers le liquide silicaté, pourrait entraîner la formation de magnétite et de chromite proche de la bordure entre les sulfures et le liquide silicaté. Notre étude a montré que ce modèle pouvait aussi s'appliquer à la formation d'ilménite.

5.3.4 PROCESSUS D'EXSOLUTION DE MSS

La distribution des EGP entre la pyrrhotite et la pentlandite a été mise en évidence dans de nombreux gisements de Ni-Cu-EGP. En comparant ces données avec nos propres données sur les lentilles riches en sulfures du Lac des Iles, il a été possible d'établir des caractéristiques générales se produisant au cours des processus d'exsolution de MSS. Il apparaît que les EGPI sont sub-également distribués entre la pyrrhotite et la pentlandite. La pentlandite est aussi largement enrichie en Pd relativement à la pyrrhotite, mais cet enrichissement est plus prononcé dans le cas des gisements d'EGP primaires. À l'inverse, la distribution du Pt entre la pyrrhotite et la pentlandite n'est pas évidente. Il semblerait que la faible proportion de Pt initialement contenue dans la MSS préfère demeurer dans la pyrrhotite dans les gisements où le taux de refroidissement est important. Dans les gisements où le refroidissement a été plus lent, le Pt semble préférer la pentlandite. Le taux de refroidissement apparait donc comme un paramêtre pouvant influencer la distribution du Pt au cours de l'exsolution de la MSS.

De plus, certaines études (Godel and Barnes, 2008; Dare et al., 2010; Chen et al., 2014) suggèrent que certaines phases discrètes (e.g., MGP) peuvent également se former au cours de ces processus d'exsolution. Notre étude apporte des informations supplémentaires à ce sujet. En effet, l'association de MGP de Pd avec des pentlandites présentant des textures d'exsolution et la présence de minéraux de Re et Mo en inclusion dans les pyrrhotites

suggèrent que certains métaux initialement contenu dans la MSS ont pu exsolver pour former des phases discrètes au sein des lentilles riches en sulfures du Lac des Iles.

5.3.5 EFFETS DE LA DEFORMATION

Dans le cas du Lac des Iles où un continuum de déformation est avéré (voir section 2.4.3) notre étude a révélé deux effets majeurs de la déformation sur les sulfures. Premièrement, notre étude montre que la déformation à haute température (stade magmatique) a pu entraîner la migration de liquides sulfurés et leur accumulation dans des zones de dilatations. Deuxièmenent, notre étude montre que la déformation à plus basse température (facies schiste vert) a pu promouvoir la diffusion de certains éléments (e.g., Ag, Bi et Pb) et leur redistribution le long de bordures de grains ou de macles dans les pentlandites et les pyrrhotites (Vukmanovic et al., 2014). Les effets de la déformation mis en évidence dans les lentilles riches en sulfures du Lac des Iles peuvent s'appliquer dans le contexte plus général des systèmes mafiques et ultramafiques.

5.3.6 RE-ÉQUILIBRATION POST-CUMULUS

Le développement de pyrite au sein des lentilles riches en sulfures du Lac des Iles a été interprété comme le résultat de redistribution du Fe ± Ni depuis la MSS ou la pyrrhotite vers les silicates intersticiels. Cette interprétation est similaire à celle proposée par Djon et

Barnes (2012) pour expliquer la présence de pyrite et de milérite au sein des sulfures disséminés. De plus, cette interprétation est consistente avec la possible redistribution du Ni suggérée par Boudreau et al. (2014). Nous montrons en plus que certains éléments, notamment Rh et Co, ont pu incorporer la pyrite par diffusion depuis les pentlandites adjacentes. Ces observations, ainsi que l'observation de zonations concentriques de certains éléments au sein des pyrites, sont semblables à celles de Dare et al. (2011) et Piña et al. (2013) et suggèrent un processus de re-équilibration commun dans les gisements de Ni-Cu-EGP.

5.3.6 EXPLORATION

Les implications pour l'exploration qui résultent de cette thèse sont multiples. Dans le cas du Lac des Iles, il a été montré que les liquides résiduels enrichis en Pd, Pt, Au et semi-métaux ont été séparés des cumulats de MSS et ont pu être relocalisés ailleurs dans la *Mine Block Intrusion*. Les zones où ces liquides riches en Pd, Pt, Au et semi-métaux ont pu être déposés représentent des cibles d'exploration potentielles. La signature géochimique des pentlandites et des pyrites des lentilles riches en sulfures du Lac des Iles en comparaison avec celles provenant d'autres gisements à permis de développer des diagrammes de discrimination. Dans des sédiments issus de l'érosion mécanique tels que les tills où les sulfures peuvent représenter une partie de la fraction dense, ces diagrammes de discrimination pourraient servir à identifier des gisements potentiels.

5.4 APPORTS AU DÉBAT ACTUEL

Notre étude montre que la signature des sulfures du Lac des Iles est similaire à celle des sulfures issus de magmas évolués tels que ceux de Sudbury (magma de composition andésitique) et d'Aguablanca (contexte d'arc continental) et différente de celles de sulfures issus de magmas plus primitifs. Par conséquence, cette thèse supporte un modèle de formation du Lac des Iles ou le magma parent serait un magma évolué de type andésite (Barnes et Gomwe, 2010) mis en place dans un contexte d'arc continental (Brügmann et al., 1997) plutôt qu'un magma plus primitif (Hinchey et al., 2005).

Cette investigation apporte aussi des évidences supplémentaires aux travaux de Hinchey et al. (2005) et Barnes et Gomwe (2011), du rôle minéralisateur des liquides sulfurés au Lac des Iles. De plus, l'étude des lentilles riches en sulfures montre que l'enrichissement en Pd des sulfures a eu lieu avant la cristallisation fractionnée des liquides sulfurés, ce qui implique un enrichissement précoce dans l'histoire du Lac des Iles. De ce fait, le contrôle potentiel de la minéralisation par des fluides hydrothermaux (Watkinson et Dunning, 1979; Talkington et Watkinson, 1984; Macdonald, 1988; Watkinson et al., 2002) n'est pas envisagé. Nous avons montré que l'altération des sulfures a pu entraîner la remobilisation locale des EGP (e.g., EGP dans les pyrites et MGP dans les silicates) tel que suggéré par les travaux de Djon et Barnes (2012), mais n'est en aucun cas à l'origine de l'enrichissement en Pd. Nos conclusions supportent un modèle de redistribution du Fe (Djon et Barnes,

2012) et du Ni (Boudreau et al., 2014), mais ne supportent pas un modèle stipulant que le S, Cu, Pt et Au aient été lessivés par des fluides au facies schiste vert (Boudreau et al., 2014). Notre étude montre plutôt que ces métaux n'ont pas été affectés par l'altération.

Bien que notre étude souligne l'importance du rôle de liquides sulfurés dans la formation de la minéralisation, elle ne nous ne permet pas de nous prononcer sur le rôle potentiel de fluides magmatiques riches en volatiles avant la formation des liquides sulfurés. Les investigations de Hanley et Gladney (2011) et Schisa et al. (2014) ont souligné la présence de tels fluides et leur influence est à préciser.

5.5 RÉFÉRENCES

Barnes, S-J., Gomwe, T.S., (2010) Composition of the Lac des Iles magma and implications for the origin of the ore. In: 11th international platinum symposium, program abstracts, Ontario Geological Survey, miscellaneous release-data 269 (abstract).

Barnes, S-J., Gomwe, T.S., (2011) The Pd Deposits of the Lac des Iles Complex, Northwestern Ontario. Reviews in Economic Geology, 17, 351-370.

Boudreau, A., Djon, L., Tchalikian, A., Corkery, J., (2014) The Lac des Iles palladium deposit, Ontario, Canada. Part I. The effect of variable alteration on the Offset Zone. Mineralium Deposita, 49, 625-654.

Brügmann, G.E., Reischrnann, T., Naldrett, A.J., Sutcliffe, R.H., (1997) Roots of an Archean volcanic arc complex; the Lac des Iles area in Ontario, Canada. Precambrian Research, 81, 223-239.

Chen, L-M., Song, X-Y., Danyushevsky L.V., Wang, Y-S., Tian, Y-L., Xiao, J-F., (2014) A laser ablation ICP-MS study of platinum-group and chalcophile elements in base metal sulfide minerals of the Jinchuan Ni–Cu sulfide deposit, NW China. Ore Geology Reviews, http://dx.doi.org/10.1016/j.oregeorev.2014.07.011

Dare, S.A.S., Barnes, S-J., Prichard, H.M., (2010) The distribution of platinum group elements and other chalcophile elements among sulfides from the Creighton Ni–Cu–PGE sulfide deposit, Sudbury, Canada, and the origin of Pd in pentlandite. Mineralium Deposita, 45, 765-793.

Dare, S.A.S., Barnes, S-J., Prichard, H.M., Fisher, P.C., (2011) Chalcophile and platinum-group element (PGE) concentrations in the sulfide minerals from the McCreedy East deposit, Sudbury, Canada, and the origin of PGE in pyrite. Mineralium Deposita, 46, 381-407.

Djon, M.L.N., Barnes, S-J., (2012) Changes in sulphides and platinum-group minerals with the degree of alteration in the Roby, Twilight, and High Grade Zones of the Lac des Iles Complex, Ontario, Canada. Mineralium Deposita, 47, 875-896.

Fonseca, R.O.C., Campbell, A.H., O'Neill, H.S.C., Fitzgerald, J.D., (2008) Oxygen solubility and speciation in sulphide-rich mattes. Geochimica and Cosmochimica Acta, 72, 2619-2635.

Godel, B., Barnes, S-J., (2008) Platinum-group elements in sulfide minerals and the whole rocks of the J-M Reef (Stillwater Complex): Implication for the formation of the reef. Chemical Geology, 248, 272-294.

Hanley, J.J., Gladney, E.R., (2011) The presence of carbonic-dominant volatiles during the crystallization of sulfide-bearing mafic pegmatites in the North Roby Zone, Lac des Iles Complex, Ontario. Economic Geology, 106, 33-54.

Hinchey, J.G., Hattori, K.H., Lavigne, M.J., (2005) Geology, petrology, and controls on PGE mineralization of the southern Roby and Twilight zones, Lac des Iles mine, Canada. Economic Geology, 100, 43-61.

Macdonald, A.J., (1988) Platinum-group element mineralisation and the relative importance of magmatic and deuteric processes: field evidence from the Lac des Iles deposit, Ontario, Canada. In Geo-Platinum ’87. Edited by Prichard, H.M., Potts, P.J., Bowles, J.F.W., Cribb, S.J. Elsevier, London, 215-236.

Piña, R., Gervilla, F., Barnes, S-J., Ortega, L., Lunar, R., (2013) Platinum-group elements-bearing pyrite from the Aguablanca Ni-Cu sulphide deposit (SW Spain): a LA-ICP-MS study. European Journal of Mineralogy, 25, 241-252.

Schisa, P., Boudreau, A., Djon, L., Tchalikian, A. and Corkery, J. (2014) The Lac des Iles palladium deposit, Ontario, Canada. Part II. Halogen variations in apatite. Mineralium Deposita, doi10.1007/s00126-014-0541-4

Talkington, R.W., Watkinson, D.H., (1984) Trends in the distribution of the precious metals in the Lac des Iles complex, Northwestern Ontario. The Canadian Mineralogist, 22, 125-136.

Vukmanovic, Z., Reddy, S.M., Godel, B., Barnes, S.J., Fiorentini, M.L., Barnes, S-J., Kilburn, M.R., (2014) Relationship between microstructures and grain-scale trace element distribution in komatiite-hosted magmatic sulphide ores. Lithos, 302-303, 42-61.

Watkinson, D.H., Dunning, G.R., (1979) Geology and platinum-group mineralization, Lac des Iles complex, Northwestern Ontario. The Canadian Mineralogist, 17, 453-462.

Watkinson, D.H., Lavigne, M.J., Fox, P.E., (2002) Magmatic-hydrothermal Cu and Pd-rich deposits in gabbroic rocks from North America. In: Cabri L.J. (ed) The geology, geochemistry, mineralogy and mineral beneficiation of platinum-group elements. Canadian Institute of Mining and Metallurgy 54, 299–320.

ANNEXES

ANNEXE 1: COORDONÉES ET DESCRIPTION DES ÉCHANTILLONS

GBNR = gabbronorite

Oxide GBNR = gabbronorite à oxydes

VT rim = varitextured rim

EGAB = east gabbro

n.a. = not available

Po = pyrrhotite

Pn= pentlandite

Ccp = chalcopyrite

Mgt = magnétite

Py = pyrite

Sample	Stratigraphic Unit	Area	Grid	UTM NAD83 easting	UTM NAD83 northing	UTM NAD83 elevation	Sampling	Depth from	Depth to	Sulfide Texture	Assemblage
CD-00150B	Oxide GBNR	Roby Zone	UTM83-16	309925,1097	5449714,235	505,1500	Drill core	283,89	284,54	massive	Po-Pn
CD-09410	VT rim	Offset Zone	UTM83-16	309545,5587	5449561,389	-93,9349	Drill core	130,19	131,12	net-textured	Po-Pn
CD-10739C	EGAB	Offset Zone	UTM83-16	309449,716	5449394,476	-155,3870	Drill core	18,70	19,41	net-textured	Po-Pn
CD-RP012	VT rim	Roby Zone	UTM83-16	n.a.	n.a.	n.a.	Grab sample from open pit	n.a.	n.a.	net-textured	Po-Pn with minor Mgt
CD-00113	EGAB	Roby Zone	UTM83-16	309730,8473	5449557,259	503,2900	Drill core	251,20	252,34	net-textured	Po-Pn with minor Py
CD-00129A	VT rim	Roby Zone	UTM83-16	308922,5574	5449369,365	517,2700	Drill core	220,90	221,33	net-textured	Po-Pn with minor Py
CD-00129C	VT rim	Roby Zone	UTM83-16	308922,5574	5449369,365	517,2700	Drill core	223,00	223,60	net-textured	Po-Pn with minor Py
CD-00139A	Oxide GBNR	Roby Zone	UTM83-16	309904,5610	5449674,807	503,4500	Drill core	324,80	326,01	net-textured	Po-Pn with minor Py
CD-00149	Oxide GBNR	Roby Zone	UTM83-16	309860,4012	5449693,335	503,1700	Drill core	151,70	152,40	net-textured	Po-Pn with minor Py
CD-00150C	Oxide GBNR	Roby Zone	UTM83-16	309925,1097	5449714,235	505,1500	Drill core	284,60	285,27	massive	Po-Pn with minor Py
CD-00256	GBNR	Roby Zone	UTM83-16	309900,9486	5449609,386	501,1800	Drill core	339,77	340,60	net-textured	Po-Pn with minor Py
CD-01083	VT rim	Roby Zone	UTM83-16	309086,1348	5449257,633	502,2800	Drill core	191,83	192,10	massive	Po-Pn with minor Py
CD-02004	Oxide GBNR	Roby Zone	UTM83-16	309905,1841	5449675,239	503,6300	Drill core	360,90	361,20	massive	Po-Pn with minor Py
CD-10603A	EGAB	Offset Zone	UTM83-16	309524,2429	5449583,924	-85,9320	Drill core	20,00	21,62	net-textured	Po-Pn with minor Py
CD-RP009	VT rim	Roby Zone	UTM83-16	n.a.	n.a.	n.a.	Grab sample from open pit	n.a.	n.a.	net-textured	Po-Pn with minor Py
CD-00089	GBNR	Roby Zone	UTM83-16	309872,8040	5449505,155	503,2200	Drill core	192,08	192,20	interconnected patch	Po-Pn with minor Py
CD-01047	VT rim	Offset Zone	UTM83-16	309949,9353	5449657,764	501,1300	Drill core	1069,22	1070,60	interconnected patch	Po-Pn with minor Py
CD-07023A	EGAB	Offset Zone	UTM83-16	309579,4656	5449475,428	90,4600	Drill core	231,00	232,95	interconnected patch	Po-Pn with minor Py
CD-07023B	EGAB	Offset Zone	UTM83-16	309579,4656	5449475,428	90,4600	Drill core	239,60	242,16	interconnected patch	Po-Pn
CD-07028	EGAB	Roby Zone	UTM83-16	309588,4378	5449448,274	90,5600	Drill core	294,90	295,34	interconnected patch	Po-Pn with minor Py
CD-07052	EGAB	Offset Zone	UTM83-16	310040,8726	5449334,744	503,2100	Drill core	1332,56	1333,12	interconnected patch	Po-Pn
CD-10603B	EGAB	Offset Zone	UTM83-16	309524,2429	5449583,924	-85,9320	Drill core	21,70	22,40	interconnected patch	Po-Pn with minor Py
CD-10739A	EGAB	Offset Zone	UTM83-16	309449,7160	5449394,476	-155,3870	Drill core	13,06	13,28	interconnected patch	Po-Pn with minor Py
CD-98041	GBNR	Baker Zone	UTM83-16	310365,1682	5450193,731	526,2700	Drill core	101,80	101,90	net-textured	Po-Pn with minor Py
CD-98042A	GBNR	Baker Zone	UTM83-16	310334,9026	5450151,180	525,8300	Drill core	31,24	31,36	net-textured	Po-Pn
CD-98042B	GBNR	Baker Zone	UTM83-16	310334,9026	5450151,180	525,8300	Drill core	61,50	61,74	net-textured	Po-Pn
CD-BZ001A	GBNR	Baker Zone	UTM83-16	310263,0000	5450248,000	509,0000	Outcrop	surface	n.a.	massive	Po-Pn with minor Py
CD-BZ001B	GBNR	Baker Zone	UTM83-16	310263,0000	5450248,000	509,0000	Outcrop	surface	n.a.	massive	Po-Pn
CD-00134	GBNR	Roby Zone	UTM83-16	309695,3668	5449610,015	504,5500	Drill core	165,89	166,50	net-textured	Ccp
CD-00129B	VT rim	Roby Zone	UTM83-16	308922,5574	5449369,365	517,2700	Drill core	221,70	222,90	net-textured	Ccp
CD-00139B	Oxide GBNR	Roby Zone	UTM83-16	309904,5610	5449674,807	503,4500	Drill core	328,35	328,50	net-textured	Ccp
CD-10739B	EGAB	Offset Zone	UTM83-16	309449,7160	5449394,476	-155,3870	Drill core	13,68	13,80	net-textured	Ccp
CD-BZ001C	GBNR	Baker Zone	UTM83-16	310263,0000	5450248,000	509,0000	Outcrop	surface	n.a.	net-textured	Ccp
CD-00118	VT rim	Roby Zone	UTM83-16	308966,8405	5449351,283	517,6300	Drill core	482,40	482,86	net-textured	Mgt
CD-00129D	VT rim	Roby Zone	UTM83-16	308922,5574	5449369,365	517,2700	Drill core	591,85	592,00	net-textured	Mgt
CD-00150A	Oxide GBNR	Roby Zone	UTM83-16	309925,1097	5449714,235	505,1500	Drill core	283,43	283,77	massive	Mgt
CD-10551	EGAB	Offset Zone	UTM83-16	310221,6028	5449279,756	501,6110	Drill core	1089,70	1089,90	massive	Mgt
CD-00109	VT rim	Roby Zone	UTM83-16	309012,0420	5449333,134	516,7700	Drill core	163,37	163,47	net-textured	Py
CD-11054	VT rim	Roby Zone	UTM83-16	309885,0603	5449245,899	502,6280	Drill core	194,33	195,08	net-textured	Py
CD-RP008	VT rim	Roby Zone	UTM83-16	n.a.	n.a.	n.a.	Grab sample from open pit	n.a.	n.a.	net-textured	Py
CD-RP010	VT rim	Roby Zone	UTM83-16	n.a.	n.a.	n.a.	Grab sample from open pit	n.a.	n.a.	net-textured	Py
CD-BZ006	GBNR	Baker Zone	UTM83-16	310365,0000	5450302,000	517,0000	Outcrop	surface	na	net-textured	Py
CD-BZ007	GBNR	Baker Zone	UTM83-16	310280,0000	5450296,000	516,0000	Outcrop	surface	na	massive	Py

ANNEXE 2: GÉOCHIMIE ROCHE TOTALE

Sample	Ag (ppm)	Al (%)	As (ppm)	Au (ppb)	Ba (ppm)	Bi (ppm)	Ca (%)	Cd (ppm)	Co (ppm)	Cr (ppm)	Cs (ppm)	Cu (%)	Fe (%)	Hg (ppm)	Ir (ppb)	Li (ppm)	Mo (ppm)	Na (%)	Mg (%)
CD-00150B	2,07	1,07	1,8	54,40	4,4	1,42	0,88	0,11	1581,47	70,95	0,40	0,26	42,88	0,01	3,92	0,32	0,96	0,02	2,15
CD-09410	0,61	5,32	1,4	152,39	7	1,52	4,88	0,09	753,48	72,16	0,48	0,13	21,73	0,01	7,57	7,07	0,54	0,44	3,42
CD-10739C	1,83	4,03	0,8	156,70	8,6	1,27	4,28	0,14	835,91	39,33	1,48	0,43	18,24	0,01	3,71	3,08	0,45	0,77	3,66
CD-RP012	0,84	4,09	4,8	93,52	7,5	0,14	3,93	0,07	698,72	110,88	0,31	0,32	27,38	<0,01	7,80	1,74	1,18	0,38	3,07
CD-00113	4,85	4,51	1	179,23	2,4	1,77	4,26	0,36	901,51	73,51	0,32	1,27	23,27	0,01	18,59	8,52	0,61	0,96	2,66
CD-00129A	1,67	1,14	2,1	2847,36	4,2	4,2	1,58	0,05	1639,80	122,35	0,28	0,16	31,99	0,01	9,33	1,87	2,14	0,00	4,75
CD-00129C	2,81	3,64	1,4	24,88	8,2	1,53	3,24	0,16	936,45	230,70	0,35	0,57	21,90	0,01	33,19	3,18	1,07	0,00	6,24
CD-00139A	2,29	4,47	<0,8	30,19	3,3	0,82	4,34	0,17	517,40	64,99	0,40	0,79	22,35	<0,01	16,02	1,61	0,44	1,08	3,47
CD-00149	5,10	5,33	1,7	2119,92	10,4	2,14	4,05	0,43	809,57	71,45	1,31	1,11	20,61	0,01	6,05	8,20	0,83	0,27	3,45
CD-00150C	4,36	2,95	1,5	60,84	8,6	0,98	3,56	0,50	582,77	159,08	0,80	1,51	22,29	0,01	35,76	0,70	0,31	0,59	6,21
CD-00256	3,39	2,43	5,7	19,65	0,9	1,38	3,04	0,39	950,86	116,89	0,29	1,40	26,06	0,01	71,75	1,56	0,73	0,08	4,93
CD-01083	3,01	2,42	1,6	90,19	3,3	1,33	3,67	0,11	1134,45	130,68	0,18	0,37	32,05	0,01	0,36	2,00	0,93	0,71	3,23
CD-02004	3,70	1,38	1,3	205,46	1	1,06	1,13	4,77	961,32	138,23	0,20	0,55	32,77	0,01	1,01	0,08	0,71	0,05	4,70
CD-10603A	3,16	6,05	2,7	339,37	8,2	1,92	4,75	0,38	698,35	51,13	0,80	0,61	18,80	0,01	1,26	10,49	0,59	0,14	3,07
CD-RP009	4,04	5,89	1,2	246,99	34	0,61	4,25	0,36	508,39	67,35	8,97	0,90	20,84	0,01	4,14	12,05	1,01	0,41	2,84
CD-00089	14,54	6,15	2,7	350,10	5,7	0,34	4,58	6,10	264,21	189,86	0,96	0,87	16,57	0,01	10,30	9,09	0,51	0,05	5,23
CD-01047	2,08	8,37	<0,8	230,46	23,4	3,04	6,15	0,24	312,82	67,62	3,32	0,24	11,48	<0,01	0,20	6,72	0,17	0,59	3,63
CD-07023A	2,24	7,70	1,1	38,81	14,9	0,48	6,34	0,34	196,79	83,86	1,64	0,59	10,89	0,01	6,42	7,49	0,15	0,21	4,26
CD-07023B	2,12	7,61	<0,8	13,15	21,1	0,71	6,86	0,31	251,43	53,68	2,11	0,51	12,69	0,01	102,87	7,77	0,23	2,46	3,99
CD-07028	3,64	2,25	2,1	17,30	2,4	1,64	3,90	0,67	541,34	375,08	1,43	0,58	19,14	0,01	8,00	2,03	0,66	0,28	8,45
CD-07052	2,27	4,46	<0,8	140,00	8,2	2,37	5,88	0,26	394,82	67,01	2,11	0,34	18,63	0,01	28,91	4,66	0,19	1,94	4,71
CD-10603B	2,33	7,91	<0,8	9,67	14,4	1,04	6,62	0,52	236,95	33,99	1,26	0,53	10,28	<0,01	0,99	9,33	0,37	3,28	3,82
CD-10739A	5,31	5,99	<0,8	3090,05	8,7	0,55	5,59	0,48	270,22	92,26	2,13	1,47	11,98	0,01	10,62	9,46	0,16	0,29	5,13
CD-98041	2,73	5,36	0,9	149,10	14	1,22	3,23	0,04	1017,85	72,97	0,72	0,22	25,11	0,01	9,26	9,19	4,33	1,65	2,88
CD-98042A	1,67	2,24	6	88,60	0,9	0,61	3,14	0,04	847,73	257,72	0,18	0,37	22,64	0,01	0,13	1,98	0,42	0,37	7,13
CD-98042B	1,55	5,99	2,9	29,50	12,5	0,49	5,08	0,11	756,55	63,62	0,22	0,32	20,22	0,01	6,00	7,82	0,74	2,70	2,49
CD-BZ001A	2,28	0,43	1,4	3,11	0,4	2,67	0,14	0,10	1872,73	32,45	0,04	0,21	43,97	<0,01	34,15	1,91	0,97	0,06	0,27
CD-BZ001B	2,22	0,34	1,5	1,81	0,9	3,05	0,11	0,07	2071,86	42,24	0,03	0,23	44,37	<0,01	32,58	1,19	0,70	0,01	0,14
CD-00134	4,87	5,76	5,3	64,23	2	0,7	3,67	0,61	512,26	193,68	0,41	1,72	18,18	0,01	6,20	11,01	0,33	0,05	4,46
CD-00129B	33,34	0,88	<0,8	93,64	1,3	4,14	1,63	1,53	401,48	135,53	0,10	9,46	18,15	0,01	29,90	0,90	0,87	0,13	6,05
CD-00139B	17,86	2,70	<0,8	9,93	1,7	1,08	5,17	1,87	218,67	137,59	0,24	8,87	18,97	0,01	23,69	1,08	0,38	0,24	4,75
CD-10739B	28,09	2,70	1,4	182,98	2,8	1,14	5,17	4,25	115,17	59,11	1,03	12,49	18,24	0,02	5,46	4,42	0,30	0,40	4,75
CD-BZ001C	33,82	5,83	<0,8	228,92	5,6	1,4	3,25	5,06	374,24	73,44	0,32	4,68	16,80	<0,01	10,44	24,30	0,21	1,84	3,54
CD-00118	5,67	5,57	1,8	302,33	6,6	3,89	5,62	0,30	1056,11	74,82	1,40	1,02	21,04	<0,01	11,60	7,02	21,42	0,23	2,78
CD-00129D	10,19	2,98	1,2	434,35	19,9	6,12	4,68	1,81	762,63	10,32	5,20	2,75	19,68	0,01	29,84	4,39	0,47	0,49	2,33
CD-00150A	2,64	1,45	1,8	77,67	3,9	2,32	1,81	0,13	1379,27	125,41	0,25	0,31	38,43	0,01	124,72	0,45	0,75	0,33	2,89
CD-10551	1,60	1,19	1,4	118,80	12,7	4,78	0,70	0,03	1276,78	26,37	1,45	0,11	52,77	<0,01	0,78	1,23	0,52	0,27	0,72
CD-00109	3,64	2,95	2,6	37,79	25,1	3,72	2,49	0,04	2552,24	14,13	3,98	0,19	33,71	<0,01	26,29	6,35	12,02	0,18	0,86
CD-11054	3,17	2,17	30,2	300,50	0,4	11,8	2,33	0,08	941,72	101,47	0,09	0,26	27,87	0,05	12,03	10,61	0,62	0,01	3,26
CD-RP008	6,47	3,24	10,1	55,32	40,3	3,25	2,63	0,02	1566,66	57,32	8,19	0,07	29,81	<0,01	23,07	9,43	4,19	0,33	2,06
CD-RP010	3,61	2,15	23,6	76,62	0,7	0,93	0,94	0,09	1615,17	69,88	0,27	0,07	32,22	0,01	27,05	5,22	1,43	0,10	2,17
CD-BZ006	0,31	0,12	12,3	273,56	0,7	2,15	0,15	0,02	381,68	8,55	<0,023	0,06	23,63	<0,01	0,02	0,61	0,10	0,00	0,40
CD-BZ007	1,35	1,55	72,4	158,21	2,5	50	1,95	0,09	1681,27	69,43	0,11	0,03	33,59	<0,01	12,96	2,13	8,32	0,02	1,64

Sample	Mn (ppm)	Ni (%)	Os (ppb)	Pb (ppm)	Pd (ppb)	Pt (ppb)	Rb (ppm)	Rh (ppb)	Ru (ppb)	S (%)	Sb (ppm)	Sc (ppm)	Se (ppm)	Sn (ppm)	Ti (ppm)	Te (ppm)	Tl (ppm)	V (ppm)	Zn (ppm)	δ34S
CD-00150B	837,96	5,18	6,22	1,10	13445,39	687,80	0,71	32,90	14,99	28,71	<0,06	11,82	121,35	0,06	1303,32	16,13	0,88	158,46	22,23	0,26
CD-09410	780,65	1,51	4,62	4,90	2171,56	215,24	0,54	22,05	9,46	12,61	<0,06	32,76	25,89	0,07	1327,71	3,42	0,67	205,51	14,15	-0,06
CD-10739C	861,19	2,91	5,61	1,60	17978,84	1894,13	1,57	22,89	11,43	14,10	<0,06	31,71	62,91	<0,04	910,61	6,08	0,27	124,29	22,89	0,00
CD-RP012	1016,85	1,19	9,93	1,70	49224,29	10773,42	0,36	54,60	27,83	14,71	<0,06	31,19	36,57	0,12	5633,19	2,82	0,65	721,11	34,67	0,63
CD-00113	892,94	2,83	30,65	3,70	31161,37	873,49	0,23	121,63	80,81	15,28	<0,06	28,49	57,62	<0,04	3,00	3,18	1,67	288,12	62,56	-0,25
CD-00129A	1095,07	6,60	14,69	5,40	67612,06	1343,63	0,50	102,19	28,97	22,04	<0,06	18,67	123,26	0,12	954,07	10,55	0,81	85,88	16,41	-0,16
CD-00129C	1184,14	3,80	13,59	1,70	4361,40	182,57	0,73	60,53	31,80	13,79	<0,06	27,33	74,61	0,07	1423,66	10,18	0,43	145,12	35,24	-0,13
CD-00139A	1222,86	1,98	6,27	5,30	10707,90	5501,62	0,28	86,83	14,54	11,54	<0,06	43,68	49,20	0,06	3294,73	7,13	0,84	341,18	49,52	-0,06
CD-00149	988,97	2,41	2,73	8,30	4321,84	2205,57	2,42	33,10	4,54	11,41	<0,06	32,52	43,32	0,06	2716,55	5,54	2,38	329,87	74,17	0,18
CD-00150C	1400,98	1,55	81,25	0,90	35275,81	410,60	0,88	163,95	177,54	10,75	<0,06	40,82	53,08	0,10	2115,80	10,69	0,57	206,42	123,57	0,15
CD-00256	977,36	3,03	22,53	1,60	2443,29	119,79	0,22	222,16	54,54	16,07	<0,06	36,27	68,52	0,07	1128,90	7,18	1,37	174,09	77,74	-0,02
CD-01083	480,93	5,45	<0,065	4,70	1759,92	203,36	0,23	3,03	0,56	21,46	<0,06	23,34	130,40	0,04	650,66	10,09	1,42	83,02	16,38	-0,20
CD-02004	1294,88	3,40	<0,065	1,70	2210,06	188,09	0,29	12,89	2,47	19,90	<0,06	22,76	71,26	0,14	752,32	5,03	1,64	150,40	432,89	-0,03
CD-10603A	857,32	2,06	<0,065	2,10	4753,96	1244,50	1,35	10,88	0,69	10,81	<0,06	35,09	49,10	0,06	934,45	9,61	0,44	139,53	49,58	0,15
CD-RP009	893,72	3,04	5,41	7,30	26712,18	1267,10	13,43	39,63	12,70	12,04	<0,06	21,17	70,83	0,04	4960,02	8,56	2,25	402,27	92,78	-0,35
CD-00089	1389,36	0,85	18,85	133,20	30350,09	1949,19	0,76	73,27	39,30	5,28	0,06	28,73	27,82	0,04	1591,45	1,56	2,20	242,42	239,9	-0,47
CD-01047	917,72	1,47	<0,065	0,90	1603,82	258,20	3,47	1,45	0,23	5,80	<0,06	25,27	36,85	0,08	1151,91	5,09	0,30	134,71	30,96	0,03
CD-07023A	1199,62	0,49	<0,065	1,30	1823,35	791,95	2,13	43,04	4,22	3,20	<0,06	35,52	19,50	0,05	1305,31	3,45	0,09	197,19	53,4	0,08
CD-07023B	1194,20	0,72	50,73	0,90	540,10	27,95	2,88	200,31	100,51	4,12	0,06	38,78	20,70	0,07	2267,24	2,64	0,16	245,56	47,56	-0,12
CD-07028	1819,96	1,34	2,42	0,90	21283,04	1934,19	1,06	40,10	16,99	8,71	<0,06	44,25	40,75	<0,04	1047,68	2,42	0,30	197,47	87,74	0,02
CD-07052	1443,58	1,11	18,45	0,80	4694,22	391,72	1,42	72,98	33,57	8,00	<0,06	47,24	29,90	<0,04	2473,68	5,20	0,31	357,06	31,42	-0,02
CD-10603B	1097,40	0,68	0,65	1,90	3913,51	114,26	2,02	12,65	1,66	4,06	<0,06	40,83	18,81	0,09	998,64	4,67	0,16	173,45	52,05	-0,14
CD-10739A	1252,29	0,75	23,99	1,70	43501,20	699,76	2,34	133,38	52,36	4,92	<0,06	44,45	25,70	<0,04	1750,18	3,71	0,17	205,56	90,12	-0,03
CD-98041	865,06	2,08	11,78	7,80	5233,54	534,25	1,17	109,69	45,06	15,91	<0,06	18,29	66,05	<0,04	1221,05	11,06	2,58	113,67	19,73	0,40
CD-98042A	1755,68	1,31	<0,065	2,20	34074,50	259,17	0,15	9,33	1,36	12,29	<0,06	39,24	30,74	0,04	2912,27	4,37	1,38	312,69	19,3	0,25
CD-98042B	697,01	2,19	1,97	7,40	2174,52	178,39	0,47	40,96	2,57	14,35	<0,06	24,04	41,10	<0,04	1635,13	3,81	2,98	176,51	29,74	0,22
CD-BZ001A	138,63	4,49	66,50	7,60	4924,32	30,40	<0,15	86,45	137,40	38,21	<0,06	2,15	66,53	<0,04	92,06	1,58	6,52	20,80	10,87	0,61
CD-BZ001B	109,97	4,71	59,69	7,20	5512,72	46,85	<0,15	129,79	127,09	37,67	<0,06	1,88	77,90	0,04	250,07	1,93	6,14	25,33	8,56	0,50
CD-00134	971,94	1,13	1,80	6,00	3810,52	847,92	0,38	58,04	3,67	9,60	<0,06	31,74	34,35	<0,04	1498,53	6,04	0,71	275,77	93,46	-0,20
CD-00129B	1425,76	2,56	10,01	2,50	2251,50	314,83	0,21	134,13	25,34	17,37	<0,06	21,54	83,16	0,05	1977,14	12,89	0,48	135,77	231,46	0,34
CD-00139B	1345,22	0,08	8,92	7,90	9111,00	915,25	0,24	126,09	18,03	12,21	<0,06	51,54	46,38	0,06	3183,42	6,89	0,33	340,58	323,61	0,24
CD-10739B	1345,22	0,31	7,96	2,50	10968,08	651,28	0,87	19,43	19,43	13,77	<0,06	28,38	66,54	0,05	3183,42	10,02	0,34	340,58	567,86	-0,05
CD-BZ001C	810,08	0,71	19,43	6,90	1937,79	8,55	0,79	41,19	43,88	11,77	<0,06	22,14	15,94	0,06	775,55	0,56	2,73	72,24	389,67	0,38
CD-00118	1064,87	3,04	20,25	8,30	33728,17	1454,39	1,18	86,17	49,24	12,01	0,07	30,22	66,62	0,07	7138,53	10,68	1,38	824,03	62,45	-0,21
CD-00129D	1036,99	6,22	12,15	3,10	3021,16	384,79	4,76	92,56	40,06	17,18	<0,06	26,54	63,07	0,19	9649,68	7,22	2,10	1001,92	271,17	-0,21
CD-00150A	834,08	4,20	54,58	2,20	8786,84	440,14	0,60	310,62	139,31	23,90	<0,06	18,94	129,00	0,06	1096,08	24,31	1,17	108,68	26,02	0,15
CD-10551	315,20	3,86	0,31	2,80	2147,26	355,53	3,09	6,27	1,04	18,74	<0,06	4,42	49,50	0,07	1042,53	9,43	0,65	444,02	8,82	-0,38
CD-00109	603,30	6,55	45,85	13,10	67803,58	2336,54	3,15	124,33	100,30	26,63	0,12	15,79	121,06	0,07	7919,52	17,19	5,64	628,40	11,09	-0,48
CD-11054	639,70	3,59	23,01	6,20	9010,68	188,54	<0,15	51,54	54,34	28,44	1,52	20,29	86,34	0,04	664,39	8,96	0,08	88,65	28,97	0,32
CD-RP008	841,05	2,53	54,45	16,80	26849,17	1657,96	10,14	125,01	134,10	22,24	<0,06	24,11	118,35	0,15	8119,39	10,64	0,86	630,95	30,64	0,23
CD-RP010	358,57	4,63	45,88	14,10	24677,87	594,65	0,21	232,28	98,42	32,44	<0,06	10,23	131,73	0,04	2232,18	6,34	6,62	205,19	29,65	0,36
CD-BZ006	77,45	0,04	<0,065	5,70	596,08	22,97	<0,15	0,18	0,04	25,22	<0,06	15,68	25,05	0,08	173,22	0,85	0,06	4,93	6,71	1,26
CD-BZ007	515,78	0,25	16,86	8,00	7609,42	453,28	0,27	48,98	37,02	39,59	<0,06	15,85	34,58	0,09	3047,39	62,75	0,87	79,44	8,27	1,49

ANNEXE 3: MATÉRIAUX DE RÉFÉRENCE POUR LES ANALYSES ROCHE TOTALE

n.a. = not available

Reference material		Ag (ppm)	Al (%)	As (ppm)	Au (ppb)	Ba (ppm)	Bi (ppm)	Ca (%)	Cd (ppm)	Co (ppm)	Cr (ppm)	Cs (ppm)	Cu (%)	Fe (%)
WMS-1a	This study	2,94	1,32	28,90	238,18	15,60	0,99	2,96	1,29	1353,31	78,24	0,49	1,35	43,46
	Working values	3,7 ± 0,5	1,35 ± 0,051	30,9 ± 2,9	300 ± 18	n.a.	n.a.	3,09 ± 0,11	n.a.	1450 ± 80	68 ± 10	n.a.	1,396 ± 0,021	45,4 ± 1,2
KPT-1	This study	0,71	14,28	1,90	n.a.	330,80	0,72	6,64	0,36	76,56	140,12	4,16	0,11	12,27
	Working values	0,75 ± 0,15	14,41 ± 0,39	2,2 ± 0,53	n.a.	465,27 ± 29,53	0,95 ± 0,15	6,89 ± 0,21	0,43 ± 0,09	78,92 ± 5,6	152,24 ± 11,43	4,42 ± 0,57	0,111 ± 0,010	12,24 ± 0,34

Reference material		Hg (ppm)	Ir (ppb)	Li (ppm)	Mo (ppm)	Na (%)	Mg (%)	Mn (ppm)	Ni (%)	Os (ppb)	Pb (ppm)	Pd (ppb)	Pt (ppb)	Rb (ppm)
WMS-1a	This study	0,26	328,09	1,24	2,17	0,02	0,25	669,90	3,54	145,91	15,60	1440,60	1875,91	1,21
	Working values	n.a.	322 ± 19	n.a.	n.a.	0,0329 ± 0,0065	0,331 ± 0,022	600 ± 70	3,02 ± 0,07	150,00	n.a.	1450 ± 50	1910 ± 50	na
KPT-1	This study	0,01	n.a.	32,59	1,26	2,71	3,98	1445,00	0,12	n.a.	72,20	n.a.	n.a.	55,97
	Working values	n.a.	n.a.	35,1 ± 3,29	1,7 ± 0,28	2,61 ± 0,09	4,3 ± 0,14	1430 ± 100	0,101 ± 0,007	n.a.	81,07 ± 6,69	n.a.	n.a.	61,45 ± 5,29

Reference material		Rh (ppb)	Ru (ppb)	S (%)	Sb (ppm)	Sc (ppm)	Se (ppm)	Sn (ppm)	Ti (ppm)	Te (ppm)	Tl (ppm)	V (ppm)	Zn (ppm)
WMS-1a	This study	245,97	144,15	27,80	6,74	3,54	99,63	1,36	814,23	4,00	0,18	132,15	118,84
	Working values	222 ± 38	145 ± 7	28,17 ± 0,69	6,92 ± 0,96	n.a.	n.a.	n.a.	840 ± 80	n.a.	n.a.	140 ± 21	130 ± 8
KPT-1	This study	n.a.	n.a.	n.a.	10,00	24,82	3,59	18,14	5169,52	0,41	0,53	216,08	77,95
	Working values	n.a.	n.a.	n.a.	10,01 ± 1,13	24,84 ± 2,45	2,93 ± 0,4	19,13 ± 1,96	9000 ± 400	0,35 ± 0,09	0,54 ± 0,09	197,22 ± 14,24	120,24 ± 9,35

ANNEXE 4: ANALYSES ROCHE TOTALE DU SE DES SULFURES DISSÉMINÉS

Sample	Se (ppb)
TZ-01	6144,6
TZ-30	2481,9
TZ-21	8360,2
TZ-41	198,3
TZ-42	675,4
RZ-44=200N 310 EST	2771,8
RZ-42=180N 270 EST	2184,8
TZ-07	1968,2
R2-50	2843,1
RZ-54	317,4
RZ-35=265N 240EST	496,3
TZ-04	1723,4
RZ45=135N 360 EST	10251,7
RZ-26	511,6
TZ-26	701,1
TZ-40	65,8
RZ-16=99-105 492.3-494	977,1
RZ-09=99-96 637-639	176,1

Reference material		Se (ppb)
MRG-1	This study	201,2
	Working value	199

ANNEXE 5: ANALYSES MICROSONDE DE PYRRHOTITES

Element		S	Mn	Fe	Ni	Co	Zn	Cu	As	Total	S	Mn	Fe	Ni	Co	Zn	Cu	As
		wt.%	wt.%	wt.%	wt.%	wt.%	wt.%	wt.%	wt.%		at.%	at.%	at.%	at.%	at.%	at.%	at.%	at.%
CD-10551	1	39,7	bdl	59,5	0,952	0,016	bdl	0,153	bdl	100	53,3	bdl	45,9	0,699	0,012	bdl	0,104	bdl
	2	39,9	bdl	59,7	1,02	0,046	0,160	0,034	0,036	101	53,3	bdl	45,8	0,741	0,033	0,105	0,023	0,021
	3	39,7	bdl	59,6	0,975	bdl	bdl	bdl	bdl	100	53,3	bdl	45,9	0,715	bdl	bdl	bdl	bdl
CD-00150A	1	39,7	0,005	59,5	0,831	bdl	0,101	0,024	0,007	100	53,4	0,004	45,9	0,610	bdl	0,066	0,016	0,004
	2	39,9	0,010	59,5	0,946	0,013	bdl	0,143	0,005	101	53,4	0,008	45,8	0,692	0,010	bdl	0,097	0,003
	3	39,9	0,008	59,6	0,610	0,088	0,041	0,065	0,035	100	53,5	0,006	45,9	0,447	0,064	0,027	0,044	0,020
CD-02004	1	39,8	bdl	59,7	0,889	0,047	0,041	bdl	0,020	100	53,3	bdl	46,0	0,651	0,034	0,027	bdl	0,011
	2	39,6	bdl	59,6	0,859	bdl	bdl	bdl	bdl	100	53,3	bdl	46,0	0,631	bdl	bdl	bdl	bdl
	3	39,7	bdl	59,5	0,786	0,041	0,055	bdl	0,022	100	53,4	bdl	46,0	0,578	0,030	0,036	bdl	0,013
	4	39,6	bdl	60,0	0,756	0,073	bdl	0,034	0,035	100	53,2	bdl	46,2	0,554	0,054	bdl	0,023	0,020
	5	39,7	bdl	59,7	0,801	bdl	0,101	0,014	0,026	100	53,3	bdl	46,0	0,587	bdl	0,066	0,009	0,015
CD-98042A	1	39,7	0,010	59,5	0,695	0,012	0,023	bdl	0,010	100	53,5	0,008	46,0	0,511	0,009	0,015	bdl	0,006
	2	39,9	0,001	59,5	0,771	0,014	bdl	bdl	0,036	100	53,5	0,001	45,9	0,566	0,010	bdl	bdl	0,021
	3	39,6	bdl	59,3	0,770	0,054	0,004	0,075	bdl	100	53,4	bdl	45,9	0,567	0,039	0,003	0,051	bdl
	4	39,7	bdl	59,4	0,713	0,005	0,019	0,037	bdl	100	53,5	bdl	46,0	0,524	0,004	0,012	0,025	bdl
	5	39,6	bdl	59,3	0,754	bdl	0,137	0,061	0,013	100	53,4	bdl	45,9	0,555	bdl	0,091	0,042	0,007
CD-00150C	1	39,9	bdl	59,4	0,863	0,036	0,050	0,126	0,013	100	53,5	bdl	45,7	0,632	0,026	0,033	0,085	0,007
	2	39,3	bdl	58,9	0,772	0,030	0,114	0,068	0,012	99,2	53,4	bdl	45,9	0,572	0,022	0,076	0,047	0,007
	3	39,5	bdl	59,1	0,848	bdl	bdl	bdl	0,030	100	53,5	bdl	45,9	0,626	bdl	bdl	bdl	0,018
CD-RP012	1	39,5	0,021	59,0	0,775	0,031	bdl	0,116	0,010	99,5	53,4	0,016	45,9	0,573	0,022	bdl	0,079	0,006
	2	39,7	bdl	59,1	0,790	0,060	0,092	0,112	0,036	100	53,5	bdl	45,7	0,581	0,044	0,061	0,076	0,021
CD-00109	1	39,5	0,010	58,5	1,12	0,052	0,078	bdl	0,007	99,3	53,6	0,008	45,5	0,829	0,038	0,052	bdl	0,004
	2	39,7	0,012	59,2	0,680	bdl	bdl	0,078	0,035	100	53,5	0,009	45,9	0,501	bdl	bdl	0,053	0,020
	3	39,7	bdl	59,3	0,682	0,035	bdl	0,048	bdl	100	53,5	bdl	45,9	0,502	0,025	bdl	0,032	bdl

Pour les annexes 5 à 10

bdl = below detection limit

ANNEXE 6: ANALYSES MICROSONDE DE PENTLANDITES

Element		S	Mn	Fe	Ni	Co	Zn	Cu	As	Total	S	Mn	Fe	Ni	Co	Zn	Cu	As
		wt.%	wt.%	wt.%	wt.%	wt.%	wt.%	wt.%	wt.%		at.%	at.%	at.%	at.%	at.%	at.%	at.%	at.%
CD-10551	1	33,1	bdl	29,2	37,4	1,08	0,073	0,153	0,037	101	46,7	bdl	23,6	28,7	0,829	0,051	0,109	0,023
	2	33,3	bdl	29,0	37,9	0,927	bdl	0,083	0,055	101	46,7	bdl	23,4	29,1	0,708	bdl	0,059	0,033
	3	33,2	0,003	29,1	37,7	1,14	bdl	bdl	0,035	101	46,7	0,002	23,5	28,9	0,875	bdl	bdl	0,021
CD-00150A	1	33,4	bdl	28,5	38,8	0,692	bdl	bdl	0,011	101	46,8	bdl	22,9	29,7	0,528	bdl	bdl	0,007
	2	33,3	bdl	28,4	38,7	0,839	0,036	bdl	0,017	101	46,8	bdl	22,9	29,7	0,640	0,025	bdl	0,010
CD-02004	1	33,3	bdl	28,8	38,8	0,539	0,068	bdl	bdl	101	46,7	bdl	23,2	29,7	0,411	0,047	bdl	bdl
	2	33,1	bdl	28,9	39,0	0,519	bdl	bdl	bdl	102	46,4	bdl	23,3	29,9	0,396	bdl	bdl	bdl
	3	33,0	bdl	28,9	38,6	0,427	0,051	0,027	bdl	101	46,5	bdl	23,4	29,7	0,328	0,035	0,019	bdl
	4	33,4	bdl	28,6	38,8	0,481	bdl	bdl	0,041	101	46,9	bdl	23,0	29,7	0,367	bdl	bdl	0,024
	5	33,2	bdl	28,9	38,6	0,612	bdl	bdl	bdl	101	46,6	bdl	23,3	29,6	0,468	bdl	bdl	bdl
CD-98042A	1	33,1	bdl	28,6	36,7	2,31	bdl	bdl	0,003	101	46,8	bdl	23,2	28,3	1,77	bdl	bdl	0,002
	2	33,2	bdl	28,8	36,9	2,13	0,119	0,027	0,020	101	46,7	bdl	23,2	28,4	1,63	0,082	0,019	0,012
	3	33,3	bdl	28,5	36,5	2,47	0,073	bdl	0,022	101	46,9	bdl	23,1	28,1	1,89	0,051	bdl	0,013
	4	33,3	bdl	28,3	36,8	2,17	bdl	bdl	0,034	101	47,0	bdl	22,9	28,4	1,66	bdl	bdl	0,021
	5	33,1	0,029	28,7	36,6	2,17	bdl	bdl	0,040	101	46,8	0,024	23,3	28,2	1,67	bdl	bdl	0,024
	6	33,3	bdl	28,8	36,6	2,14	bdl	bdl	0,036	101	46,9	bdl	23,3	28,2	1,64	bdl	bdl	0,022
CD-00150C	1	32,9	0,002	28,6	38,1	1,04	bdl	bdl	bdl	101	46,6	0,002	23,2	29,4	0,797	bdl	bdl	bdl
	2	33,4	bdl	29,0	37,8	0,988	0,119	bdl	0,036	101	46,8	bdl	23,4	29,0	0,754	0,082	bdl	0,022
	3	33,2	bdl	28,6	37,7	0,999	bdl	bdl	0,004	100	46,9	bdl	23,2	29,1	0,769	bdl	bdl	0,002
	4	33,2	0,018	28,5	37,8	1,19	bdl	bdl	bdl	101	46,8	0,015	23,1	29,1	0,913	bdl	bdl	bdl
CD-RP012	1	33,1	bdl	29,2	37,5	0,709	bdl	0,060	0,032	101	46,8	bdl	23,7	28,9	0,545	bdl	0,043	0,020
	2	32,9	0,006	28,8	37,5	0,820	bdl	0,063	0,036	100	46,8	0,005	23,5	29,1	0,633	bdl	0,045	0,022
CD-00109	1	33,1	bdl	29,5	37,9	0,180	0,133	bdl	0,018	101	46,7	bdl	23,9	29,2	0,138	0,092	bdl	0,011
	2	32,9	0,005	29,7	37,8	0,076	0,128	bdl	0,009	101	46,6	0,004	24,1	29,2	0,058	0,089	bdl	0,005
CD-RP008	1	32,9	0,008	25,5	42,2	0,029	0,023	bdl	bdl	101	46,6	0,006	20,8	32,6	0,023	0,016	bdl	bdl
	2	32,9	bdl	24,9	42,3	0,013	0,169	bdl	0,003	100	46,8	bdl	20,3	32,8	0,010	0,118	bdl	0,002

ANNEXE 7: ANALYSES MICROSONDE DE CHALCOPYRITES

Element		S	Mn	Fe	Ni	Co	Zn	Cu	As	Total	S	Mn	Fe	Ni	Co	Zn	Cu	As
		wt.%	wt.%	wt.%	wt.%	wt.%	wt.%	wt.%	wt.%		at.%	at.%	at.%	at.%	at.%	at.%	at.%	at.%
CD-10551	1	34,8	0,003	30,7	0,026	0,063	0,151	33,9	0,014	99,7	50,0	0,003	25,3	0,021	0,049	0,106	24,5	0,009
	2	34,7	bdl	30,7	bdl	bdl	bdl	34,6	0,012	100	49,7	bdl	25,3	bdl	bdl	bdl	25,0	0,007
	3	34,7	0,008	30,8	bdl	bdl	bdl	33,4	0,029	98,9	50,1	0,007	25,5	bdl	bdl	bdl	24,3	0,018
CD-98042A	1	34,9	bdl	30,8	bdl	0,004	bdl	32,5	0,007	98,3	50,6	bdl	25,6	bdl	0,003	bdl	23,8	0,004
	2	34,7	bdl	30,5	0,049	0,078	0,004	33,9	bdl	99,2	50,0	bdl	25,3	0,039	0,061	0,003	24,7	bdl
	3	34,9	bdl	30,8	0,013	0,085	bdl	33,2	0,003	99,0	50,3	bdl	25,5	0,01	0,067	bdl	24,1	0,002
CD-00150C	1	35,2	bdl	30,6	bdl	bdl	bdl	34,0	bdl	99,8	50,4	bdl	25,1	bdl	bdl	bdl	24,6	bdl
	2	34,7	bdl	30,4	0,024	0,033	0,031	33,9	0,002	99,2	50,1	bdl	25,2	0,019	0,026	0,022	24,7	0,001
CD-RP012	1	34,7	0,001	30,6	bdl	0,026	bdl	34,4	bdl	99,7	49,8	0,001	25,2	bdl	0,021	bdl	24,9	bdl
	2	34,7	bdl	30,6	0,005	0,021	0,049	34,4	0,001	99,8	49,8	bdl	25,2	0,004	0,016	0,034	24,9	bdl
CD-00109	1	34,6	0,007	30,3	bdl	0,038	bdl	34,5	0,030	99,5	49,9	0,006	25,0	bdl	0,030	bdl	25,1	0,018
	2	34,6	0,015	30,5	bdl	0,075	bdl	34,4	0,011	99,7	49,8	0,012	25,2	bdl	0,059	bdl	24,9	0,007
CD-RP008	1	34,8	0,002	30,3	bdl	bdl	bdl	34,3	bdl	99,4	50,1	0,002	25,0	bdl	bdl	bdl	24,9	bdl

ANNEXE 8: ANALYSES MICROSONDE DE PYRITES

Element		S	Mn	Fe	Ni	Co	Zn	Cu	As	Total	S	Mn	Fe	Ni	Co	Zn	Cu	As
		wt.%	wt.%	wt.%	wt.%	wt.%	wt.%	wt.%	wt.%		at.%	at.%	at.%	at.%	at.%	at.%	at.%	at.%
CD-10551	1	53,5	0,005	46,9	0,211	0,054	0,172	0,114	0,004	101	66,3	0,004	33,3	0,143	0,036	0,105	0,071	0,002
	2	53,4	bdl	43,1	4,44	bdl	bdl	bdl	0,023	101	66,3	bdl	30,7	3,01	bdl	bdl	bdl	0,012
	3	53,5	bdl	46,3	0,055	1,08	bdl	0,059	0,019	101	66,3	bdl	32,9	0,037	0,726	bdl	0,037	0,010
	4	53,7	bdl	46,1	bdl	1,35	0,009	bdl	bdl	101	66,4	bdl	32,7	bdl	0,910	0,006	bdl	bdl
CD-00150A	1	53,4	0,002	44,1	2,97	0,194	0,233	bdl	0,018	101	66,3	0,001	31,4	2,01	0,131	0,141	bdl	0,010
	2	53,7	bdl	45,6	bdl	1,67	bdl	0,083	0,016	101	66,4	bdl	32,4	bdl	1,13	bdl	0,052	0,008
	3	53,3	0,024	47,3	0,028	bdl	0,052	bdl	0,002	101	66,2	0,018	33,8	0,019	bdl	0,031	bdl	0,001
	4	53,7	bdl	44,7	2,17	0,431	0,033	bdl	0,011	101	66,5	bdl	31,8	1,47	0,290	0,020	bdl	0,006
CD-02004	1	52,4	bdl	47,2	bdl	bdl	0,121	0,079	bdl	100	65,8	bdl	34,0	bdl	bdl	0,075	0,050	bdl
	2	53,9	bdl	45,0	0,476	1,71	bdl	0,014	0,031	101	66,6	bdl	31,9	0,321	1,15	bdl	0,009	0,017
	3	53,4	bdl	44,0	2,13	1,61	bdl	bdl	0,002	101	66,2	bdl	31,3	1,44	1,08	bdl	bdl	0,001
	4	53,3	0,006	45,6	0,769	0,945	bdl	0,007	bdl	101	66,3	0,005	32,5	0,522	0,639	bdl	0,004	bdl
	5	53,2	bdl	43,3	3,83	0,075	bdl	0,010	0,015	100	66,3	bdl	31,0	2,61	0,051	bdl	0,006	0,008
	6	53,5	bdl	45,3	1,43	0,751	bdl	0,024	0,034	101	66,3	bdl	32,2	0,967	0,506	bdl	0,015	0,018
CD-98042A	1	53,9	bdl	46,0	bdl	0,942	0,275	bdl	bdl	101	66,6	bdl	32,6	bdl	0,633	0,166	bdl	bdl
	2	53,7	bdl	45,8	0,013	1,08	0,047	bdl	bdl	101	66,6	bdl	32,6	0,009	0,727	0,028	bdl	bdl
	3	53,6	bdl	46,0	0,001	0,812	0,060	bdl	bdl	100	66,6	bdl	32,8	0,001	0,549	0,037	bdl	bdl
	4	53,5	bdl	45,8	bdl	1,02	0,214	bdl	bdl	101	66,5	bdl	32,7	bdl	0,687	0,131	bdl	bdl
CD-00150C	1	53,9	bdl	45,9	bdl	0,757	bdl	0,055	bdl	101	66,8	bdl	32,7	bdl	0,511	bdl	0,035	bdl
	2	53,6	bdl	42,4	4,62	0,131	0,075	bdl	0,013	101	66,5	bdl	30,2	3,13	0,088	0,045	bdl	0,007
	3	53,6	bdl	45,2	0,054	2,17	0,112	0,010	0,026	101	66,3	bdl	32,1	0,037	1,46	0,068	0,006	0,014
	4	53,6	bdl	45,7	bdl	1,12	bdl	bdl	bdl	100	66,6	bdl	32,6	bdl	0,757	bdl	bdl	bdl
	5	52,9	bdl	43,1	3,61	0,085	0,033	0,425	0,018	100	66,2	bdl	30,9	2,47	0,058	0,020	0,268	0,010
CD-RP012	1	53,2	bdl	45,9	bdl	1,03	bdl	0,062	0,008	100	66,4	bdl	32,9	bdl	0,701	bdl	0,039	0,004
	2	53,7	bdl	42,9	1,87	2,04	0,102	0,083	0,001	101	66,7	bdl	30,6	1,27	1,37	0,062	0,052	bdl
	3	53,5	bdl	46,5	0,001	0,678	0,135	bdl	0,018	101	66,3	bdl	33,1	0,001	0,457	0,082	bdl	0,009
	4	53,5	bdl	45,4	bdl	1,71	0,121	0,017	0,013	101	66,4	bdl	32,3	bdl	1,15	0,074	0,011	0,007
	5	53,1	bdl	45,0	bdl	1,89	0,116	bdl	bdl	100	66,4	bdl	32,3	bdl	1,28	0,071	bdl	bdl
	6	53,4	bdl	45,3	0,008	1,51	bdl	0,069	bdl	100	66,5	bdl	32,4	0,005	1,03	0	0,044	bdl
CD-00109	1	53,4	bdl	46,0	bdl	0,792	0,056	0,007	bdl	100	66,5	bdl	32,9	bdl	0,537	0,034	0,004	bdl
	2	53,4	bdl	44,9	bdl	1,74	bdl	bdl	0,004	100	66,6	bdl	32,2	bdl	1,18	bdl	bdl	0,002
	3	53,3	bdl	46,3	0,002	0,759	bdl	0,055	0,037	100	66,3	bdl	33,1	0,001	0,514	bdl	0,035	0,020
	4	53,9	0,003	46,3	bdl	0,728	bdl	0,052	0,004	101	66,6	0,002	32,9	bdl	0,490	bdl	0,032	0,002
	5	53,5	bdl	45,4	0,037	1,58	0,149	0,003	0,021	101	66,4	bdl	32,4	0,025	1,07	0,091	0,002	0,011
CD-RP008	1	53,4	0,021	46,5	0,033	0,610	bdl	0,076	0,034	101	66,3	0,015	33,2	0,022	0,412	bdl	0,048	0,018
	2	53,5	0,004	46,4	0,149	0,367	0,023	0,149	bdl	101	66,5	0,003	33,1	0,101	0,248	0,014	0,093	bdl
	3	53,7	bdl	46,2	0,019	0,609	0,070	bdl	0,027	101	66,6	bdl	32,9	0,013	0,411	0,042	bdl	0,014
	4	53,4	0,011	45,9	0,075	0,882	bdl	bdl	0,001	100	66,5	0,008	32,8	0,051	0,598	bdl	bdl	bdl
	5	53,5	bdl	46,3	0,064	0,384	bdl	0,062	0,017	100	66,6	bdl	33,1	0,044	0,260	bdl	0,039	0,009

ANNEXE 9: ANALYSES MICROSONDE DE MAGNÉTITES

Element		SiO2	TiO2	Al2O3	Cr2O3	Fe2O3	MgO	CaO	MnO	FeO	CoO	NiO	ZnO	Total
		wt.%	wt.%	wt.%	wt.%	wt.%	wt.%	wt.%	wt.%	wt.%	wt.%	wt.%	wt.%	
CD-10551	1	0,019	0,012	0,197	0,016	69,5	0,009	bdl	0,040	31,3	bdl	0,043	0,019	101
	2	0,019	0,099	0,230	bdl	69,1	0,032	bdl	0,071	31,1	bdl	0,024	bdl	101
	3	0,016	0,033	0,293	0,025	69,5	0,025	bdl	bdl	31,3	bdl	0,075	0,069	101
	4	0,017	0,054	0,491	bdl	68,8	0,017	0,014	0,005	31,2	bdl	0,074	0,033	101
	5	bdl	0,015	0,242	bdl	69,1	0,030	0,002	0,028	31,0	0,051	0,091	bdl	101
CD-00150A	1	0,028	0,027	0,190	0,042	69,6	0,016	bdl	0,055	31,3	0,051	0,031	0,053	101
	2	0,038	0,045	0,196	0,067	68,9	0,062	bdl	bdl	30,9	0,062	0,043	0,060	100
	3	0,040	0,042	0,190	0,014	68,9	0,015	bdl	bdl	31,1	bdl	0,063	bdl	100
CD-02004	1	0,063	0,055	0,109	0,785	68,1	0,006	bdl	bdl	31,0	0,048	0,068	bdl	100
CD-98042A	1	bdl	0,083	0,126	2,17	65,5	0,028	0,001	bdl	30,5	bdl	0,059	bdl	98,5
	2	0,013	0,059	0,152	2,25	64,9	0,046	0,001	0,071	30,2	bdl	0,066	bdl	97,7
CD-00150C	1	0,019	0,026	0,243	0,450	68,7	0,033	bdl	bdl	31,2	0,062	0,011	bdl	101
	2	0,038	0,142	0,358	0,483	67,9	0,033	bdl	bdl	31,0	0,062	0,026	bdl	100
CD-RP012	1	0,027	0,100	0,451	0,253	67,5	0,045	bdl	0,038	30,7	bdl	bdl	bdl	99,1
	2	0,030	0,421	0,474	0,227	66,9	0,024	bdl	0,053	30,7	bdl	bdl	bdl	98,8
	3	0,034	0,059	0,228	0,259	67,4	0,021	bdl	bdl	30,4	0,026	0,082	0,077	98,6
CD-00109	1	0,035	0,703	0,213	0,062	66,8	0,023	bdl	bdl	30,4	0,066	0,111	bdl	98,3
	2	0,028	0,067	0,186	0,090	68,6	0,002	0,037	0,043	30,9	bdl	0,075	0,016	100
CD-RP008	1	0,056	0,712	0,147	0,112	67,6	0,017	0,003	0,040	30,8	bdl	0,072	bdl	99,5
	2	0,018	0,123	0,158	0,093	68,5	0,013	bdl	0,088	30,8	0,035	0,036	0,038	99,9

Element		SiO2	TiO2	Al2O3	Cr2O3	Fe2O3	MgO	CaO	MnO	FeO	CoO	NiO	ZnO
		at.%	at.%	at.%	at.%	at.%	at.%	at.%	at.%	at.%	at.%	at.%	at.%
CD-10551	1	0,006	0,003	0,071	0,004	15,9	0,004	bdl	0,010	7,97	bdl	0,011	0,004
	2	0,006	0,023	0,083	bdl	15,9	0,015	bdl	0,018	7,96	bdl	0,006	bdl
	3	0,005	0,008	0,105	0,006	15,9	0,011	bdl	bdl	7,95	bdl	0,018	0,016
	4	0,005	0,012	0,177	bdl	15,8	0,008	0,005	0,001	7,96	bdl	0,018	0,007
	5	bdl	0,003	0,087	bdl	15,9	0,014	0,001	0,007	7,94	0,013	0,022	bdl
CD-00150A	1	0,008	0,006	0,068	0,01	15,9	0,007	bdl	0,014	7,95	0,012	0,008	0,012
	2	0,012	0,010	0,071	0,016	15,9	0,029	bdl	bdl	7,93	0,015	0,010	0,014
	3	0,012	0,010	0,069	0,003	15,9	0,007	bdl	bdl	7,98	bdl	0,016	bdl
CD-02004	1	0,019	0,013	0,040	0,190	15,7	0,003	bdl	bdl	7,97	0,012	0,017	bdl
CD-98042A	1	bdl	0,019	0,046	0,535	15,4	0,013	bdl	bdl	7,97	bdl	0,015	bdl
	2	0,004	0,014	0,056	0,560	15,4	0,021	bdl	0,019	7,94	bdl	0,017	bdl
CD-00150C	1	0,006	0,006	0,088	0,109	15,8	0,015	bdl	bdl	7,97	0,015	0,003	bdl
	2	0,012	0,033	0,130	0,117	15,7	0,015	bdl	bdl	7,96	0,015	0,007	bdl
CD-RP012	1	0,008	0,023	0,165	0,062	15,7	0,021	bdl	0,010	7,97	bdl	bdl	bdl
	2	0,009	0,098	0,173	0,056	15,6	0,011	bdl	0,014	7,96	bdl	bdl	bdl
	3	0,011	0,014	0,084	0,064	15,8	0,010	bdl	bdl	7,94	0,007	0,021	0,018
CD-00109	1	0,011	0,165	0,078	0,015	15,7	0,011	bdl	bdl	7,92	0,016	0,028	bdl
	2	0,009	0,016	0,067	0,022	15,9	0,001	0,012	0,011	7,95	bdl	0,018	0,004
CD-RP008	1	0,017	0,165	0,053	0,027	15,7	0,008	0,001	0,011	7,94	bdl	0,018	bdl
	2	0,006	0,029	0,057	0,023	15,9	0,006	bdl	0,023	7,94	0,009	0,009	0,009

ANNEXE 10: ANALYSES MICROSONDE D'ILMÉNITES

Element		SiO2	TiO2	Al2O3	Cr2O3	Fe2O3	MgO	CaO	MnO	FeO	CoO	NiO	ZnO	Total
		wt.%	wt.%	wt.%	wt.%	wt.%	wt.%	wt.%	wt.%	wt.%	wt.%	wt.%	wt.%	
CD-02004	1	0,002	50,6	bdl	0,044	19,7	0,030	bdl	0,790	30,7	bdl	0,054	bdl	102
CD-98042A	1	0,005	47,3	0,003	0,281	22,2	0,226	bdl	2,15	28,8	0,006	bdl	0,030	101
	2	0,022	48,0	0,026	0,140	21,6	0,186	bdl	2,15	28,9	0,038	bdl	bdl	101
	3	0,005	46,1	0,018	0,306	23,1	0,176	bdl	1,99	28,9	0,059	0,016	0,033	101
CD-00150C	1	0,140	49,3	0,012	0,093	20,7	0,136	bdl	1,51	29,8	0,067	bdl	bdl	102
	2	0,006	48,6	0,037	0,099	21,1	0,017	bdl	2,12	29,2	bdl	bdl	0,076	101
CD-RP012	1	0,017	51,4	0,016	bdl	18,2	0,040	bdl	1,23	29,9	bdl	0,076	bdl	101
	2	0,016	50,7	0,026	bdl	19,2	0,037	bdl	1,29	30,1	0,011	bdl	bdl	101
	3	0,023	49,6	0,046	0,059	20,2	0,025	bdl	1,40	29,9	0,026	bdl	bdl	101
CD-00109	1	0,009	49,0	0,008	0,044	20,7	0,044	bdl	1,39	29,8	0,063	bdl	0,017	101
	2	bdl	49,2	0,027	0,050	21,1	0,072	0,002	1,22	30,2	0,069	bdl	bdl	102
	3	bdl	48,6	0,029	0,028	21,5	0,106	bdl	1,33	29,9	0,077	bdl	0,045	102
	4	0,023	48,6	0,009	0,048	20,8	0,091	bdl	1,45	29,6	0,029	0,026	bdl	101
CD-RP008	1	bdl	47,9	0,022	0,039	21,4	0,006	bdl	1,60	29,5	0,037	bdl	0,032	101
	2	bdl	48,6	0,008	0,021	21,6	0,007	bdl	1,49	30,0	bdl	0,033	0,042	102

Element		SiO2	TiO2	Al2O3	Cr2O3	Fe2O3	MgO	CaO	MnO	FeO	CoO	NiO	ZnO
		at.%	at.%	at.%	at.%	at.%	at.%	at.%	at.%	at.%	at.%	at.%	at.%
CD-02004	1	bdl	9,76	bdl	0,009	3,79	0,011	bdl	0,171	6,59	bdl	0,011	bdl
CD-98042A	1	0,001	9,27	0,001	0,058	4,35	0,088	bdl	0,474	6,27	0,001	bdl	0,006
	2	0,006	9,38	0,008	0,029	4,23	0,072	bdl	0,472	6,28	0,008	bdl	bdl
	3	0,001	9,10	0,005	0,063	4,56	0,069	bdl	0,442	6,33	0,012	0,003	0,006
CD-00150C	1	0,036	9,54	0,004	0,019	4,01	0,052	bdl	0,329	6,41	0,014	bdl	bdl
	2	0,002	9,48	0,011	0,020	4,12	0,007	bdl	0,466	6,33	bdl	bdl	0,015
CD-RP012	1	0,004	9,97	0,005	bdl	3,53	0,015	bdl	0,269	6,45	bdl	0,016	bdl
	2	0,004	9,82	0,008	bdl	3,72	0,014	bdl	0,282	6,47	0,002	bdl	bdl
	3	0,006	9,64	0,014	0,012	3,92	0,010	bdl	0,306	6,47	0,005	bdl	bdl
CD-00109	1	0,002	9,55	0,002	0,009	4,05	0,017	bdl	0,305	6,47	0,013	bdl	0,003
	2	bdl	9,52	0,008	0,010	4,09	0,027	0,001	0,266	6,50	0,014	bdl	bdl
	3	bdl	9,45	0,009	0,006	4,18	0,041	bdl	0,290	6,46	0,016	bdl	0,009
	4	0,006	9,52	0,003	0,010	4,08	0,035	bdl	0,319	6,44	0,006	0,005	bdl
CD-RP008	1	bdl	9,41	0,007	0,008	4,22	0,002	bdl	0,355	6,45	0,008	bdl	0,006
	2	bdl	9,44	0,002	0,004	4,19	0,003	bdl	0,327	6,48	bdl	0,007	0,008

ANNEXE 11: ANALYSES LA-ICP-MS DE PYRRHOTITES

Pour les annexes 11 à 14

Calcul du facteur de correction pour l'interférence de Ru^{101} avec $Ni^{61}Ar^{40}$ (varie en fonction des journées d'analyses).

$$* Ru^{101} = Ru^{101}\ mesuré - (Ni^{61} * \frac{Ru^{101}\ dans\ Ni\ blank}{Ni^{61}\ dans\ Ni\ blank})$$

$$\frac{Ru^{101}\ dans\ Ni\ blank}{Ni^{61} dans\ Ni\ blank} = 2{,}67944 * 10^{-6}\ ou\ 3{,}03917 * 10^{-6}\ ou\ 2{,}57444 * 10^{-6}$$

Calcul du facteur de correction pour l'interférence de Rh^{103} avec $Cu^{63}Ar^{40}$ (varie en fonction des journées d'analyses).

$$* Rh^{103} = Rh^{103}\ mesuré - (Cu^{63} * \frac{Rh^{103}\ dans\ MASS1}{Cu^{63}\ dans\ MASS1})$$

$$\frac{Rh^{103}\ dans\ MASS1}{Cu^{63} dans\ MASS1} = 2{,}72814 * 10^{-5}\ ou\ 3{,}42195 * 10^{-5}\ ou\ 2{,}62174 * 10^{-5}$$

Calcul du facteur de correction pour l'interférence de Pd^{108} avec Cd^{111}

$$* Pd^{108} = Pd^{108}\ mesuré - \left(\frac{abondance\ \%\ de\ Cd^{108}}{abondance\ \%\ de\ Pd^{108}}\right) * Cd^{111}$$

$$\frac{abondance\ \%\ de\ Cd^{108}}{abondance\ \%\ de\ Pd^{108}} = 0{,}0336$$

Element		Co	Ni	Cu	Zn	As	Se	Mo	Ru	Rh	Pd	Ag	Cd	Sn	Sb	Te	Re	Os	Ir	Pt	Au	Pb	Bi
		(ppm)	(ppm)	(ppm)	(ppm)	(ppm)	(ppm)	(ppm)	(ppm)	(ppm)	(ppm)	(ppm)	(ppm)	(ppm)	(ppm)	(ppm)	(ppm)	(ppm)	(ppm)	(ppm)	(ppm)	(ppm)	(ppm)
Isotope		^{59}Co	^{61}Ni	^{65}Cu	^{66}Zn	^{75}As	^{82}Se	^{95}Mo	^{101}Ru*	^{103}Rh*	^{108}Pd*	^{109}Ag	^{111}Cd	^{118}Sn	^{121}Sb	^{128}Te	^{185}Re	^{189}Os	^{193}Ir	^{195}Pt	^{197}Au	^{208}Pb	^{209}Bi
CD-00129A	1	64,9	3727	0,567	0,158	0,550	158	0,170	0,179	0,008	<0,010	0,167	<0,054	0,187	0,017	0,231	0,008	0,138	0,068	0,019	0,033	0,477	0,046
	2	72,5	4612	0,381	0,417	1,15	143	0,165	0,145	0,080	0,303	0,929	0,068	56,1	0,030	0,210	0,017	0,069	0,032	0,018	0,041	1,18	0,070
CD-00150B	1	201	9356	0,274	<0,090	1,12	185	0,183	<0,017	0,043	0,034	0,215	<0,054	0,145	0,026	0,499	0,071	0,017	0,028	<0,014	0,041	0,103	0,056
	2	161	8134	0,349	<0,090	1,51	186	0,167	<0,017	0,061	<0,010	0,335	<0,054	0,148	0,038	0,611	0,075	<0,016	0,019	<0,014	0,040	0,171	0,127
	3	206	8689	0,405	2,62	1,68	170	0,188	0,022	0,072	0,038	0,169	<0,054	0,086	0,027	0,573	0,103	<0,016	0,033	<0,014	0,026	0,090	0,038
	4	196	8346	0,505	2,43	1,68	155	0,297	<0,017	0,095	0,014	0,233	<0,054	0,134	0,031	0,380	0,249	0,020	0,033	<0,014	0,030	0,100	0,029
CD-RP010	1	22,3	4369	0,549	<0,090	2,05	341	0,210	<0,017	<0,003	0,084	0,535	0,056	0,148	0,025	0,841	0,262	0,021	0,007	0,015	0,017	2,03	0,040
	2	21,7	4151	0,155	1,71	0,754	146	0,175	<0,017	0,004	0,095	0,191	<0,054	0,185	0,035	0,258	0,012	0,040	<0,004	<0,014	0,014	1,22	0,017
	3	24,4	4887	0,499	0,474	1,24	293	0,202	<0,017	<0,003	0,197	0,346	<0,054	0,077	0,019	0,262	0,014	<0,016	<0,004	<0,014	0,008	1,82	0,020
CD-10603A	1	47,9	4625	0,067	0,393	1,09	165	0,161	0,019	0,003	<0,010	0,309	<0,054	0,203	0,032	0,238	0,009	0,046	0,058	<0,014	0,008	0,885	0,131
	2	48,3	4288	0,262	0,238	1,07	199	0,140	0,028	<0,003	0,033	0,484	<0,054	0,252	0,023	<0,194	0,009	0,054	0,070	<0,014	<0,008	0,659	0,112
	3	40,1	3553	0,161	0,132	1,39	252	0,128	<0,017	<0,003	0,027	1,02	0,112	1,93	0,027	0,399	<0,006	0,021	0,014	<0,014	0,014	6,79	0,485
CD-00150C	1	125	7860	0,168	1,49	0,711	128	0,153	0,024	0,003	<0,010	0,268	<0,054	0,109	0,019	0,355	<0,006	0,018	0,011	0,018	<0,008	0,117	0,042
	2	156	8302	0,143	0,455	0,611	128	0,249	0,026	0,011	<0,010	0,166	<0,054	0,126	0,012	0,312	0,024	0,019	0,024	0,019	0,050	0,098	0,044
	3	153	8034	1,184	0,573	<0,456	120	0,255	0,018	0,003	<0,010	0,536	0,112	0,085	0,042	<0,194	0,092	0,062	0,024	<0,014	0,010	0,161	0,079
	4	158	8514	0,061	0,723	0,891	113	0,213	<0,017	0,035	<0,010	0,139	<0,054	0,088	0,016	<0,194	0,110	<0,016	0,022	<0,014	0,011	0,084	0,027
	5	164	8090	0,141	0,330	0,636	111	0,279	<0,017	0,015	0,043	0,972	<0,054	0,089	0,029	<0,194	0,144	<0,016	0,024	<0,014	0,011	0,140	0,037
	6	162	6171	0,146	0,266	0,673	124	0,265	<0,017	0,042	0,040	1,16	<0,054	0,069	0,015	<0,194	0,120	<0,016	0,015	<0,014	0,009	0,326	0,064
	7	214	9007	0,174	0,287	0,941	125	0,251	<0,017	0,081	<0,010	0,156	<0,054	0,131	0,013	0,277	0,128	0,016	0,025	<0,014	0,013	0,075	0,020
CD-00118	1	76,2	4376	0,492	1,12	0,773	275	0,188	<0,017	0,009	0,023	0,287	<0,054	0,130	<0,012	0,280	<0,006	<0,016	<0,004	<0,014	<0,008	0,303	0,062
	2	43,7	3048	0,879	0,280	0,997	243	0,122	<0,017	0,002	0,070	0,561	<0,054	0,110	0,012	0,218	<0,006	0,019	0,004	<0,014	<0,008	1,26	0,193
CD-00150A	1	127	10671	0,288	<0,090	1,40	182	0,264	0,034	0,015	<0,010	0,187	<0,054	0,087	0,016	0,330	0,324	0,031	0,007	<0,014	0,011	0,159	0,050
	2	114	10284	87,3	<0,090	0,773	170	0,158	0,014	0,001	0,026	1,03	<0,054	0,122	0,025	0,467	0,009	<0,016	0,006	<0,014	0,012	1,02	0,335
CD-09410	1	232	5896	0,199	0,405	0,499	71,1	0,187	0,224	0,045	0,037	0,198	0,374	0,146	0,024	0,386	0,013	0,175	0,020	0,019	0,009	0,461	0,352
	2	233	5653	0,330	0,312	<0,456	65,4	0,199	0,220	0,041	<0,010	0,338	0,187	0,090	0,027	0,312	0,009	0,102	0,016	0,023	0,011	2,04	1,353
	3	221	5628	0,150	0,100	<0,456	72,1	0,110	0,242	0,047	<0,010	0,221	0,056	0,089	0,027	0,224	0,050	0,119	0,021	0,056	0,011	1,04	0,748
	4	205	5354	0,100	0,505	<0,456	66,9	0,108	0,209	0,032	0,017	0,388	0,077	0,103	0,056	0,430	0,012	0,108	0,012	<0,014	0,009	2,30	1,47
	5	353	7205	0,143	0,337	<0,456	70,8	0,180	0,257	0,054	0,019	0,164	0,092	0,117	0,027	0,486	0,022	0,137	0,055	0,016	0,013	0,187	0,290
	6	170	5379	0,262	0,386	<0,456	66,9	0,224	0,303	0,022	0,014	0,341	0,086	0,368	0,018	0,330	0,016	0,150	0,014	0,014	0,008	1,14	0,854
CD-98042A	1	271	6626	38,6	0,443	<0,456	104	0,109	0,030	0,014	0,112	0,303	0,065	0,173	0,028	0,654	0,014	<0,016	0,015	0,021	0,008	0,444	0,029
	2	275	7099	0,187	0,804	<0,456	103	0,115	0,040	0,006	0,016	0,203	0,061	8,91	0,037	0,355	0,007	0,029	0,007	<0,014	<0,008	0,319	0,025
	3	350	7461	0,280	0,262	0,972	71,1	0,139	0,081	0,007	0,025	0,542	0,074	0,145	0,025	0,555	0,007	0,032	0,019	<0,014	0,015	0,430	0,024
	4	232	6713	0,324	0,237	1,08	84,1	0,165	0,037	0,019	0,041	0,372	0,077	0,174	0,014	0,196	0,013	0,016	0,013	<0,014	0,008	0,985	0,064
CD-RP012	1	124	7723	0,118	0,181	<0,456	80,7	0,181	0,077	0,006	0,035	0,954	0,096	0,101	0,018	0,299	0,016	0,023	0,010	0,017	0,010	0,611	0,004
	2	116	7417	0,237	0,237	0,785	91,7	0,199	0,070	0,009	0,030	0,446	0,084	0,075	0,021	0,280	0,052	0,038	0,015	0,023	0,008	0,403	0,006
	3	123	7685	<0,098	0,362	<0,456	94,3	0,129	0,075	0,005	0,011	0,355	0,100	0,118	0,022	<0,194	0,012	0,024	0,014	<0,014	<0,008	0,402	0,004
	4	139	8072	0,274	0,262	<0,456	91,6	0,219	0,097	0,037	0,307	0,282	0,137	0,076	0,024	0,206	0,054	0,053	0,017	0,017	0,012	0,357	0,006

ANNEXE 12: ANALYSES LA-ICP-MS DE PENTLANDITES

Element		Co	Ni	Cu	Zn	As	Se	Mo	Ru	Rh	Pd	Ag	Cd	Sn	Sb	Te	Re	Os	Ir	Pt	Au	Pb	Bi
		(ppm)	(ppm)	(ppm)	(ppm)	(ppm)	(ppm)	(ppm)	(ppm)	(ppm)	(ppm)	(ppm)	(ppm)	(ppm)	(ppm)	(ppm)	(ppm)	(ppm)	(ppm)	(ppm)	(ppm)	(ppm)	(ppm)
Isotope		^{59}Co	^{61}Ni	^{65}Cu	^{66}Zn	^{75}As	^{82}Se	^{95}Mo	^{101}Ru*	^{103}Rh*	^{108}Pd*	^{109}Ag	^{111}Cd	^{118}Sn	^{121}Sb	^{128}Te	^{185}Re	^{189}Os	^{193}Ir	^{195}Pt	^{197}Au	^{208}Pb	^{209}Bi
CD-00129A	1	3787	217175	1,50	0,182	2,93	90,2	0,046	0,167	0,739	278	4,18	0,041	0,117	0,017	<0,194	<0,006	0,043	0,015	0,100	0,021	9,74	0,257
	2	4513	241595	1,05	1,60	0,697	78,6	0,081	0,185	0,235	98,9	1,61	0,087	22,5	0,098	<0,194	0,011	0,033	0,022	0,277	0,028	1,42	0,044
	3	1172	229385	0,326	<0,090	0,749	86,9	0,039	0,084	0,043	17,6	0,612	0,093	0,147	0,012	0,218	0,029	0,038	0,018	0,023	0,020	1,30	0,019
CD-00150B	1	7932	244851	0,938	<0,090	<0,456	107	0,068	0,021	0,043	13,2	1,95	<0,054	0,132	0,013	0,218	<0,006	<0,016	0,015	0,014	0,015	0,394	0,078
	2	8124	268946	1,23	<0,090	0,752	115	0,043	<0,017	0,053	18,4	3,26	<0,054	0,092	<0,012	0,296	<0,006	<0,016	0,018	<0,014	0,013	0,947	0,199
	3	8010	261782	1,99	<0,090	0,456	116	0,086	<0,017	0,069	18,3	6,02	<0,054	0,068	<0,012	0,527	<0,006	<0,016	0,020	<0,014	0,012	2,96	0,658
	4	7980	251363	1,44	<0,090	<0,456	101	0,082	0,020	0,043	15,4	1,57	<0,054	0,065	<0,012	<0,194	0,048	<0,016	0,012	<0,014	0,011	0,352	0,067
	5	7619	264062	5,57	0,544	0,690	92,5	0,060	0,080	0,048	15,8	3,94	<0,054	<0,032	0,039	<0,194	<0,006	<0,016	0,011	0,029	0,016	0,638	0,274
	6	8628	266015	1,66	0,466	0,586	89,9	0,097	<0,017	0,053	18,3	2,37	<0,054	0,067	<0,012	<0,194	0,057	<0,016	0,005	0,026	0,010	0,606	0,179
CD-RP010	1	537	220236	0,944	<0,090	<0,456	159	0,189	0,060	0,069	42,0	3,19	<0,054	0,039	<0,012	0,687	<0,006	<0,016	<0,004	0,029	0,016	11,1	0,071
	2	1426	222710	1,80	<0,090	1,56	203	0,125	0,120	0,200	102	2,79	<0,054	0,054	0,020	2,53	0,007	<0,016	0,006	0,078	0,021	13,8	0,300
	3	1146	231502	0,970	<0,090	1,01	201	0,064	0,080	0,172	89,2	1,31	<0,054	0,056	0,018	1,270	<0,006	<0,016	<0,004	0,026	0,012	6,12	0,079
	4	1101	216850	1,71	<0,090	1,04	121	0,098	0,060	0,148	72,8	2,60	<0,054	0,048	0,012	0,283	0,008	<0,016	<0,004	<0,014	0,012	10,1	0,017
	5	137	222710	0,391	16,0	0,586	114	0,080	<0,017	0,022	9,44	2,34	<0,054	0,050	<0,012	<0,194	0,006	<0,016	0,005	<0,014	<0,008	4,00	0,010
	6	1206	238014	1,25	2,28	<0,456	102	0,095	0,105	0,189	97,3	1,92	<0,054	0,089	0,017	0,287	0,007	<0,016	<0,004	<0,014	0,016	8,43	0,020
	7	1550	192104	104	1,76	0,762	165	0,106	0,049	0,178	89,9	3,55	<0,054	0,179	0,019	3,09	0,009	<0,016	0,005	0,035	0,023	24,7	1,368
CD-10603A	1	3471	257875	1,00	0,612	2,60	147	1,661	0,019	0,019	10,9	0,681	<0,054	0,036	0,014	5,14	25,7	0,039	<0,004	0,021	0,033	3,61	0,446
	2	3813	213268	11,7	2,77	2,60	171	0,056	<0,017	0,021	9,83	0,804	0,241	0,098	0,038	2,18	<0,006	0,016	0,005	<0,014	0,008	2,74	0,778
	3	3324	238990	0,759	0,199	0,729	112	0,076	<0,017	0,021	11,0	0,488	<0,054	3,29	0,018	1,04	<0,006	0,017	0,009	<0,014	<0,008	1,37	0,088
	4	3363	238014	0,664	0,137	0,886	114	0,050	0,098	0,022	11,5	0,376	<0,054	0,335	0,018	0,563	0,008	0,032	0,009	<0,014	<0,008	0,482	0,021
	5	3116	227920	1,53	3,48	1,33	118	0,062	0,047	0,018	8,37	0,723	<0,054	0,147	0,030	1,74	0,021	<0,016	0,004	<0,014	0,010	2,62	0,206
CD-00150C	1	7622	272202	0,931	0,681	0,488	72,9	0,081	<0,017	0,035	12,1	1,34	<0,054	0,078	<0,012	<0,194	0,119	0,016	0,015	0,018	0,015	0,329	0,023
	2	7847	236711	40,7	0,557	0,781	65,1	0,091	0,033	0,039	11,0	3,97	<0,054	0,055	<0,012	<0,194	0,068	<0,016	0,010	0,015	0,016	0,856	0,062
	3	7697	255922	1726	1,75	1,14	72,0	0,131	<0,017	0,031	9,24	6,09	<0,054	<0,032	<0,012	<0,194	0,063	0,029	0,004	0,014	0,008	2,22	0,218
	4	7619	249735	2,18	1,45	1,04	71,2	0,119	<0,017	0,020	9,64	5,86	<0,054	0,042	0,014	<0,194	0,024	<0,016	0,009	<0,014	0,013	1,86	0,184
	5	8215	271550	0,947	1,17	0,498	65,1	0,115	0,031	0,070	10,1	3,06	<0,054	0,061	<0,012	<0,194	0,074	0,016	0,014	<0,014	<0,008	0,449	0,054
	6	7349	249084	2,41	0,479	<0,456	64,9	0,120	0,021	0,026	8,02	3,16	<0,054	0,361	<0,012	<0,194	0,117	<0,016	0,016	0,014	<0,008	1,15	0,083
	7	8414	256247	1,02	0,251	<0,456	66,6	0,103	0,017	0,018	7,09	2,57	<0,054	0,059	0,015	<0,194	0,042	<0,016	0,009	<0,014	<0,008	0,814	0,077
	8	8694	268946	0,990	1,27	0,755	72,0	0,139	0,036	0,066	10,4	1,85	<0,054	0,049	0,015	<0,194	0,066	<0,016	0,012	<0,014	<0,008	0,083	0,027
	9	8381	263410	2,05	9,77	1,56	75,1	0,092	0,092	0,035	8,97	2,82	0,140	0,054	0,012	<0,194	0,043	<0,016	0,015	<0,014	<0,008	0,599	0,045
	10	7391	216198	1,40	12,7	1,99	79,1	0,086	0,043	0,036	4,88	0,576	<0,054	0,046	0,326	0,195	0,048	<0,016	0,012	<0,014	<0,008	0,137	0,067

Element		Co	Ni	Cu	Zn	As	Se	Mo	Ru	Rh	Pd	Ag	Cd	Sn	Sb	Te	Re	Os	Ir	Pt	Au	Pb	Bi
		(ppm)	(ppm)	(ppm)	(ppm)	(ppm)	(ppm)	(ppm)	(ppm)	(ppm)	(ppm)	(ppm)	(ppm)	(ppm)	(ppm)	(ppm)	(ppm)	(ppm)	(ppm)	(ppm)	(ppm)	(ppm)	(ppm)
Isotope		^{59}Co	^{61}Ni	^{65}Cu	^{66}Zn	^{75}As	^{82}Se	^{95}Mo	^{101}Ru*	^{103}Rh*	^{108}Pd*	^{109}Ag	^{111}Cd	^{118}Sn	^{121}Sb	^{128}Te	^{185}Re	^{189}Os	^{193}Ir	^{195}Pt	^{197}Au	^{208}Pb	^{209}Bi
CD-RP008	1	1553	200895	1,98	14,5	3,35	908	0,449	0,145	0,342	182	4,40	0,057	0,058	0,032	2,74	<0,006	0,026	<0,004	<0,014	0,021	94,1	0,524
	2	1241	201872	342	22,2	7,91	1931	0,124	0,679	1,41	785	13,4	0,107	0,080	0,016	3,32	0,008	<0,016	<0,004	0,037	0,062	234	2,78
	3	3875	128286	4689	1,75	2,21	262	0,070	0,128	0,122	53,1	27,7	<0,054	2,54	0,023	0,811	0,013	<0,016	<0,004	0,028	0,079	89,2	1,53
	4	1361	220431	105	1,02	4,23	1120	0,078	0,170	0,127	70,3	70,3	<0,054	1,05	0,013	0,807	<0,006	<0,016	<0,004	0,073	0,133	213	0,661
CD-00118	1	4213	246805	882	348	0,821	119	0,045	0,331	0,582	305	5,14	2,214	0,125	0,038	<0,194	<0,006	<0,016	<0,004	<0,014	<0,008	3,81	0,368
	2	3891	222059	251	9,44	0,189	169	0,048	0,289	0,565	311	6,54	0,106	0,182	0,013	<0,194	<0,006	<0,016	<0,004	<0,014	<0,008	6,77	0,560
CD-00150A	1	5848	258526	2,47	<0,090	0,654	99,3	0,185	0,080	0,037	20,1	6,41	<0,054	0,208	<0,012	<0,194	0,007	<0,016	0,005	<0,014	<0,008	2,28	0,485
CD-09410	1	13350	260480	1,12	0,309	1,50	44,9	0,068	0,033	0,027	1,32	1,15	0,078	<0,032	0,014	1,74	0,008	0,084	0,007	<0,014	0,019	3,61	0,944
	2	12731	260806	0,928	4,88	0,977	39,4	0,046	0,204	0,048	1,30	0,208	0,074	0,049	0,016	1,63	0,020	0,094	0,017	<0,014	<0,008	0,100	0,052
	3	5079	202588	0,514	0,326	0,847	37,6	0,052	0,073	0,013	0,402	0,397	0,098	0,043	0,026	0,628	0,008	0,046	0,007	0,020	0,008	2,74	0,560
	4	9866	204477	1,23	0,152	0,586	45,3	0,147	0,307	0,020	0,712	2,42	0,093	0,058	0,022	1,29	0,020	0,062	0,029	0,023	0,030	8,40	2,59
	5	7131	129914	0,651	1,50	2,28	55,4	0,055	0,323	0,048	0,564	0,492	0,166	0,107	0,027	2,51	0,032	0,414	0,029	0,061	0,025	6,06	1,15
	6	7228	157265	0,459	0,163	<0,456	45,2	0,046	0,211	0,025	0,567	0,293	0,078	0,037	0,036	0,391	0,009	0,068	0,012	<0,014	<0,008	1,65	0,651
CD-98042A	1	14847	233455	1,03	0,163	1,07	56,0	0,212	0,158	0,329	175	1,99	0,065	0,081	0,017	0,303	0,028	0,031	0,007	0,027	<0,008	3,26	0,063
	2	16736	269922	1,25	0,198	1,11	62,5	0,124	0,279	0,394	221	3,18	0,163	0,456	0,028	0,292	0,013	0,021	0,015	0,150	0,030	3,58	0,063
	3	13545	239967	91,2	3,94	1,30	69,0	0,199	0,219	0,489	267	3,87	0,111	<0,032	0,023	0,472	0,012	0,033	0,009	0,041	0,016	13,8	0,238
	4	10191	174847	1,04	8,27	3,03	53,7	0,355	0,357	0,499	274	3,05	<0,054	0,091	0,020	0,501	0,030	0,026	0,014	0,485	0,016	10,5	0,137
	5	2344	229548	11,4	20,3	<0,456	41,4	0,267	0,018	0,058	31,3	1,33	0,085	0,066	0,048	0,560	0,036	0,016	0,006	0,127	0,015	8,30	0,303
CD-RP012	1	3386	254001	104	0,567	<0,456	54,1	0,228	0,246	0,352	199	2,47	0,065	0,540	0,025	<0,194	<0,006	0,022	0,008	0,015	<0,008	1,05	0,003
	2	1267	256084	53,1	0,632	0,479	54,4	0,081	0,085	0,092	48,8	2,80	0,078	0,280	0,015	<0,194	0,130	0,023	0,007	0,063	0,021	2,05	0,004
	3	4363	271550	33,1	27,0	<0,456	46,2	2,963	0,184	0,450	221	4,85	0,280	7,81	0,094	<0,194	1,14	0,017	0,026	0,029	0,031	4,69	0,012
	4	7912	255596	5,86	3,29	1,73	54,7	0,068	0,387	0,645	359	4,00	<0,054	0,104	<0,012	<0,194	0,017	0,028	0,009	0,025	<0,008	2,44	0,039
	5	6720	278714	0,990	0,156	0,518	57,3	0,050	0,230	0,191	102	1,84	0,078	0,254	<0,012	<0,194	<0,006	<0,016	0,010	<0,014	<0,008	0,420	0,004
	6	7769	280342	1,16	0,150	<0,456	56,7	0,039	0,538	1,16	621	5,14	0,081	0,153	0,015	<0,194	0,025	0,020	0,008	0,063	<0,008	2,12	<0,003

ANNEXE 13: ANALYSES LA-ICP-MS DE CHALCOPYRITES

Element		Co	Ni	Cu	Zn	As	Se	Mo	Ru	Rh	Pd	Ag	Cd	Sn	Sb	Te	Re	Os	Ir	Pt	Au	Pb	Bi
		(ppm)	(ppm)	(ppm)	(ppm)	(ppm)	(ppm)	(ppm)	(ppm)	(ppm)	(ppm)	(ppm)	(ppm)	(ppm)	(ppm)	(ppm)	(ppm)	(ppm)	(ppm)	(ppm)	(ppm)	(ppm)	(ppm)
Isotope		^{59}Co	^{61}Ni	^{65}Cu	^{66}Zn	^{75}As	^{82}Se	^{95}Mo	^{101}Ru*	^{103}Rh*	^{108}Pd*	^{109}Ag	^{111}Cd	^{118}Sn	^{121}Sb	^{128}Te	^{185}Re	^{189}Os	^{193}Ir	^{195}Pt	^{197}Au	^{208}Pb	^{209}Bi
CD-RP010	1	1159	2042	318298	0,396	1,151	149	0,596	0,260	n.a.	141	5,78	0,067	0,222	0,026	1,34	0,050	0,049	0,011	0,027	0,018	10,0	0,010
	2	429	22823	329129	50,5	0,565	156	0,052	0,030	n.a.	14,9	43,2	0,615	0,040	0,022	1,31	<0,006	<0,016	0,004	0,014	0,075	42,0	1,643
CD-10603A	1	5538	420	347358	40,5	0,472	97,4	0,134	0,018	n.a.	0,033	1,13	0,791	0,052	<0,012	3,20	0,265	<0,016	<0,004	<0,014	0,012	2,71	4,72
	2	4230	14120	342185	77,0	8,125	215	0,094	0,034	n.a.	0,736	2,68	2,10	1,64	0,049	4,84	0,008	<0,016	<0,004	<0,014	0,009	7,91	4,26
CD-00118	1	0,344	2042	343250	679	0,882	201	0,074	0,136	n.a.	1,81	74,4	3,45	0,082	0,013	0,329	<0,006	<0,016	<0,004	<0,014	<0,008	2,82	0,099
	2	0,402	2033	347815	840	0,843	208	0,063	0,131	n.a.	1,35	58,9	5,51	0,136	0,017	0,237	<0,006	0,024	<0,004	<0,014	<0,008	2,38	0,105
	3	0,354	2008	348424	660	0,624	205	0,087	0,114	n.a.	0,944	43,5	5,22	0,216	0,018	0,265	<0,006	<0,016	<0,004	<0,014	<0,008	2,29	0,109
	4	0,429	1996	351162	545	0,898	171	0,072	0,130	n.a.	0,683	31,9	3,13	0,135	0,018	<0,194	<0,006	<0,016	<0,004	<0,014	<0,008	2,15	0,048
	5	0,481	2012	345381	512	0,904	197	0,083	0,143	n.a.	1,96	82,3	3,29	0,174	0,017	0,259	<0,006	<0,016	<0,004	<0,014	0,008	3,62	0,126
	6	0,362	1987	346902	457	0,773	189	0,080	0,129	n.a.	1,84	83,3	2,60	0,145	0,013	<0,194	<0,006	<0,016	<0,004	<0,014	<0,008	1,50	0,056
CD-00150A	1	0,320	2005	346598	0,045	0,770	165	0,103	0,137	n.a.	1,28	56,2	4,32	0,158	0,013	0,551	0,039	<0,016	<0,004	<0,014	0,012	2,86	0,523
	2	1,29	1993	338990	0,045	<0,456	106	0,075	0,134	n.a.	1,23	57,1	7,36	0,210	0,029	0,329	<0,006	<0,016	<0,004	<0,014	0,013	2,83	0,390
CD-98042A	1	2465	1923	253482	122	1,400	108	0,125	0,138	n.a.	0,525	6,27	0,493	<0,032	0,016	1,55	0,015	0,026	0,017	0,520	0,028	23,6	2,22
	2	55,4	2784	275544	97,7	0,596	77,3	0,228	0,084	n.a.	0,124	4,59	0,204	0,049	0,017	0,411	0,011	0,018	0,027	0,024	0,018	11,4	0,060
	3	1187	22518	297605	136	0,822	90,4	0,660	0,088	n.a.	50,5	18,4	0,539	0,183	0,013	<0,194	0,286	0,029	0,024	0,026	0,025	27,0	0,079
CD-RP012	1	140	6116	345381	48,7	<0,456	65,1	0,073	0,065	n.a.	5,99	3,71	0,268	0,176	<0,012	<0,194	0,024	0,034	0,027	<0,014	0,014	2,95	0,017
	2	59,6	3682	291215	128	<0,456	74,2	0,198	0,072	n.a.	2,84	10,0	0,493	0,092	0,019	<0,194	0,012	0,025	0,015	0,070	0,014	9,92	0,027
CD-11054	1	9,65	2684	344772	36,2	4,199	239	0,107	0,115	n.a.	1,18	35,3	0,110	0,134	<0,012	<0,194	0,081	0,017	0,012	<0,014	0,012	6,79	2,77
	2	0,279	2304	346598	131	<0,456	42,7	0,110	0,121	n.a.	0,652	29,5	0,895	1,55	0,033	<0,194	0,008	0,033	0,005	<0,014	0,012	3,13	0,657
	3	1,40	2270	342946	67,2	<0,456	70,9	0,134	0,133	n.a.	0,841	41,6	0,341	0,246	0,026	<0,194	0,010	0,030	0,015	<0,014	0,013	3,65	0,962

ANNEXE 14: ANALYSES LA-ICP-MS DE PYRITES

Element		Co	Ni	Cu	Zn	As	Se	Mo	Ru	Rh	Pd	Ag	Cd	Sn	Sb	Te	Re	Os	Ir	Pt	Au	Pb	Bi
		(ppm)	(ppm)	(ppm)	(ppm)	(ppm)	(ppm)	(ppm)	(ppm)	(ppm)	(ppm)	(ppm)	(ppm)	(ppm)	(ppm)	(ppm)	(ppm)	(ppm)	(ppm)	(ppm)	(ppm)	(ppm)	(ppm)
Isotope		^{59}Co	^{61}Ni	^{65}Cu	^{66}Zn	^{75}As	^{82}Se	^{95}Mo	^{101}Ru*	^{103}Rh*	^{108}Pd*	^{109}Ag	^{111}Cd	^{118}Sn	^{121}Sb	^{128}Te	^{185}Re	^{189}Os	^{193}Ir	^{195}Pt	^{197}Au	^{208}Pb	^{209}Bi
CD-00129A	1	12475	4274	2234	1,86	1,04	154	0,122	1,12	1,21	131	2,33	<0,054	0,035	0,047	1,25	<0,006	0,400	0,256	1,26	0,031	11,4	3,96
	2	5912	12662	303	0,954	0,708	222	0,132	0,137	0,060	0,487	6,66	0,062	<0,032	0,028	0,950	0,042	0,048	0,027	0,091	0,354	9,54	1,68
	3	6722	61,1	4,00	51,2	1,77	104	0,115	0,213	0,798	<0,010	0,081	0,996	0,114	0,065	1,15	0,090	0,154	0,071	<0,014	0,010	0,903	0,056
	4	8365	98,7	135	1,07	1,81	68,4	0,132	0,912	2,49	0,113	0,128	0,237	0,177	0,036	0,973	0,013	0,526	0,280	1,12	0,088	0,456	0,391
CD-00150B	1	2160	29932	470	6,28	0,843	214	0,111	<0,017	0,234	0,277	5,23	0,089	<0,032	0,021	4,69	<0,006	<0,016	0,014	<0,014	0,045	3,49	3,01
CD-RP010	1	5121	1289	92,2	<0,090	185	196	0,264	0,038	0,095	0,984	1,13	10,2	0,656	2,57	13,7	0,081	0,038	0,062	0,065	0,307	5,45	2,51
	2	5186	773	83,3	1099	217	50,5	0,247	0,163	0,645	0,315	0,875	6,70	0,466	1,80	2,03	0,032	0,201	0,106	0,503	0,126	4,00	1,59
	3	2923	1052	50,7	656	210	110	0,466	0,593	0,953	<0,010	1,98	14,8	1,11	2,93	2,23	0,092	0,466	0,220	0,117	0,158	5,07	2,36
	4	3049	745	125	22,8	128	61,1	0,121	0,164	0,085	0,205	0,149	0,326	0,074	0,100	1,56	0,024	0,099	0,095	0,186	0,034	0,898	0,331
CD-10603A	1	6978	614	111	549	216	54,5	0,559	0,948	2,84	0,512	3,35	27,6	2,75	6,89	3,67	0,076	0,256	0,422	0,097	0,284	15,3	5,82
	2	587	3272	30,7	5,54	1,02	87,5	0,106	<0,017	0,003	0,141	1,52	0,178	4,52	0,115	1,74	<0,006	<0,016	<0,004	<0,014	0,010	132	1,82
	3	7369	382	74,5	470	139	83,8	0,298	0,200	0,053	<0,010	1,47	18,9	0,773	3,03	2,48	0,191	0,114	0,245	0,048	0,200	7,68	2,59
	4	9845	428	372,4	167	78,2	165	0,228	0,061	0,031	0,030	0,791	5,63	1,69	1,23	3,66	0,040	0,056	0,059	0,042	0,084	3,91	2,56
	5	7234	372	6,70	0,512	34,0	66,8	0,126	0,218	0,028	0,017	0,040	<0,054	<0,032	<0,012	1,15	0,017	0,088	0,142	<0,014	<0,008	0,954	0,271
CD-00150C	1	8751	9217	2588	638	0,898	153	0,152	<0,017	0,021	0,573	6,33	2,21	0,034	0,027	4,62	<0,006	<0,016	0,011	<0,014	0,030	6,24	6,56
	2	2746	11125	2272	172	0,596	121	0,131	<0,017	0,014	0,233	7,54	0,945	0,044	0,038	1,63	<0,006	<0,016	0,008	<0,014	0,041	10,2	4,75
	3	7960	11032	2011	479	0,996	164	0,169	0,024	0,289	0,276	9,26	1,59	<0,032	0,076	4,37	0,088	<0,016	0,020	<0,014	0,055	29,8	5,24
	4	10427	97,3	74,5	2,28	3,19	109	0,159	0,169	13,1	<0,010	0,340	<0,054	<0,032	<0,012	0,857	0,035	0,031	0,110	<0,014	<0,008	0,335	0,452
	5	1788	32957	6,33	0,312	<0,456	136	0,117	<0,017	<0,003	0,075	2,04	<0,054	0,419	<0,012	0,466	<0,006	<0,016	<0,004	<0,014	<0,008	0,633	0,098
	6	6796	23461	512	35,8	0,745	130	0,114	<0,017	0,141	0,204	5,82	0,349	0,058	0,133	3,58	<0,006	<0,016	0,008	<0,014	0,066	22,0	8,24
	7	6103	48878	540	3,03	0,870	174	0,141	0,040	0,149	1,311	6,79	<0,054	<0,032	0,095	2,71	0,017	<0,016	0,014	<0,014	0,059	15,9	3,74
CD-RP008	1	4227	537	405	59,6	148	63,4	0,159	0,153	0,044	0,258	0,507	3,12	0,233	0,633	2,70	0,024	0,067	0,048	0,103	0,082	1,96	0,931
	2	3901	642	79,6	310	240	60,1	0,470	0,128	0,129	<0,010	1,13	12,8	0,777	1,75	4,38	0,035	0,049	0,045	0,062	0,078	3,03	1,71
	3	4669	726	62,8	179	160	35,6	0,303	0,594	0,087	<0,010	1,12	10,2	0,973	2,12	1,20	0,038	0,105	0,099	0,064	0,076	4,93	1,80
	4	4739	600	144	97,3	111	35,1	0,244	5,26	0,154	0,110	0,614	4,75	0,531	0,982	0,875	0,033	0,745	0,466	0,081	0,052	2,51	0,745
	5	4664	917	284	400	155	56,4	0,312	0,021	0,045	0,589	1,09	6,70	0,787	1,60	1,81	0,056	0,031	0,039	0,154	0,171	7,77	2,57
	6	5200	534	41,0	196	47,9	113	0,191	0,018	0,010	0,184	0,442	4,24	0,363	1,54	1,26	0,040	0,039	0,019	0,102	0,058	2,09	1,18
	7	3766	517	23,7	99,2	65,6	273	0,217	<0,017	0,006	0,115	0,587	4,61	0,433	0,959	1,75	0,015	<0,016	0,017	0,182	0,054	3,54	1,07
	8	4906	524	1,04	0,605	6,38	209	0,117	<0,017	<0,003	0,027	0,200	<0,054	0,037	<0,012	0,493	0,047	0,127	0,022	0,020	<0,008	2,84	0,003
	9	4892	469	1,91	0,220	85,3	33,2	0,109	0,083	0,680	0,015	0,008	<0,054	<0,032	<0,012	0,628	0,009	<0,016	0,018	0,035	<0,008	0,033	0,012
	10	5498	532	0,368	0,684	43,2	248	0,149	<0,017	<0,003	0,055	0,014	<0,054	<0,032	0,013	2,23	0,051	0,063	0,007	<0,014	<0,008	0,061	0,027
	11	4967	463	0,344	0,196	82,4	39,6	0,114	0,046	0,012	0,012	<0,012	<0,054	0,033	<0,012	0,540	0,010	<0,016	<0,004	0,073	<0,008	0,016	0,060

Element		Co	Ni	Cu	Zn	As	Se	Mo	Ru	Rh	Pd	Ag	Cd	Sn	Sb	Te	Re	Os	Ir	Pt	Au	Pb	Bi
		(ppm)	(ppm)	(ppm)	(ppm)	(ppm)	(ppm)	(ppm)	(ppm)	(ppm)	(ppm)	(ppm)	(ppm)	(ppm)	(ppm)	(ppm)	(ppm)	(ppm)	(ppm)	(ppm)	(ppm)	(ppm)	(ppm)
Isotope		^{59}Co	^{61}Ni	^{65}Cu	^{66}Zn	^{75}As	^{82}Se	^{95}Mo	^{101}Ru*	^{103}Rh*	^{108}Pd*	^{109}Ag	^{111}Cd	^{118}Sn	^{121}Sb	^{128}Te	^{185}Re	^{189}Os	^{193}Ir	^{195}Pt	^{197}Au	^{208}Pb	^{209}Bi
CD-00118	1	60,9	4520	0,419	0,354	0,731	202	0,109	0,018	0,004	<0,010	0,542	<0,054	0,099	<0,012	<0,194	<0,006	<0,016	0,004	<0,014	<0,008	1,89	0,398
CD-00150A	1	13779	240	242	<0,090	242	226	0,312	0,054	0,110	<0,010	1,33	19,2	0,773	1,97	3,01	0,068	0,023	0,034	0,066	0,112	4,89	4,70
	2	7076	1531	1536	<0,090	145	107	0,540	0,123	0,291	<0,010	3,96	33,5	1,45	5,21	4,24	0,084	0,028	0,069	0,068	0,185	12,4	5,21
	3	433	573	51,7	5,03	0,647	55,0	<0,028	<0,017	0,005	0,040	2,34	0,131	0,032	0,661	1,88	<0,006	<0,016	<0,004	<0,014	<0,008	117	0,321
	4	6894	1243	777	<0,090	131	155	0,307	0,075	0,045	0,336	2,35	15,8	1,30	3,03	4,66	0,016	<0,016	0,039	0,038	0,169	11,5	5,73
	5	8458	342	1653	1569	43,3	150	0,246	0,030	0,115	1,365	2,18	7,59	0,819	1,94	11,0	0,024	<0,016	0,021	0,067	0,133	7,63	7,77
	6	7616	517	270	1289	84,7	178	0,289	0,025	0,039	1,752	2,00	9,22	0,884	2,33	11,9	0,069	<0,016	0,018	0,182	0,142	10,9	9,08
CD-09410	1	6145	698	0,591	0,256	101	18,8	0,112	<0,017	9,50	0,084	1,95	<0,054	0,011	<0,012	15,3	0,076	0,023	<0,004	<0,014	0,073	1,82	12,0
	2	2225	1704	41,9	1,78	0,694	33,2	0,135	0,032	0,043	0,177	7,45	0,461	0,115	0,101	0,740	0,011	0,028	0,006	0,017	0,099	1220	18,2
CD-98042A	1	8379	749	13872	13,3	104	57,3	0,213	0,159	3,62	2,977	5,77	0,065	0,053	0,025	15,9	0,242	0,045	0,069	4,05	0,078	11,6	6,19
	2	10613	517	25603	20,2	47,0	66,6	0,106	0,250	2,16	0,639	1,98	0,107	<0,032	<0,012	1,86	0,013	0,082	0,038	0,470	0,034	12,1	4,50
	3	8035	600	186	358	131	54,7	0,503	0,253	0,180	0,023	2,04	19,6	1,21	5,40	1,44	0,136	0,081	0,074	0,164	0,142	11,3	4,00
	4	9124	591	54,9	382	108	39,9	0,456	0,450	1,01	<0,010	1,91	19,0	1,20	4,89	1,78	0,115	0,102	0,108	0,089	0,120	9,82	3,54
CD-RP012	1	8100	223	163	0,549	0,596	75,4	0,116	0,232	3,11	0,368	0,034	<0,054	0,233	<0,012	0,279	0,016	0,048	0,031	0,053	0,002	0,549	0,045
	2	7364	261	172	205	62,8	57,1	0,307	0,297	2,66	<0,010	1,49	12,1	1,01	2,47	0,852	0,042	0,091	0,055	0,082	0,072	4,66	2,20
	3	7308	377	67,5	475	148	65,4	0,400	0,339	11,0	<0,010	2,72	22,7	1,50	5,03	1,63	0,072	0,073	0,061	0,079	0,133	12,0	4,61
	4	9850	531	112	624	161	88,3	0,377	0,641	8,47	<0,010	2,29	23,3	1,13	4,79	1,66	0,072	0,146	0,135	0,163	0,114	10,1	3,91
	5	6377	11963	4376	63,3	12,9	103	0,138	0,079	0,134	4,881	2,53	2,98	0,475	0,479	0,694	0,026	0,035	0,025	0,282	0,069	24,3	0,600
CD-11054	1	4008	260	56,8	228	119	63,3	0,219	0,113	0,529	0,269	0,614	5,45	0,372	1,72	0,614	0,029	0,092	0,152	0,661	0,090	6,52	1,58
	2	6443	261	26,5	200	46,6	51,3	0,326	0,035	0,089	<0,010	0,754	9,22	0,442	1,87	0,810	0,072	0,030	0,015	0,057	0,034	3,96	2,21
	3	4087	391	233	185	54,9	76,3	0,284	0,086	0,107	0,398	1,38	8,24	0,596	2,65	1,10	0,025	0,051	0,031	0,088	0,060	11,4	5,21
	4	4883	326	251	0,526	32,4	655	2,65	0,031	0,015	0,918	1,42	0,242	6,24	0,074	2,37	0,021	0,022	0,008	0,024	0,265	7,49	4,28
	5	2169	246	25,1	107	37,7	67,0	0,169	0,045	0,024	0,063	0,763	4,47	0,447	1,17	0,619	0,013	<0,016	0,011	0,048	0,033	3,03	1,55
	6	334	535	41,0	400	111	129	0,368	0,043	0,038	0,025	1,55	16,7	1,11	3,82	1,34	0,036	0,040	0,034	0,089	0,085	7,49	2,93
	7	2788	847	46,1	321	105	102	3,17	0,040	0,031	0,086	1,75	14,2	0,787	2,56	1,01	0,074	<0,016	0,023	0,071	0,108	11,0	3,96

ANNEXE 15: MATÉRIAUX DE RÉFÉRENCES POUR LES ANALYSES LA-ICP-MS DES SULFURES

Element		Co	Ni	Cu	Zn	As	Se	Mo	Ru	Rh	Pd	Ag	Cd	Sn	Sb	Te	Re	Os	Ir	Pt	Au	Pb	Bi
Isotope		^{59}Co	^{61}Ni	^{65}Cu	^{66}Zn	^{75}As	^{82}Se	^{95}Mo	^{101}Ru*	^{103}Rh*	^{108}Pd*	^{109}Ag	^{111}Cd	^{118}Sn	^{121}Sb	^{128}Te	^{185}Re	^{189}Os	^{193}Ir	^{195}Pt	^{197}Au	^{208}Pb	^{209}Bi
Po-727	Working value (ppm)								36,26	41,62	43,82							46,85	47,81	35,37	45,79		
	Mean (ppm) n=27								36,46	41,56	43,36							46,65	47,96	35,47	45,92		
	Standard Derivation								0,626	0,524	0,829							0,984	0,944	0,691	1,522		
	RSD (%)								1,72	1,26	1,91							2,11	1,97	1,95	3,32		
Mass-1	Working value (ppm)	67		134000	210000	65	53	61				67	70	55	55	21,1						80,26	66,43
	Mean (ppm) n=27	67,16		134288	176627	65,14	53,15	61,10				67,06	69,97	55,22	55,14	21,17						80,10	66,05
	Standard Derivation	1,39		1912	76934	1,14	1,49	0,88				1,01	2,34	1,26	0,96	0,46						1,44	1,02
	RSD (%)	2,06		1,42	43,56	1,76	2,81	1,43				1,51	3,34	2,28	1,74	2,17						1,80	1,55
JB-mss-5	Working value (ppm)		10487	205		79	48,35	0,23	21,72	61,40	65,20	53	0,13	0,34	61,3	44	20,7	42,52	43,98	39,90	35,90	71,5	76,1
	Mean (ppm) n=27		10468	215		58	56,83	0,74	21,52	62,88	60,29	66	0,10	0,66	51,5	42	20,7	57,00	41,69	42,62	37,87	83,5	84,2
	Standard Derivation		132	31,8		4,39	7,60	0,054	1,07	2,17	1,89	2,33	0,04	0,152	2,35	5,23	0,395	5,59	3,34	1,34	2,92	2,9	2,84
	RSD (%)		1,26	14,8		7,54	13,38	7,21	4,95	3,45	3,13	3,51	39,2	23,0	4,56	12,4	1,91	9,81	8,01	3,14	7,72	3,5	3,38
GSE	Working value (ppm)	380	440	380				390				200		280								378	320
	Mean (ppm) n=27	334	424	386				415				219		302								412	343
	Standard Derivation	20,2	12,0	7,71				9,04				8,58		6,65								10,5	11,6
	RSD (%)	6,07	2,84	1,99				2,18				3,92		2,20								2,6	3,39

ANNEXE 16: ANALYSES LA-ICP-MS DE MAGNÉTITES

Element		Mg	Al	Si	Ca	Sc	Ti	V	Cr	Mn	Co	Ni	Cu	Zn	Ga	Ge	Y	Zr	Nb	Mo	Sn	Hf	Ta	W	Pb
		(ppm)	(ppm)	(ppm)	(ppm)	(ppm)	(ppm)	(ppm)	(ppm)	(ppm)	(ppm)	(ppm)	(ppm)	(ppm)	(ppm)	(ppm)	(ppm)	(ppm)	(ppm)	(ppm)	(ppm)	(ppm)	(ppm)	(ppm)	(ppm)
Isotope		^{25}Mg	^{27}Al	^{29}Si	^{44}Ca	^{45}Sc	^{47}Ti	^{51}V	^{52}Cr	^{55}Mn	^{59}Co	^{60}Ni	^{63}Cu	^{66}Zn	^{71}Ga	^{74}Ge	^{89}Y	^{90}Zr	^{93}Nb	^{95}Mo	^{118}Sn	^{178}Hf	^{181}Ta	^{182}W	^{208}Pb
CD-00150C	1	288	2798	<648	<12,3	1,72	722	5200	2683	335	22,3	535	<0,095	48,3	52,5	0,856	<0,013	0,030	0,021	<0,143	0,155	<0,015	<0,006	<0,015	0,045
	2	395	1805	1510	18,0	1,87	741	5509	2795	298	16,9	485	6,47	27,5	55,6	0,992	0,052	0,047	0,035	<0,143	0,165	<0,015	<0,006	<0,015	0,020
	3	813	3531	<648	15,1	1,70	816	6703	2927	309	23,0	529	180	53,4	52,6	1,06	0,095	0,114	0,022	<0,143	0,278	<0,015	<0,006	<0,015	0,029
	4	103	883	<648	<12,3	0,990	436	5876	2956	2718	34,5	748	4,03	27,3	48,9	0,899	<0,013	<0,015	<0,018	0,396	0,083	<0,015	<0,006	<0,015	0,058
	5	62,1	845	<648	<12,3	3,67	2208	6199	3092	2790	17,6	488	4,32	27,3	51,9	0,856	<0,013	0,040	0,178	0,194	0,135	0,016	<0,006	<0,015	0,022
CD-RP012	1	148	2171	<648	<12,3	1,28	636	9754	1385	235	14,8	256	0,992	21,9	70,1	0,730	<0,013	<0,015	<0,018	<0,143	0,089	<0,015	<0,006	<0,015	0,567
	2	474	2713	3259	30,9	0,899	590	9797	1374	223	12,3	279	0,779	53,1	68,0	0,779	0,095	0,038	<0,018	<0,143	0,112	<0,015	<0,006	<0,015	0,425
	3	106	1482	<648	29,0	0,800	572	9393	1396	222	15,7	269	0,305	35,4	66,6	0,871	<0,013	0,030	<0,018	<0,143	0,137	<0,015	<0,006	<0,015	0,312
	4	227	3003	<648	744	1,63	758	9209	1381	263	20,7	298	0,210	179	71,8	0,645	<0,013	0,113	0,018	<0,143	0,176	<0,015	<0,006	<0,015	0,638
	5	189	2804	<648	<12,3	1,40	938	9832	1415	265	25,5	354	0,659	19,9	75,7	0,758	<0,013	0,026	<0,018	<0,143	0,147	<0,015	<0,006	0,015	0,205
	6	79,3	2493	878	<12,3	1,99	661	9563	1551	2543	18,5	281	0,432	12,8	72,6	1,04	<0,013	<0,015	<0,018	0,347	0,482	<0,015	<0,006	<0,015	0,312
	7	142	2543	1417	333	3,57	1197	9606	1459	2727	135	322	4,39	34,7	71,6	0,822	<0,013	0,046	0,124	<0,143	2,20	<0,015	<0,006	0,016	0,034
	8	248	1941	1672	22,7	1,40	506	9110	1332	2720	18,8	694	6,02	9,28	79,3	0,885	0,022	<0,015	<0,018	0,184	0,772	0,016	<0,006	0,018	0,305
	9	2338	5667	7863	66,6	1,74	716	10420	1544	2706	27,6	295	3,26	46,0	77,0	1,01	0,101	0,375	<0,018	0,312	2,55	0,020	<0,006	0,099	0,106
	10	1169	6305	4250	26,2	2,62	393	9868	1927	2578	15,7	237	6,38	170	82,8	0,857	0,030	0,099	<0,018	0,411	8,50	0,028	<0,006	0,018	0,035
CD-00150A	1	167	930	<648	<12,3	0,463	328	217	93,9	357	33,0	584	30,5	24,7	18,8	0,506	<0,013	0,059	<0,018	<0,143	0,095	<0,015	<0,006	<0,015	0,054
	2	133	937	<648	<12,3	0,403	309	174	950	327	26,5	537	0,232	15,5	19,9	0,616	<0,013	0,019	<0,018	<0,143	0,104	<0,015	<0,006	<0,015	0,094
	3	122	870	<648	<12,3	0,408	321	167	18,13	309	20,6	516	0,674	65,3	19,6	0,499	<0,013	0,028	<0,018	<0,143	0,135	<0,015	<0,006	<0,015	0,111
	4	87,0	876	<648	<12,3	0,441	339	202	7,55	374	36,9	621	2,68	23,9	19,0	0,573	<0,013	<0,015	<0,018	<0,143	0,080	<0,015	<0,006	<0,015	0,043
	5	219	1146	870	<12,3	0,885	96	39,9	21,03	2944	36,3	711	0,740	102	32,5	1,001	0,017	0,028	<0,018	0,428	8,70	<0,015	<0,006	<0,015	0,392
	6	189	949	1958	<12,3	0,841	127	34,2	6,82	2929	24,4	567	0,435	24,7	28,2	0,508	<0,013	<0,015	<0,018	0,305	11,6	<0,015	<0,006	<0,015	0,116
	7	194	1079	1885	15,2	0,877	124	42,6	312	2987	22,8	624	8,92	18,6	29,1	0,718	0,019	<0,015	<0,018	0,471	0,645	<0,015	<0,006	<0,015	0,181
	8	198	980	3698	79,8	2,00	468	84,3	6,74	2792	22,0	560	218	30,5	27,5	0,711	<0,013	<0,015	<0,018	0,196	8,70	<0,015	<0,006	<0,015	0,080
	9	290	885	2908	16,7	1,55	431	142	246	2857	15,3	342	1160	1305	23,9	0,769	0,047	0,025	<0,018	0,152	7,32	0,028	<0,006	0,036	0,370
	10	152	816	1443	12,4	0,850	368	189	107	2755	43,4	500	268	31,3	25,1	0,638	<0,013	<0,015	<0,018	0,261	2,97	<0,015	<0,006	0,018	0,160
	11	602	1805	3169	45,7	1,07	579	323	120	2799	29,4	840	0,435	19,6	21,2	0,566	0,032	0,031	<0,018	<0,143	0,885	<0,015	<0,006	0,025	0,067
	12	1407	1987	4786	732	1,08	539	1682	9390	2719	59,5	732	5,08	26,8	20,4	0,689	0,066	0,088	<0,018	0,160	1,67	<0,015	<0,006	0,045	0,167
	13	226	1196	1711	12,7	0,924	114	27,8	7,27	2719	25,5	669	0,406	21,0	29,6	0,674	0,016	0,015	0,030	0,232	6,89	<0,015	<0,006	<0,015	0,203
	14	428	1196	2429	334	1,25	101	28,9	27,7	2683	26,5	730	0,660	18,8	29,4	0,573	0,065	0,025	<0,018	0,225	3,99	<0,015	<0,006	0,019	0,048
	15	125	845	1131	20,3	0,892	168	63,4	11,7	2686	21,6	785	29,0	25,6	30,2	0,805	<0,013	<0,015	<0,018	0,232	2,10	0,017	<0,006	<0,015	0,099

Element		Mg	Al	Si	Ca	Sc	Ti	V	Cr	Mn	Co	Ni	Cu	Zn	Ga	Ge	Y	Zr	Nb	Mo	Sn	Hf	Ta	W	Pb
		(ppm)	(ppm)	(ppm)	(ppm)	(ppm)	(ppm)	(ppm)	(ppm)	(ppm)	(ppm)	(ppm)	(ppm)	(ppm)	(ppm)	(ppm)	(ppm)	(ppm)	(ppm)	(ppm)	(ppm)	(ppm)	(ppm)	(ppm)	(ppm)
Isotope		^{25}Mg	^{27}Al	^{29}Si	^{44}Ca	^{45}Sc	^{47}Ti	^{51}V	^{52}Cr	^{55}Mn	^{59}Co	^{60}Ni	^{63}Cu	^{66}Zn	^{71}Ga	^{74}Ge	^{89}Y	^{90}Zr	^{93}Nb	^{95}Mo	^{118}Sn	^{178}Hf	^{181}Ta	^{182}W	^{208}Pb
CD-10551	1	155	2085	<648	44,3	0,592	583	1003	5,67	329	19,4	575	0,116	24,0	118	0,611	<0,013	<0,015	<0,018	<0,143	0,104	<0,015	<0,006	0,120	0,083
	2	179	2150	1743	96,6	0,617	601	991	5,40	313	15,7	522	0,799	30,5	115	0,647	0,044	0,022	<0,018	0,145	0,126	<0,015	<0,006	0,161	0,056
	3	182	2862	726	50,8	0,513	458	989	5,67	246	18,8	632	0,320	11,0	109	0,959	<0,013	0,029	<0,018	<0,143	0,166	<0,015	0,006	0,033	0,160
	4	814	5375	3341	67,6	1,18	1830	989	5,52	320	20,0	601	1,09	9,73	115	0,908	0,020	0,111	0,071	<0,143	0,097	<0,015	0,174	1,068	0,068
	5	269	1068	<648	14,2	1,33	599	946	5,04	341	20,6	590	<0,095	15,2	123	0,697	<0,013	0,026	<0,018	<0,143	0,106	<0,015	<0,006	<0,015	1,53
	6	132	1954	<648	83,5	1,21	607	956	5,70	350	20,7	596	1,89	16,1	125	0,692	<0,013	0,049	<0,018	<0,143	0,097	<0,015	<0,006	0,017	0,044
CD-98042A	1	2318	2228	2076	82,4	0,554	433	21800	10167	748	36,7	370	0,270	107	48,0	0,561	<0,013	0,257	0,095	<0,143	0,098	<0,015	<0,006	<0,015	0,070
	2	122	724	<648	<12,3	0,567	632	14707	13530	480	26,4	341	0,235	46,4	47,1	0,443	<0,013	0,089	0,105	<0,143	0,094	<0,015	<0,006	<0,015	0,173
CD-02004	1	58,9	518	<648	<12,3	2,02	353	3828	4880	277	14,9	352	0,110	24,1	18,2	0,797	<0,013	0,034	0,042	<0,143	0,130	<0,015	<0,006	<0,015	0,315
	2	1794	2304	<648	14,1	2,34	286	3775	4694	245	14,4	322	1,87	27,9	19,2	0,866	0,024	0,047	0,044	<0,143	0,110	<0,015	<0,006	<0,015	3,23
CD-RP008	1	128	773	1788	<12,3	1,41	3305	5308	501	446	7,34	618	0,630	42,6	34,3	0,913	<0,013	0,020	1,409	<0,143	0,134	<0,015	0,042	0,051	0,182
	2	1223	4457	6725	451	1,09	410	5301	596	2624	24,3	979	4,15	44,9	32,6	0,851	<0,013	0,074	<0,018	0,229	3,36	<0,015	<0,006	<0,015	1,29
	3	73,7	538	<648	29,3	1,14	658	4908	579	2583	24,8	638	9,30	150	27,3	0,823	0,019	<0,015	0,089	0,272	9,30	<0,015	<0,006	<0,015	0,143
	4	58,9	700	<648	<12,3	1,11	431	5737	584	2567	16,7	685	5,72	49,0	36,8	0,966	<0,013	<0,015	<0,018	0,293	6,65	<0,015	<0,006	<0,015	0,103
	5	98,7	779	980	30,8	1,13	456	5845	710	2625	12,9	765	10,7	57,2	37,2	1,29	<0,013	<0,015	<0,018	<0,143	8,08	<0,015	<0,006	0,018	0,122
	6	73,0	699	672	<12,3	1,02	423	5752	567	2747	9,77	723	0,680	57,2	40,5	1,19	<0,013	<0,015	<0,018	<0,143	3,00	<0,015	<0,006	<0,015	0,179
	7	1502	5652	8298	201	1,17	391	5501	607	2654	45,1	871	0,744	39,3	31,7	1,09	0,030	0,072	<0,018	0,186	6,22	<0,015	<0,006	<0,015	0,994
CD-00109	1	46,3	1045	<648	<12,3	2,87	798	10980	138	262	36,6	715	1,64	43,1	53,8	0,708	0,021	0,052	0,036	<0,143	0,246	<0,015	<0,006	<0,015	0,363
CD-00118	1	124	770	1346	27,4	0,924	467	1871	7,01	2815	16,3	871	1901	21,2	44,9	0,691	<0,013	0,016	<0,018	0,295	1,80	<0,015	0,006	<0,015	0,065
	2	79,2	675	2520	<12,3	1,56	727	1753	394	2765	27,9	1145	4,10	28,9	49,5	0,835	<0,013	<0,015	<0,018	0,396	7,99	<0,015	<0,006	0,065	0,092
	3	109	589	1094	57,6	1,56	490	1757	6,70	2621	18,3	986	245	16,6	49,0	0,698	0,045	<0,015	<0,018	<0,143	3,74	<0,015	<0,006	0,035	0,115
CD-00150B	1	83,3	630	<648	<12,3	1,50	488	5227	2434	2729	25,3	922	0,410	19,6	53,8	0,799	<0,013	0,043	<0,018	<0,143	0,245	<0,015	<0,006	<0,015	5,76
	2	2930	5544	8856	142	2,61	700	6134	2851	2657	25,2	850	0,533	86,4	53,6	0,886	0,288	0,194	<0,018	0,151	2,30	<0,015	0,043	0,022	0,051
	3	585	2369	1548	59,8	1,39	683	5731	2398	2650	41,0	1015	1,10	94,3	55,5	0,914	0,035	0,018	<0,018	0,166	0,454	<0,015	<0,006	<0,015	0,034
	4	2736	6768	6192	180	3,05	590	5954	2830	2678	166	655	4,46	547	61,9	1,10	0,071	0,044	0,037	0,194	0,461	<0,015	<0,006	0,864	1,44

ANNEXE 17: ANALYSES LA-ICP-MS D'ILMÉNITES

Element		Mg	Al	Si	Ca	Sc	Ti	V	Cr	Mn	Co	Ni	Cu	Zn	Ga	Ge	Y	Zr	Nb	Mo	Sn	Hf	Ta	W	Pb
		(ppm)	(ppm)	(ppm)	(ppm)	(ppm)	(ppm)	(ppm)	(ppm)	(ppm)	(ppm)	(ppm)	(ppm)	(ppm)	(ppm)	(ppm)	(ppm)	(ppm)	(ppm)	(ppm)	(ppm)	(ppm)	(ppm)	(ppm)	(ppm)
Isotope		^{25}Mg	^{27}Al	^{29}Si	^{44}Ca	^{45}Sc	^{47}Ti	^{51}V	^{52}Cr	^{55}Mn	^{59}Co	^{60}Ni	^{63}Cu	^{66}Zn	^{71}Ga	^{74}Ge	^{89}Y	^{90}Zr	^{93}Nb	^{95}Mo	^{118}Sn	^{178}Hf	^{181}Ta	^{182}W	^{208}Pb
CD-00150C	1	284	101	2252	25,5	99,2	281924	1867	496	17043	11,0	20,5	2,60	106	0,890	<0,125	0,446	13,0	34,0	2,00	0,766	1,00	1,97	1,62	0,045
	2	200	56,7	4505	125	304	258649	1731	443	8634	18,8	28,5	1,88	38,3	0,938	<0,125	0,083	8,67	27,0	0,420	0,623	0,439	0,935	0,999	0,043
CD-RP012	1	138	116	3855	28,6	52,7	285647	2834	321	10291	9,13	11,7	3,12	44,9	0,683	<0,125	0,460	13,0	24,6	1,41	1,20	1,69	0,768	0,180	0,312
	2	698	738	1990	126	308	252970	2038	385	5177	9,14	29,4	2,47	169	3,79	0,140	1,358	176	34,6	0,991	4,59	6,28	1,73	0,193	<0,011
	3	279	67,9	1366	191	294	261782	2486	298	5474	11,5	297	2,06	54,3	0,485	<0,125	0,174	17,7	35,9	0,474	5,36	3,07	2,00	0,180	0,019
	4	460	48,5	977	109	301	251869	2853	321	5427	10,8	58,7	10,6	69,4	0,734	0,242	0,191	20,5	36,7	0,565	3,41	4,41	2,13	0,202	0,044
	5	477	1046	3231	389	282	236815	2467	315	5236	182	1322	1689	42,6	1,20	0,147	0,219	22,8	33,4	0,587	6,98	2,68	1,52	0,190	0,485
CD-98042A	1	1457	24,3	2054	44,5	46,1	281071	5252	1852	15495	43,4	19,0	1,90	93,6	0,848	0,143	0,511	6,87	33,7	2,10	0,211	0,962	1,72	1,01	0,228
	2	1391	21,6	2967	25,1	44,8	277648	5652	1134	15894	40,4	26,6	1,92	87,1	0,958	0,126	0,517	7,97	33,8	1,93	0,251	0,913	1,82	0,936	0,913
	3	1731	19,8	1092	120	307	276507	6238	809	7702	72,3	23,0	179	71,8	0,947	<0,125	0,119	9,32	15,1	0,475	0,951	0,407	0,400	0,650	0,152
	4	1369	18,6	1103	415	288	271562	4450	1685	7881	46,0	87,5	17,5	116	0,856	0,156	0,162	11,6	25,9	0,403	1,98	1,08	1,32	1,44	0,129
	5	1012	137	2815	2130	289	276507	4180	519	8189	39,3	61,6	4,79	97,4	0,738	0,445	0,221	5,66	24,9	0,422	3,73	0,825	1,41	5,44	0,087
CD-RP008	1	108	33,0	2327	20,2	67,0	274303	1835	52,3	10987	1,22	41,0	2,37	33,8	0,492	<0,125	0,439	1,58	125	2,12	1,71	0,340	6,56	2,90	0,515
	2	121	52,0	1831	19,9	63,0	273921	1824	52,3	11174	1,40	34,9	1,92	28,3	0,543	<0,125	0,451	1,66	125	1,89	1,40	0,373	6,08	2,39	0,282
	3	116	41,1	1373	17,9	65,6	267817	1816	49,7	10984	1,39	36,0	1,93	27,9	0,571	<0,125	0,418	1,72	122	2,02	1,66	0,502	5,44	2,71	0,214
	4	237	519	2060	1091	332	280788	1083	28,0	5574	10,5	130	1,96	33,2	0,454	<0,125	0,068	0,61	87,1	0,420	11,8	0,041	8,06	0,942	0,298
CD-00109	1	475	516	4365	27,0	137	293050	3382	330	10401	23,9	77,3	2,66	29,5	0,790	<0,125	0,506	5,60	29,1	1,53	0,471	0,542	1,59	23,4	0,205
	2	434	116	911	15,9	130	294189	2968	178	10105	28,8	49,7	2,24	33,9	0,881	<0,125	0,489	6,57	29,2	1,53	0,345	0,679	1,56	25,7	0,683
	3	419	197	1822	326	177	282421	4753	82,6	10120	19,5	94,0	7,97	19,0	0,616	<0,125	0,915	2,71	31,4	1,69	0,509	0,448	1,74	25,6	0,156
	4	438	148	1708	30,4	44,7	285837	3223	72,3	10021	29,6	85,4	8,35	37,2	0,854	<0,125	0,676	8,62	25,6	1,59	0,611	0,562	1,42	24,2	0,131
CD-00118	1	209	629	2786	1976	308	254930	612	5,62	6079	4,77	56,2	233	31,5	1,41	0,178	0,081	3,97	10,4	0,500	2,44	0,189	0,258	10,6	0,244
	2	88,4	174	1957	1332	323	267880	566	5,25	6312	6,42	40,4	222	28,0	0,744	0,211	0,130	3,57	11,9	0,318	5,55	0,189	0,333	8,73	0,093
	3	105	21,8	766	381	293	230140	1339	29,6	6338	9,88	192	15,91	33,2	1,01	0,185	0,075	5,40	14,4	0,899	32,6	1,27	1,16	2,66	0,181
	4	96,9	174	1432	152	323	251600	582	4,59	6556	6,18	40,8	1,68	27,2	0,751	0,174	0,078	4,56	9,93	0,574	14,4	0,307	0,273	10,1	0,192
	5	68,2	72,9	1820	1554	322	253820	580	4,51	6294	5,56	38,3	4,37	31,1	0,825	0,137	0,080	4,87	13,0	0,481	7,55	0,178	0,185	10,7	0,307

ANNEXE 18: MATÉRIAUX DE RÉFÉRENCES POUR LES ANALYSES LA-ICP-MS DES OXIDES DE FE-TI

Element		Mg	Al	Si	Ca	Sc	Ti	V	Cr	Mn	Co	Ni	Cu	Zn	Ga	Ge	Y	Zr	Nb	Mo	Sn	Hf	Ta	W	Pb
Isotope		^{25}Mg	^{27}Al	^{29}Si	^{44}Ca	^{45}Sc	^{47}Ti	^{51}V	^{52}Cr	^{55}Mn	^{59}Co	^{60}Ni	^{63}Cu	^{66}Zn	^{71}Ga	^{74}Ge	^{89}Y	^{90}Zr	^{93}Nb	^{95}Mo	^{118}Sn	^{178}Hf	^{181}Ta	^{182}W	^{208}Pb
GSE	Working value (ppm)	21106	68804	250994	52858	530	450	440	400	590	380	440	380	460	490	320	410	410	420	390	280	395	390	430	378
	Mean (ppm) n=17	21119	68724	252212	52882	530	452	443	401	590	383	442	381	465	491	322	410	411	420	393	282	395	391	431	380
	Standard Derivation	262	1611	5655	1080	12,3	11,3	11,6	4,84	7,91	13,1	8,24	6,07	19,3	6,78	8,70	10,6	9,98	5,7	10,5	6,57	9,12	8,63	7,38	6,81
	RSD (%)	1,24	2,34	2,24	2,04	2,32	2,50	2,61	1,21	1,34	3,42	1,87	1,59	4,14	1,38	2,70	2,57	2,43	1,36	2,68	2,33	2,31	2,21	1,71	1,79
GSD	Working value (ppm)	21709	70922	248657	51429	52	7432	44	42	220	40	58	42	54	54	32	42	42	42	39	29	39	40	43	50
	Mean (ppm) n=15	21865	72952	253963	51975	62,9	7685	46,2	50,6	365	40,5	60,7	42,5	55,3	52,3	32,2	42,5	44,6	42,9	39,8	28,7	41,8	40,4	44,3	47,3
	Standard Derivation	365	2152	7184	1049	4,96	266	0,954	1,23	109	0,356	1,72	1,79	5,72	1,49	1,50	2,09	1,76	0,83	1,66	1,46	2,02	1,33	1,67	2,81
	RSD (%)	1,67	2,95	2,83	2,02	7,88	3,46	2,06	2,43	29,9	0,881	2,83	4,22	10,3	2,85	4,66	4,92	3,95	1,93	4,16	5,07	4,83	3,30	3,76	5,93
BC-28	Working value (ppm)	11618	20787				87615	9603	1172	2125	241	573		588	41,1	0,856	0,080	27,5	1,72	0,760	2,20	0,583	0,070		
	Mean (ppm) n=18	10962	17376				65386	8341	1286	2296	286	708		392	43,3	0,749	0,126	19,1	1,34	0,611	1,79	0,754	0,109		
	Standard Derivation	839	1717				3849	208	58,3	404	19,5	378		64,0	2,42	0,058	0,017	1,86	0,099	0,075	0,64	0,069	0,016		
	RSD (%)	7,65	9,88				5,89	2,50	4,53	17,6	6,82	53,5		16,3	5,59	7,77	13,2	9,75	7,38	12,2	35,8	9,14	14,4		

ANNEXE 19: MICROPHOTOGRAPHIES DES OXIDES DE FE-TI PRÉSENTS DANS LA GABBRONORITE À OXIDES

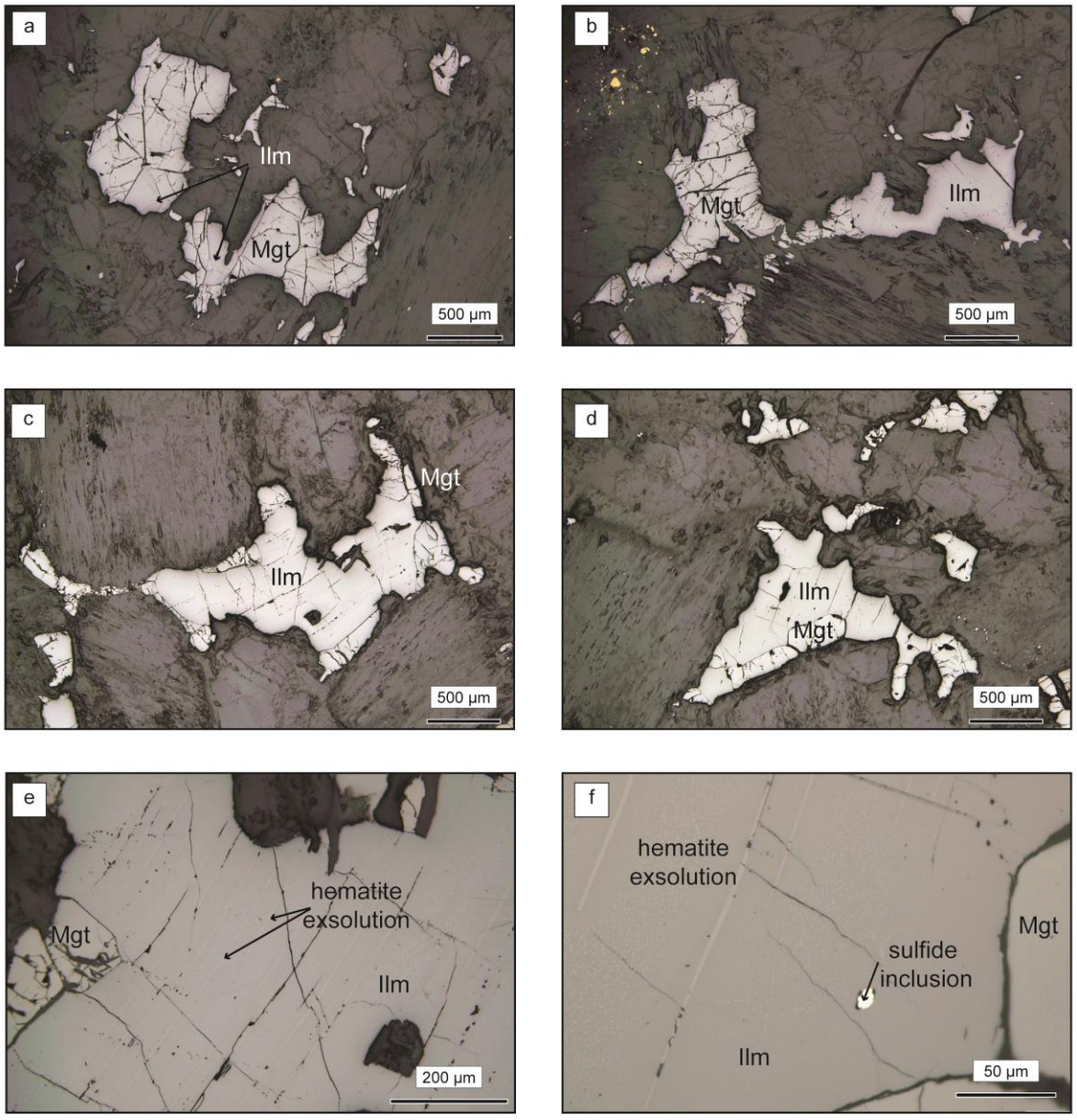

ANNEXE 20: ANALYSES LA-ICP-MS DES OXIDES DE FE-TI DE LA GABBRONORITE À OXIDES

Les oxides de Fe-Ti présents dans la gabbronorite à oxides ont été analysés par LA-ICP-MS suivant le protocole décrit dans le chapitre 2. Un faisceau de laser de 33 µm, une fréquence de 15 Hz, une puissance de 5 mJ et un stade de vitesse de 5 $\mu.s^{-1}$ ont été utilisés au cours de l'analyse.

Element		Mg	Al	Si	P	Ca	Sc	Ti	V	Cr	Mn	Co	Ni	Cu	Zn	Ga	Ge	As	Y	Zr	Nb	Mo	Sn	Hf	Ta	W	Pb
		(ppm)	(ppm)	(ppm)	(ppm)	(ppm)	(ppm)	(ppm)	(ppm)	(ppm)	(ppm)	(ppm)	(ppm)	(ppm)	(ppm)	(ppm)	(ppm)	(ppm)	(ppm)	(ppm)	(ppm)	(ppm)	(ppm)	(ppm)	(ppm)	(ppm)	(ppm)
Isotope		^{24}Mg	^{27}Al	^{29}Si	^{31}P	^{44}Ca	^{45}Sc	^{47}Ti	^{51}V	^{52}Cr	^{55}Mn	^{59}Co	^{60}Ni	^{63}Cu	^{66}Zn	^{71}Ga	^{74}Ge	^{75}As	^{89}Y	^{90}Zr	^{93}Nb	^{95}Mo	^{118}Sn	^{178}Hf	^{181}Ta	^{182}W	^{208}Pb
Magnetite																											
CD-00139B	1	56,4	510	< 978	< 1,94	< 31,1	0,213	448	8502	2373	325	22,0	341	0,174	11,0	14,1	0,868	1,07	< 0,005	< 0,008	< 0,006	0,069	< 0,237	< 0,010	< 0,004	< 0,020	0,083
	2	50,7	519	< 978	8,54	< 31,1	0,313	417	8032	3178	351	21,7	219	0,166	12,4	13,9	0,933	0,991	0,007	0,009	< 0,006	0,072	< 0,237	< 0,010	< 0,004	< 0,020	0,033
CD-00150C	1	34,8	1125	1230	9,77	< 31,1	0,161	673	9523	2695	246	73,2	414	0,253	119	33,9	0,738	0,781	< 0,005	< 0,008	0,011	< 0,041	< 0,237	< 0,010	< 0,004	< 0,020	0,131
	2	42,5	1100	< 978	< 1,94	< 31,1	0,183	687	7931	2892	260	64,3	359	0,259	104	38,1	0,716	0,666	< 0,005	< 0,008	< 0,006	< 0,041	< 0,237	< 0,010	< 0,004	0,058	0,144
	3	24,1	1014	< 978	< 1,94	< 31,1	0,274	340	10470	2580	234	85,4	435	0,239	40,5	35,4	0,905	0,680	< 0,005	< 0,008	< 0,006	< 0,041	0,434	< 0,010	< 0,004	< 0,020	0,130
	4	28,5	1295	< 978	< 1,94	< 31,1	0,384	543	9841	2460	231	74,8	419	0,182	98,4	41,5	0,738	0,615	< 0,005	< 0,008	< 0,006	0,061	< 0,237	< 0,010	< 0,004	< 0,020	0,104
CD-02004	1	25,4	459	1693	13,0	< 31,1	0,463	250	9067	5460	237	33,6	337	0,152	22,4	20,1	0,644	0,745	< 0,005	< 0,008	0,011	0,208	< 0,237	< 0,010	< 0,004	< 0,020	0,031
	2	36,3	577	< 978	< 1,94	< 31,1	0,412	174	10246	5362	259	36,8	303	0,362	31,7	21,9	0,724	0,564	< 0,005	0,018	0,009	0,260	< 0,237	0,043	< 0,004	< 0,020	0,042
Ilmenite																											
CD-00139B	1	692	861	2356	10,7	78,8	23,1	294480	2187	266	17312	17,1	17,6	43,4	75,8	0,674	0,140	1,13	0,098	0,482	3,38	0,762	0,479	0,059	0,110	0,357	3,20
	2	151	265	3350	25,4	210	23,9	279388	2864	202	16675	16,1	19,5	6,26	41,5	0,637	0,206	1,15	0,077	0,909	10,7	0,718	1,73	0,401	0,626	0,493	0,401
	3	593	769	6110	8,10	6184	30,7	295216	2801	578	18206	17,5	31,0	545	302	1,44	0,508	1,15	0,126	3,13	7,14	0,751	2,50	0,578	0,307	0,398	27,2
	4	223	110	1804	7,36	442	27,3	296873	2007	221	16877	15,4	8,01	3,79	34,1	0,427	0,225	1,26	0,088	0,758	2,50	0,629	< 0,237	0,056	0,073	0,629	0,283
	5	246	151	< 978	< 1,94	902	42,6	319400	3000	293	19841	16,8	9,75	5,82	41,8	0,545	0,180	0,924	0,089	1,48	9,17	0,994	1,07	0,567	0,920	0,353	0,530
CD-00150C	1	253	107	< 978	25,8	< 31,1	16,5	267609	2720	515	8584	87,2	30,0	3,61	79,9	0,640	0,177	0,854	0,091	2,58	3,22	0,431	< 0,237	0,124	0,084	0,099	0,276
	2	227	96,1	< 978	< 1,94	50,8	14,5	254099	2444	453	8297	65,0	59,5	3,52	67,0	2,11	0,155	1,06	0,070	2,60	3,08	0,401	0,258	0,217	0,127	1,05	0,390
	3	352	13,4	< 978	< 1,94	< 31,1	25,4	259731	2201	350	8588	96,7	41,6	2,67	67,7	0,485	0,133	0,744	0,086	5,21	7,60	0,409	< 0,237	0,571	0,608	0,677	0,163
CD-02004	1	249	102	1638	13,0	< 31,1	56,9	256934	2405	423	12714	36,8	52,4	2,76	45,4	1,73	0,158	0,541	0,100	2,47	51,2	1,13	2,86	2,72	2,51	0,666	0,112
	2	171	11,6	1288	6,63	< 31,1	65,2	278652	3052	508	13947	35,0	24,9	2,13	47,9	0,501	0,144	0,596	0,169	1,34	22,0	0,950	1,97	0,744	0,384	0,206	0,049
	3	229	23,6	< 978	6,63	< 31,1	67,9	288590	2680	296	14323	44,5	20,9	2,98	47,9	0,479	0,140	0,596	0,075	1,82	53,3	1,02	0,663	0,523	3,02	0,571	0,124
	4	166	110	< 978	< 1,94	< 31,1	62,7	242946	2650	575	11919	44,2	58,9	2,09	65,2	2,04	0,162	0,648	0,082	4,86	43,2	1,07	2,93	2,85	2,36	0,589	0,022
	5	522	331	1940	7,80	< 31,1	45,8	246921	3449	814	12641	43,0	37,7	3,01	49,6	1,66	0,206	0,497	0,071	0,626	19,5	1,05	2,19	1,26	0,535	0,066	0,130

ANNEXE 21: MATÉRIAUX DE RÉFÉRENCES POUR LES ANALYSES LA-ICP-MS DES OXIDES DE FE-TI DE LA GABBRONORITE À OXIDES

Element		Mg	Al	Si	P	Ca	Sc	Ti	V	Cr	Mn	Co	Ni	Cu	Zn	Ga	Ge	As	Y	Zr	Nb	Mo	Sn	Hf	Ta	W	Pb
Isotope		^{24}Mg	^{27}Al	^{29}Si	^{31}P	^{44}Ca	^{45}Sc	^{47}Ti	^{51}V	^{52}Cr	^{55}Mn	^{59}Co	^{60}Ni	^{63}Cu	^{66}Zn	^{71}Ga	^{74}Ge	^{75}As	^{89}Y	^{90}Zr	^{93}Nb	^{95}Mo	^{118}Sn	^{178}Hf	^{181}Ta	^{182}W	^{208}Pb
GSE	Working value (ppm)	21106	68804	250994	70	52858	530	450	440	400	590	380	440	380	460	490	320	260	410	410	420	390	280	395	390	430	378
	Mean (ppm) n=4	21110	68825	250825	70,2	52938	530	450	440	400	590	380	440	380	460	490	320	260	411	411	421	390	280	395	390	430	378
	Standard Derivation	115	222	3397	4,70	562	6,43	3,34	3,57	2,65	3,56	2,48	1,07	2,40	2,05	2,90	3,78	4,75	3,72	6,47	3,53	1,66	0,48	6,36	6,68	4,56	2,05
	RSD (%)	0,543	0,322	1,35	6,69	1,06	1,21	0,741	0,811	0,663	0,603	0,653	0,242	0,631	0,445	0,592	1,18	1,83	0,905	1,57	0,838	0,425	0,171	1,61	1,71	1,06	0,542
GSD	Working value (ppm)	21709	70922	248657	860	51429	52	7432	44	42	220	40	58	42	54	54	32	27	42	42	42	39	29	39	40	43	50
	Mean (ppm) n=4	22110	73035	254400	1243	53238	61,3	8040	48,0	54,6	239	41,1	61,4	45,4	58,3	53,5	33,2	28,5	41,8	43,4	43,3	40,7	29,4	39,5	39,2	43,8	47,9
	Standard Derivation	180	629	3374	440	682	4,47	163	0,337	4,88	2,08	0,259	0,709	1,51	1,75	0,522	0,430	1,21	0,110	0,200	0,399	1,29	0,431	0,538	0,408	0,500	1,85
	RSD (%)	0,815	0,861	1,33	35,4	1,28	7,30	2,03	0,70	8,95	0,9	0,631	1,16	3,34	3,01	0,976	1,30	4,23	0,262	0,460	0,921	3,18	1,47	1,36	1,04	1,14	3,86
BC-28	Working value (ppm)	11618	20787				31	87615	9603	1172	2125	241	573		588	41,1	0,856		0,080	27,5	1,72	0,760	2,20	0,583	0,070		
	Mean (ppm) n=4	8635	12790				25,8	73680	9135	1348	1764	261	606		563	48,0	0,868		0,053	20,7	1,44	0,504	2,52	0,758	0,117		
	Standard Derivation	1159	2024				0,439	588	52,6	29,7	86,5	15,5	5,02		227	1,11	0,055		0,027	3,33	0,154	0,026	0,446	0,130	0,006		
	RSD (%)	13,4	15,8				1,70	0,798	0,576	2,20	4,90	5,95	0,828		40,3	2,32	6,28		52,1	16,1	10,7	5,24	17,7	17,1	5,16		

ANNEXE 22: 4ÈMES JOURNÉES DE LAUNAY

Présentation orale aux 4èmes Journées De Launay (Montréal, Canada) du 8 au 9 Mai 2012.

Résumé soumis :

Les sulfures massifs du complexe du Lac-des-Îles, Ontario, Canada

C. Duran[1,2] et S.-J. Barnes[1,2]
[1] Chaire de Recherche du Canada en Métallogénie Magmatique
[2] Université du Québec À Chicoutimi

Les processus d'enrichissement extrême en palladium (Pd) du complexe du Lac-des-Îles, notamment par rapport aux éléments du groupe du platine (EGP : Ru, Rh, Os, Ir, et surtout Pt), demeurent toujours énigmatiques bien que de nombreux modèles aient été proposés. Quatrième producteur de Pd au monde et unique en son genre, le complexe du Lac-des-Îles est localisé dans la province archéenne du Supérieur, au Nord-Ouest de l'Ontario, Canada. Formé à la suite de plusieurs injections mafiques à ultramafiques, il se caractérise par un assemblage chaotique de lithologies, résultant d'une activité magmatique très intense. Le tout est associé à des épisodes d'altération deutérique, de métamorphisme, de déformation et possiblement d'hydrothermalisme. Initialement considéré comme pauvre en sulfures (< 3%), les occurrences de sulfures massifs récemment découvertes remettent en question les investigations antérieures, et offrent un nouvel axe de recherche.

Des observations pétrographiques et des analyses géochimiques sur roche totale ont été effectuées pour caractériser les sulfures massifs. Les assemblages de sulfures sont essentiellement composés de pyrrhotite et pentlandite aux textures magmatiques, associés à des quantités importantes de pyrite et/ou magnétite (entre 10 et 75 % des sulfures). Des minéraux du groupe du platine (MGP) sont associés avec les sulfures et les silicates matriciels. La corrélation positive du Ni avec le S et la corrélation négative du Cu avec le S suggèrent la formation des sulfures massifs par l'accumulation de *monosulfide solid solution* (*mss*) lors du fractionnement du liquide sulfuré. Cependant les faibles concentrations en Ir (< 0,15 ppm) et les fortes concentrations en Pd (jusqu'à 67,8 ppm) ne sont pas en accord avec cette hypothèse. De plus la présence de pyrite et de magnétite associées aux assemblages magmatiques, témoigne d'une modification par des processus d'altération, soulignés dans les travaux antérieurs. Les ratios S/Se montrent une corrélation positive et ne suggèrent aucune perte ou addition de S significative, impliquant une mobilisation d'autres éléments pour former la pyrite et la magnétite.

Ces résultats préliminaires suggèrent que les sulfures massifs, originellement

magmatiques, ont subis des modifications. Cependant la nature de ces modifications et leur influence sur l'enrichissement en Pd reste à déterminer. La pyrite pourrait s'être formée par perte de Fe et/ou de Cu lors de l'altération de la pyrrhotite et/ou de la chalcopyrite. La magnétite pourrait s'être formée dans un contexte d'oxydation. La minéralogie ainsi que la signature géochimique roche totale des sulfures massifs traduisent la complexité de l'environnement de formation du gisement. L'étude détaillée des sulfures massifs s'avère alors essentielle pour retracer l'évolution du liquide sulfuré et faire le lien avec les sulfures disséminés porteurs des minéralisations actuellement exploitées. Subséquemment il sera possible de mieux comprendre le comportement du Pd au cours des processus magmatiques et post-magmatiques, et d'établir un modèle génétique susceptible d'être utilisé pour l'exploration minière des gisements potentiels de type Lac-des-Îles.

Mots clés : sulfures massifs – Lac-des-Îles, Ontario – palladium – altération

ANNEXE 23: 12TH INTERNATIONAL NICKEL SYMPOSIUM

Photoaffiche présentée au 12th International Nickel Symposium (Guiyang, Chine) du 16 au 21Juin 2012.

Résumé étendu soumis :

12th International Ni-Cu-(PGE) Symposium, Guiyang, China *June 16-21, 2012*

Massive Sulfides from the Lac-des-Iles Palladium Ore Deposits, Ontario, Canada

C. Duran, S.-J. Barnes
Sciences de la Terre, Université du Québec à Chicoutimi, 555 Boulevard de l'Université, Chicoutimi, Québec, Canada G7H 2B1
charley.duran1@uqac.ca
J.T. Corkery
North American Palladium, 556 Tenth Avenue, Thunder Bay, Ontario, Canada P7B 2R2

ABSTRACT. We have studied newly discovered massive sulfides from the Lac-des-Iles Pd ore deposits (i.e. Roby and Offset zones). Petrographical investigations show that four distinct assemblages can be identified based on the degree of alteration. Massive pods and lenses of sulfides evolve from magmatic to very altered. The magmatic ones mainly consist of pyrrhotite and pentlandite (Pn) where Pn displays typical igneous morphological features. The amount of pyrite (Py) and chalcopyrite are minor. The very altered ones consist of Py and/or magnetite widely replacing the primary assemblages. Whole rock geochemical analyses from massive sulfides compared to disseminated show that Ni, Se and Ir are well correlated with S, whereas values of Pd for massive sulfides fall below the trend line extrapolated from the disseminated sulfides. We found that there was no evidence between the petrographical features and the whole rock geochemical analyses. Thus we suggest that massive sulfides formed by mss accumulation.

1 INTRODUCTION

The Archean Lac-des-Iles (LDI) Complex, northwestern Ontario, Canada, is the world's fourth largest palladium (Pd) producer. In contrast to most of platinum-group element (PGE) ore deposits, which occur as reefs within large layered intrusions (e.g. Bushveld and Stillwater) or associated with Ni-Cu sulfides at the base of mafic intrusions (e.g. Noril'sk and Sudbury), the LDI ore deposits (i.e. Roby and Offset zones) occur within a small concentrically zoned intrusion. The mineralization consists of disseminated sulfides associated with magmatic breccias and varitextured gabbronorites (Lavigne et al. 2001). The latest work (Hinchey et al. 2005; Barnes & Gomwe 2011) suggest that both PGE collection by a magmatic sulfide liquid and Pd remobilization by an aqueous fluid have contributed in the ore formation. However, the contribution of each process is poorly understood, and relatively little is known about how the extreme and variable Pd-enrichment was achieved. This enrichment is highlighted by unusually high Pd/Pt and Pd/Ir ratios. Barnes & Gomwe (2011) proposed that these ratios might be due to the injection of a Pd-Cu rich magma into the LDI magmatic chamber derived by melting of previously crystallised sulfides. Alternatively, many authors (e.g. Brügmann et al. 1989; Lavigne & Michaud 2001; Watkinson et al. 2002; Hinchey et al. 2005) proposed that these ratios might be due to dissolution and reprecipitation of Pd by deuteric or hydrothermal fluids during late magmatic evolution or alteration events, upgrading the Pd grade.

The LDI complex has been previously characterized as sulfide poor (i.e. < 3%); however massive sulfide occurrences have recently been discovered. This raises the question of what is the relationship between the massive and disseminated sulfides. The massive sulfides could represent a monosulfide solid solution (mss) cumulate that crystallized from the sulfide liquid that later formed the disseminated sulfides. Alternatively, they could represent the mss restite proposed by Barnes &

Gomwe (2011). Or the massive sulfides may have a completely different origin to the disseminated sulfides. In the current study we document new data on the petrography, mineralogy and whole rock geochemistry of the newly discovered massive sulfides from the LDI Complex in order to constrain their signature and discuss their origin.

2 SAMPLING AND ANALYTICAL METHODS

Thirty specimens of massive sulfides were sampled from drill cores and from the open pit of LDI mine. These samples were selected to represent the Roby and Offset ore zones. Petrographical investigations of sulfide assemblages were carried out on hand specimens and polished thin sections. Major element composition of each sulfide phase was determined using a CAMECA SX-100 electron microprobe. Whole rock geochemical analyses were performed by a number of methods. Sulfur was determined using an infrared Horiba EMIA 220V sulfur and carbon analyser. Ni and Cu were analyzed by atomic absorption spectrometry, PGE and Au by Ni-sulfide fire assay and Te-coprecipitation coupled with ICP-MS. Finally, semi-metals were determined by Aqua Regia digest coupled with ICP-MS. Platinum-group minerals (PGM) were located using a JEOL 840-A scanning electron microscope. The composition of the PGM and of their host minerals were characterized by energy dispersive spectra and back-scattered electron images were also taken.

3 PRELIMINARY RESULTS

3.1 Petrographical observations

Massive sulfides from Roby and Offset zones have similar textural and petrographical characteristics. They occur as pods and lenses of sulfides. The ore mineral assemblage is mainly composed of pyrrhotite (Po), pentlandite (Pn), pyrite (Py) and magnetite (Mt) with minor amounts of chalcopyrite (Ccp), ilmenite and discrete PGM.

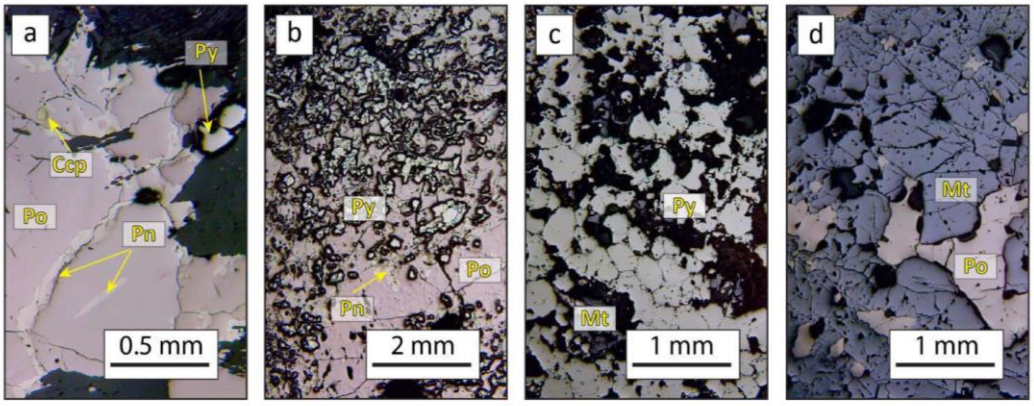

Figure 1. Photomicrographs of the different sulfide assemblages from the LDI massive sulfides in reflected light. a) Assemblage i) showing magmatic textures. b) Assemblage ii) where magmatic textures still remain but with considerable amount of Py. c-d) Respectively assemblage iii) and iv) corresponding to the most altered samples. Magmatic textures are almost lost and Py and/or Mt are the major phases.

Based on modal proportions, the massive sulfides can be divided into 4 assemblages: i) Po + Pn + minor Py (< 10%) ± Ccp (Fig. 1a). This assemblage is the least altered and exhibits magmatic textures. Pyrrhotite forms large anhedral crystals surrounded by granular polycrystalline veinlets of

Pn. Pentlandite also occurs as exsolution flames in Po; ii) Po + Pn + Py (> 10%) ± Ccp (Fig.1b). This assemblage still shows magmatic texture associated with considerable amount of Py. Pyrite textures vary from subhedral to anhedral individual grains or polycrystalline aggregates. In some rare cases Py occurs as small veins; iii) Py (>50%) + Po + Pn ± Ccp (Fig. 1c); iv) Mt (>30%) + Py (>10%) + Po + Pn ± Ccp (Fig. 1d). The last two assemblages are the most altered and Py and/or Mt intensely replace the primary assemblages observed in the first two assemblages. Some rare Ccp-rich samples have been found at the edge of massive Po-Pn pods.

3.2 Whole rock geochemistry

Sulfur concentrations in massive sulfides, range from 9.60 to 32.44 wt. %. Values of S/Se ratio are in the range of mantle-derived sulfides, varying from 1610 to 4122. Nickel commonly exceeds Cu with Ni/Cu ratios much higher than 1. These data are consistent with minor amounts of Ccp observed during petrographical description. The Pd/Ir ratios are high (~10000) as are the Pd/Pt ratios (~20), indicating a Pd-enrichment.

Combining data for disseminated sulfides (Gomwe, 2008; Hinchey & Hattori, 2005) and our data, Se and Ni show positive correlations with S (Fig. 2), indicating that S has not been added or removed from the rocks despite the changes in sulfide mineralogy. For samples with less than 1 wt % S, Pd also shows a positive correlation with S (Fig. 2). However, the massive sulfides fall below the extrapolated trend line, possibly because the massive sulfides are mss cumulates or restites. If the massive sulfides represent mss then they should be enriched in IPGE such as Ir. Many of them are, but a few of them are not (Fig. 2).

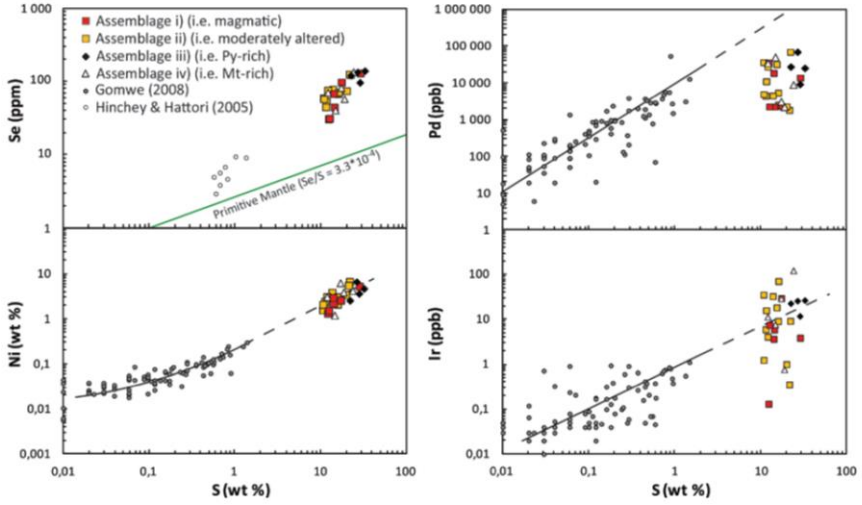

Figure 2. Bivariate plots of whole rock S (wt %) versus whole rock Ni (wt %), Se (ppm), Ir (ppb) and Pd (ppb). Values of disseminated sulfides are taken from Gomwe (2008) and Hinchey & Hattori (2005), for comparison with massive sulfides from this study. Note the good trend line between disseminated and massive sulfides for Ni, Se and Ir. However Pd values from disseminated and massive sulfides are not correlated.

3.3 Platinum-Group Minerals

Preliminary observations show that PGM occur as euhedral to anhedral single grains. Most of them are included in sulfides, along sulfide-silicate and sulfide-sulfide grain boundaries. Only few of them are included in silicates. The majority of PGM are Pd-tellurides as observed by previous workers (Watkinson & Dunning, 1979; Djon & Barnes, 2012). They consist, in decreasing order of abundance, of merenskyite ($PdTe_2$), kotulskite (PdTe), and telluropalladinite (Pd_9Te_4). Some (Pd,Pt)-bismuthotellurides and (Pd,Pt) sulfides have also been found.

4 DISCUSSION AND CONCLUSIONS

The origin of LDI massive sulfides and their relationship with disseminated sulfides have never been documented. We propose that: 1) Massive sulfides formed by mss accumulation in order to explain the Ni, Se, Ir and Pd contents in the massive sulfides compared to disseminated sulfides. 2) Massive sulfides are overprinted by Py and Mt due to intense alteration. 3) Magnetite may have formed in an oxidizing environment by O addition in the sulfide system. S/Se ratios do not show S addition, thus Py may have formed by Fe loss from the sulfide system. The major process which occurred during alteration was Fe-remobilization by oxidizing fluids. 4) No relationship between petrographical features and whole rock geochemistry have been established, thus we assume that alteration processes leading to mineralogical changes in the sulfide assemblages of Roby and Offset zones did not contribute in the Pd-enrichment of massive sulfides. 5) However alteration processes could lead to Pd redistribution at a local scale, resulting in discrete PGM associated with secondary minerals (i.e. Py, Mt and hydrous silicates).

5 REFERENCES

Barnes, S.-J. and Gomwe, T.S. 2011. The Pd-deposits of the Lac des Iles Complex, north-western Ontario; Review in Economic Geology 17, p. 351-370.

Brügmann, G.E., Naldrett, A.J. and Macdonald, A.J. 1989. Magma mixing and constitution zone refining in the Lac-des-Iles Complex, Ontario – genesis of platinum-group element mineralization; Economic Geology 84, p. 1557-1573.

Djon, M.L.N. and Barnes, S.-J. 2012. Changes in sulfide and platinum-group minerals with the degree of alteration in the Roby, Twilight, and High Grade Zones of the Lac des Iles Complex, Ontario, Canada; Mineralium Deposita in press, p. 1-22.

Gomwe, T.S. 2008. The formation of the palladium-rich Roby, Twilight and High-Grade zones of the Lac des Iles complex; unpublished PhD Thesis, Université du Québec à Chicoutimi, 296 p.

Hinchey, J.G., Hattori, K.H. and Lavigne, M.J. 2005. Geology, petrology, and controls on PGE mineralization of the southern Roby and Twilight zones, Lac des Iles mine, Canada; Economic Geology 100, p. 43-61.

Hinchey, J.G. and Hattori, K.H. 2005. Magmatic mineralization and hydrothermal enrichment of the High Grade Zone at the Lac des Iles palladium mine, northern Ontario, Canada; Mineralium Deposita 40, p. 13-23.

Lavigne, M.J. and Michaud, M.J. 2001. Geology of North American Palladium Ltd.'s Roby zone deposit, Lac des Iles; Exploration and Mining Geology 10, p. 1-17.

Watkinson, D.H. and Dunning, G. 1979. Geology and platinum-group mineralization, Lac-des-Iles complex, northwestern Ontario; Canadian Mineralogist 17, p. 453-462.

Watkinson, D.H., Lavigne, M.J. and Fox, P.E. 2002. Magmatic-hydrothermal Cu- and Pd-rich deposits in grabbroic rocks from North America; *in* Canadian Institute of Mining, Metallurgy and Petroleum Special Volume 54, p. 299-320.

ANNEXE 24: 12TH SGA BIENNIAL MEETING

Présentation orale au 12th SGA Biennial Meeting (Uppsala, Suède) du 12 au 15 Aout 2013.

Résumé étendu soumis :

Petrogenesis of massive sulphides from the Lac-des-Iles palladium ore deposits, Western Ontario, Canada

Charley J. Duran, Sarah-Jane Barnes
Sciences de la Terre, Université du Québec, Chicoutimi, Canada G7H 2B1 (charley.duran@hotmail.fr)

John T. Corkery
North American Palladium, 556 Tenth Avenue, Thunder Bay, Ontario, Canada P7B 2R2

Abstract. Previously characterised as a sulphide-poor Pd ore deposit, massive sulphides have recently been discovered in Lac-des-Iles. The massive sulphides occur across the different lithological units and show variable degrees of alteration. The least altered samples comprise a typical magmatic assemblage of pyrrhotite, pentlandite and chalcopyrite. Chalcopyrite-rich samples are found at the edges of the pyrrhotite/pentlandite-rich pods. Base metal and platinum-group element (PGE) compositions indicate that as a whole they represent a frozen sulphide liquid, different from the one that formed the sulphide-poor samples, that was injected along structural features. The altered samples are rich in pyrite and magnetite. Molecular proportions of base metals and S/Se ratios are the same for the altered and unaltered samples indicating that neither S nor Fe has been remobilized from the system. We propose instead that oxidation was responsible for the observed changes in mineralogy. This alteration event appears not to have affected the PGE content.

Keywords. Massive sulphides, structural control, Lac-des-Iles Pd ore deposits

1 Introduction

The Archean Lac-des-Iles (LDI) Complex, western Ontario, is Canada's only primary platinum-group elements (PGE) producer and the world's fourth largest palladium (Pd) producer. In contrast to most PGE ore deposits which occur either as strataform PGE-rich layers within large layered intrusions (e.g. Bushveld and Stillwater) or as PGE-rich Ni-Cu sulphides at the base of mafic intrusions (e.g. Norils'k and Sudbury), the LDI mineralization occurs as sulphides and platinum-group minerals (PGM) disseminated in a small mafic intrusion of chaotic lithologies (i.e. magmatic breccias and varitextured gabbronorites). The mineralization is characterized by extreme and variable Pd-enrichment highlighted by unusually high Pd/Pt ratios. Studies by Hinchey et al. (2005), Barnes and Gomwe (2011), and Djon and Barnes (2012), suggest that both PGE collection by a magmatic sulphide liquid followed by Pd-remobilization by later magmas or fluids have contributed in the ore formation. However, the contribution of each process is poorly understood, and relatively little is known about how the Pd-enrichment was achieved.

The LDI complex has been previously characterized as sulphide poor (i.e. < 3%). However massive sulphides have recently been discovered, which raises the question of the processes involved in their formation. Three possible origins may be considered: a) the sulphides are monosulphide solid solution (MSS) cumulates and the fractionated liquid has migrated away to form the disseminated sulphides; b) the sulphides represent a frozen sulphide liquid; c) the sulphides precipitated from late-magmatic aqueous fluids.

In the current study we document new data on the geology, petrography/mineralogy, and whole rock geochemistry of the newly discovered massive sulphides from the LDI complex in order to consider their origin.

2 Geology of LDI and location of massive sulphides

The LDI Complex consists of three mafic to ultramafic intrusions emplaced into gneissic tonalites and granodiorites, which are in turn intruded by various granitoids. The Mine Block Intrusion is the central intrusion of the complex and is the only one that hosts Pd-deposits (i.e. Roby and Offset zones). The Mine Block Intrusion is concentrically zoned in both composition and texture. Compositions range mainly from leuco- to melano-gabbros and gabbronorites, including a magnetite-rich gabbro. Magmatic breccias occur in the Roby zone but have not been observed at depth. Varitextured gabbros form a rim around the gabbroic and gabbronoritic units. Most of the rocks regardless their texture or degree of alteration, have similar compositions (Barnes and Gomwe 2011). The shape of the intrusion suggests an elongation along a SW-NE trend.

The sulphide-rich samples occur as small pods and lenses (8 to 65 cm thick), ranging from densely disseminated (~10% sulphides) to massive sulphides (~90% sulphides). These pods are found in different units and at different stratigraphic levels within the intrusion (Figs. 1 and 2). Despite being present in host rocks that formed at different stages of magma differentiation the sulphide-rich samples have similar textural, petrographical and mineralogical characteristics. The semi-massive sulphides host rounded silicate inclusions and exhibit brecciated textures. All these observations suggest that the sulphides have been injected across the stratigraphy of the intrusion implying that they were in a liquid state. The geological setting thus suggests that the sulphides were emplaced along some structural feature and either represent an immiscible sulphide liquid, or have precipitated from late-magmatic fluids.

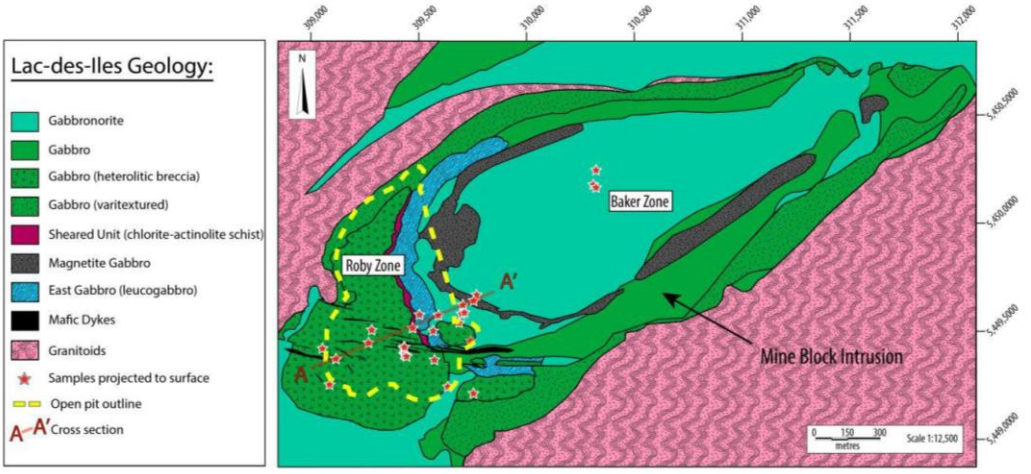

Figure 1. Simplified geological map of the Mine Block Intrusion of the Lac-des-Iles Complex with location of the sulphide-rich samples (Modified from North American Palladium). Note that the samples are projected to surface and form a SW-NE trend. The samples are hosted in the different lithological units.

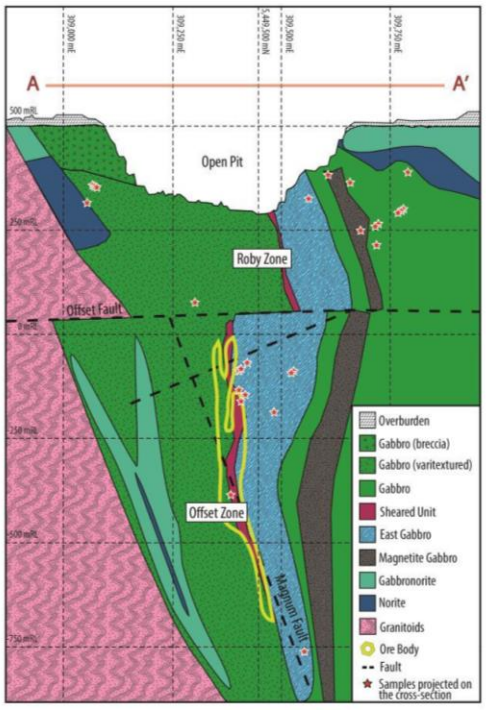

Figure 2. Idealized cross-section of the Mine Block Intrusion of the Lac-des-Iles complex with projected location of samples from drill cores (Modified from North American Palladium). Note that sulphides sampled from the open pit and from Baker zone are not plotted on the cross-section.

3 Petrography

The ore mineral assemblage is mainly composed of pyrrhotite (Po), pentlandite (Pn), pyrite (Py) and magnetite (Mt) with minor amounts of chalcopyrite (Ccp), ilmenite and discrete PGM up to 100 µm diameter. Most of the PGM are either included in sulphides, or along sulphide-silicate and sulphide-sulphide grain boundaries. Only few of them are included in silicates.

Based on modal proportions, the massive sulphides can be divided into 5 assemblages: i) Po + Pn + minor Py (< 10%) ± Ccp (Fig. 3a). This assemblage exhibits magmatic textures. Pyrrhotite forms large anhedral crystals surrounded by granular polycrystalline veinlets of Pn. Pentlandite also occurs as exsolution flames in Po; ii) Po + Pn + Py (> 10%) ± Ccp (Fig. 3b). This assemblage still shows magmatic texture, but the amount of Py present is too high for an igneous assemblage. Pyrite textures vary from subhedral to anhedral individual grains or polycrystalline aggregates. In some rare cases Py occurs as small veins; iii) Py (>50%) + Po + Pn ± Ccp (Fig. 3c); iv) Mt (>30%) + Py (>10%) + Po + Pn ± Ccp (Fig. 3d); v) Ccp (>50 %) found at the edges of the pods (Fig. 3e). All of the assemblages except v) contains too little Ccp to represent sulphide liquid. Assemblages i) and ii) could represent sulphide cumulates and assemblage v) the fractionated liquid. Assemblages iii) and iv) could be extremely altered sulphide cumulates or they could precipitate from late-magmatic fluids.

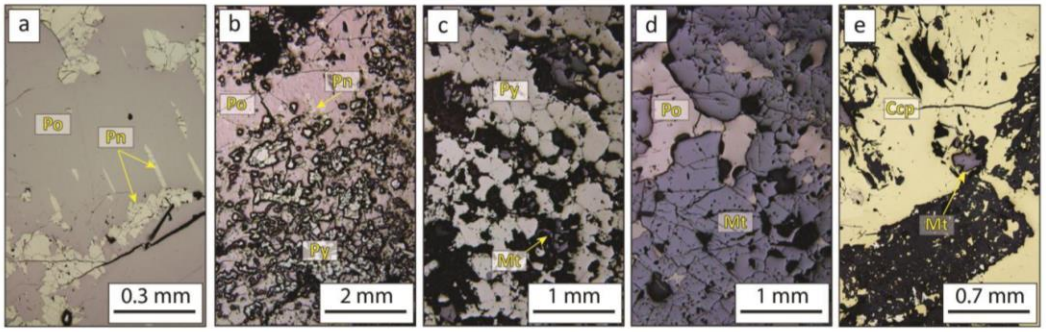

Figure 3. Photomicrographs of the different sulphide assemblages from LDI in reflected light. a) Assemblage i) showing magmatic textures; b) Assemblage ii) where magmatic textures still remain but with considerable amount of Py; c-d) Respectively assemblages iii) and iv) correspond to the most altered samples. Magmatic textures are almost lost and Py and/or Mt are the major phases; e) Assemblage v) where Ccp is the major phase.

4 Geochemistry

4.1 Relationship among the assemblages

Based on the behaviour of relatively immobile elements such as Ir and Rh, we do not think that assemblages iii) and iv) represent hydrothermal deposits. These elements fall on a single trend which includes the disseminated sulphides from the mineralized zones and the sulphide-rich assemblages (Fig. 4).

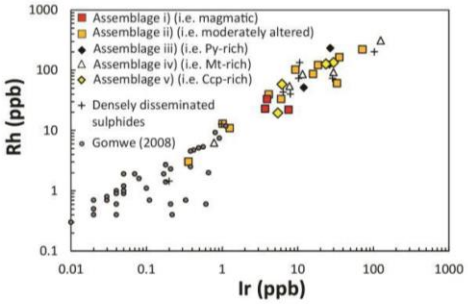

Figure 4. Bivariate plot of whole rock Ir (ppb) versus whole rock Rh (ppb). Values of disseminated sulphides (small circles) from mineralized zones are taken from Gomwe (2008).

Assuming that assemblages ii) to iv) represent altered magmatic sulphides the presence of excess Py and Mt in assemblages ii) to iv) requires either that S has been added or that Fe has been lost from the sulphide assemblage.

In igneous sulphides the molecular proportions of S to Fe + Cu + Ni is approximately 1. Most of the samples including those of assemblage iii) and iv) plot close to the igneous line (Fig. 5). This suggests that for most of the samples, neither S nor Fe has been mobile. The positive correlations between S and Se and S and Ni, combined with S/Se ratios in the mantle range, also suggest that S was not mobile (Fig. 6a,b).

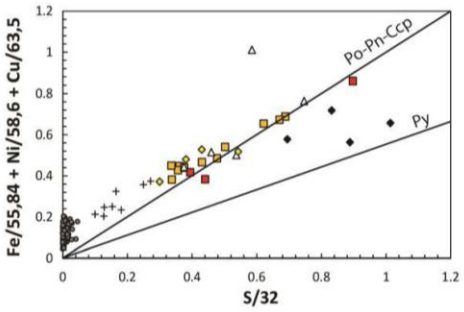

Figure 5. Bivariate plot of molecular proportions of S versus Fe + Ni + Cu. Values of disseminated sulphides (small circles) from mineralized zones are taken from Gomwe (2008).

In order to account for the excess of Py and Mt in assemblages ii) to iv), we suggest that Po was oxidized resulting in the reaction: Po + O_2 = Py + Mt. Thus neither Fe nor S was mobile and assemblages i) to iv) represent sulphides which have been partly oxidized during late-magmatic alteration.

On a plot of S versus Cu (Fig. 6c) the samples show a good correlation until approximately 5% S. After that the samples plot on either side of the trend, with the Ccp-rich samples above the trend. This could be because the Ccp-rich samples represent the fractionated liquid complimentary to the sulphide cumulate. However this does not appear to be the case because the fractionated liquid should be enriched in Pd and yet the Ccp-rich samples have similar values to the other massive sulphide samples (Fig. 6d). This suggests that the Ccp-rich samples either represent intermediate solid solution cumulates, and the most fractionated liquid has migrated away from the massive sulphide pods. Alternatively Ccp was originally present with Po and Pn in the center of the pods, and has been remobilized to the edges. At present we favour the remobilization because all the massive sulphides have very high Pd/Ir and Pd/Pt ratios (1000-10000; 10-20) which is contrary to the general observation that sulphide cumulates are depleted in Pd.

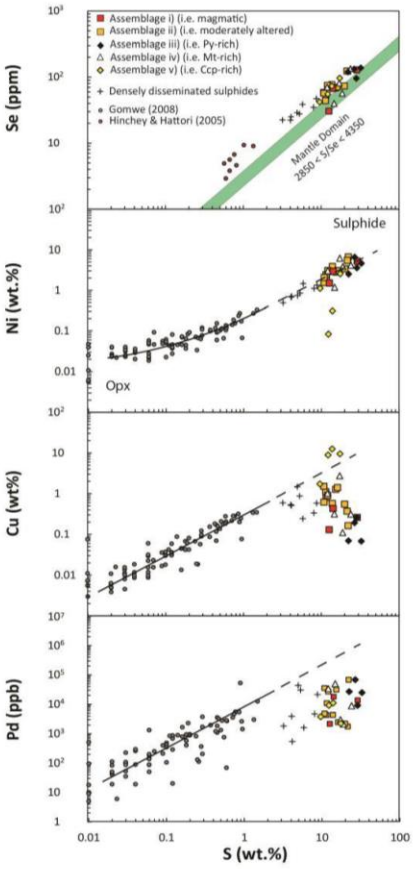

Figure 6. Bivariate plots of whole rock S (wt %) versus whole rock Ni (wt. %), Se (ppm), Cu (wt. %), and Pd (ppb). Values of disseminated sulfides are taken from Gomwe (2008) and Hinchey and Hattori (2005).

4.2 Relationship between massive and disseminated sulphides

If we consider only S, Ni and Se and allow that Cu has been remobilized on the centimeter scale, then it is possible to argue that because the compositions of massive and disseminated sulphides are co-linear, the sulphide component of all the samples represents a sulphide liquid. But when we consider the plot of Pd versus S (Fig. 6d) it is clear that the massive sulphides are depleted in Pd in comparison with the disseminated sulphides. Therefore it cannot be the same liquid.

5 Discussion

Although the position of the sulphides within the complex and their late-magmatic mineralogy could make us think that sulphides might have formed by precipitation from an aqueous fluid circulating through structures within the intrusion, the presence of typical magmatic textures and the geochemical signature of massive sulphides demonstrate their magmatic origin. Indeed the typical magmatic textures would not have been formed by fluids.

Our model suggests that late in the solidification of the Mine Block intrusion magmatic sulphide liquid was injected from a feeder chamber along structures related to regional crustal movements. Movement along the structures separated the sulphide liquid into pods. The liquid crystallized as Po-Pn-Ccp and PGM.

Deformation or fluid action caused the Ccp to migrate to the edges of the pods and thus forming Ccp-rich and Ccp-poor sulphide assemblages. Oxidation of Po led to the formation of Py and Mt, but does not appear to affect the metal content of the rocks.

6 Conclusions

We propose that: 1) Sulphide liquid accumulated in embayments of a magmatic conduit. 2) This sulphide liquid has been squeezed through dilatencies in consolidated silicate magma and accumulated as massive sulphides across the stratigraphy. 3) The sulphide liquid formed MSS cumulates and a Cu-rich portion. 4) The massive sulphides are not related to the disseminated sulphides as they are poorer in Pd. 5) The primary sulphide assemblage has been altered to Py and Mt by oxidation. 6) This oxidation event did not affect the metal concentrations in the ores; in particular it did not up-grade the Pd because there is no relationship between the sulphide assemblages and the metal contents of the rocks.

Acknowledgements

We are grateful to North American Palladium for funding this project via the Canada Research Chair in Magmatic Ore Deposits Program. We thank the North American Palladium exploration team for technical support in the field and with modelling software. We thank Dany Savard for his assistance with geochemical analyses and Philippe Pagé and Sarah Dare for their constructive comments.

References

Barnes S-J, Gomwe TS (2011) The Pd-deposits of the Lac-des-Iles Complex, north-western Ontario. Review in Economic Geology 17:351–370

Djon MLN, Barnes S-J (2012) Changes in sulfide and platinum-group minerals with the degree of alteration in the Roby, Twilight, and High Grade Zones of the Lac des Iles Complex, Ontario, Canada. Mineralium Deposita 47:875–896

Gomwe TS (2008) The formation of the palladium-rich Roby, Twilight and High-Grade zones of the Lac des Iles complex. Unpublished PhD Thesis, Université du Québec à Chicoutimi, 296 p

Hinchey JG, Hattori KH, Lavigne MJ (2005) Geology, petrology, and controls on PGE mineralization of the southern Roby and Twilight zones, Lac des Iles mine, Canada. Economic Geology 100:43–61

Hinchey JG, Hattori KH (2005) Magmatic mineralization and hydrothermal enrichment of the High Grade Zone at the Lac des Iles palladium mine, northern Ontario, Canada. Mineralium Deposita 40:13–23

ANNEXE 25: 12TH INTERNATIONAL PLATINUM SYMPOSIUM

Photoaffiche présentée au 12th International Platinum Symposium (Yekaterinburg, Russie) du 11 au 14 Aout 2014.

Résumé étendu soumis :

SULFIDE-RICH PODS FROM THE LAC-DES-ILES Pd-ORE DEPOSITS, WESTERN ONTARIO, CANADA: PART 1. A GENETIC MODEL

Duran, C.J.[1], Barnes, S.-J.[1] & Corkery, J.T.[2]

[1] Université du Québec à Chicoutimi, 555 Blvd. de l'Université, Chicoutimi, G7H 2B1, Qc, Canada
[2] North American Palladium, 556 Tenth Av., Thunder-Bay, P7B 2R2, On, Canada
e-mail: charley.duran@hotmail.fr

ABSTRACT. Massive sulfide pods from the Lac-des-Iles Pd-ore deposits (Western Ontario, Canada) show a variation in sulfide mineralogy and texture from essentially magmatic (pyrrhotite+pentlandite±chalcopyrite) to highly altered (pyrite±pentlandite±pyrrhotite±chalcopyrite). We suggest that the magmatic assemblage formed from crystallization of magmatic sulfide liquid. The pyrite (Py)-rich assemblage formed by Fe-loss to the surrounding silicates.

The Mine Block intrusion that host the Lac-des-Iles Pd deposits also hosts occasional sulfide-rich pods which have not been considered by previous studies. These pods are unusual in that they do not display typical magmatic features as they are not found at the base of the intrusion, they show a variation in sulfide mineralogy and texture ranging from magmatic to altered assemblages (Py-rich assemblages), and they are enriched in Pd (up to 67 g/t) with unusually high Pd/Ir and Pd/Pt ratios. There has been a long-standing controversy about the role played by fluids in the ore-forming processes at Lac-des-Iles (Talkington & Watkinson, 1984; Lavigne & Michaud, 2001; Hinchey & Hattori, 2005; Barnes & Gomwe, 2011; Hanley & Gladney, 2011; Djon & Barnes, 2012; Boudreau et al., 2014). The presence of unusual sulfide-rich pods adds another source of information to the ongoing debate. The present study examines the geology, petrography and whole rock geochemistry of Lac-des-Iles sulfide-rich pods in order to consider their origin and to assess the processes involved in their genesis and subsequent modifications.

The abundance of sulfides forming the pods is unlikely to be the result of cotectic precipitation from the mafic magma and therefore requires mobility and accumulation of the sulfides. Although the sulfide-rich pods occur across the stratigraphy of the intrusion, they do not form veins and are not associated with alteration halos which might indicate hydrothermal origin. Whereas some of the pods are massive, most of them are matrix and net-textured sulfides which negates the possibility of sub-solidus mobility of the sulfides. In addition, no evidence of deformation and/or recrystallization has been observed in the sulfides. Consequently the pods were more likely formed by accumulation of magmatic sulfide liquid into dilational jogs while the intrusion was emplaced and deformed (Fig. 1a.b). Nonetheless many of the pods have an excess of Py relative to the crystallization product of a magmatic sulfide liquid. Concentrations of immobile elements (IPGE+Rh) are correlated with one another regardless the amount of Py and the most soluble elements (Pd+Pt+Au) are not enriched in the most Py-rich pods. Furthermore Py-rich assemblages display similar metal patterns on a primitive mantle normalized basis to monosulfide solid solution (MSS) assemblages (i.e. decoupling between Ni and Cu, flat IPGE patterns, and Pt depletion). Therefore we suggest that the pods formed by fractional crystallization of magmatic sulfide liquid (Fig. 1c.d) and that Py-rich assemblages represent altered MSS assemblages. We also suggest that Pd enrichment was achieved prior to alteration resulting in the high Pd/Pt and Pd/Ir ratios regardless of the degree of alteration.

Instead of a strictly hydrothermal origin for the Lac-des-Iles sulfide-rich pods we favour a model whereby sulfides crystallized from a fractionating magmatic sulfide liquid prior to any modification by alteration. While alteration proceeded, trace elements were not remobilized. However the presence of excess Py requires either that S has been added or Fe has been lost from MSS. The combination

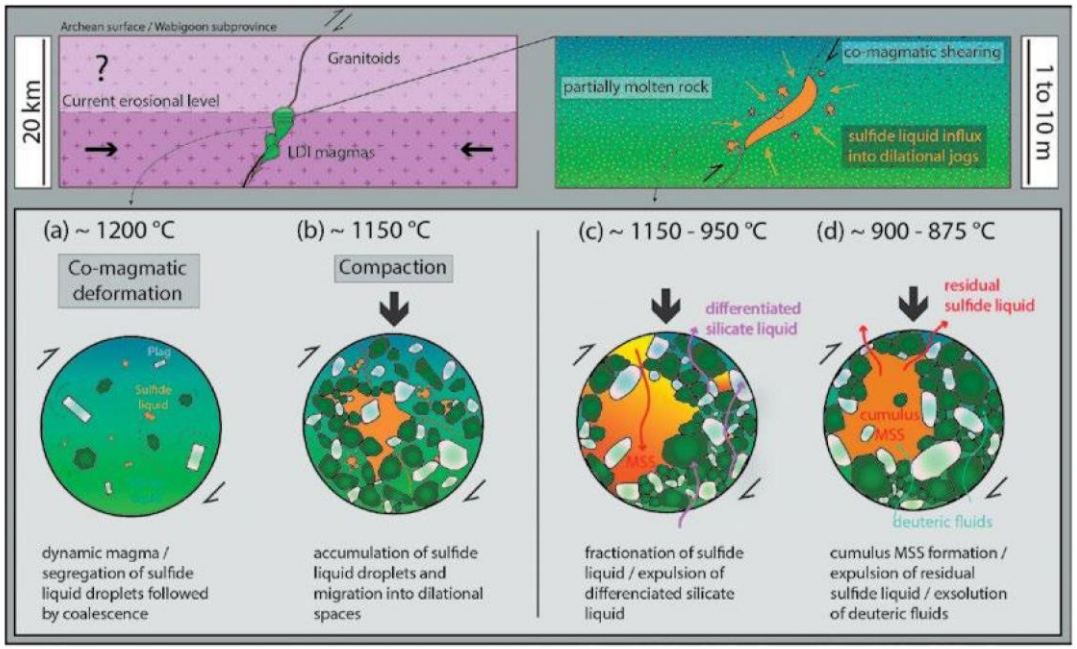

Fig. 1. Schematic model for the development of sulfide-rich pods at Lac-des-Iles: (a) segregation and coalescence of sulfide liquid droplets in a dynamic setting; (b) accumulation of sulfide liquid into dilational jogs during compaction; (c) fractional crystallization of sulfide liquid; (d) MSS formation and incipient alteration by deuteric fluids

of S/Se ratios and δ^{34} S values in the mantle range suggests that S was not mobile. As a result, we propose a model whereby Fe has been lost from MSS to surrounding silicates, promoting the formation of Py. However this raises the questions of how Py formed and how trace elements behaved during the formation of Py. Thus in Part 2 we discuss the implications of modifying the MSS assemblages during alteration on the distribution of PGE and the origin of PGE-bearing Py (Duran et al., 2014).

Acknowledgements. We are grateful to North American Palladium for funding this project via the Canada Research Chair in Magmatic Ore Deposits.

REFERENCES

1. BOUDREAU, A., DJON, L., TCHALIKIAN, A. & CORKERY, J. (2014): The Lac des Iles palladium deposit, Ontario, Canada part I. The effect of variable alteration on the Offset Zone. Mineralium Deposita, 49, 625-654.
2. BARNES, S-J. & GOMWE, T.S. (2011): The Pd deposits of the Lac des Iles Complex, Northwestern Ontario. Rev. Economic Geology, 17, 351-370.
3. DJON, M.L.N. & BARNES, S-J. (2012): Changes in sulfides and platinum-group minerals with the degree of alteration in the Roby, Twilight, and High Grade Zones of the Lac des Iles Complex, Ontario, Canada. Mineralium Deposita, 47, 875-896.
4. DURAN, C.J., BARNES, S-J. & CORKERY, J.T. (2014): Sulfide-rich pods from the Lac-des-Iles Pd ore deposits, Western Ontario, Canada: Part 2. The origin of platinum-group elements bearing pyrites. 12th IPS abstract volume.
5. HANLEY, J.J. & GLADNEY, E.R. (2011): The presence of carbonic-dominant volatiles during the crystallization of sulfide-bearing mafic pegmatites in the North Roby Zone, Lac des Iles Complex, Ontario. Economic Geology, 106, 33-54.
6. HINCHEY, J.G. & HATTORI, K.H. (2005): Magmatic mineralization and hydrothermal enrichment of the High Grade Zone at the Lac des Iles palladium mine, northern Ontario, Canada. Mineralium Deposita, 40, 13-23.
7. LAVIGNE, M.J. & MICHAUD, M.J. (2001): Geology of North American Palladium Ltd's Roby Zone deposit, Lac des Iles. Exploration and Mining Geology, 10, 1-17.
8. TALKINGTON, R.W. & WATKINSON, D.H. (1984): Trends in the distribution of the precious metals in the Lac-Des Iles Complex, Northwestern Ontario. Canadian Mineralogist, 22, 125-136.

ANNEXE 26: 12TH INTERNATIONAL PLATINUM SYMPOSIUM

Présentation orale au 12th International Platinum Symposium (Yekaterinburg, Russie) du 11 au 14 Aout 2014.

Résumé étendu soumis :

SULFIDE-RICH PODS FROM THE LAC-DES-ILES Pd-ORE DEPOSITS, WESTERN ONTARIO, CANADA: PART 2. THE ORIGIN OF PLATINUM-GROUP ELEMENTS-BEARING PYRITES

Duran, C.J.[1], Barnes, S.-J.[1] & Corkery, J.T.[2]

[1] Université du Québec à Chicoutimi, 555 Blvd. de l'Université, Chicoutimi, G7H 2B1, Qc, Canada
[2] North American Palladium, 556 Tenth Av., Thunder-Bay, P7B 2R2, On, Canada
e-mail: charley.duran@hotmail.fr

ABSTRACT. Pyrite from Lac-des-Iles sulfide-rich pods host substantial amounts of platinum-group elements (PGE). In this contribution we discuss the origin of pyrite and their PGE content.

Recent studies have shown that pyrite (Py) may be a significant host for PGE in magmatic Ni-Cu-PGE deposits (Oberthür et al., 1997; Dare et al., 2011; Djon and Barnes, 2012; Piña et al., 2012, 2013). Although common, Py is usually an accessory phase in these deposits. Consequently very little attention has been paid to processes controlling the distribution of PGE into Py which may form over a wide range of conditions (i.e. exsolution from monosulfide solid solution (MSS) to hydrothermal precipitation). The Mine Block intrusion that hosts the Lac-des-Iles Pd ore deposits also hosts occasional sulfide-rich pods which are unusual in that many of them are extensively enriched in Py. Despite the presence of significant amount of Py in most of our samples, we have interpreted the sulfide-rich pods to have formed by accumulation of MSS separating from fractionating sulfide liquids in equilibrium with surrounding silicate magma (Duran et al., 2014). In order to account for the excess of Py we suggested a model whereby formation of Py was promoted by modifications of MSS (i.e. Fe-loss during alteration). Therefore sulfide-rich pods from Lac-des-Iles provide ideal material to investigate processes that might affect MSS. Thus, to assess the role played by Py as a carrier of PGE and to consider the processes involved in its formation, we have determined by LA-ICP-MS the concentrations of PGE and chalcophile elements in pyrrhotite (Po), pentlandite (Pn) and Py from Lac-des-Iles sulfide-rich pods.

When comparing the distribution of PGE and chalcophile elements between Po and Py (Fig. 1a),

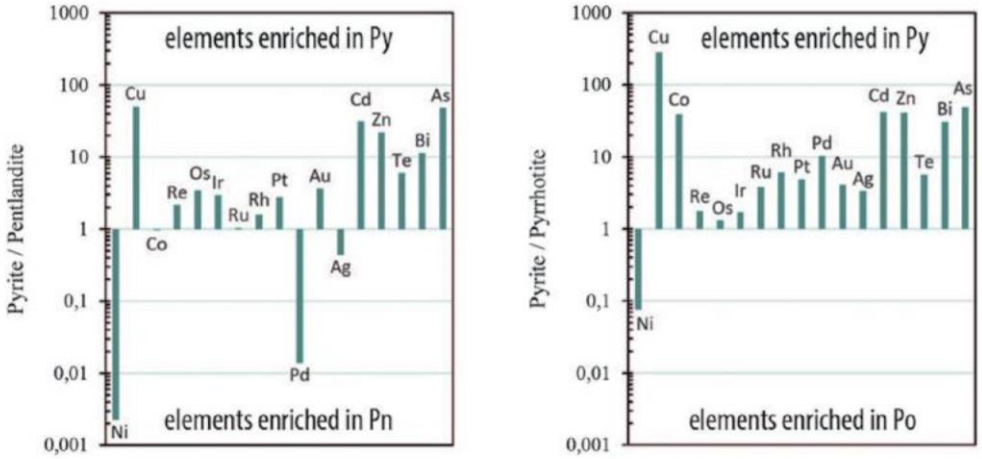

Fig. 1. Histograms showing the mean trace element contents in Py (n=57) vs. (a) co-existing Po (n=37); (b) co-existing Pn (n=57)

Re, IPGE (Os, Ir, Ru), Rh, Pt, Au, Ag and Te show a slight (< 1 order of magnitude) preference for Py over Po whereas Cu, Zn, Co, Pd, As, Cd, Sn, Sb, Pb and Bi show a considerable (> 1 order of magnitude) preference for Py over Po. Only Ni shows a preference for Po over Py. A similar distribution is observed between Pn and Py except that Pd and Ag are enriched in Pn instead of Py and Co is equally distributed (Fig. 1b). Considering that IPGE+Rh are immobile elements, their presence in Py could not have resulted from hydrothermal introduction and is more likely to be inherited from MSS or Po and Pn which exsolved from MSS. Furthermore Pt, Pd and Au which are the most soluble elements and which are incompatible with MSS are not significantly enriched in Py. On a primitive mantle normalized basis, Py display similar Re, Os and Ir patterns to co-existing Po (Fig. 2). Assuming that Py might replace Po, it is reasonable to argue that Py inherited Re, Os and Ir contents from Po. On the other hand Po is not a significant host for Co, Ru and Rh, and yet Py is much more enriched in these elements (Fig. 2). Therefore Co and some of Ru and Rh in Py cannot be inherited from Po. Pentlandite however hosts significant amount of Co, Ru and Rh and display similar primitive mantle normalized profiles to Py for these elements (Fig. 2). Nonetheless Py does not host significant amount of Ni and any Ni sulfides have not been observed, therefore Py could not have extensively replaced Pn. As a result we suggest that Py formed while Pn was exsolving in order to promote competition of Co, Ru and Rh between Py and Pn.

Based on the distribution of PGE and chalcophile elements among Po, Pn and Py, 2 models may be considered for the origin of Py during alteration: (1) Fe diffused out from Po while Pn was still exsolving from MSS. Therefore Py replaced Po and inherited its Re, Os and Ir contents and allowed Co, Ru and Rh to choose between Pn and Py (2) Fe diffused out from MSS prior or during Po and Pn exsolution, thus forming a S-rich MSS and allowing exsolution of important amounts of Py. At this point we do not favour a particular model but in both cases the formation of Py was likely promoted by alteration of MSS/Po during exsolution of Pn, thus providing a new host to compete for Co, IPGE and Rh.

Acknowledgements. We are grateful to North American Palladium for funding this project via the Canada Research Chair in Magmatic Ore Deposits.

REFERENCES

1. DARE, S.A.S., BARNES, S-J., PRICHARD, H.M. & FISHER, P.C. (2011): Chalcophile and platinum-group element (PGE) concentrations in the sulfide minerals from the McCreedy East deposit, Sudbury, Canada, and the origin of PGE in pyrite. Mineralium Deposita, 46, 381-407.
2. DJON, M.L.N. & BARNES, S-J. (2012): Changes in sulfides and platinum-group minerals with the degree of alteration in the Roby, Twilight, and High Grade Zones of the Lac des Iles Complex, Ontario, Canada. Mineral. Deposita, 47, 875-896.
3. DURAN, C.J., BARNES, S-J. & CORKERY, J.T. (2014): Sulfide-rich pods from the Lac-des-Iles Pd ore deposits, Western Ontario, Canada: Part 1. A genetic model. 12th IPS abstract volume.
4. OBERTHÜR, T., CABRI, L.J., WEISER, T.W., McMAHON, G. & MULLER, P. (1997): Pt, Pd and other trace elements in sulfides of the Main Sulfide Zone, Zimbabwe: a reconnaissance study. Canadian Mineralogist, 35, 597-609.
5. PINA, R., GERVILLA, F., BARNES, S-J., ORTEGA, L. & LUNAR, R. (2012): Distribution of platinum-group and chalcophile elements in the Aguablanca Ni-Cu sulfide dposit (SW Spain): Evidence from a LA-ICP-MS study. Chemical Geology, 302-303, 61-75.
6. PINA, R., GERVILLA, F., BARNES, S-J., ORTEGA, L. & LUNAR, R. (2013): Platinum-group elements-bearing pyrite from the Aguablanca Ni-Cu sulphide deposit (SW Spain): a LA-ICP-MS study. Eropean Journal of Mineralogy, 25, 241-252.

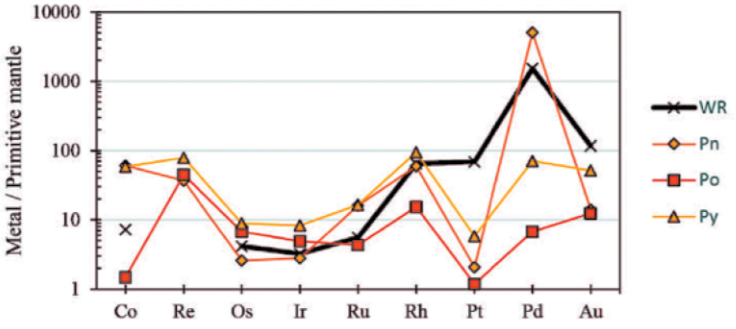

Fig. 2. Primitive mantle normalized metal profiles for Po, Pn and Py and whole rock (WR)

ANNEXE 27: 68TH GAC-MAC MEETING (JOINT ASSEMBLY WITH AGU AND CGU)

Présentation orale at the AGU-CGU-GAC-MAC joint assembly (Montréal, Canada) du 03 au 07 Mai 2015.

Résumé soumis :

The Use of Pentlandite and Pyrite Compositions for Exploration

Charley J. Duran[1], Sarah-Jane Barnes[1], John T. Corkery[2]

[1]Université du Québec A Chicoutimi, Sciences de la Terre, 555 Boulevard de l'Université, Chicoutimi, QC, Canada, G7H 2B1
[2]North American Palladium, Metals Exploration Division, 556 Tenth Avenue, Thunder Bay, ON, Canada, P7B 2R2

We have analyzed pentlandites and pyrites of sulfide-rich pods from the Lac des Iles Pd-deposits (Western Ontario, Canada) using LA-ICP-MS. In comparing our data with those from the literature, we noticed that pentlandites from primary PGE deposits are significantly enriched in Pd and Rh relative to pentlandites from Ni-Cu sulfide deposits. We also noticed that pyrites found in magmatic Ni-Cu-PGE deposits are enriched in Co and Se and depleted in Sb and As relative to pyrites found in low-temperature hydrothermal deposits (e.g. orogenic gold deposits and volcanogenic-hosted massive sulfides). A plot of Pd vs Rh in pentlandite appears to be effective at distinguishing pentlandites from primary PGE deposits to those from Ni-Cu deposits. In addition, a plot of Co/Se vs Sb/As in pyrite allows to distinguish pyrites from magmatic settings to those from hydrothermal settings. In detrital rocks such as tills, pentlandite and pyrite can be found in the heavy mineral fraction. Therefore, the two plots that we developed can be used in exploration to fingerprint potential targets. Furthermore, we identified that the primitive mantle normalized patterns of pentlandites derived from primitive magmas (e.g. layered intrusions, flood basalts, and ultramafic intrusions and flows) are different to those of pentlandites derived from evolved magmas (e.g. andesites). Thus, the geochemical signature of pentlandite may be used to infer the nature of its parental magma. This result can be of key importance to adapt exploration strategies.